Towards C+L Band Elastic Optical Networks: A Solution to Overcome the Optical Fiber Capacity Crunch Problem

By

Rana Kumar Jana

PhD19103

Under the Supervision of

Prof. Anand Srivastava and Dr. Abhijit Mitra

Department of Electronics & Communication Engineering
Indraprastha Institute of Information Technology, Delhi

September, 2024

Towards C+L Band Elastic Optical Networks: A Solution to Overcome the Optical Fiber Capacity Crunch Problem

By

Rana Kumar Jana

PhD19103

Under the Supervision of

Prof. Anand Srivastava and Dr. Abhijit Mitra

Submitted
in partial fulfillment of the requirements for the degree of
Doctor of Philosophy

to the

Indraprastha Institute of Information Technology, Delhi

September, 2024

Dedicated to my loving wife for her unconditional and uncountable support throughout this journey…

Certificate

This is to certify that the thesis titled "**Towards C+L Band Elastic Optical Networks: A Solution to Overcome the Optical Fiber Capacity Crunch Problem**" being submitted by **Rana Kumar Jana** to the Indraprastha Institute of Information Technology Delhi, for the award of the degree of **Doctor of Philosophy**, is an original research work carried out by him under my supervision. In my opinion, the thesis has reached the standards fulfilling the requirements of the regulations relating to the degree.

The results contained in this thesis have not been submitted in part or full to any other university or institute for the award of any degree/diploma.

Prof. Anand Srivastava

Dr. Abhijit Mitra

Indraprastha Institute of Information Technology Delhi
New Delhi, 110020
September, 2024

Declaration

This is to certify that the thesis titled "**Towards C+L Band Elastic Optical Networks: A Solution to Overcome the Optical Fiber Capacity Crunch Problem**" being submitted by **Rana Kumar Jana** to the Indraprastha Institute of Information Technology Delhi, for the award of the degree of **Doctor of Philosophy**, is a bonafide research work carried out by me under the supervision of **Prof. Anand Srivastava** and **Dr. Abhijit Mitra**.

The results contained in this thesis have not been submitted in part or full to any other university or institute for the award of any degree/diploma.

Rana Kumar Jana
PhD19103

Indraprastha Institute of Information Technology Delhi
New Delhi, 110020
September, 2024

Acknowledgements

"The important thing is not to stop questioning. Curiosity has its own reason for existence."

– Albert Einstein, Life Magazine, May 2, 1955

The key principle of successful research depends on the willpower, curiosity, patience, and hard work of the researcher. I am thankful to countless individuals who have supported me in this journey in numerous ways and helped me to maintain these essential aspects of research.

First and foremost, I am deeply thankful to my supervisors, Prof. Anand Srivastava and Dr. Abhijit Mitra, for their constant support, guidance, and encouragement throughout the last five years. I would like to take this opportunity to express my sincere gratitude to both of my supervisors because without the opportunity provided by them at IIIT Delhi, starting my PhD journey five years ago would have been difficult. I am also grateful to my yearly monitoring committee members, Dr. Sayak Bhattacharya (IIIT Delhi, India) and Prof. Motoharu Matsuura (UEC, Japan), for their insightful feedback on my research output. In addition, I am also thankful to my comprehensive examiners, Prof. Vivek Ashok Bohara (IIIT Delhi, India), and Dr. Abhishek Dixit (IIT Delhi, India), for their valuable advice in my work. Moreover, I am also grateful to my thesis examiners, Prof. Y. N. Singh (IIT Kanpur, India), Prof. Eiji Oki (Kyoto University, Japan), and Prof. Vimal Bhatia (IIT Indore, India), whose constructive comments have significantly improved the flow of the thesis.

My heartfelt appreciation goes to my international mentors, Mr. Andrew Lord (British Telecom, UK) and Prof. Biswanath Mukherjee (UC, Davis), for arranging time for me from their very busy schedules and for providing their in-depth advice throughout my research. Their constructive criticism has challenged me to think critically and has greatly improved the quality of my research work.

I am also immensely thankful to Prof. Wladek Forysiak and Prof. Sergei K. Turitsyn for hosting my overseas research visit in the UK. I was very fortunate to work under their kind guidance as a visiting researcher at Aston University (Birmingham, UK). I would also like to express my special thanks to the selected members of the Aston Institute of Photonic Technologies (AiPT) Group, namely, Dr. Pratim Hazarika, Dr. Shabnam Noor, and Dr. Mingming Tan, for their in-kind suggestions in my overseas research. I would also like to acknowledge the great effort of Ms. Tatiana Kilina (member of AiPT) for smoothly organizing my overseas journey from India to the UK. I am very thankful to Prof. Wladek Forysiak for giving me the excellent opportunity to visit University College London (UCL) and meet the leading research team of Prof. Polina Bayvel. I am very thankful to Mr. Henrique Buglia for spending valuable hours with me for insightful discussions. I am also very grateful to Prof. Gerard Parr for his kind hosting at the University of East Anglia (Norwich) and for providing valuable time to discuss possible collaboration opportunities.

In my UK days, I was fortunate to visit the beautiful campus of the BT group at Adastral Park (Ipswich) and visualize the growth of cutting-edge research areas. I am very thankful to Andrew Lord for giving me this unforgettable opportunity. Many thanks to Ms. Lakshmi Rajagopal and Mr. Kristan Farrow for introducing me to the exceptional research facilities of BT at Adastral Park. I am very grateful to Dr. Md Asif Iqbal for his uncountable guidance and help in every aspect of my Ipswich days. I am also very much thankful to my other collaborators from the BT optics research team, namely Mr. Paul Wright and Mr. Neil Parkin, who have contributed their valuable inputs to my different research problem statements.

I would also like to take this opportunity to thank Netlab members of the University of California (UC, Davis), especially Dr. Sifat Ferdousi, Mr. Ramanuja Kalkunte, Mr. Subhadeep Sahoo, Dr. Tanjila Ahmed, Dr. Forough Shirin Abkenar, and Prof. Massimo Tornatore, for their technical inputs. I am immensely thankful to Prof. Biswanath Mukherjee for providing me with the opportunity to participate in Netlab weekly meetings. I would also like to express my special thanks to Dr. Bijoy Chand Chatterjee (South Asian University, India) for providing his valuable opinions to my numerous queries related to our collaborative work. I am also thankful to my other industrial collaborators, especially Dr. Arvind Kumar Mishra (STL), Dr. Parthasarathi Palai (Tejas Networks, India), and Mr. Sowmendran (Tejas Networks, India), for providing their in-kind input in different aspects of my research.

My heartfelt appreciation goes to IIIT-Delhi for providing an excellent research infrastructure, precious facilities, and fellowship support. I am grateful to the numerous administrative officers, staff, faculty, and team of IIIT-Delhi, especially the Admin PhD, IRD Team, Finance Team, IT Team, Library Team, Department Admin, and Head of the Department, for their kind help in different aspects throughout my journey. I am very much thankful to the selected alumni of the BITS-ON group of IIIT-Delhi (mainly Mr. Aniket Pradhan and Mr. Abhishek Pratap Singh) for their insightful input in our collaborative works.

This PhD journey would not be possible without the support of some of my special friends, and they deserve special recognition. To begin with, I would like to convey my sincere gratitude to Mr. Rahul and Ms. Akanksha Sneh for their in-kind financial, mental, and moral support throughout the last five years. Next, I want to express my heartfelt thanks to Mr. Sayantan Roy and Mr. Sagnik Chatterjee for their unwavering love, encouragement, and financial support in this tough journey. Furthermore, I would also like to thank Ms. Akshita Gupta, Dr. Saumya Chaturvedi, Mrs. Kainat Yasmeen, Dr. Sandeep Sharma, and Dr. Dilnashin Anwar for their unconditional financial and strategic support in my various overseas journeys. I am also very much thankful to former lab members, especially Dr. Dhananjay Kimothi, Dr. Charul Paliwal, and Dr. Anand Singh, for providing their valuable suggestions in the early days of my Ph.D. I would also like to thank the rest of the members of the CoE-Lifi and BITS-ON groups of IIIT-Delhi for participating with me in various stimulating research discussions.

I also want to convey my gratitude to my former supervisors, especially Prof. Abhirup Das Barman (University of Calcutta, India) and Prof. Debasish Datta (IIT Kharagpur, India), for bringing me into the field of optical networks seven years ago. I would also like to express my heartfelt thanks to my beloved seniors, Mr. Arnav Mukhopadhyay and Dr. Rangana Banerjee Chaudhuri, who are the constant source of motivation, support, and inspiration. My PhD journey would not have even started at IIIT-Delhi without the limitless support from Mr. Arnav at the end of my M.Tech. I am also grateful to my beloved school friend, Dr. Sourav Bej, and my respected teacher, Mr. Raju Manna, for their valuable encouragement. I am immensely thankful to my Parents (Mrs. Mousumi Jana and Mr. Rabi Jana) and my in-laws (Mrs. Chhabi Chakraborty and Mr. Dilip Kumar Chakraborty) for their constant support and motivation.

Last but not least, survivability in this journey would not have been possible without the unconditional and uncounted support from my wife, Mrs. Sudipta Chakraborty, who is the

backbone of all of my achievements. I cannot thank her enough, but I would like to surely thank god for blessing me with a wonderful, supportive life partner. I dedicate this thesis to her as a token of gratitude.

Rana Kumar Jana
PhD19103

Abstract

Over the past decade, there has been an exponential rise of high-data-rate, ultra-low-latency, and bandwidth-hungry applications at the client's end, which has increased data traffic many-fold. Recent developments in 5G and cloud-based services have driven the compound annual growth rate (CAGR) of global Internet protocol (IP) traffic by nearly 30%. Hence, in the near future, per-month IP traffic growth will reach the zetta-bytes era. The COVID-19 pandemic has also catalyzed the usage of online services, leading to a 50% increase in data traffic compared to the pre-pandemic scenario. Recent forecasts indicate that, for the next ten years, the deployed infrastructure of the optical fiber backbone network will need to be upgraded to support this exponential growth of IP traffic to avoid the fiber-capacity-crunch problem. This has compelled network operators to seek out new strategies for enhancing network capacity while increasing minimum capital expenditure (CapEx).

The use of multiband (MB) and multifiber technologies appears to be a promising alternative immediate solution in recent studies while having its own trade-off to address this fiber capacity crunch problem and enhance the overall network capacity. MB technology considers the exploitation of the deployed standard single-mode fiber while enabling transmission on other bands (such as O, E, S, and L) along with the traditional C-band (1530 - 1565 nm). Although the multiband technology can use the full capacity of the existing deployed infrastructure, the challenges come from nonlinear impairments such as interchannel stimulated Raman scattering (ISRS). On the contrary, the multifiber-based solution focuses on the enlightenment of available dark fibers or the addition of additional parallel fibers. However, the CapEx for additional fiber resource deployment can play a crucial role in this context.

The research in this thesis has focused on addressing the following fundamental questions in this context:

- What is the cost-effective solution between MB and multifiber transmission? We justify this by performing techno-economic comparisons between these two solutions. As the L-band wavelengths provide the minimum attenuation after the C-band and as the L-band amplification appears as the most viable solution using the available commercial amplifiers, this thesis entirely focuses on C+L band transmission for analyzing the multiband scenarios.

- Do the conventional resource allocation and spectrum management policies also work well for C+L band systems while considering the impact of physical layer impairments?

- What will be the effective strategy to upgrade the existing C-band network towards the C+L band solution?

- How can network survivability be ensured in the C+L band environment for geographically diverse networks?

In the first part of this thesis, we have considered the C+L band physical layer model for estimating the quality of transmission (QoT) in multi-hop links while considering nonlinear interference (NLI) due to ISRS and other linear impairments (such as amplified spontaneous emission (ASE) noise). Consequently, we have made the techno-economic comparisons between the C+L band optical network with the multifiber C band scenario in the context of geographically diverse networks. Our results capture the variation of cost-per-bit with network traffic growth and fiber leasing cost. The numerical result indicates that the transmission over C+L bands is cost-effective compared to the multifiber C band scenario, particularly for large link-based geographies while considering the fiber leasing scenario. However, for smaller geographies, C+L band transmission becomes advantageous only if the fiber lease cost is high. As an alternate solution to fiber leasing, cable deployment scenarios are also considered separately for techno-economic comparison. The reported result shows that the C+L band system can postpone the need for extra cable deployment compared to the C band system and thereby minimizes the cost-per-bit in the long run. Furthermore, the comparison between optical cable deployment and fiber leasing is captured to minimize cost-per-bit while considering an operator's domain knowledge about their network.

After showcasing the benefits of C+L band transmission on cost-per-bit minimization, the next part of this thesis is focused on efficient spectrum management policies for the C+L band network to enhance the overall network capacity. Hitless spectrum defragmentation is mainly considered for the efficient utilization of spectral resources. The proposed work provides insights for network operators to develop the quality of service (QoS) maintenance strategy while doing spectrum defragmentation in the C + L bands. The proposed scheme prioritizes the minimization of the fragmentation index while maintaining the quality of transmission (QoT) for two different defragmentation algorithms, namely, nonlinear-impairment (NLI)-aware defragmentation (NAD) and NLI-unaware defragmentation (NUD). We leverage machine learning (ML) techniques for QoT estimation of ongoing lightpaths during spectrum reprovisioning. The optical signal-to-noise ratio (OSNR) of a lightpath is predicted for each choice of spectrum reprovisioning, which helps to monitor the effect of defragmentation on the quality of active lightpaths (in terms of assigned modulation format). Numerical results show that, compared to a baseline algorithm (NUD), the proposed NAD algorithm provides significant capacity increment for smaller and as well as larger networks.

As the C+L band network is highly vulnerable to NLI, appropriate channel allocation during lightpath provisioning also becomes crucial for boosting the achievable capacity of the overall network. As a consequence, we have developed an efficient spectrum allocation strategy for C+L band networks. Unlike conventional schemes, the proposed scheme takes the effect of physical layer impairments (PLI) before the choice of the spectrum during resource allocation to reduce the likelihood of blocking. An algorithm under this scheme, namely, OSNR adaptive first–last-fit (OA-FLF), is proposed while leveraging the heterogeneity of the C+L band elastic optical network. The proposed algorithm selectively chooses the available channels among C and L bands to achieve the maximum network capacity in the long run. However, as the network evolves from the beginning-of-life (BoL) or end-of-life (EoL) situation, the analytical method of OSNR estimation under this OA-FLF algorithm becomes computationally intensive. We have leveraged the computational advantage of ML techniques to resolve this issue and utilized a deep neural network (DNN) model to predict the OSNR of all lightpaths during provisioning. Reported results show that, compared to the baseline algorithms, the proposed OA-FLF algorithm can provide gain in terms of traffic admissibility for smaller and as well as larger networks.

As the existing C-band-based network can't adopt these emerging technologies instantaneously, strategic planning needs to be done to upgrade the existing network infrastructure. Hence, the later part of this thesis focuses on efficient network upgrade strategies. First, the ad-

vantage of resource re-provisioning via selective movement of lightpaths from C-band to L-band is explored before upgrading the C-band network to C+L-bands. Later on, a novel strategy, named C to C+L Upgrade (CLU), is proposed to upgrade links from C to C+L bands gradually. We develop a recurrent neural network (RNN)-based model to efficiently predict links for the upgrade based on network state and spectrum utilization to reduce blocking and upgrade costs. Our results show that CLU outperforms baseline strategies (which do not employ predictive decisions) by upgrading fewer links at appropriate times. As the parallel multifiber C-band-based solution is beneficial for the network operators in the presence of their own dark-fibers availability, the later section of this thesis also explored the strategic network upgrade methodologies in this context. The advantage of adaptive margin allocation on network upgrades while effectively utilizing the monitoring data from optical performance monitoring equipment is shown for multifiber-based upgrade scenarios. The proposed approach considers periodic feedback from the network to gain domain knowledge and prioritizes adequate margin allocation before network upgrade initiation. Reported results show that usage of domain knowledge-assisted adaptive margin can postpone the requirement of the network upgrade, enhance the spectrum efficiency, and minimize cost-per-bit in the long run.

Although operations over the C+L band can be an immediate and cost-effective solution for minimizing network upgrade costs, the impact on overall network reliability due to component failures needs to be considered for comprehensively assessing the true potential of the C+L band solution. Hence, the last part of this thesis is focused on the network survivability for C+L band networks while considering geographically diverse networks. In this context, we consider only single-band (either C or L band) inline amplifier failure scenarios. The provisioning of the backup lightpaths is prioritized over the same route as primary lightpaths using the alternate band. If the spectrum is unavailable in the primary routes, alternate routes are explored for backup path provisioning. Our approach measures the overall protection space of the network and the quality of the allocated lightpaths in geographically diverse networks. As a final step, we show the effect of the required Fill Margin (FM) on the achievable protection space and reliability of the network.

To summarize, the research in this thesis is entirely focused on the C+L band optical networks while considering the impact of the physical layer impairments. Numerous significant aspects, such as techno-economic comparisons, cost-per-bit minimization, efficient spectrum resource management, periodic network upgrades, and reliability issues, have been explored in various parts of this thesis. The research output on these perspectives will be truly essential for network operators and vendors for practically enabling C+L band transmission in the core optical network.

Table of Contents

List of Figures

List of Tables

List of Abbreviations

ANN	Artificial Neural Network
ASE	Amplified Spontaneous Emission
BDM	Band-Division Multiplexing
BoL	Beginning of Life
BP	Blocking Probability
CAGR	Compound Annual Growth Rate
CapEx	Capital Expenditure
CASSR	Contiguous-Aligned Available Slot Ratio
CLU	C to C+L Upgrade
DNN	Deep Neural Network
DSP	Digital Signal Processing
EDFA	Erbium-Doped Fiber Amplifier
EoL	End of Life
EON	Elastic Optical Network
FF	First Fit
FLF	Last Fit
FM	Fill Margin
GFF	Gain-Flattening Filters
GN	Gaussian Noise
HoM	Higher-Order Modulation
IoT	Internet of Things
IP	Internet Protocol
ISRS	Interchannel Stimulated Raman Scattering

KSP	k-Shortest Paths
LF	First Last Fit
LoM	Lower-Order Modulation
M2M	Machine-to-Machine
MB	Multiband
MB-EON	Multiband Elastic Optical Network
MCF	Multicore Fibers
ML	Machine Learning
MLP	Multi-Layer Perceptron
MoL	Mid of Life
NAD	NLI-Aware Defragmentation
NF	Noise Figure
NLI	Nonlinear Interference
NUD	NLI-Unaware Defragmentation
OA-FLF	OSNR Adaptive First-Last-Fit
OpEx	Operational Expenditure
OSNR	Optical Signal-to-Noise Ratio
PLI	Physical-layer Impairments
PLI	Physical Layer Impairments
QoS	Quality of Service
QoT	Quality of Transmission
RF	Random Fit
RMSA	Routing, Modulation and Spectrum Allocation
RNN	Recurrent Neural Network
ROADM	Reconfigurable Add-Drop Multiplexer
ROI	Return on Investment
SDM	Space Division Multiplexing
SE	Spectrum Efficiency
SINR	Signal-to-Interference-plus-Noise Ratio
SLA	Service Level Agreements

SPM	Self-Phase Modulation
SSFM	Split-Step Fourier Method
WDM	Wavelength Division Multiplexing
WSS	Wavelength Selective Switch
XPM	Cross-Phase Modulation

Chapter 1

Introduction

1.1 Background

In the era of machine-to-machine (M2M) communications, the Internet of Things (IoT), cloud computing, and ultra HD video live-streaming services, core network traffic is expected to increase manifold in the upcoming years. In order to support these next-generation services under the advancement of 5G and beyond technologies, the overall capacity of the core optical fiber networks needs to be enriched. Research into elastic optical networks over the C-band has been carried out over the past decade to address the capacity crunch problem while allocating optical spectrum in granularity of 12.5 GHz [1]–[3]. In parallel, significant research has also been reported on overall spectrum efficiency (SE) improvement while using advanced modulation format and constellation shaping [4]. However, the saturation in SE improvement due to the Shannon limit indicates that operators need to find some other alternatives in this context. As a consequence, the requirement for additional spectral resources still persists to solve the capacity crunch problem.

Two different technologies, namely, multiband (MB) optical transmission and space division multiplexing (SDM), emerge as potential candidates in this context [5]. The former is focused on the effective utilization of the already deployed single-mode optical fiber (ITU-T G.652.D) by exploring the optical transmission over other wavelength bands in addition to transmission over only the traditional C-band (1530 - 1565 nm). Whereas the SDM approach is focused on providing redundant C-band optical spectrum either by activating the dark fibers or deploying novel multicore fibers (MCF). As the commercial deployment of new MCF fiber cables requires enormous CapEx, multiband transmission emerges as an immediate option compared to the SDM solution [6].

Figure 1.1 captures the wavelength range and the dispersion and attenuation parameters of different optical bands, along with the details of the doped fiber amplifiers technologies [7]. As the amplification in the long wavelength band (L-band, 1565 - 1625 nm) can be supported using the current-deployed erbium-doped fiber amplifiers (EDFA), C+L band transmission becomes the first viable solution in the context of multiband technology [8].

1.2 Objectives

The main aim of this dissertation is to evaluate the net capacity and cost benefits of the C+L band elastic optical networks while considering the impact of nonlinear interference (NLI) due to inter-channel stimulated Raman scattering (ISRS) and other linear impairments. In order to achieve this aim, the following objectives have been addressed in different parts of this thesis:

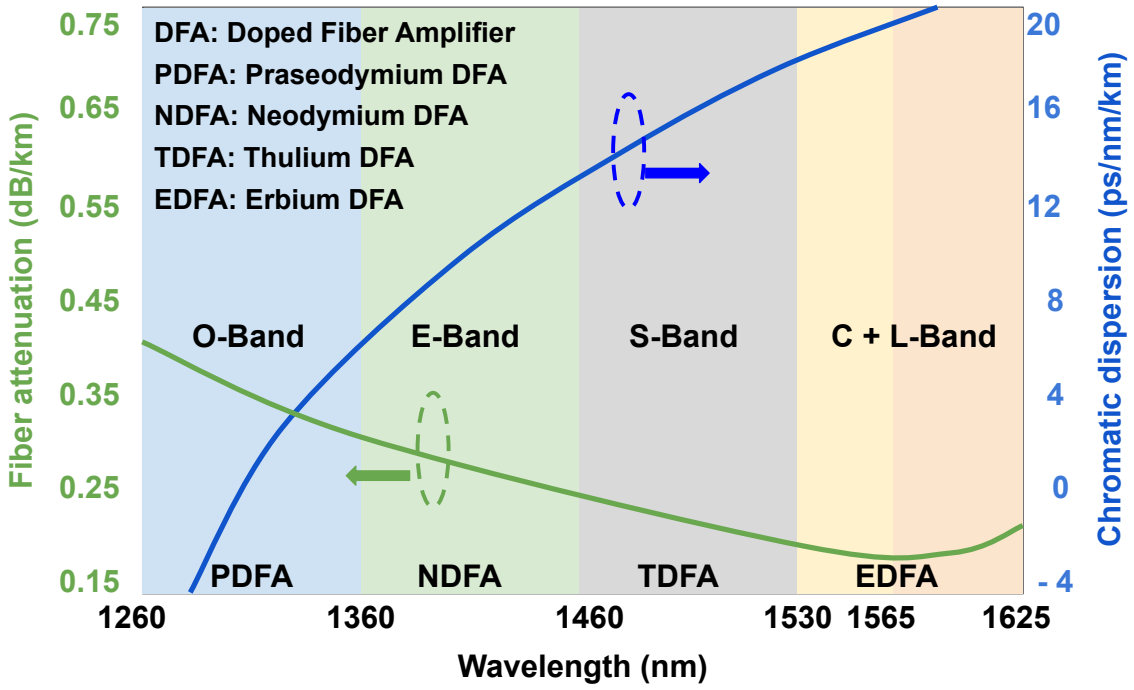

Figure 1.1: Bands of optical transmission in ITU-T G.652.D SMF fiber [5].

- **Objective 1:** To perform the techno-economic comparison between C+L band and multifiber-based C-band technology in the context of geographically diverse networks.
- **Objective 2:** To design efficient spectrum management policies for the C+L band network to enhance the overall network capacity while considering the underlying physical layer impairments.
- **Objective 3:** To propose efficient network upgrade methodologies for the designing of next-generation optical networks.
- **Objective 4:** To analyze the network survivability for C+L band networks while considering geographically diverse networks.

Figure 1.2 captures the flow of the overall thesis and the relationship between each chapter according to the above-mentioned objectives. To begin with, chapter 2 illustrates the physical layer model for the C+L band optical network while predicting the optical signal-to-noise ratio (OSNR) of a lightpath in the presence of linear and non-linear impairments. Later on, chapters 3 and 4 describe the strategies for techno-economic comparisons (objective 1) while considering the physical layer model from Chapter 2. Furthermore, objectives 2 and 3 have been analyzed in chapters 5, 6, and chapters 7, 8, and 9, respectively. In addition, the last objective of this thesis (objective 4) is discussed in Chapter 10 while considering the similar input on the physical player model from Chapter 2 as Objectives 2 and 3. Finally, chapter 11 summarizes the overall contribution of this dissertation in order to justify the aforementioned aim of this thesis and to illustrate the potential benefits of the C+L band network.

1.3 Major Contributions

The key contributions and outcomes of the research under this thesis are summarized below, along with relevant publications.

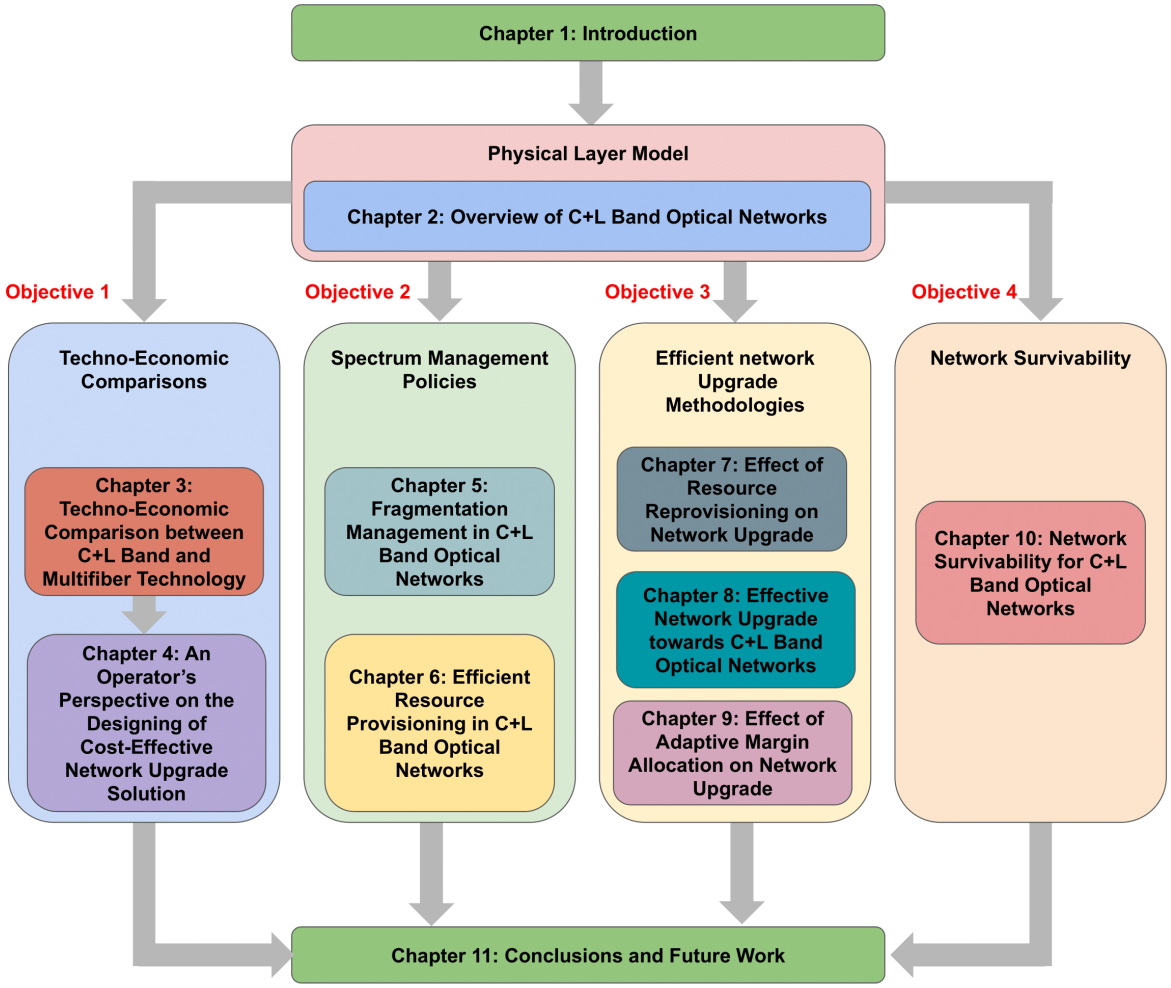

Figure 1.2: Relationship between chapters to grasp the key objectives.

- The research in this thesis first focused on multiband physical layer modeling while investigating the presence of significant challenges from several non-linear physical-layer impairments (PLIs), such as ISRS, and band-dependent transmission impairments, such as attenuation, dispersion, etc. In order to enhance the overall capacity of the network while mitigating the effect of PLIs, the use of gain-flattering filters (GFFs) in different parts of the network has been explored. Reported results show that the placement of GFF at every inline amplifier module instead of its placement at the reconfigurable optical add-drop multiplexer (ROADM) module can provide significant gain in traffic admissibility for smaller and as well as larger networks. In addition, the effect of launch power and symbol rate variation is also explored in this context. Numerical results show that the placement of GFF at the ROADM modules outperforms in terms of return on investment (ROI), whereas the placement of GFF at the EDFA module outperforms in terms of quality of transmission (QoT).

  – **R. K. Jana**, A. Srivastava, A. Lord, and A. Mitra, "Effect of Gain Flattening Filter Placement for Nonlinear Impairment Mitigation in Multiband Optical Transport Network," ***2023 IEEE International Conference on Advanced Networks and Telecommunications Systems (ANTS)***, Jaipur, India, 2023, pp. 102-107, doi: 10.1109/ANTS59832.2023.10469529.

- The next part of this thesis is focused on the techno-economic comparisons between C and C + L band technologies while taking the cost of different in-line components. A domain-knowledge-assisted, cost-effective network upgrade algorithm is proposed to enhance the overall capacity of the network while minimizing CapEx. The performance of the proposed algorithm is assessed in terms of network upgrade cost, overall CapEx, and cost-per-bit while considering flex-grid with incremental static traffic. In addition, the comparison between optical cable deployment and fiber leasing is captured to upgrade the capacity of the optical core network with minimum cost-per-bit. Moreover, geographically diverse networks are considered in this study to highlight the effect of longer link length on the network upgrade cost.

  - **R. K. Jana**, A. Mitra, A. Pradhan, K. Grattan, A. Srivastava, B. Mukherjee, and A. Lord, "When Is Operation Over C + L Bands More Economical than Multifiber for Capacity Upgrade of an Optical Backbone Network?," ***2020 European Conference on Optical Communications (ECOC)***, Brussels, Belgium, 2020, pp. 1-4, doi:10.1109/ECOC48923.2020.9333276.

  - **R. K. Jana**, M. A. Iqbal, N. Parkin, A. Srivastava, A. Mishra, J. Balakrishnan, P. Coppin, A. Lord and A. Mitra, "Multifiber vs. Ultra-Wideband Upgrade: A Techno-Economic Comparison for Elastic Optical Backbone Network," ***2022 European Conference on Optical Communications (ECOC)***, Basel, Switzerland, 2022, pp. 1-4, doi: 10.1364/ECEOC.2022.We1A.5.

  - **R. K. Jana**, A. Srivastava, A. Lord, and A. Mitra, "Optical Cable Deployment vs. Fiber Leasing: An Operator's Perspective on CapEx Savings for Capacity Upgrade in Elastic Optical Core Network," in ***Journal of Optical Communications and Networking***, vol. 15, no. 8, pp. C179-C191, August 2023, doi: 10.1364/JOCN.483200, [**Impact Factor: 4.0**].

- After showcasing the benefits of multiband (C+L band) transmission on cost-per-bit minimization, the consequent part of this thesis is concentrated on the designing of efficient spectrum management policies for the C+L band network. This work proposes, for the first time, a quality-aware proactive defragmentation scheme for the multiband (C+L band) EON system while analyzing the trade-off between NLI and defragmentation. This work provides insights for network operators to develop the QoS maintenance strategy while doing spectrum defragmentation in the C + L bands. During the development of the proposed schemes, this work shows the impact of the lightpath selection strategy on the overall network capacity. The proposed scheme prioritizes the minimization of the fragmentation index (FI) and QoT maintenance for two different defragmentation algorithms, namely, NLI-aware defragmentation (NAD) and NLI-unaware defragmentation (NUD). Moreover, to leverage the computational advantage of machine learning (ML) techniques, a robust deep neural network (DNN) model is also used to predict the OSNR of all lightpaths while performing proactive spectrum reprovisioning.

  - **R. K. Jana**, B. C. Chatterjee, A. P. Singh, A. Srivastava, B. Mukherjee, A. Lord, and A. Mitra, "Machine learning-assisted nonlinear-impairment-aware proactive defragmentation for C+L band elastic optical networks," in ***Journal of Optical Communications and Networking***, vol. 14, no. 3, pp. 56-68, March 2022, doi: 10.1364/JOCN.440214 [**Impact Factor: 4.0**].

- As the multiband network is highly vulnerable to NLI, appropriate channel allocation during lightpath provisioning also becomes crucial for enhancing the achievable capacity of the overall network. As a consequence, the next part of this thesis is focused on the development of efficient spectrum allocation policies over C+L band networks. First, the performance of the conventional spectrum allocation policies is investigated in different geographies with different channel launch powers for C+L band systems. Hence, a novel quality-aware resource provisioning scheme is proposed to enhance the overall network capacity while capturing the physical layer impairments for the C+L band.

  - **R. K. Jana**, B. C. Chatterjee, A. P. Singh, A. Srivastava, B. Mukherjee, A. Lord, and A. Mitra, "Performance Evaluation of Conventional Spectrum-Allocation Policies for C+L Band Elastic Optical Networks," ***2021 IEEE International Conference on Advanced Networks and Telecommunications Systems (ANTS)***, Hyderabad, India, 2021, pp. 348-353, doi: 10.1109/ANTS52808.2021.9937024.

  - **R. K. Jana**, B. C. Chatterjee, A. P. Singh, A. Srivastava, B. Mukherjee, A. Lord, and A. Mitra, "Quality-Aware Resource Provisioning for Multiband Elastic Optical Networks: A Deep Learning-Assisted Approach," in ***Journal of Optical Communications and Networking***, vol. 14, no. 11, pp. 882-893, Nov 2022, doi: 10.1364/JOCN.465782, [**Impact Factor: 4.0**].

- As the existing C-band-based network cannot adopt these above-mentioned emerging technologies instantaneously, strategic planning needs to be done to upgrade the existing network infrastructure. Hence, the later part of this thesis focuses on efficient network upgrade methodologies. First, the advantage of resource re-provisioning is explored for upgrading the C-band network to C+L bands while leveraging the benefits of selective lightpaths's movement from C-band to L-band. Later on, a novel strategy, named C to C+L Upgrade (CLU), is proposed to upgrade links from C to C+L bands gradually. Moreover, as the parallel multifiber C-band-based solution is beneficial for the network operators in the presence of their own dark-fibers availability, the later section of this thesis also explored the strategic network upgrade methodologies in this context. Mainly, the advantage of adaptive margin allocation on network upgrades while effectively utilizing the monitoring data from optical performance monitoring equipment is shown for multifiber-based upgrade scenarios.

  - R. Kalkunte, **R. K. Jana**, S. Ferdousi, A. Srivastava, A. Mitra, M. Tornatore, A. Lord, and B. Mukherjee, "GSNR-aware resource re-provisioning for C to C+L-bands upgrade in optical backbone networks," in ***Photonic Network Communications***, vol. 47, pp. 139-153, July 2024, doi: 10.1007/s11107-024-01023-6, [**Impact Factor: 1.8**].

  - R. Kalkunte, F. S. Abkenar, **R. K. Jana**, D. Aureli, S. Ferdousi, A. Srivastava, A. Mitra, M. Tornatore and B. Mukherjee, "An Effective Strategy for Link Upgrade from C to C+L Band in Elastic Optical Backbone Networks," ***2023 IEEE International Conference on Advanced Networks and Telecommunications Systems (ANTS)***, Jaipur, India, 2023, pp. 437-440, doi: 10.1109/ANTS59832.2023.10469649.

– **R. K. Jana**, A. Lord, A. Srivastava, and A. Mitra., "An Operator's Perspective on the Introduction of Domain Knowledge-Assisted Adaptive Margin Ahead of Network Upgrade," ***2024 European Conference on Optical Communications (ECOC)***, Frankfurt, Germany, 2024, pp. 1-4, (Accepted).

- Although operations over the multiband can be a short-term, cost-effective solution for minimizing network upgrade cost and the cost-per-bit in the long run, the overall network reliability due to component failures needs to be further studied in order to assess the overall true potential of the multiband solution. Hence, the last part of this thesis is focused on the network survivability for C+L band networks while considering geographically diverse networks. In this context, we consider only single-band (either C or L band) inline amplifier failure scenarios. Our proposed approach measures the overall protection space of the network and the quality of the allocated lightpaths in two geographically diverse networks. As a final step, we have shown the effect of the required OSNR margin variation for absorbing adjacent channel impairments (called Fill Margin (FM)) on the achievable protection space and reliability of the network.

  – **R. K. Jana**, A. Srivastava, A. Lord, and A. Mitra, "Effect of fill margin on network survivability for C+L band optical networks," ***49th European Conference on Optical Communications (ECOC)***, Glasgow, UK, 2023, pp. 1453-1456, doi: 10.1049/icp.2023.2589.

1.4 Thesis Layout

The rest of the thesis is organized as follows:

Chapter 2 presents the overview of multiband optical networks while capturing the NLI due to ISRS and other linear impairments. In chapter 3, the techno-economic comparisons between the C+L band optical network and the multifiber C band system are captured while considering fiber leasing and cable deployment scenarios. Chapter 4 minimizes the cost-per-bit with increasing traffic load while exploring the domain-knowledge-assisted network upgrade methodologies. After showcasing the benefits of the multiband optical network, the next part of the thesis is focused on the development of efficient spectrum management and spectrum allocation policies in chapter 5 and 6, respectively. The later part of this thesis is focused on the upgradation of the existing C-band-based infrastructure towards the C+L band. At first, the advantage of resource re-provisioning from C-band to L-band is explored in this context in chapter 7. Hence, an ML-based model is also developed in chapter 8 for efficiently predicting links for the upgrade as per the network's current status. Furthermore, chapter 9 explores the advantage of optical performance monitoring equipment and shows the impact of utilizing the monitoring data on the network upgrade requirement. The last part of this thesis is focused on the network survivability for multiband networks where the reliability aspects are compared between C+L band and C-band systems for geographically diverse networks in chapter 10. Finally, Chapter 11 concludes this dissertation and indicates possible future research directions.

Chapter 2

Overview of C+L Band Optical Networks

2.1 Introduction

As indicated in Chapter 1, many sophisticated technologies, including M2M communication, IoT, cloud computing, etc., have significantly boosted the compound annual growth rate (CAGR) of global Internet protocol (IP) traffic in the 5G era [9]. In addition, the rise of online activities during the COVID-19 pandemic also increased the overall network traffic globally by approximately 50% [10]. Recent projections show that, in order to prevent the optical fiber capacity crunch problem, the existing infrastructure of the optical fiber transport network should be increased in order to accommodate this exponential rise of IP traffic over the next 10 years [11]. As a result, the optical network industry's research focuses on increasing the capacity of existing infrastructure while minimizing capital expenditures (CapEx).

In recent studies, MB and SDM technologies have been proposed as potential candidates for optical transport network upgrades. As mentioned in Chapter 1, research in MB solution focuses on the effective utilization of additional bands (such as L (1565 - 1625 nm), S (1460 - 1530 nm), E (1360 - 1460 nm), and O (1260 - 1360 nm) bands) of deployed single-mode fibers along with the conventional C band (1530 - 1565 nm) transmission. On the other hand, the use of parallel single-mode fibers and several new types of fibers, such as multimode fibers and multicore fibers, are the key focus of SDM technology.

Although the MB solution enhances the transmission bandwidth, a drawback is the presence of inter-channel stimulated Raman scattering (ISRS) [12]. As a result of ISRS, nonlinear interaction occurs between the active channels in the network, and a significant amount of power transfer happens from higher-frequency active channels to lower-frequency active channels. This redistribution of launch power enhances the nonlinear interference (NLI) for certain channels and reduces the overall transmission reach of the network.

The use of gain flattening filters (GFF) for the mitigation of ISRS is a useful technique in the context of the MB technology [13], [14]. However, the position of GFF needs to be localized as it can severely impact the quality of transmission and the achievable capacity of the network. We have explored the effect of GFF localisation in MB scenarios while considering the presence of various geographies, launch power, and symbol rates.

This work compares the effect of GFF placement in the C+L band system in two different positions, namely, GFF at each of the inline amplifier modules and GFF at each of the reconfigurable optical add-drop multiplexer (ROADM) modules. As less number of GFF is required for the latter approach, the impact of the deployed GFF count is analyzed here for geographically diverse networks in terms of traffic admissibility, quality of transmission (QoT), and return on

investment (ROI).

The remaining parts of this work are arranged as follows. Section 2.2 discusses the underlying physical layer of the network. Section 2.3 captures the details of GFF-assisted routing, modulation, and spectrum allocation (RMSA) strategy. The simulation setup and simulated results are reported in Section 2.4 and 2.5, respectively. Finally, Section 2.6 concludes the work.

2.2 Physical-Layer Model

This section explains the details of the physical layer model, which is needed to estimate the QoT of a lightpath in terms of OSNR. Figure 2.1 shows the end-to-end system model for the C+L band where the transmission of a lightpath over multiple hops is illustrated. During multi-hop transmission between a source and destination node, a lightpath travels over different links, inline amplifiers, and ROADM modules. Band-specific inline amplifiers such as C band EDFA (noise figure (NF) = 5.5 dB [5]) and L band EDFA (NF = 6 dB [5]) are used in every link between successive spans. In order to mitigate the effect of ISRS, two positions for GFF placement are considered, and the corresponding physical layer model is elaborately described below.

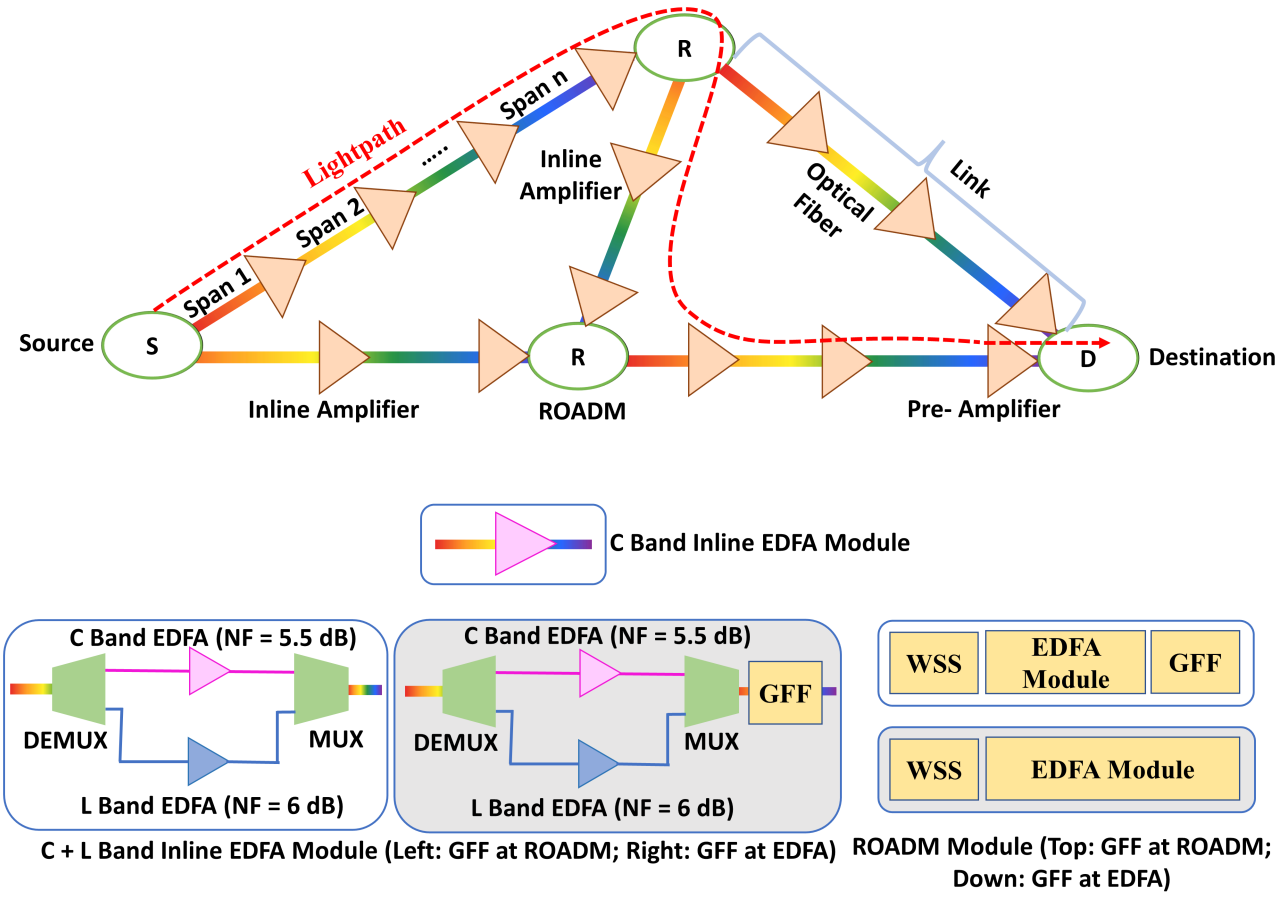

Figure 2.1: End-to-end physical layer model.

2.2.1 GFF at ROADM module

If the GFF is placed in the ROADM module, the band-specific amplifiers and MUX/DEMUX elements (insertion loss = 1 dB) for multiplexing/demultiplexing purposes are considered within

the inline amplifier module. The gain of the inline amplifiers (g_{in}) is set as the previous span losses, and the accumulated amplified spontaneous emission (ASE) noise power (in Watts) of the lightpath at frequency f after traversing the i^{th} link are considered as follows [15]:

$$P^i_{ASE}(f) = N^i_S 2n_{sp}(g_{in} - 1)hfB_{Ref}, \tag{2.1}$$

where B_{Ref}, h, N^i_s and $2n_{sp}$ denote reference bandwidth, Planck constant, number of spans in the i^{th} link and NF of the amplifier, respectively.

$$P^{R_i}_{ASE}(f) = N^i_S 2n_{sp}(g_R(f) - 1)hfB_{Ref}, \tag{2.2}$$

Equation 2.2 captures the component of ASE noise ($P^{R_i}_{ASE}(f)$) power from the ROADM module, where the combined gain (i.e., $g_R(f)$ in linear scale) of the GFF block and amplifier module at the ROADM can be written (in dB scale) as follows [16]:

$$G_R(f)(dB) = \begin{cases} 18 - \sum_{k=1}^{N^i_s} \rho_k(f) & \text{positive ISRS gain,} \\ 18 & \text{no ISRS gain,} \\ 18 + \sum_{k=1}^{N^i_s} \rho_k(f) & \text{negative ISRS gain,} \end{cases} \tag{2.3}$$

where 18 and $\rho_k(f)$ denote the insertion loss (in dB) for the wavelength-selective switches (WSSs) [17] and accumulated ISRS gain, respectively. The details of ISRS gain are captured in Appendix A.

$$P^i_{NLI}(f) = (P^i_{ch})^3 N^i_s \eta_{XPM}(f) + (P^i_{ch})^3 N^i_s \eta_{SPM}(f), \tag{2.4}$$

On the other hand, the total NLI power ($P^i_{NLI}(f)$) (in watt) can be expressed using Equation 2.4, where the component of self-phase modulation (SPM) ($\eta_{SPM}(f)$) and cross-phase modulation (XPM) ($\eta_{XPM}(f)$) can be written using Equation 2.5 and 2.6, respectively [13].

$$\begin{aligned} \eta_{\text{SPM}}(f) \approx{}& \frac{4}{9}\frac{\gamma^2}{B_z^2}\frac{\pi}{\phi_z \bar{\alpha}\,(2\alpha + \bar{\alpha})} \\ &\cdot \left[\frac{T_z - \alpha^2}{a}\text{asinh}\left(\frac{\phi_z B_z^2}{\pi a}\right) + \frac{A^2 - T_z}{A}\text{asinh}\left(\frac{\phi_z B_z^2}{\pi A}\right)\right], \end{aligned} \tag{2.5}$$

$$\begin{aligned} \eta_{\text{XPM}}(f) \approx{}& \frac{32}{27}\sum_{k=1,k\neq z}^{N_{\text{ch}}}\left(\frac{P_k}{P^i_{ch}}\right)^2 \frac{\gamma^2}{B_k \phi_{z,k}\bar{\alpha}\,(2\alpha + \bar{\alpha})} \\ &\cdot \left[\frac{T_k - \alpha^2}{\alpha}\text{atan}\left(\frac{\phi_{z,k} B_z}{\alpha}\right) + \frac{A^2 - T_k}{A}\,\text{atan}\left(\frac{\phi_{z,k} B_z}{A}\right)\right], \end{aligned} \tag{2.6}$$

where N_{ch} denotes total number of active channels. P_k is the power of the k^{th} interfering channel, γ is the fiber nonlinear coefficient, $\phi_{z,k}$ is the phase mismatch term between k^{th} interfering channel and channel of interest, and T_k denotes the frequency-dependent constant of the k^{th} channel for ISRS power transfer [12].

Moreover, the OSNR of a lightpath after traversing through the N_L number of links at the frequency f can be summarized as follows [15]:

$$\frac{1}{OSNR(f)} = \sum_{i=1}^{N_L}\left(\frac{P^i_{ASE}}{P^i_{ch}} + \frac{P^i_{NLI}(f)}{P^i_{ch}} + \frac{P^{R_i}_{ASE}(f)}{P^i_{ch}}\right), \tag{2.7}$$

where P^i_{ch}, $P^i_{NLI}(f)$ and $P^{R_i}_{ASE}$ denote the launch power, accumulated NLI power and accumulated ASE noise power due to EDFAs of ROADM module in the i^{th} optical link, respectively.

2.2.2 GFF at EDFA module

If the GFF is placed after every span in every inline amplifier (EDFA) module, the combined gain of EDFAs and GFF can be summarized as follows [13]:

$$G(f)[dB] = \begin{cases} \alpha L^i_{span} - \rho^{i_{span}}(f) & \text{positive ISRS Gain at f,} \\ \alpha L^i_{span} & \text{no ISRS gain at f,} \\ \alpha L^i_{span} + \rho^{i_{span}}(f) & \text{negative ISRS Gain at f} \end{cases} \tag{2.8}$$

where α, L^i_{span} and $\rho^{i_{span}}(f)$ denote fiber attenuation, span length of i^{th} link and ISRS gain in each span, respectively.

Moreover, the ISRS gain for a single span at frequency f can be written as follows [13]:

$$\rho(z, f) = \frac{P_{tot} e^{-\alpha z - P_{tot} C_r L_{eff} f}}{\int G_{Tx}(\nu) e^{-P_{tot} C_r L_{eff} \nu} d\nu} \tag{2.9}$$

where P_{tot}, C_r, and G_{Tx} denote total signal power, Raman gain slope, and power spectral density, respectively.

On the other hand, as the GFF block is absent at the ROADM unit, the gain of the amplifier modules at ROADM becomes equivalent to total WSS switching loss (18 dB), and the overall OSNR of a lightpath can be expressed as follows:

$$\frac{1}{OSNR(f)} = \sum_{i=1}^{N_L} \left(\frac{(P^i_{ASE}(f))' + (P^i_{NLI}(f))'}{P^i_{ch}} \right) + \left(\frac{(P^{R_i}_{ASE})'}{P^i_{ch}} \right) \tag{2.10}$$

where $(P^i_{ASE}(f))'$, $(P^i_{NLI}(f))'$ and $(P^{R_i}_{ASE})'$ denote total ASE noise power due to inline EDFAs, NLI power and ASE noise power from ROADM modules, respectively, for GFF at EDFA scenario.

2.3 GFF-assisted RMSA

This section describes the overview of the proposed RMSA methodology (Algorithm 1) while considering the position of GFF in the network. This algorithm considers several parameters as input, such as network topology, channel launch power, symbol rate, supportable modulation formats, associated OSNR threshold, and GFF positions. Moreover, it returns the information about traffic admissibility, QoT, and ROI as output.

Initially, the possibility of spectrum allocation is checked in the k^{th} shortest path for every incoming request (lines 1-2). If there is spectrum availability in any of the available routes, the position of GFF is checked in the selected route (lines 3-4). Hence, the OSNR of the lightpath is calculated according to the position of GFF (lines 5-9), as discussed in Section 2.2. If the OSNR of the lightpath exceeds the threshold according to the supportable modulation formats, the incoming requests are served in the network while operating the lightpath over the selected modulation format (lines 10-12). On the contrary, if there is an unavailability of spectrum in all of the allowable routes or the OSNR of the corresponding lightpath of a request can not meet the threshold requirement of any modulation formats, the requests are blocked in the network (lines 16 - 18). Next, the overall traffic admissibility is captured in terms of total accepted requests and blocked requests (lines 26-27). Finally, the algorithm calculates the QoT using the distribution of modulation formats across the allocated lightpath in the network (line 28) and also evaluates the ROI while monitoring the CapEx and allocated traffic in the network (line 29).

Algorithm 1 GFF-Assisted RMSA

Input: Network topology, Channel launch power, Symbol rate, Supportable modulation formats, Traffic array, GFF position, k-shortest paths for every request, k^{max};
Output: Allocated requests, Blocked requests, QoT, ROI;
Initialisation: # of Blocked requests = 0, # of allocated requests = 0, $k = 1$

1: **for** each request in traffic array **do**
2: Check the possibility of spectrum allocation in the selected route k;
3: **if** (spectrum allocation == True) **then**
4: Check GFF position in the selected route;
5: **if** (GFF at ROADM == True) **then**
6: Calculate the OSNR of the lightpath using Eq. 2.7;
7: **else**
8: Calculate the OSNR of the lightpath using Eq. 2.10;
9: **end if**
10: **if** (OSNR of the lightpath $\geq$ threshold of minimum allowable modulation format) **then**
11: Allocate the lightpath in the network;
12: # of Allocated requests += 1;
13: **else**
14: Check the alternate route;
15: k += 1;
16: **if** ($k > K_{max}$) **then**
17: # of Blocked requests += 1;
18: **else**
19: Go to Step 2;
20: **end if**
21: **end if**
22: **else**
23: Go to Step 14;
24: **end if**
25: **end for**
26: Total allocated requests == # of allocated requests;
27: Total blocked requests == # of blocked requests;
28: QoT == Distribution of modulation formats in the allocated lightpaths;
29: ROI == CapEx / Allocated traffic;

2.4 Simulation Setup

In this work, simulations are done using a custom-built, event-driven, Python simulator while considering two diverse geographies, such as the BT-UK network (22 nodes, 35 links, average link length of 147 km) [18] and the Indian RailTel network (19 nodes, 28 links, average link length of 531 km) [18]. The details of these topologies are discussed in Appendix B. Moreover, three conventional launch powers (0 dBm, -1.5 dBm, and -3 dBm) per channel [19] are considered for analysis, along with symbol rates of 28 GBaud with 37.5 GHz channel spacing. Table 2.1 captures the supported modulation formats for individual lightpaths and corresponding OSNR thresholds. An optical bandwidth of 10 THz is considered for every link with a guard band of 200 GHz between the C and L bands.

Table 2.1: Supported modulation formats for lightpaths in 28 GBaud system [13].

Modulation	Data Rate (Gbps)	OSNR Threshold (dB)
PM-BPSK	50	9
PM-QPSK	100	12
PM-8QAM	150	16
PM-16QAM	200	18.6
PM-32QAM	250	21.6
PM-64QAM	300	24.6

2.5 Results and Discussion

This section first discusses the scenario of a point-to-point link where the distribution of power across all the active channels is monitored for different positions of GFF. Later on, the effect of GFF placement on the overall network performance is analyzed in terms of traffic admissibility, QoT, and ROI. Traffic admissibility is defined as the number of allocated connections in the network till predefined thresholds (such as 1% blocking in the network). The QoT is captured in terms of the distribution of the modulation formats across all the established connections in the network. ROI is defined as the ratio of the cost of the required GFF [20] to the allocated capacity.

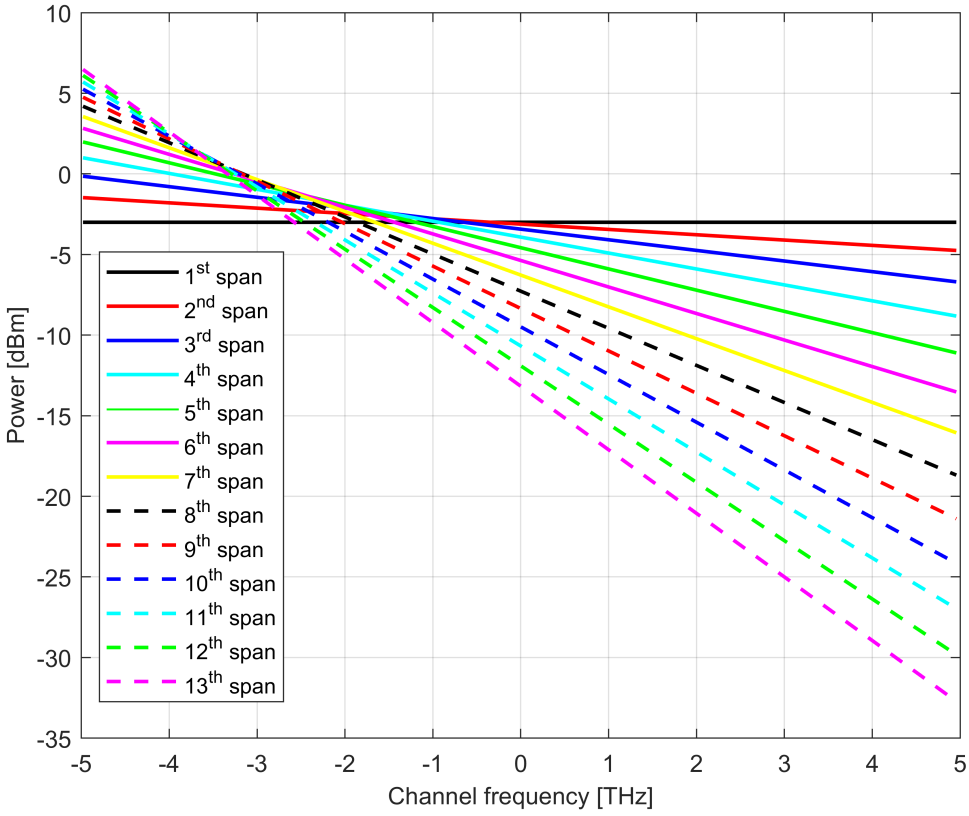

Figure 2.2: Effect of ISRS on power profile of each channel (-3 dBm of uniform launched power is considered at first span, as shown by the black solid line).

2.5.1 Point-to-point link analysis

Figure 2.2 captures the effect of the ISRS on the power profile across the C+L band spectrum for a point-to-point link. The x-axis represents the normalized frequencies for the overall 10 THz C+L band spectrum, whereas the y-axis represents the launch power profile at the beginning of every span due to ISRS non-compensation. Here, the 0 to 5 THz range on the x-axis indicates the C-band channels, whereas the 0 to -5 THz range denotes the L-band channels. Reported results show that if the ISRS effect is not compensated by GFF placement at the end of the span, the flat launch power distribution becomes tilted from one span to another due to power transfer from higher frequency channels to lower frequency channels. Figure 2.2 also depicts that if the number of spans with ISRS non-compensation increases in a point-to-point link, drastic power differences between the different channels in the 10 THz spectrum can be observed. For example, as shown by the red dotted line in Figure 2.2, if the ISRS is uncompensated for the eight consecutive spans (i.e., 480 km while taking 60 km as span length), launch power at the input of ninth span becomes - 21 dBm at 5 THz frequency and 5 dBm at -5 THz frequency. As the NLI on a particular span depends on the power profile of different active channels, the variation of launch power from one span to another due to tunability in GFF localization results in different NLIs for the active channels in the link. Consequently, the quality of transmission across different channels becomes dependent on GFF localization.

2.5.2 Network Analysis

This section describes the effect of GFF placement on the overall network performance in terms of traffic admissibility, QoT, and ROI.

2.5.2.1 Traffic Admissibility

Figures 2.3 and 2.4 show the traffic admissibility till 1% blocking for the BT-UK network and Indian RailTel network, respectively. The reported result shows that the placement of GFF at every EDFA module can provide a 37.7% gain in traffic admissibility compared to GFF at the ROADM scenario for 0 dBm launch power in the BT-UK network. However, as the launch power decreases from 0 dBm to -3 dBm, ISRS gain decreases significantly in every span of the C+L band link. As a result, the advantage of GFF placement at ROADM becomes similar to the GFF at EDFA scenario.

Figure 2.4 shows that the GFF placement at every EDFA in the Indian RailTel network can provide traffic admissibility gain of 38.9%, 74.9%, and 118.7% for 0 dBm, -1.5 dBm, and -3 dBm launch power, respectively, compared to the placement of GFF at ROADM scenario. As the average link length of the Indian RailTel network is higher compared to the BT-UK network, the ISRS compensation at ROADM reduces the QoT and achievable traffic admissibility. Whereas the placement of GFF at every EDFA mitigates the ISRS effect after every span and provides significant gains compared to GFF at the ROADM scenario.

2.5.2.2 Quality of Transmission

The QoT is captured in terms of the distribution of modulation formats across the established lightpaths in the network. Figures 2.5 and 2.6 capture the QoT in BT-UK and Indian RailTel network, respectively. The reported result shows that the shifting of the GFF position from EDFA to ROADM degrades the QoT in both of the networks. Mainly, lower-order modulation (LoM)-based lightpaths, such as PM-BPSK and PM-QPSK, increase in both of the networks for GFF at the ROADM scenario compared to GFF at the EDFA scenario. In smaller networks like BT-UK, the shifting of GFF at ROADM enhances the LoM from 3.7% to 11.6%, whereas

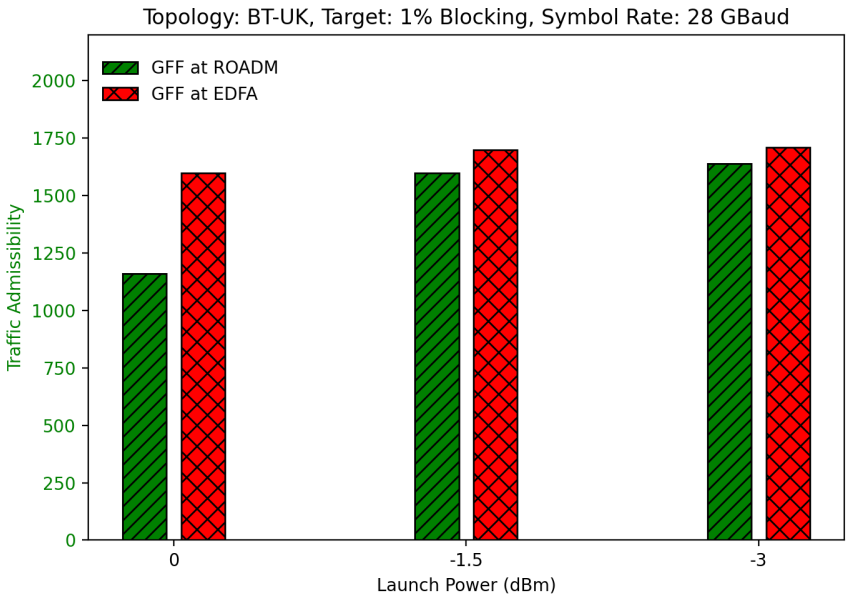

Figure 2.3: Traffic admissibility in BT-UK Network.

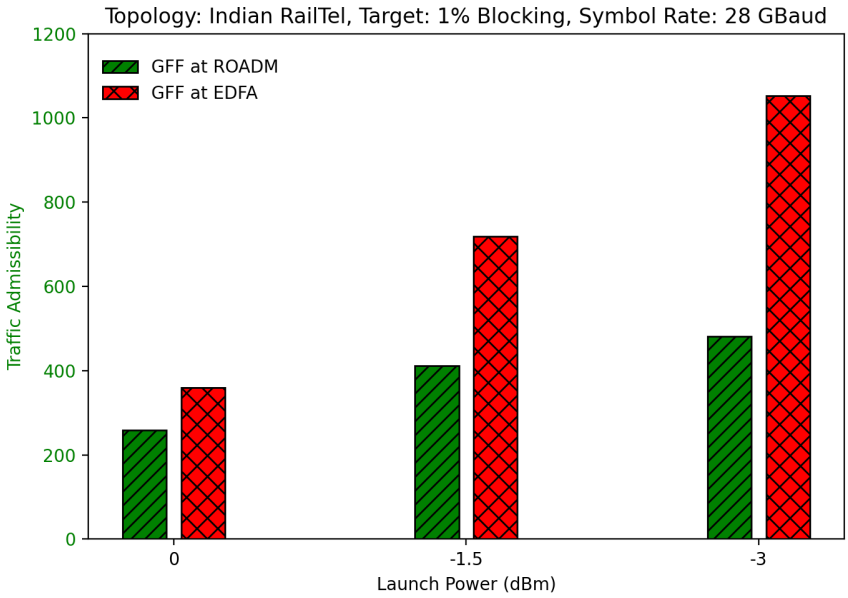

Figure 2.4: Traffic admissibility in Indian RailTel network.

the LoM-based lightpaths increase from 55.8% to 64.3% in the considered longer network (i.e., Indian RailTel Network). This 7.9% increment of LoM lightpaths due to the shifting of the GFF position does not severely impact the traffic admissibility in the BT-UK network as the majority of lightpaths are provisioned over higher-order modulation (HoM). Here, PM-8QAM, PM-16QAM, and PM-32QAM are considered as HoM. However, the enhancement of LoM-based lightpaths due to the shifting of the GFF position from EDFA to ROADM in the Indian network significantly dropped the traffic admissibility as the majority of lightpaths in this longer network are provisioned over low-efficiency oriented LoM formats.

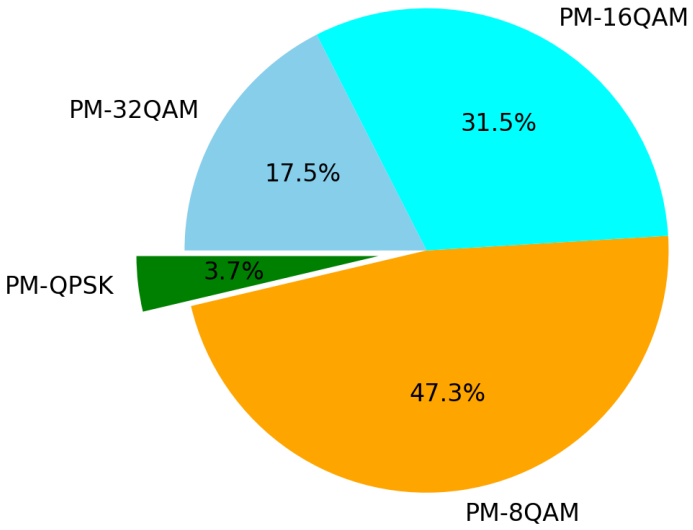

(a) GFF at EDFA

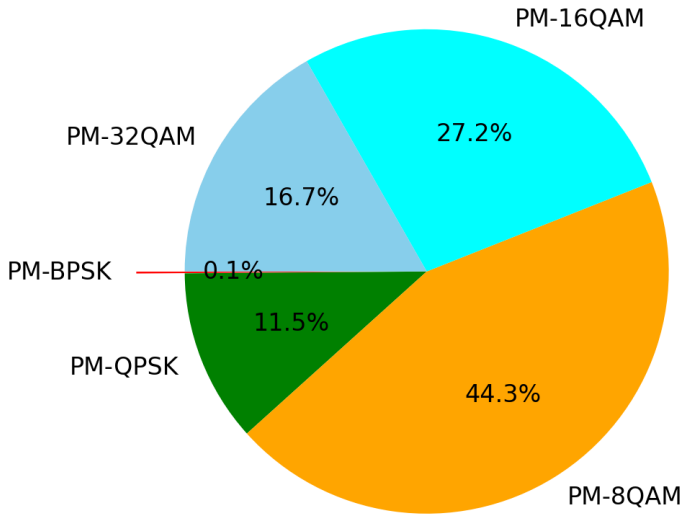

(b) GFF at ROADM

Figure 2.5: Quality of Transmission in BT-UK Network (Launch Power = -3 dBm).

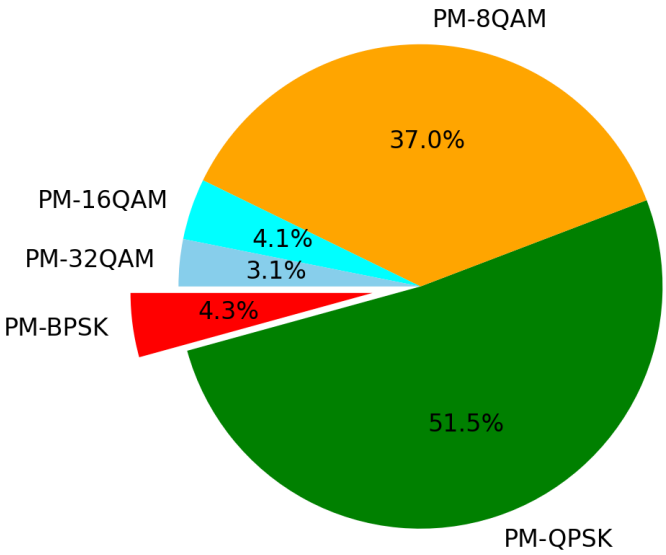

(a) GFF at EDFA

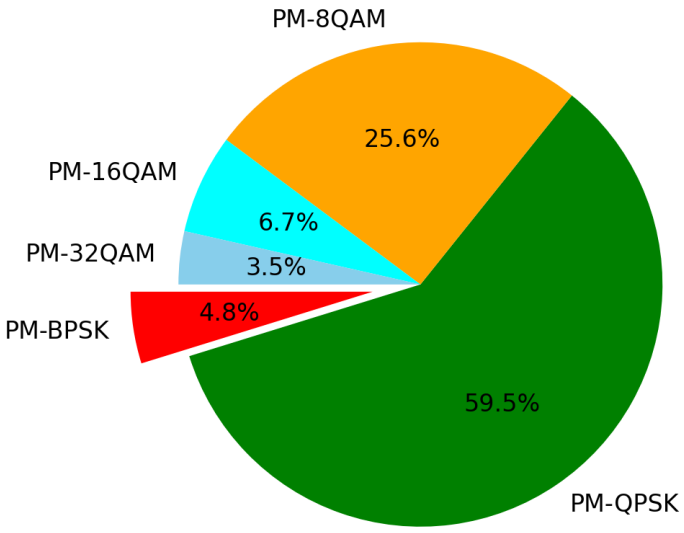

(b) GFF at ROADM

Figure 2.6: Quality of Transmission in Indian RailTel Network (Launch Power = -3 dBm).

Table 2.2: ROI for BT-UK network till 1% blocking.

GFF Position	Launch Power (dBm)	ROI ($ /bit/sec)
ROADM	0	15.2
ROADM	-1.5	11.0
ROADM	-3	10.7
EDFA	0	44
EDFA	-1.5	40.4
EDFA	-3	40.0

Table 2.3: ROI for Indian RailTel network till 1% blocking.

GFF Position	Launch Power (dBm)	ROI ($ /bit/sec)
ROADM	0	60
ROADM	-1.5	36.9
ROADM	-3	31.6
EDFA	0	560
EDFA	-1.5	275.9
EDFA	-3	188.6

2.5.2.3 Return on Investment

Tables 2.2 and 2.3 capture the RoI for BT-UK and Indian RailTel networks, respectively. Simulated results indicate that GFF placement at ROADM can provide a maximum gain of 73.2% in the BT-UK network, whereas the number becomes 89.2% for the Indian RailTel network. As the allocated capacity till 1% blocking is higher in the BT-UK network compared to the Indian network scenario, ROI becomes generally higher in the Indian network.

2.6 Conclusion

In terms of traffic acceptance, quality of service, and return on investment (ROI), this work examines the impact of GFF installation at various locations across geographically diversified networks. The reported result shows that the placement of GFF at the ROADM module can provide gain in terms of return on investment. However, the placement of GFF at EDFA outperforms in terms of traffic admissibility and quality of transmission for shorter and as well as longer geography.

Chapter 3

Techno-Economic Comparison between C+L Band and Multifiber Technology

3.1 Introduction

The primary objective of the network operators is the increment of the overall network capacity while incurring minimum CapEx. Although the use of multiple parallel fibers and MB solutions appear as potential candidates for increasing network capacity, both of these solutions are associated with their individual trade-offs. As discussed in Chapter 2, transmission over MB can use the full capacity of the existing infrastructure; however, the quality of the transmission becomes susceptible to NLIs such as ISRS [21]. In addition, the MB system needs the development of several advanced amplifier modules for long-reach transmission over different bands. On the contrary, leasing or deployment of additional fibers is needed to enable transmission over the multifiber C band-based solution.

Moreover, the geographical size of the network plays a crucial factor for the network operator. Mainly, the cost of additional equipment and fiber lease costs varies based on the size of the network. Therefore, the choice of technology for a network upgrade may vary from operator to operator. Recently, an optimum way to multifiber C+L bands link upgrade has been studied for the Italian network, considering geographical population locations [22]. Similarly, it has been shown that the MB Elastic Optical Network (EON) needs a higher migration cost than that of the parallel fiber system for the Telefónica-Spain national network [23].

In this work, at first, the effect of fiber lease cost on network cost upgrade (measured in cost-per-bit metric) has been analyzed for geographically diverse networks (such as BT-UK and Indian network [24]). Optical signal transmission over the C+L band and multifiber C-band solution are also compared. As the addition of spectral resources in the network can practically be possible only by leasing or deploying whole new fiber cables, we have also concentrated on additional cable deployment. The later part of this study considered more realistic assumptions and demonstrated the strategy of additional cable deployment at different required locations in the network. Mainly, the impact of additional cable deployment on traffic growth is analyzed in this work. Two scenarios, namely, multifiber C band and multifiber C+L band, are focused in this study. We have indicated the former case as nC and the latter case as n(C+L), where the notation n is used to resemble the multifiber scenario. A techno-economic comparison is performed between the nC and n(C+L) in terms of CapEx and cost-per-bit of the network while assuming a bidirectional single fiber pair in all of the links of the network initially.

3.1.1 Key Contributions

The overall contribution of this study can be summarized as shown below:

- Network operation over C+L bands compared to multifiber (nC) band is investigated for the capacity upgrade of optical backbone networks. Mainly, the effect of fiber leasing cost on the cost-per-bit of the network is captured for geographically-diverse networks. The reported result shows the advantage of the C+L band network for larger networks, even for the presence of low fiber lease cost.
- Two methods are proposed to upgrade the network capacity by following two principles, namely, placement of extra cable and lease of extra fibers.
- The effect of network upgrade instances on the total cost of the system is analyzed for both nC band and n(C+L) band scenarios. Reported results indicate that the n(C+L) band systems can save 30% of the total cost while using 22.2% fewer upgrades compared to the nC band scenario.

3.2 Cost Model

In order to do the techno-economic comparison between multifiber and C+L band systems, we consider the relative cost of several components while considering C band EDFA cost as a baseline, as shown in Table. 3.1. As the L-band EDFA consists of longer EDF coils [8], the cost of an L-band EDFA is assumed to be 20% higher compared to the C band EDFA. According to the specifications from Sterlite Technologies Limited [25], we have considered the '8-FC' optical cable for analyzing the cable deployment scenarios. Mainly, the availability of eight parallel fibers is considered for transmission over the considered '8-FC' optical cable. Moreover, different fiber lease costs based on the network operator's geography have also been focused on during the analysis. For a European country, fiber lease cost is considered as approximately 0.33x ($\sim$ \$1308) per fiber/km/year for five years of leasing package. Whereas the lease cost in the Indian network is considered as about 0.007x ($\sim$ \$ 29) per fiber/km/year, which is significantly less compared to European countries.

3.3 Link Upgrade Strategy

3.3.1 Scenario 1: Fiber Leasing

In this study, we have considered two scenarios. At first (scenario 1), leasing of extra fibers is considered at the specific links to upgrade the network capacity. Initially, the lightpaths are allocated until 1% blocking for single fiber C+L bands. Then, for the nC case, we start with single C band fiber links and repeat the simulation until an equal number of lightpaths matching the C+L bands is achieved. In order to achieve an equal number of lightpaths as the C+L band scenario, additional fibers are leased at specific positions in the network during nC band operations. Mainly, the route of the lightpath for each 1% blocked demand is considered during nC band upgrade operations, and additional parallel fibers are leased to the most exhausted links in the considered route. The links with the highest spectral occupancy in the considered route during the instance of network upgrade are referred to as exhausted links. This process of extra fiber leasing in the most exhausted link of the route continues until the upgraded links help to reroute the last 1% blocked connection. In the later part of this work (scenario 2), we have taken more realistic assumptions and upgraded the network by deploying new cables consisting of 8 parallel fibers.

Table 3.1: Approx. relative cost of different equipment [20], [26].

Equipment	Relative Cost
EDFA (C band)	x ($\sim$ 4000 \$)
EDFA (L band)	1.2x
DEMUX	0.04x
MUX	0.04x
EDFA module (C+L)	2.28x
8-FC Cable Purchase	0.05x / km
8-FC Cable Deployment	0.5x / km
GFF at EDFA module	0.2x
WSS (C band)	5x
WSS (L band)	6x
Transponder	36x
Average fiber lease cost	Nx
(per fiber per km per year)	(N = 0 to 0.5)

3.3.2 Scenario 2: Cable Deployment

This section presents the proposed methodology for scenario 2, which has been considered to upgrade specific links of the network as per the requirement of traffic growth. The links are upgraded by placing extra multifiber cables and their associated additional amplifiers. Mainly, the selection of the link for upgrade is determined based on the spectrum occupancy. Fig. 3.1 illustrates the flowchart of the proposed link upgrade strategy. The proposed strategy starts with the allocation of upcoming new traffic requests while doing routing, modulation, and spectrum allocation (RMSA). If the unavailability of spectrum resources leads to the blocking of certain requests, the strategy compares the state of current blocking probability (BP) with the predefined acceptable threshold (BP_{th}). If BP becomes equal to BP_{th}, the strategy stops the allocation of a new connection and monitors the state of the network. As a start, it takes the route of the last blocked demand and upgrades the most congested links one by one in the route by placing additional cables until the successful rerouting of the last blocked connection. Consequently, the allocation process of new requests is resumed after the successful rerouting of the last blocked request. The process of new connection establishment and additional cable addition continues until the network reaches its targeted capacity.

3.4 Simulation Setup

3.4.1 Scenario 1: Fiber Leasing

In this work, for techno-economic comparison between nC and C+L bands EON, the cost-per-bit metric is analyzed for the small BT-UK network and the larger Indian network. The average link length of BT-UK is 147 km, whereas for the Indian network, it is 531 km. The details of these topologies are illustrated in Appendix B. In this work, a biased traffic matrix is generated to resemble traffic flow among high-demand generating nodes in both networks. For BT-UK, we use the population and dropped wavelength data of each node to choose source-destination pairs probabilistically. For the Indian network, we use a population metric for each city [27]. We have used the 28 GBaud system with 37.5 GHz channel spacing. As the positions of GFF for ISRS compensation impact the QoT (as shown in Chapter 2), placement of GFF at every

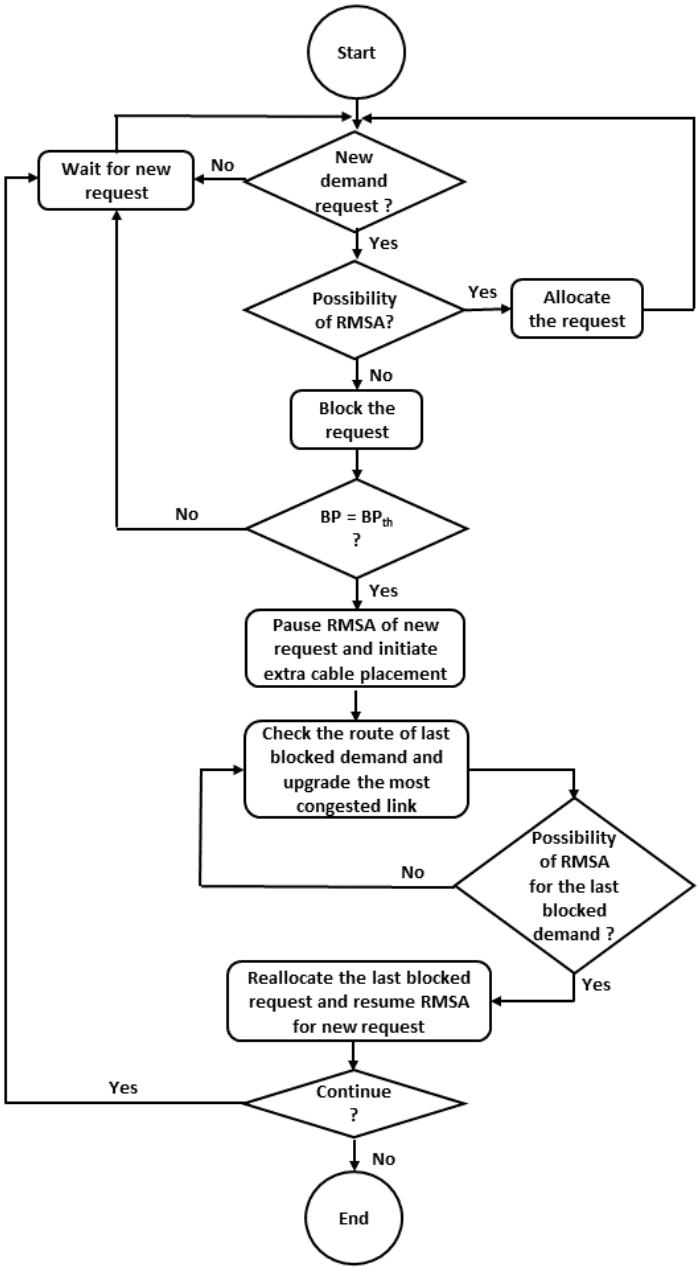

Figure 3.1: Flowchart of link upgrade strategy.

EDFA module is considered for the larger Indian network in order to provision lightpaths over longer distances. Whereas, for smaller networks like BT-UK, we have compensated the ISRS at each ROADM block using GFF.

A total of 10,000 demands, each of 100 Gpbs, are generated to fill the network spectrum. Moreover, three launch powers (-5.25 dBm, -3 dBm, and -1.5 dBm) are also considered for both of the networks. In addition, the channel bandwidth of 37.5 GHz for C+L band transmission is assumed, with a guard band of 200 GHz between C and L bands. Figures 3 and 4 present average results of 100 random traffic generations while considering three shortest paths for each lightpath; and C band is considered first for filling the spectrum in case of C+L bands.

3.4.2 Scenario 2: Cable Deployment

A custom-built, event-driven Python simulator is developed to make the techno-economic comparison. BT-UK network topology is considered for simulation with 0 dBm launch power while considering GFF at every ROADM scenario (as discussed in Chapter 2). Moreover, a 64 Gbaud system with 75 GHz of channel spacing is considered while taking three modulation formats, PM-QPSK, PM-8QAM, and PM-16QAM. On the other hand, 200 GHz guard band is considered between C and L band due to non-ideal WSS passband assumption. A biased traffic matrix is generated by following the same methodology as described in Section 3.4.1 to capture the traffic growth rate of 35% with baseline traffic of 20 Tb/s. A total of 1500 requests, each of 100 Gbps, are considered as a targeted capacity of the network during simulation, which resembles seven years of network traffic growth with a pre-determined blocking threshold (BPth) of 1%. We run the simulations for twenty seeds, and the average results are reported with less than a 5% margin of error at a 95% confidence interval.

3.5 Results and Discussion

3.5.1 Scenario 1: Fiber Leasing

This section analyzed the normalized cost-per-bit metric with the fiber lease cost for C+L band and nC scenarios. Figures 3.2 and 3.3 shows the scenario of BT-UK and Indian networks, respectively, while considering five years of leasing and three different launch powers. As the fiber leasing cost varies from country to country, we have considered different fiber leasing costs and captured their impact on the cost-per-bit. The reported result shows that the rise of leasing cost multiplicative factor (indicated by N in Table 3.1) increases the cost-per-bit value in both of the scenarios. At N = 0.0 (i.e., no fiber leasing cost), the C+L band becomes expensive compared to the nC scenario due to the requirement of costly L-band subsystems. However, as the value of N enhances, the cost of leased fiber (labeled as 'extra added fiber' in Fig. 3.2 and 3.3) dominates. The **crossover point** represented by the arrow in Fig. 3.2 and 3.3 indicates the corresponding fiber lease cost, after which the operation over C+L bands will incur lower cost-per-bit compared to the nC scenarios. The launch power of individual channels plays a crucial role in this context, and their impacts are also illustrated in Fig. 3.2 for the BT-UK network. At -5.25 dBm launch power, 1222 lightpaths, on average, are provisioned in the C+L band scenario until 1% blocking as shown in the top sub-figure of Fig. 3.2). In order to achieve the same capacity in the nC scenario, multiple fibers are leased, and the total leased fiber distance becomes 2193 km. These extra leased fibers enhance the cost-per-bit in the nC scenario and lead to a crossover at N = 0.13. Furthermore, as the launch power increases from -5.25 dBm to -3 dBm, the number of allocated lightpaths till 1% blocking in the C+L band enhances to 1247 (as shown in the middle sub-figure of Fig. 3.2) due to the enhancement of received optical signal power. The improvement of this signal power also improves the QoT in the C-band system and postpones the requirement for additional spectrum resources. As a result, the crossover point shifted toward the right from N = 0.13 to N = 0.22. Nonetheless, at the typical lease cost of fiber for the BT-UK network, as shown by the green dotted vertical line, the C+L band scenario still shows its cost-effectiveness compared to the nC scenario. If the launched power is further enhanced from -3 dBm to -1.5 dbm, the number of provisioned lightpaths till 1% blocking reduces in the C+L band to 1151 due to the enhancement of ISRS-based NLI. As a consequence, the crossover point shifted further right from N = 0.22 to N = 0.33 as indicated in the last sub-figure of Fig. 3.2.

Figure 3.3 shows the normalized cost-per-bit for the Indian network under C+L bands and nC case. Similar results like the BT-UK network are also observed here. Nevertheless, the

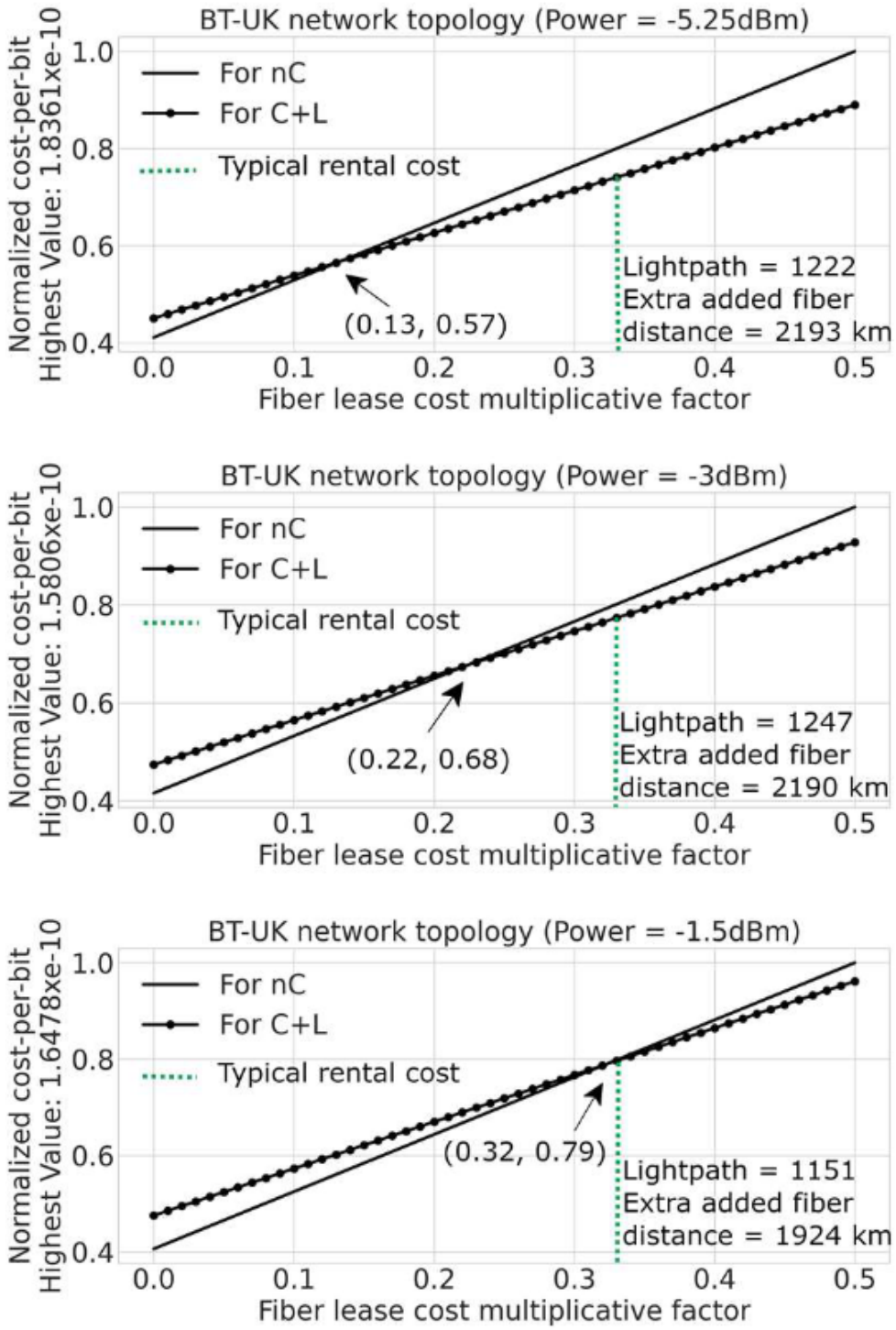

Figure 3.2: Normalized cost-per-bit for BT-UK network with five years of leasing.

presence of longer link lengths in the Indian network prepones the crossover point in the Indian network compared to the BT-UK scenario. Reported results show that a maximum number of lightpaths are provisioned in the C+L band scenario for -5.25 dBm of launch power. As the launch power of each channel increases from -5.25 dBm to -3 dBm, the number of provisioned lightpaths decreases significantly in the C+L band scenario due to the increment of NLI over longer link lengths. Consequently, the total length of required leased fibers for the nC scenario is also dropped from 9974 km to 6094, as shown by the top and middle sub-figure of Fig. 3.3. As the link lengths are much larger and the leased fiber distance is greater for the Indian network

compared to the BT-UK scenario, the nC solution becomes costlier even for lower fiber lease costs. If the launch power is further increased to -1.5 dBm, NLI becomes significant over longer links of the Indian network under the C+L band transmission. As a result, only 691 lightpaths are provisioned till 1% blocking in the Indian network under C+L band scenario as indicated in the bottom sub-figure of Fig. 3.3. Consequently, minimal fibers are leased for the nC scenario with -1.5 dBm launch power, and the gap between nC and C+L bands after crossover becomes less significant compared to other power profiles.

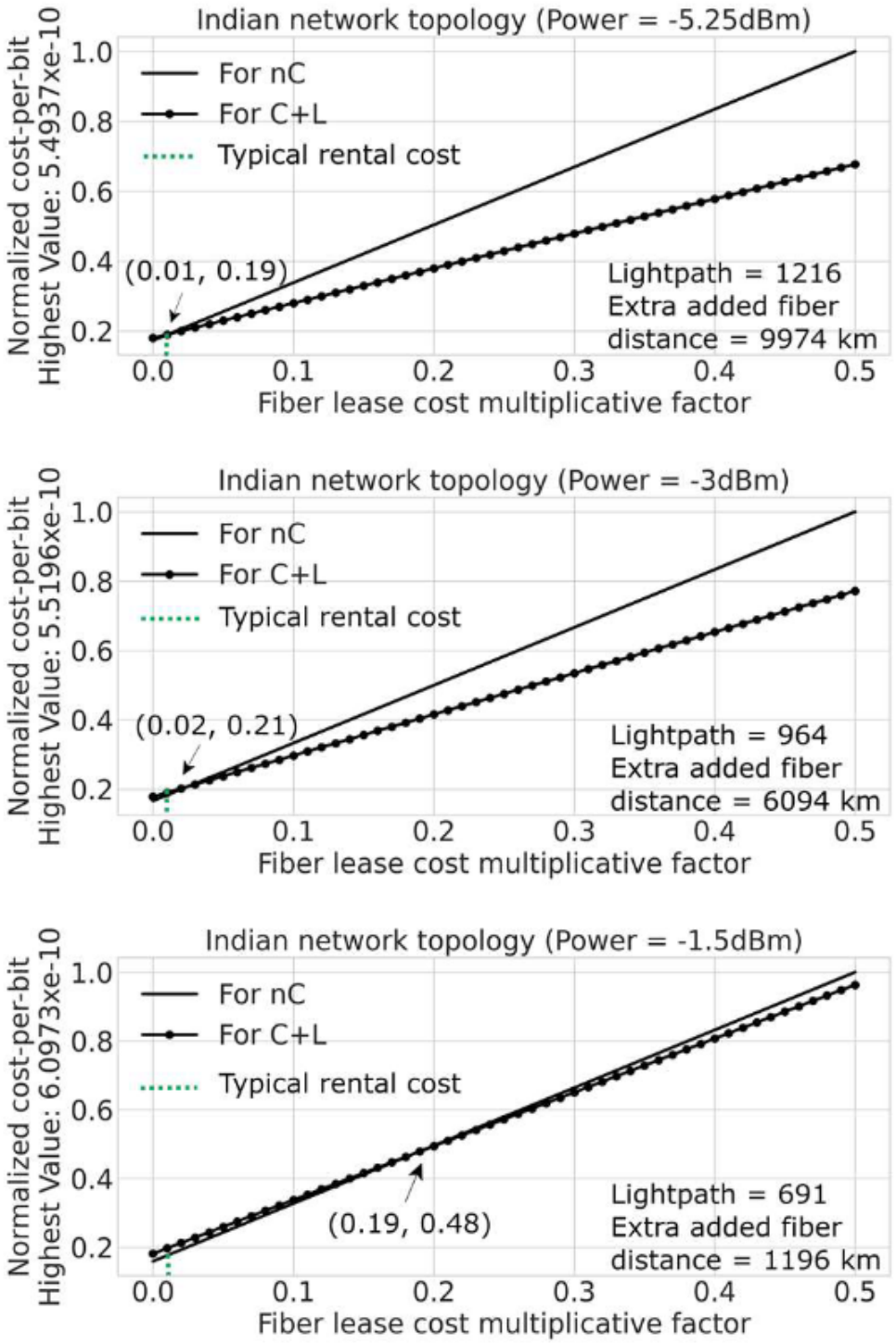

Figure 3.3: Normalized cost-per-bit for Indian network with five years of leasing.

3.5.2 Scenario 2: Cable Deployment

In order to accommodate the exponential traffic growth, multiple cables (8-FC) are deployed in specific links of the network for both C and C+L band systems using the mentioned link upgrade strategy.

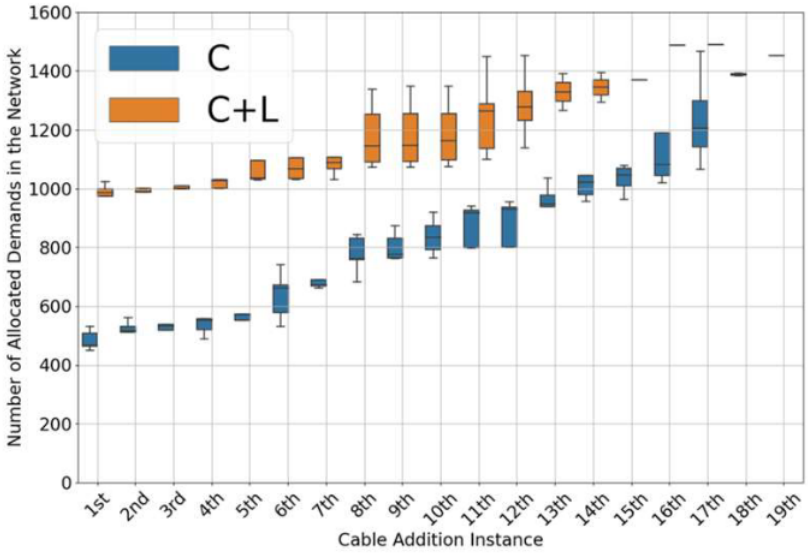

Figure 3.4: Cable addition instances with traffic loading.

The results of multiple independent simulations are captured in Fig. 3.4, where the number on the y-axis represents the number of allocated traffic demands in the network. Whereas, the number on the x-axis represents the corresponding cable addition instances in order to support the targeted traffic demand in the network. Individual box plots have been used to depict the variation of allocated demands in the network over multiple simulations under each cable addition instance. On average, for the C band system, the first cable addition occurs after the allocation of 500 100G demands in the network, as indicated by the left-most (or first) blue box in Fig. 3.4. Whereas the availability of extra resources in the C+L band system provides 50% more capacity and postpones this instance of the first upgrade till 1000 100G demands. Moreover, the presence of the small number of channels in the C band system results in the addition of more cables compared to the C+L band system in order to serve the same amount of traffic. Figs. 3.5 and 3.6 show the variation of overall cost and cost-per-bit of the network with instances of cable addition and traffic loading. As the cables are added at different instances, the slope of the total cost curve rises. Due to the costly amplifier module, although the C+L band system appears costly for low traffic, a crossover happens between C and C+L band systems when allocated demand touches 600 100G capacity as indicated in Figure 3.5.

The numerical result suggests that out of 35 links in BT-UK, 51.4% of the links are upgraded for nC system, whereas a 22.2% reduction in the number of link upgrades is achievable using the n(C+L), which leads to 30% total cost savings.

Moreover, simulation results also show that, on average, n(C+L) needs to activate 41.6% fewer additional fibers than the nC case (number of extra active fibers is 24) in order to cater for the same amount of traffic and thereby indicates the availability of a large surplus capacity of n(C+L) compared to nC.

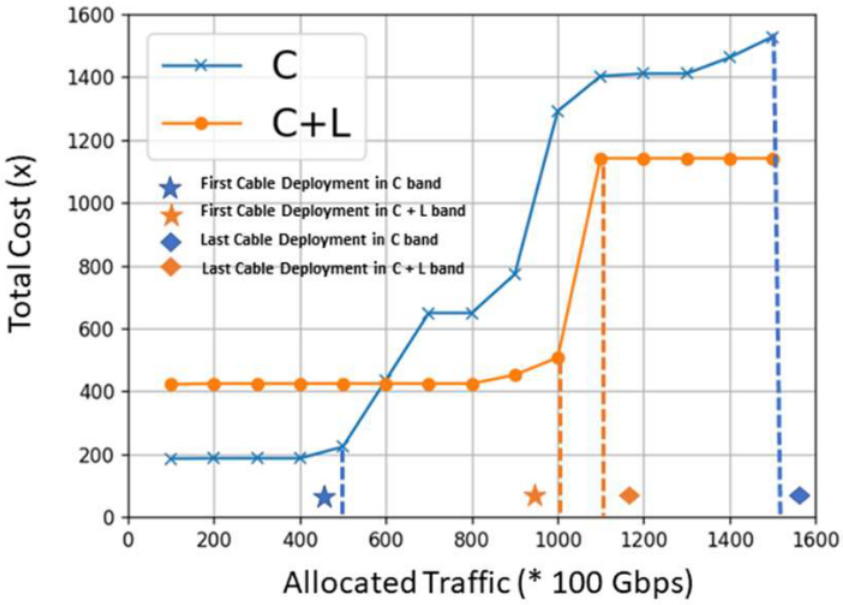

Figure 3.5: Total cost variation with traffic loading (Crossover Point: (600, 425)).

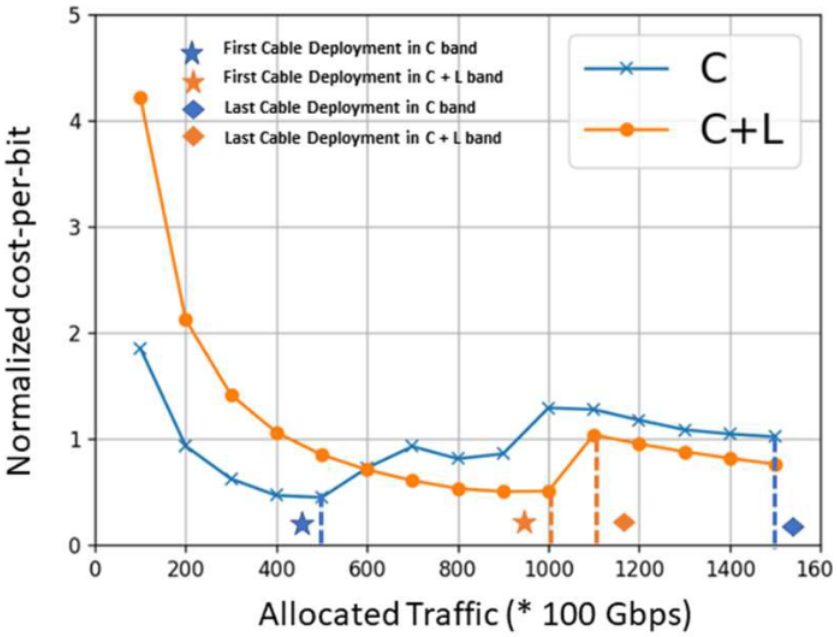

Figure 3.6: Cost-per-bit variation with traffic loading.

3.6 Conclusion

This study shows that C+L band EON is cost-effective compared to nC band EON scenarios, particularly for larger geographies (Indian network). But, for smaller geographies (BT-UK network), C+L bands are advantageous only if the fiber lease cost is high. It is also observed that the C+L band system can postpone the need for extra cable deployment compared to the C band system and thereby minimizes the cost-per-bit in the long run.

Chapter 4

An Operator's Perspective on the Designing of Cost-Effective Network Upgrade Solution

4.1 Introduction

Chapter 3 performs the techno-economic comparison between MB and multifiber technology while considering fiber leasing and cable deployment scenarios separately. Although several attempts have been made in the literature to inspect the behavior of these two technologies regarding network upgrades, there still exists some fundamental questions:

- Is it possible to lease the dark fiber or deploy the new optical cable in any link of the network?
- Is the same upgrade solution beneficial for every network operator?
- What is the cost-effective upgrade solution if the baseline system consists of multiband and multifiber-based infrastructure?

To address these questions, this chapter proposes a cost-effective network upgrade algorithm by considering CapEx for several in-line equipment and different parameters related to network infrastructure. A couple of realistic scenarios have been considered in the simulation in order to provide solutions relevant to different network operators.

In brief, the following are the main contributions of this work:

- A domain knowledge-assisted, cost-effective network upgrade algorithm is proposed to enhance the overall capacity of the network while minimizing CapEx.
- The performance of the proposed algorithm is assessed in terms of network upgrade cost, overall CapEx, and Cost-per-bit while considering EON with incremental traffic.
- Geographically diverse networks are considered in this work to highlight the effect of longer link length on the network upgrade cost.

The rest of this work is divided into the following sections. Section 4.2 summarizes the building blocks of the techno-economic comparison, where the cost model and network upgrade strategy are discussed in detail. The simulation setup, along with traffic matrix generation methodology, is presented in Section 4.3. Furthermore, the results of the techno-economic comparison are elaborated in Section 4.4. Finally, Section 4.5 concludes the work.

4.2 Building Blocks for Techno-economic Comparison

This section describes the methodology of the techno-economic comparison while describing the problem statement followed by a discussion on the cost model and proposed network upgrade algorithm.

4.2.1 Problem Statement

According to the discussion in Chapter 3, it can be realized that the capacity of the optical network needs to be upgraded while minimizing the CapEx. From operator to operator, the choice of upgrade can vary based on the availability of owned fiber, third-party dark fiber distribution, the possibility of new cable deployment in the owned or the third-party duct, and the cost of new duct deployment. In this work, we proposed a domain knowledge-assisted network upgrade algorithm, which can help the operator to choose the best way of upgrading as per their network condition.

Table 4.1: Approximate relative cost of different equipment.

Equipment	Relative Cost
EDFA (C band) [28]	x ($\sim$ \$4000) (reference cost)
EDFA (L band)	$1.2x$
DEMUX [29]	$0.04x$
MUX [29]	$0.04x$
EDFA module (C+L band)	$2.28x$
8-FC Cable Purchase	$0.05x$ / km
8-FC Cable Deployment	$0.5x$ / km
Optical Fiber Leasing Cost [30]	$0.33x$ /fiber/km/year
Duct Rental Cost	$0.0875x$ /km/year
New Duct Deployment Cost with New Fiber Roll-out (Rural area) [5]	$6.58x$ /km
New Duct Deployment Cost with New Fiber Roll-out (Metropolitan area) [5]	$131.65x$ /km

4.2.2 Cost Model

Table 4.1 captures the relative cost of different inline equipment's, where the cost of C band EDFA is taken as the baseline or reference cost. The cost of L band equipment is considered 20% higher compared to the C band (since the L band EDFA needs longer EDF coils than C band EDFA [8]). Sterlite's 8-FC cable is considered for the cable deployment, which has eight parallel fibers and is the least granular feasible cable currently available.

4.2.3 Proposed Algorithm of Network Upgrade

Conventional approaches for network upgrades assume that the leasing of dark fibers or new cable deployment can be possible in all the links of the considered topology. However, the network upgrade methodology can vary from operator to operator based on various factors,

such as the distribution of dark fibers, duct space availability, and the cost of cable deployment. This specialized information about the network is generally known as Domain knowledge, and network operators can leverage the benefits of this existing information during their network upgrade. This section describes the proposed algorithm, which considers all of these areas of domain knowledge of the network and returns the most cost-effective solution for network upgrade.

Table 4.2 and 4.3 lists the notations for the different parameters, decision variables, and functions which are used in the proposed algorithm. Algorithm 2 starts by taking multiple inputs such as network topology, traffic matrix, channel launch power, OSNR threshold, and tolerable blocking probability, along with a couple of domain knowledge parameters. The cost of network upgrades varies as per its associated methodology. For example, an operator can choose to light up its own pre-existing dark fibers (if any) during a network upgrade, whereas another operator can choose to deploy a new cable in its own duct if the duct spaces are available. Similarly, if an operator does not have its own duct at any particular location, it can choose to deploy new cables in another existing operator's (third-party) duct. On the other hand, operators can also choose to lease fibers from a third party or can deploy their new duct. Therefore, it can be easily understood that all the possible cases need different costs of the upgrade (as listed in Table 4.1). On the other hand, as the characteristics of different links in the network varies based on several factors such as it's geographical location, traffic generation probability, availability of third party dark fibers, etc., it is also important to check the possibility of all these options in different links of the network. All of this information is taken as input in Algorithm 2.

Initially, for each demand request, the possibility of traffic grooming is checked in order to effectively use the remaining capacity of the existing lightpaths (lines 1 - 9) [16]. At first, the traffic grooming function (TG) takes every incoming demand request (t) and tries to place them in the network using the spare capacity of the existing lightpaths. If the spare capacity of any existing lightpath L_{TG} matches the requirement of request t, traffic grooming is initiated by allocating the demand request t using L_{TG}. If traffic grooming is not possible, the possibility of routing and spectrum allocation over a new lightpath is checked using the function CRSA (line 11). This function takes the details of the network topology and demand request as input and returns the availability of continuous and contiguous spectrum slots (ACCSS) in the feasible route. The CRSA function explores the k-shortest path routing policy for individual traffic requests and checks the ACCSS in the allowable routes.

If there exists continuous and contiguous spectrum slots in any of the k route, the GAF function takes the information of spectrum occupancy for that k route as input and results the list of all available frequencies. Consequently, the SAP function takes all of these available frequencies as input and returns the preferable frequency among them for provisioning new lightpaths in the network (lines 12 - 14) according to the allowable spectrum allocation policy. Hence, the OSNR of the lightpath is calculated at the preferable frequency while considering the assumptions of the physical layer model (as discussed in Chapter 2) (line 15). If the OSNR of the lightpath appears greater than the predefined threshold, the corresponding highest-order modulation format is chosen, and the spectrum is allocated for this lightpath (lines 16 - 19). Generally, if any lightpath does not find a continuous and contiguous spectrum in its route, it's considered as a blocked connection. When the network touches its predefined tolerable blocking probability, network upgrade methodology is initiated (lines 23 - 24) while pausing the next demand allocation. The route of the last blocked connection is analyzed, and the most congested link is chosen first for upgrade (lines 25 - 26). The possibility of link upgrade is analyzed using the function CPL and all the domain knowledge (line 27). Furthermore, all the possibilities are compared, and the cost-effective solution is calculated (lines 28 - 29). After upgrading the selected link in the last blocked route cost-effectively, the RBC function tries to

Table 4.2: List of notations for different given parameters, decision variables, sets, and functions used in the algorithm.

Notation	Description
	Given Parameters:
$G(V, E)$	Network topology; V = set of nodes, E = set of links.
T	Traffic matrix.
P_{Ch}	Launch power of each channel.
O_{Th}^{m}	OSNR threshold for all allowable modulation formats.
QoT^{Cal}	Quality of transmission calculator.
BP^{Th}	Blocking probability threshold.
C^{LODF}	Cost for lighting-up owned dark fiber.
C^{CDOD}	Cost for cable deployment in owned duct.
C^{CDTD}	Cost for cable deployment in third-party duct.
C^{LDF}	Cost for leasing dark fibers from third-party.
C^{DD}	Cost for duct deployment.
P_{e}^{LODF}	Possibility of LODF in link $e \in E$.
P_{e}^{CDOD}	Possibility of CDOD in link $e \in E$.
P_{e}^{CDTD}	Possibility of CDTD in link $e \in E$.
P_{e}^{LDF}	Possibility of LDF in link $e \in E$.
P_{e}^{DD}	Possibility of DD in link $e \in E$.
	Decision Variables:
T_A	Traffic admissibility $\in \mathbb{W}$.
BP	Blocking Probability.
$CapEx$	Capital Expenditure.
${P_{TG}}^{t}$	Possibility of traffic grooming for demand request $t \in$ {True, False}.
L_{TG}	Location of traffic grooming.
R_t	Route for the t^{th} demand request.
$ACCSS$	Availability of continuous and contiguous spectrum slots $\in$ {True, False}.
$F_{Available}$	Available set of frequencies.
f	Selected frequency.
$OSNR_f$	OSNR at selected frequency f.
M_{OSNR_f}	Modulation format according to OSNR at frequency f
AS	Available solutions.
CS	Cost-effective solution.
SU	Successful Upgrade $\in$ {True, False}.

reallocate the blocked connection by rerouting over the upgraded new link. If the last blocked connection can be provisioned into the network using the upgraded link, the network upgrade methodology is paused, and resource allocation for the next requests is initiated. However, if the last link upgrade is not sufficient to reallocate the blocked demand, the variable SU is set as False, and the upgrade methodology continues over the other links in the blocked route (lines

Table 4.3: List of notations for different sets and functions used in the algorithm.

Notation	Description
	Sets:
S_O	Spectrum occupancy.
L_{All}	Set of all ongoing lightpaths.
	Functions:
TG	Traffic grooming.
CRSA	Check route and spectrum availability.
GAF	Get available frequencies.
SAP	Spectrum allocation policy.
SLDSO	Sort the link in descending order of spectrum occupancy.
CPL	Check the possibility of link upgrade.
COMPARE	Compare the available solutions.
LUC	Link Upgrade cost.
RBC	Reroute the blocked connection.

30 - 34). After upgrading selected links as per the domain knowledge, the algorithm returns the most cost-effective solution of network upgrade with its associated CapEx.

In Algorithm 2, the time complexity to find the possibility of traffic grooming for each incoming request t ∈ T in every existing lightpath $LP \in L_{All}$ using lines 1 to 9 is $O(|T| \times |L_{All}|)$. In line 11, the Dijkstra's algorithm is used with time complexity of $O(|T| \times (|V| + |E| \log |V|))$ to find the shortest path routing for each lightpath. In addition, availability of spectrum is also checked using CRSA function with time complexity of $O(|T| \times |S| \times |E|)$, where S represents the set of frequencies in each link. In lines 12-19, spectrum and modulation allocation is done for each request with time complexity of $O(|T| \times |S| \times |M|)$, where M denotes the set of modulation formats. Consequently, during the network upgrade stage, SLDSO function is executed first with time complexity of $O(|E| \times \log |E|)$. In lines 26-34, the cost effective link upgrade strategy is calculated with time complexity of $O(|E|)$. Therefore, the overall time complexity of Algorithm 2 can be written as $O(|T||L_{All}| + |T|(|V| + |E| \log |V|) + |T||S||E| + |T||S||M| + |E| \log |E| + |E|)$.

4.3 Simulation Methodology

This section describes the simulation setup in order to provide detailed information about various considered parameters, such as channel launch power, attenuation coefficient, channel spacing, etc. In addition, biased traffic matrix generation procedure, domain knowledge and all the related assumptions are also discussed later on.

4.3.1 Simulation Setup

To make the techno-economic comparison, an event-driven, custom-built Python simulator is developed. In addition, Intel(R) Xeon(R) CPU E5-2670 v2 @ 2.50 GHz and Intel(R) Xeon(R) Gold 5220 CPU @ 2.20 GHz with 264 cores and 96 GB of memory is used to generate all of the reported results. Simulations are considered first on smaller geography, such as the BT-UK network (22 nodes, 35 links, average link length of 147 km). Later on, the scenario of the longer network (Pan-Europe network) is also considered in this study and elaborately discussed

Algorithm 2 Domain Knowledge Assisted Network Upgrade for MB-EON

Input: $G(V, E)$, T, P^{Ch}, O^{m}_{Th}, QoT^{Cal}, BP^{Th}, C^{LODF}, C^{CDOD}, C^{CDTD}, C^{LDF}, C^{DD}, P_e^{LODF}, P_e^{CDOD}, P_e^{CDTD}, P_e^{LDF}, P_e^{DD};
Output: T_A, BP, S_O, CS, $CapEx$;
***Initialisation*:** $T_A = 0$, $BP = 0$, $S_O = \{\emptyset\}$, $L_{All} = \{\emptyset\}$, ${P_{TG}}^t$ = False;

```
for each demand request t in T sequentially do
  for each lightpath LP in L_All do
    L_TG ← TG(t, LP);
    Update P_TG^t;
  end for
  if (P_TG^t == True) then
    Allocate demand request t using L_TG;
    T_A = T_A + 1;
    Update S_O, L_All;
  else
    R_t, ACCSS ← CRSA(G(V, E), t);
    if (ACCSS == True) then
      F_Available ← GAF(ACCSS, S_O, R_t);
      f ← SAP(F_Available);
      OSNR_f ← QoT^Cal(t, R_t, P^Ch, f ∈ F_Available, S_O);
      if (OSNR_f ≥ min(O^m_Th)) then
        Select M_OSNR_f, Occupy f;
        T_A = T_A + 1;
        Update S_O, L_All;
      end if
    else
      Update BP;
      if (BP ≥ BP^Th) then
        Pause CRSA for next demand request;
        L = SLDSO(R_t, S_O);
        for each link l in L do
            AS = CPL(l, P_e^LODF, P_e^CDOD, P_e^CDTD, P_e^LDF, P_e^DD);
            CS = COMPARE (AS);
            CapEx = LUC(CS, C^LODF, C^CDOD, C^CDTD, C^LDF, C^DD);
            SU = RBC (CS)
            if (SU == True) then
              Skip other links in L;
            else
              Continue;
        Resume CRSA for next demand request;
      else
        Start the allocation of next demand request;
      end if
    end if
  end if
end for
```

in Section 4.4. The details of these topologies are illustrated in Appendix B. Furthermore, Table 4.4 captures the allowable modulation formats that are taken into account for modeling the 64

Gbaud system with 75 GHz of channel spacing. A total optical bandwidth of 10 THz is taken for transmission over C+L band in each fiber, while considering guard band of 200 GHz at the junction of C and L band due to non-ideal WSS passband assumption [20]. Consequently, the number of channels in every link is considered as 59 and 135 for C and C+L band systems, respectively. Furthermore, the presence of ITU-T G.652.D fibers is assumed in each link of the network along with the other system parameters as listed in Table 4.5. Mainly, the last-fit spectrum allocation policy is considered here where the spectrum allocation is started from the highest frequency (C-band wavelength.) Moreover, k-shortest path (k=3) routing is considered for every traffic demand. The blocking probability threshold is considered as 1%. The average results are presented with less than a 5% margin of error at a 95% confidence interval after performing the simulations over 20 random seeds.

Table 4.4: Allowable modulation formats and corresponding OSNR threshold [31], [32].

Modulation	Data Rate (Gbps)	OSNR Threshold (dB)
PM-QPSK	200	16
PM-8QAM	300	21
PM-16QAM	400	24

Table 4.5: System parameters [13].

Parameters	Symbol	Values
P_{ch}	Channel launch power [dBm]	0
B_{CH}	Channel spacing [GHz]	75
α	Attenuation coefficient [dB/km]	0.2
D	Dispersion [ps/nm/km]	17
S	Dispersion slope [ps/nm^2/km]	0.067
γ	NL coefficient [1/W/km]	1.2
C_r	Raman gain slope [1/W/km/THz]	0.028

4.3.2 Traffic Matrix

We have considered baseline traffic of 20 Tb/s along with the 35% annual growth rate. Since static traffic builds up in core networks, a total of 1500 static demand requests, each of 100 Gbps, are taken into account for the simulation, which emulates network traffic growth over the seven-year time frame. Therefore, when a total of 1500 requests (with an individual data rate of 100G) exist in the network, the total capacity of the network becomes 1500 * 100 G = 150 Tbps. As described in [20], a biased traffic matrix is generated by probabilistically choosing the source-destination pairs using the dropped wavelength data of individual nodes. The data of dropped wavelength for each node is listed in Appendix B. This methodology helps to resemble the high traffic flow between special nodes in different geographic locations of the BT-UK network. The current analysis solely takes into account requests with data rates of 100 Gbps, however using traffic grooming demands with variable data rates can also be allocated into the network.

4.3.3 Assumptions

We assume that no leasing cost is required if the operator has their own dark fibers, whereas the cost of other inline equipment, such as EDFAs are only necessary to decide the cost of the upgrade. The usable bandwidth of additional fibers is assumed based on whether the C or C+L band network has been considered from the beginning. For example, if additional fibers are placed in the C+L band-based link, it's assumed that the extra fiber will also operate in the C+L band.

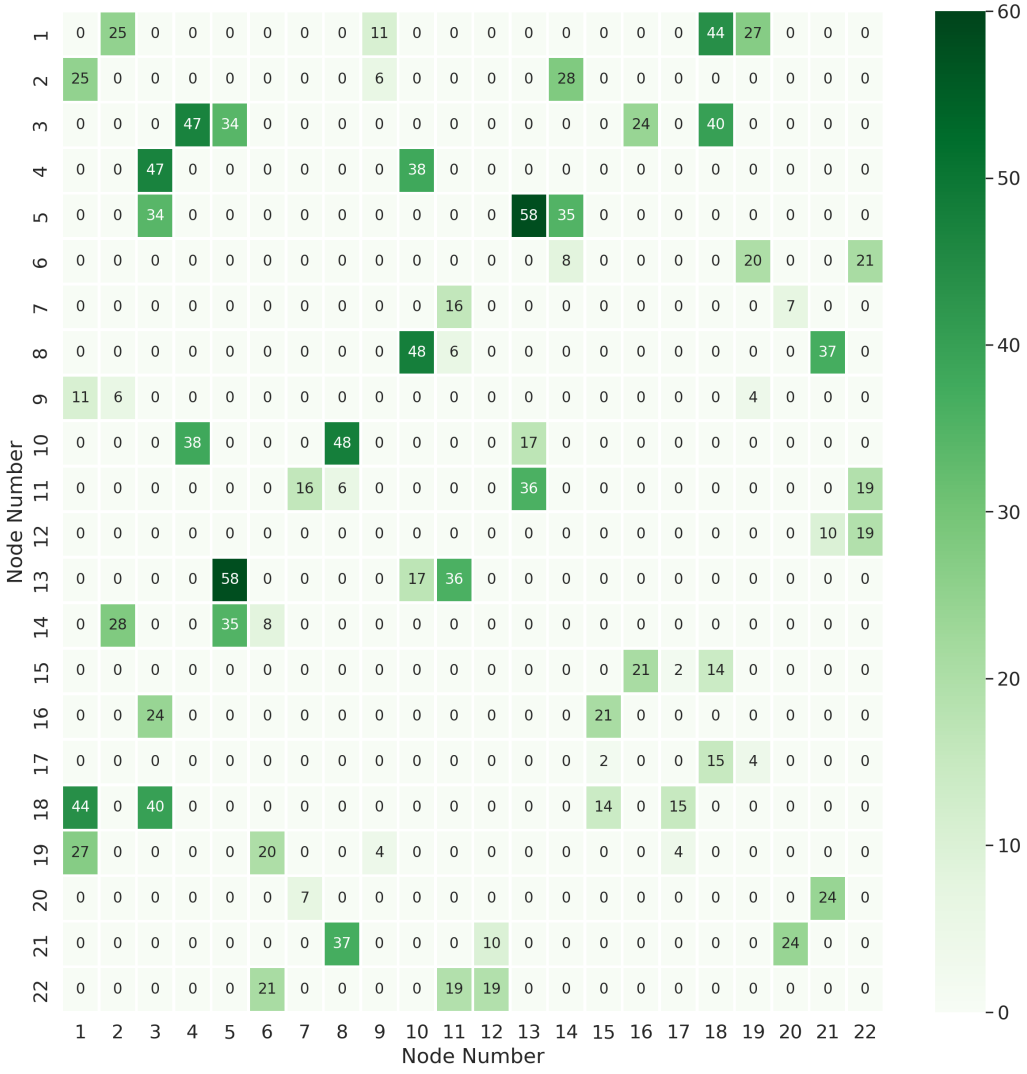

Figure 4.1: Shortest path heat map.

4.3.4 Domain Knowledge

For the current study, we have not considered cable deployment in third party ducts for the BT-UK network. Since the availability of operator-owned dark fibers can vary from operator

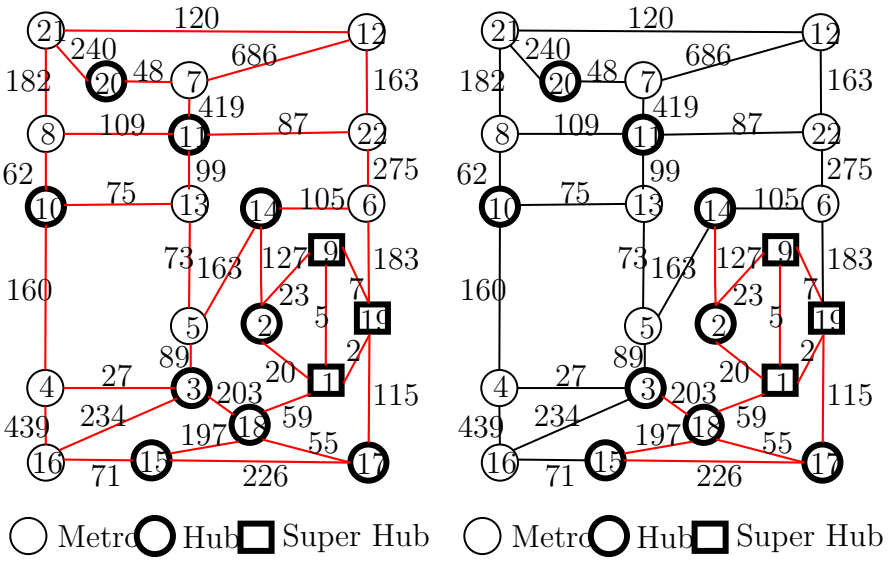

(a) Case 1: D_{All}.

(b) Case 2: D_{SN}.

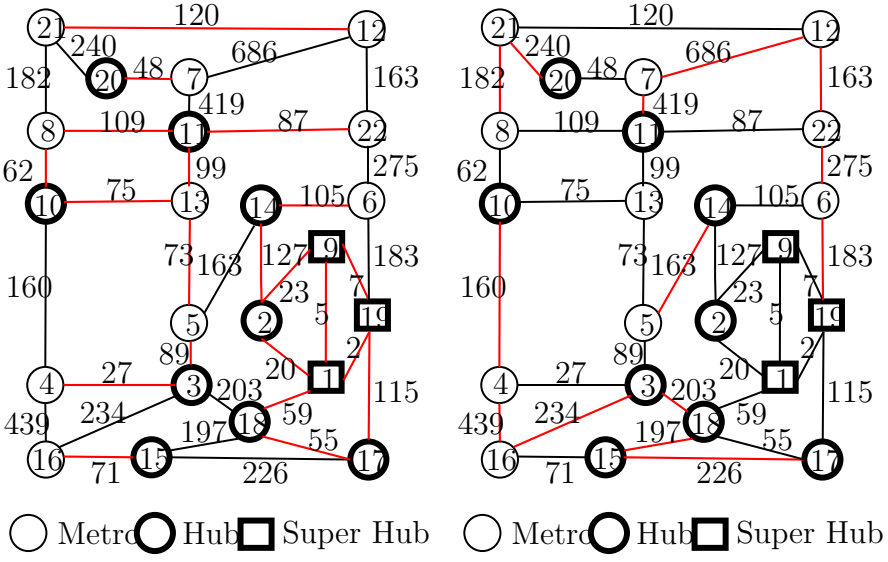

(c) Case 3: D_{SL}.

(d) Case 4: D_{LL}.

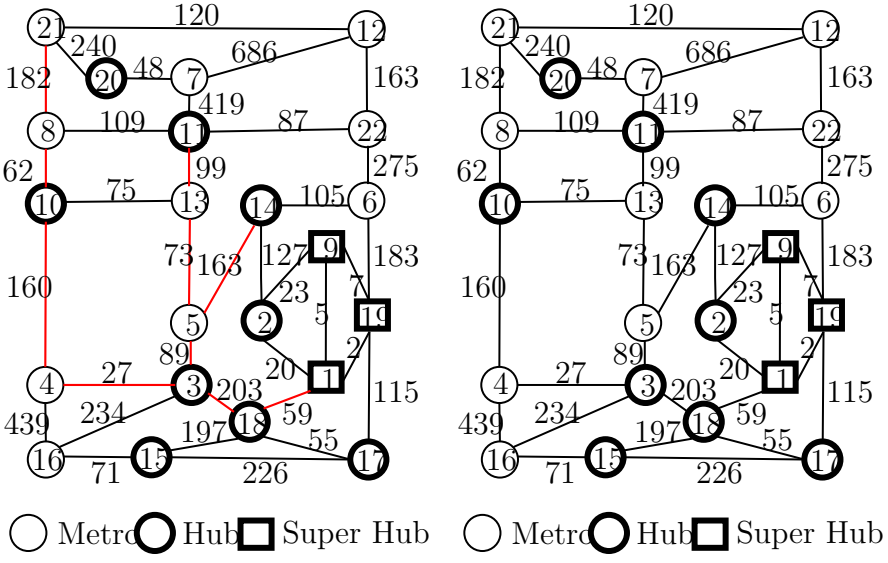

(e) Case 5: D_{SPL}.

(f) Case 6: D_{NL}.

Figure 4.2: Availability of operator's owned dark fiber (red links: dark fibers are available; black links: dark fibers are absent).

to operator based on their deployment strategy, various distributions of operator's owned dark fibers are considered in the simulation as listed below:

1. **Case 1 (D_{All}):** Operator's owned dark fibers are available in all the links.
2. **Case 2 (D_{SN}):** Operator's owned dark fibers are available only between the special nodes (SN) of the network. For the BT-UK network, the 'Hubs' and 'Super Hub' labeled nodes (as shown in the Appendix B) are considered as the special nodes.
3. **Case 3 (D_{SL}):** Operator's owned dark fibers are available at shortest links (SL). For the BT-UK network, the links with distance less than 147 km (the average link length) are considered as shorter links.
4. **Case 4 (D_{LL}):** Operator's owned dark fibers are available at the larger links (LL). For the BT-UK network, the links with distance greater than 147 km (the average link length) are considered as larger links.
5. **Case 5 (D_{SPL}):** In every topology, a total of $\binom{n}{2}$ unique demand requests can be generated among n number of nodes of the topology. Dijkstra's shortest path algorithm can be used to determine the shortest route between the source and destination node of each of these individual requests. If the probability of occurrence for each demand request is equal, the likelihood of link congestion can be determined by the majority voting rule. This rule indicates that if the route of most of the requests passes over a link, the chances of blocking/congestion will be more in that link compared to other parts of the topology. Therefore, it is crucial for the operators to place extra resources into these specific links for achieving high network throughput. For case 5, it is considered that operator's owned dark fibers are available in all of these links where the shortest path of most of the unique requests is likely to overlap. Figure 4.1 captures the shortest path heat map for the BT-UK network while taking $\binom{n}{2}$ unique requests, where n = 35. The individual boxes represent the links between two nodes which are indicated on the two axes. The denoted number in the box indicates how many unique requests are expected to route through that particular link. The midpoint of the right side vertical bar (i.e., 30) of Figure 4.1 is considered as the threshold to choose the maximum overlapped links.
6. **Case 6 (D_{NL}):** Operator's owned dark fibers are not available in any of the links.

Overall, Figure 4.2 summarizes the distribution of dark fibers in the BT-UK network for all the above-mentioned cases. The red links in the figure indicate the availability of the operator's owned dark fibers. In contrast, the dark link represents the deficiency of dark fibers at different locations in the network.

4.4 Results and Discussions of Techno-economic Comparison

This section evaluates the performance of the proposed algorithm in terms of the cost of the upgrade, total CapEx, and normalized cost-per-bit. The metric cost of the upgrade is defined as the amount of additional investment which is required in order to place additional spectrum resources at certain links of the networks for achieving the targeted network capacity. Total CapEx is calculated by adding the cost of the upgrade with the baseline infrastructure cost. Normalized cost-per-bit is measured by dividing the total CapEx of the network by the achievable overall network capacity.

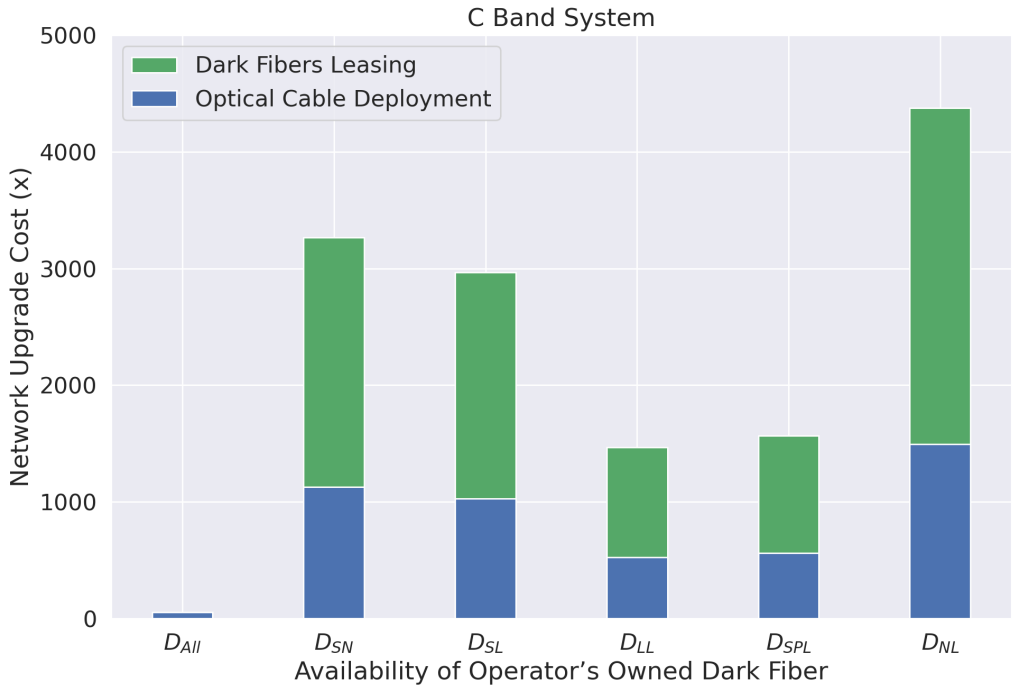

(a)

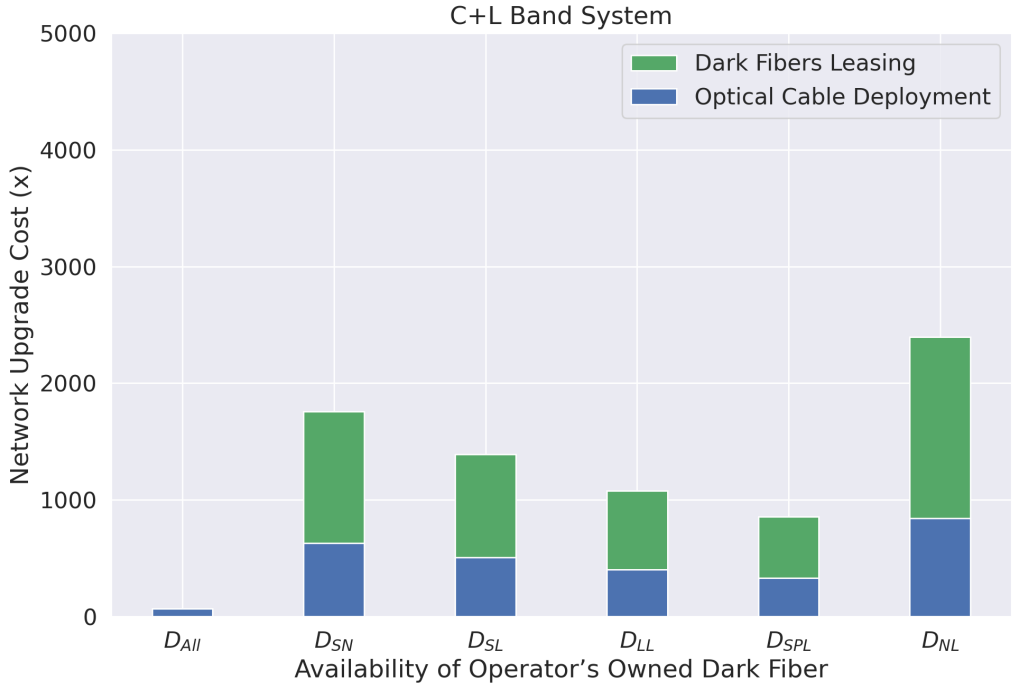

(b)

Figure 4.3: Cost of network upgrade: (a) C band system, (b) C+L band system.

4.4.1 Cost of Upgrade Analysis

Figure 4.3 compares the cost of network upgrade for different cases as indicated in Section 4.3.4. In Figure 4.3(a), the cost of network upgrade is plotted while considering the underlying system as C band. On the other hand, the C+L band system is considered in Figure 4.3(b). For case 1 (D_{All}), additional EDFAs are only considered to upgrade the network as all the links consist

of the operator's owned dark fiber. Therefore, it provides the minimum cost of the upgrade for both the C and C+L band systems.

Algorithm 2 selects third party fiber leasing and optical cable deployment in the owned duct as the choice of two minimum upgrades in those links where the operators do not have their pre-existing dark fibers. For other cases (except case 1), the cost of network upgrade using third party dark fiber leasing appears large compared to optical cable deployment in the operator's own duct while considering 5 years of leasing contract. As the number of channels in the C+L band system is approximately twice compared to that of the C band-only system, the requirement of the network upgrade for achieving a targeted capacity becomes smaller for the C+L band. As a result, the cost of network upgrade becomes smaller in the C+L band system compared to the C band system for each of the cases. As case 6 (D_{NL}) considers the absence of the operator's owned dark fibers in all the links, the cost of network upgrade becomes maximum compared to the rest of the cases for both the C and C+L band systems.

4.4.2 Total CapEx Analysis

The variation of the overall CapEx with the instances of traffic loading for different cases is captured in Figures 4.4, 4.5, 4.6, 4.7, 4.8 and 4.9. For case 1, as there is the availability of the operator's owned dark fibers in all the links, the minute increment is observed in total CapEx with the increment of traffic load. Moreover, as the cost of the C+L band EDFA module is 2.28 times higher compared to C band EDFA, the overall CapEx remains higher for the C+L band system compared to the C band scenario. However, for other cases (except case 1), instances of extra resource addition (cable deployment/fiber leasing) change the slope of the curves. For example, Figure 4.5(a) indicates that first fiber leasing occurs when the network touches a total capacity of 60 Tbps while allocating 600 requests, each of 100 Gbps, in the network for the C band system. On the contrary, the C+L band system indicates a 66.67% gain in-terms of traffic admissibility while postponing the need for additional resources until 1000 requests each of 100 Gbps exist in the network. Moreover, a crossover happens when 600 requests each of 100 Gpbs are provisioned in the network, after which the C band-based system becomes costly compared to the C+L band system. As the network is loaded with more traffic, certain links of the C+L band system are also upgraded using the leasing of dark fibers. However, to achieve the targeted capacity of 150 Tbps, the multifiber C+L band system provides a gain of 35.2% in CapEx savings compared to the C band system. The remaining cases of total CapEx analysis (as highlighted in Figures 4.5, 4.6, 4.7, 4.8 and 4.9) have also shown a similar nature of crossover for fiber leasing and cable deployment scenarios. If we consider the worst-case scenario (case 6) as shown in Figure 4.9(a) and 4.9(b), the multifiber C+L band system provides CapEx savings of 36.9% compared to the multifiber C band system when the network touches 1500 100G capacity.

4.4.3 Cost-per-bit Analysis

The effect of traffic increment on the normalized cost-per-bit of the network is shown in Figures 4.10, 4.11, 4.12, 4.13, 4.14 and 4.15 while considering different strategies of network upgrade. All the cost-per-bit data are mainly normalized by a common integer $(10^{11})/x$, where x is the cost of C-band EDFA (as discussed in Table 4.1). Ideally, if there is no network upgrade, the cost-per-bit reduces along with the traffic increment. Additionally, if the network is upgraded by the operator's own dark fibers, the cost-per-bit decreases almost exponentially, as shown in Figures 4.10(a) and 4.10(b).

However, if the network is upgraded by third party fiber leasing or cable deployment in its own duct, the slope of the cost-per-bit curve changes. Generally, single fiber C+L band solution

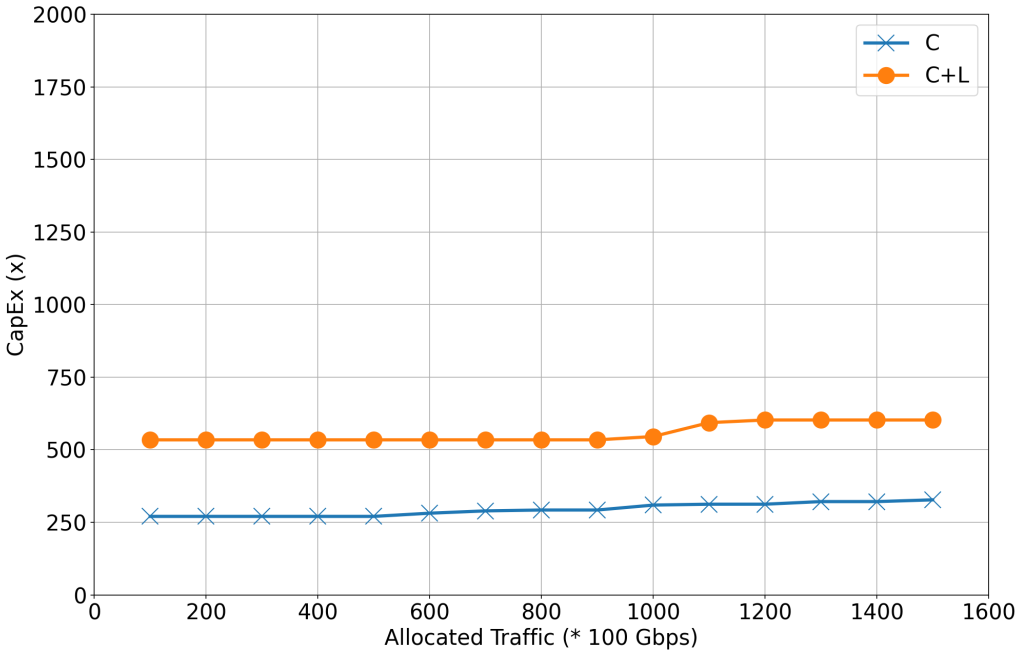

(a)

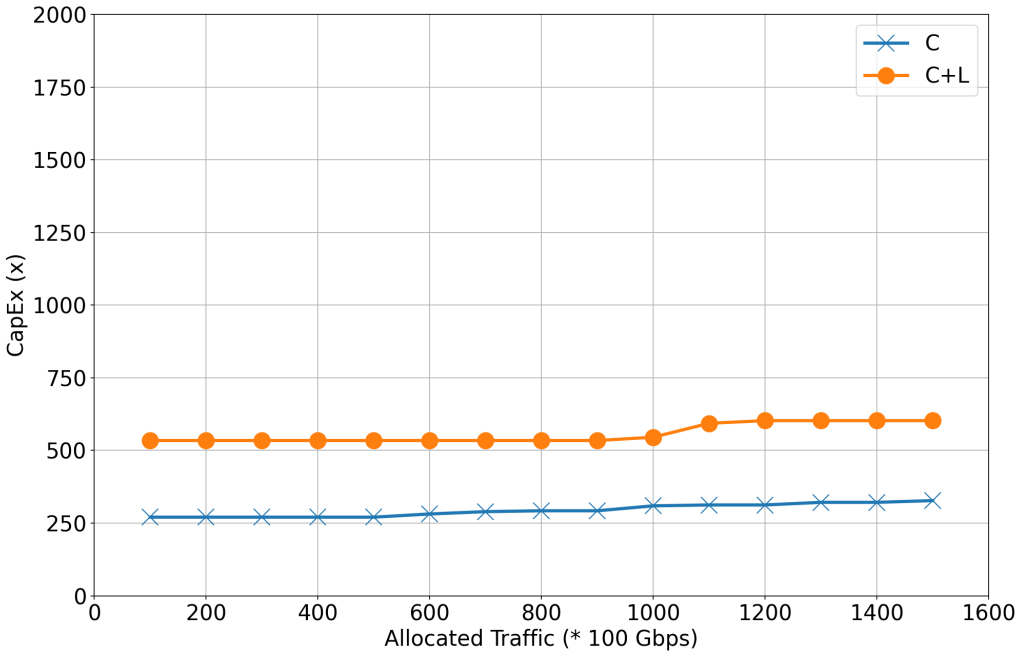

(b)

Figure 4.4: Total CapEx analysis: (a) case 1 with dark fiber leasing, (b) case 1 with optical cable deployment.

achieves larger cost-per-bit at small traffic instances due to the presence of the costly EDFA module. Nevertheless, when the cost of network upgrades becomes dominant along with the traffic load increment, the cross-over occurs between two cost-per-bit curves, as shown in Figures

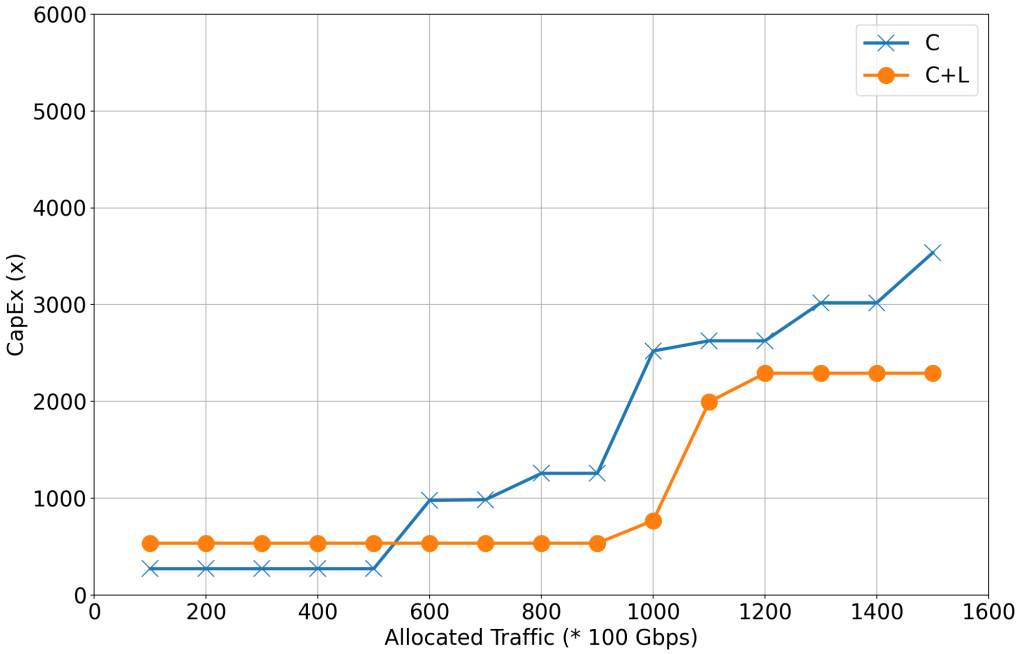

(a)

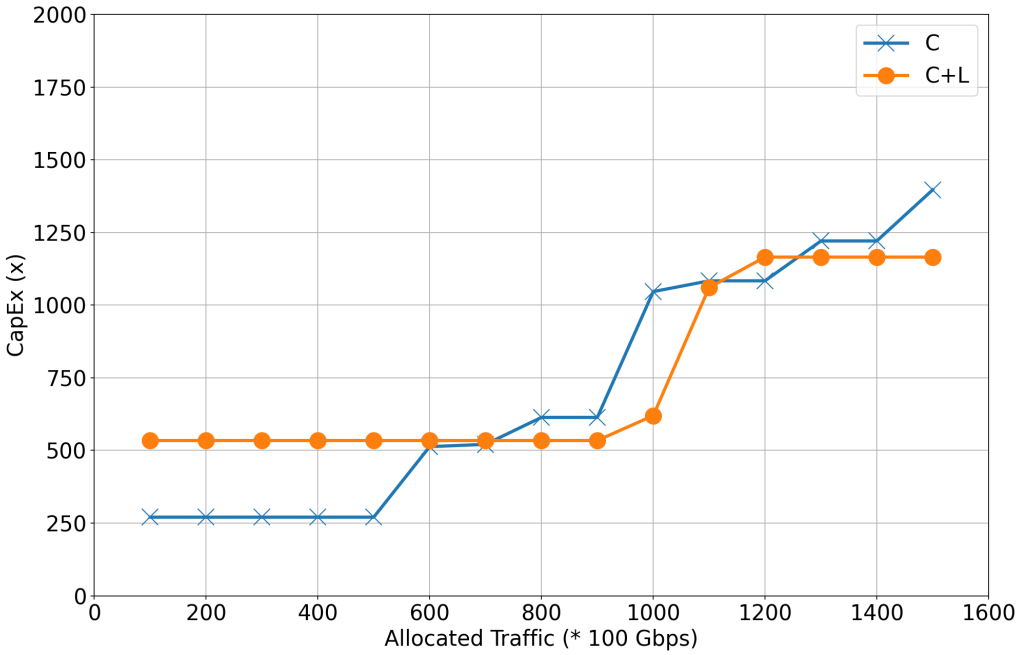

(b)

Figure 4.5: Total CapEx analysis: (a) case 2 with dark fiber leasing, (b) case 2 with optical cable deployment.

4.11, 4.12, 4.13, 4.14 and 4.15. Therefore, the operation over the C+L band becomes cheaper in terms of cost-per-bit and indicates the best return on investment in the long term. The simulated result shows a maximum gain of 40.5% (case 3) can be achievable in terms of cost-per-

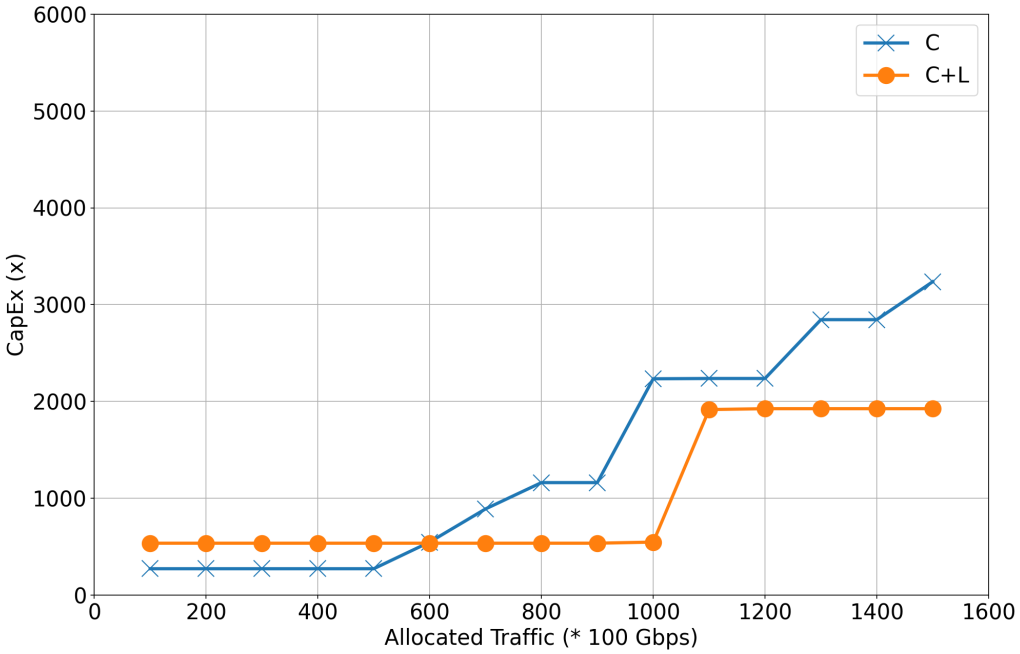

(a)

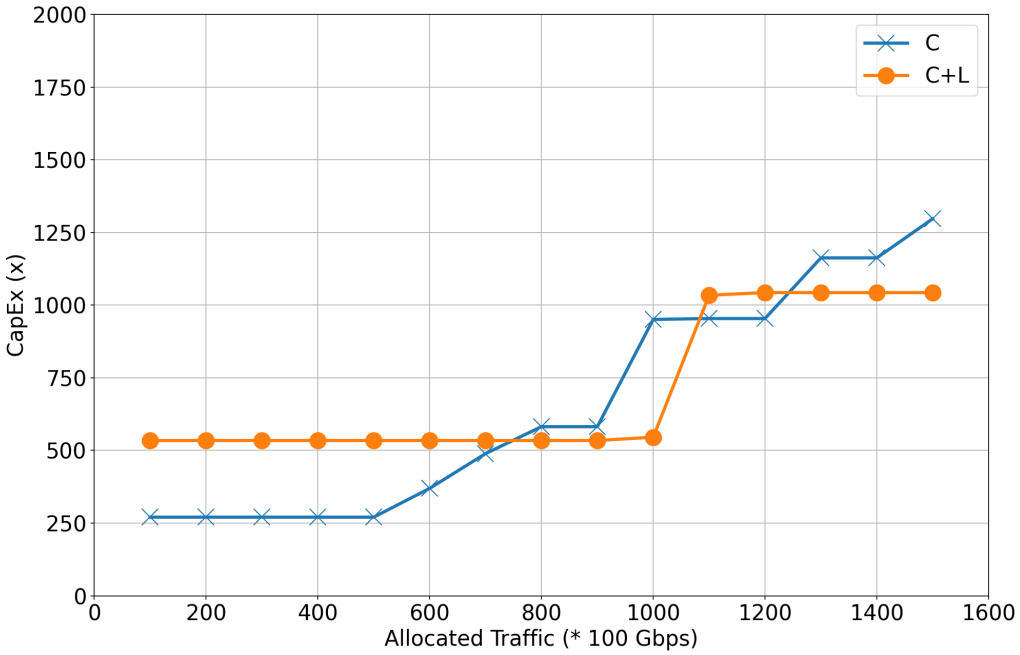

(b)

Figure 4.6: Total CapEx analysis: (a) case 3 with dark fiber leasing, (b) case 3 with optical cable deployment.

bit reduction using the C+L band, whereas, in the worst-case scenario (case 6), the multifiber C+L band solution can reduce the cost-per-bit of the network at least by 21.9% compared to the multifiber C band solution. Ideally, the instances of extra cable deployment/fiber leasing

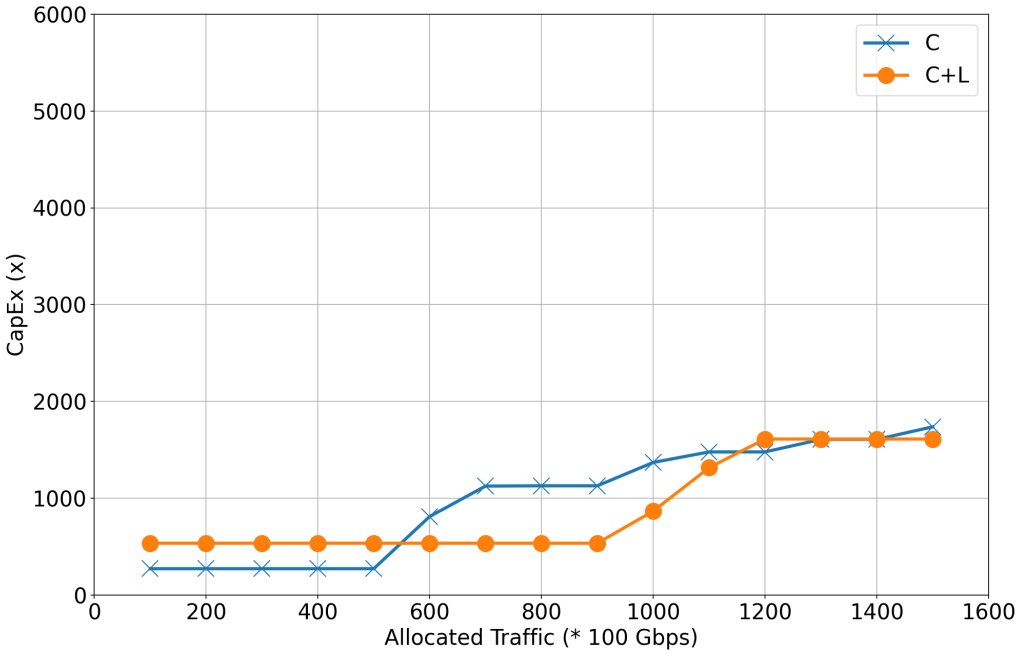

(a)

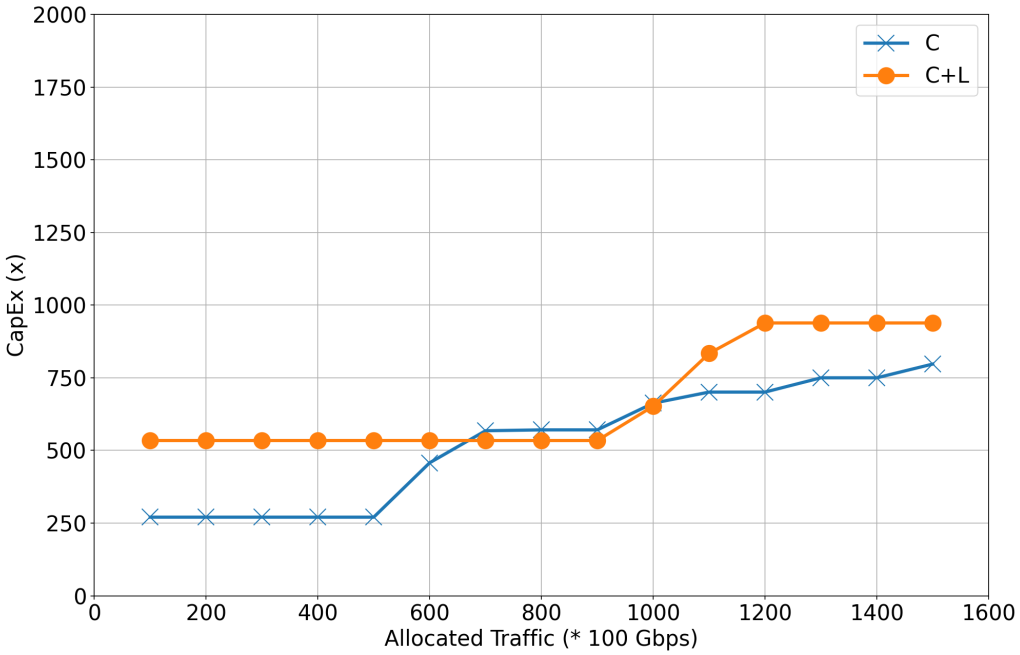

(b)

Figure 4.7: Total CapEx analysis: (a) case 4 with dark fiber leasing, (b) case 4 with optical cable deployment.

occur more in the C band compared to the C+L band due to the lack of spectrum resources. As a result, in the long run, the C+L band provides minimum network upgrade cost compared to the C band scenario. However, the distribution operator's own dark fiber can improve the

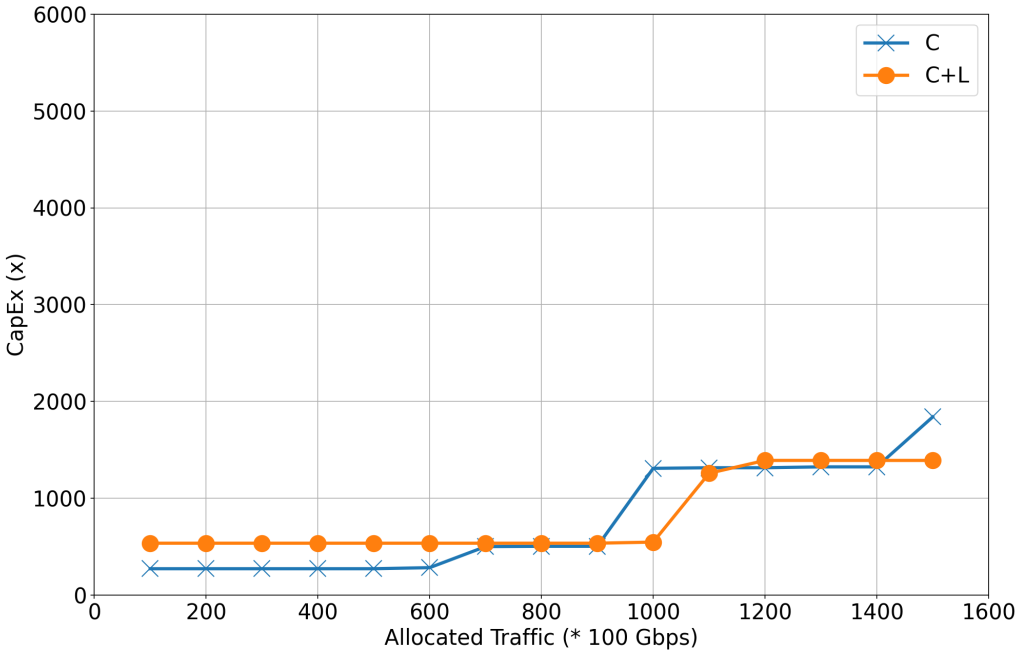

(a)

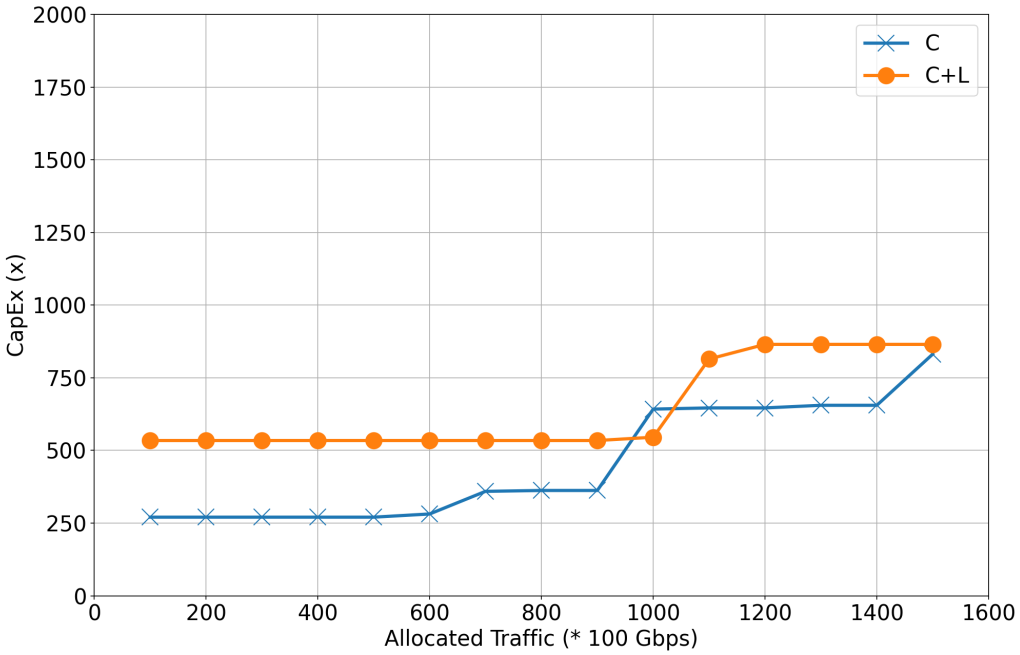

(b)

Figure 4.8: Total CapEx analysis: (a) case 5 with dark fiber leasing, (b) case 5 with optical cable deployment.

performance of the C band system and minimizes the upgrade cost difference between C and C+L band. Figure 4.14(b) depicts such kind of scenarios where the availability of the dark fibers on overlapped shortest-path-based routes (case 5) decreases the cost of upgrades in the

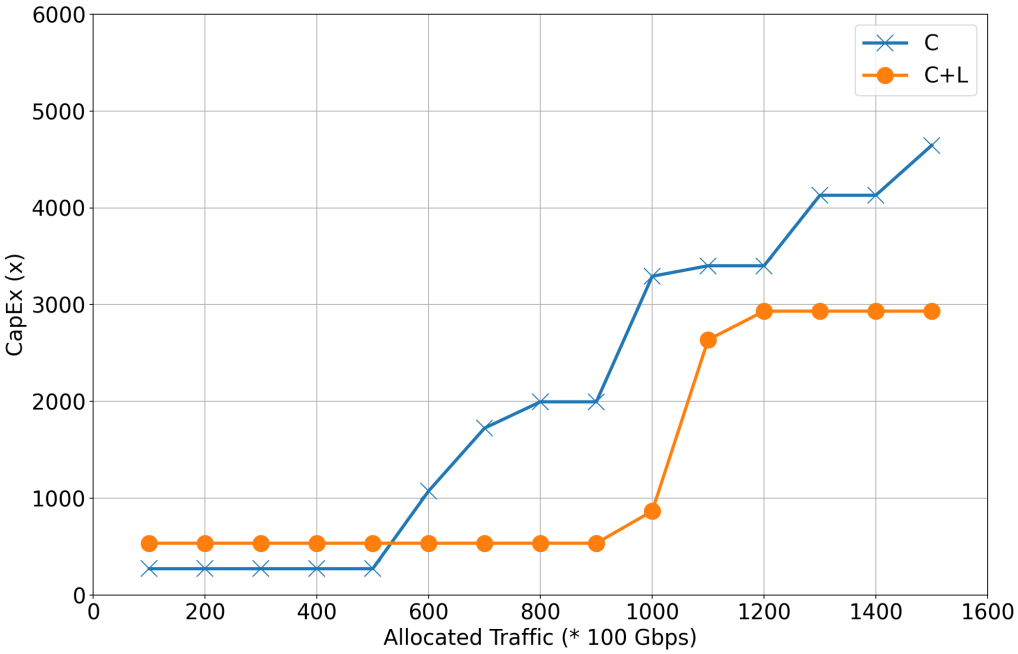

(a)

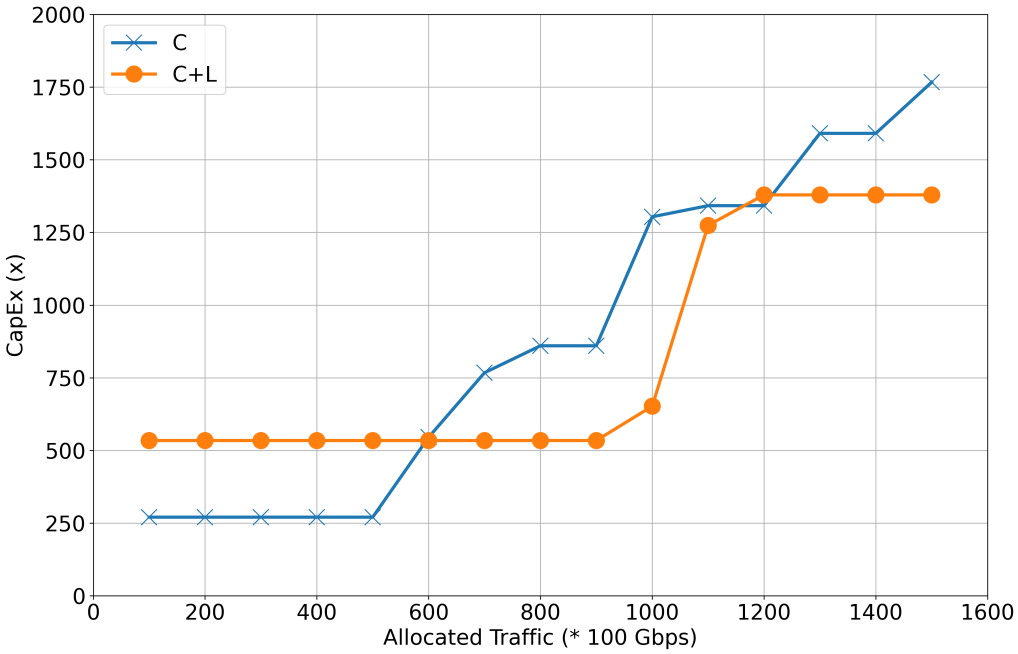

(b)

Figure 4.9: Total CapEx analysis: (a) case 6 with dark fiber leasing, (b) case 6 with optical cable deployment.

C band. As a result, the multifiber C band system achieves similar to multifiber C+L bands for these special cases.

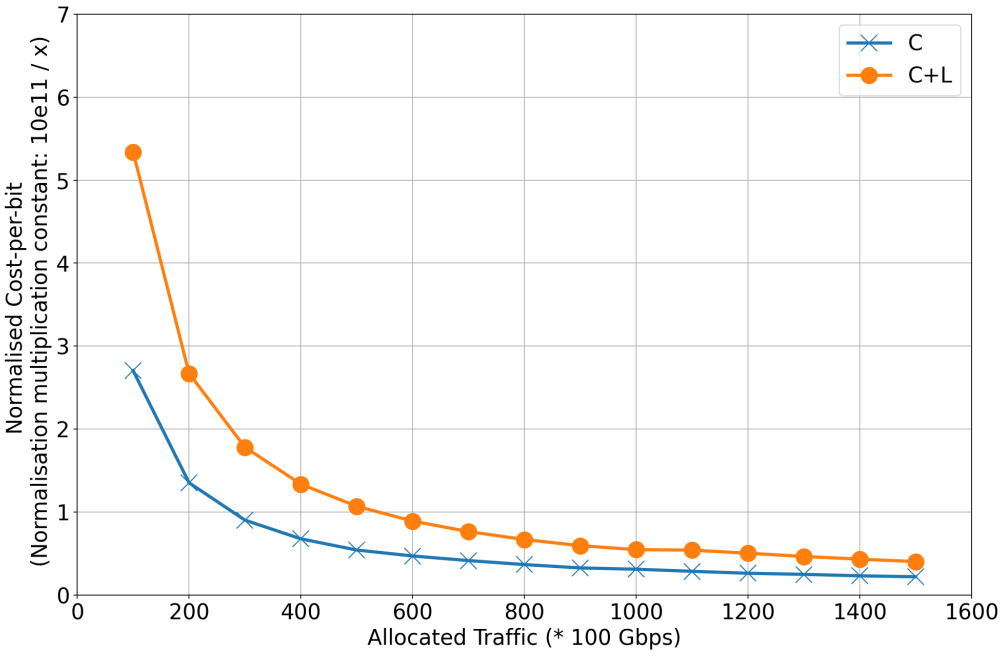

(a)

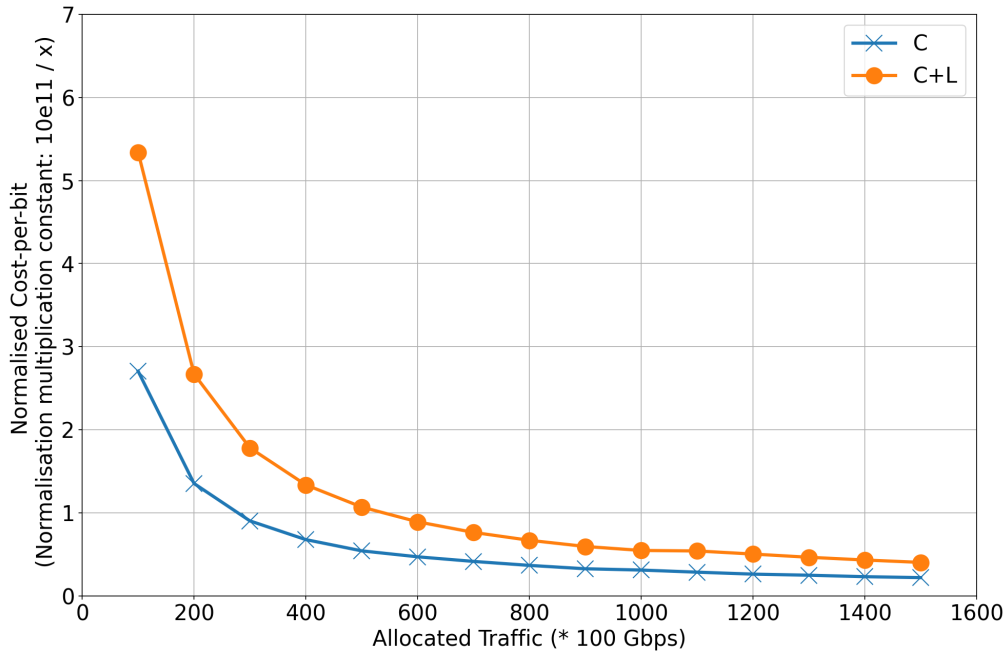

(b)

Figure 4.10: Cost-per-bit Analysis: (a) case 1 with dark fiber leasing, (b) case 1 with optical cable deployment.

4.4.4 Effect of Link Length and Channel Launch Power

So far, we have considered a smaller network (BT-UK, average link length = 147 km) in our analysis. However, it will be interesting to study the longer networks as well since the link

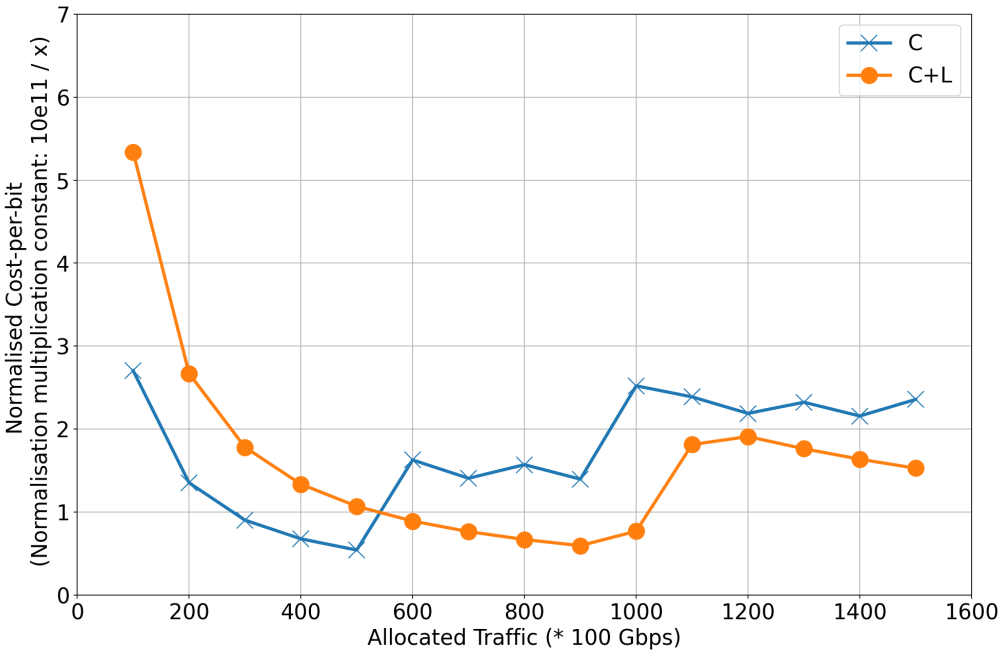

(a)

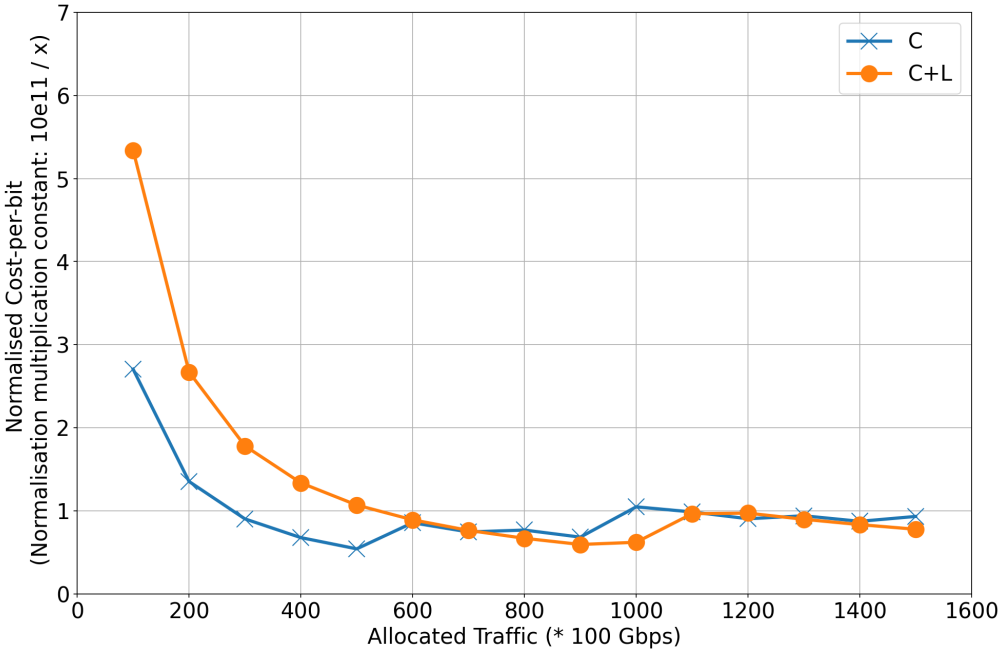

(b)

Figure 4.11: Cost-per-bit Analysis: (a) case 2 with dark fiber leasing, (b) case 2 with optical cable deployment.

length of the network plays an important role in the overall achievable capacity of the network. We have taken Pan Europe networks [average link length = 486 km][13] in this context and described the performance of our proposed algorithm on it. All of the physical layer parameters

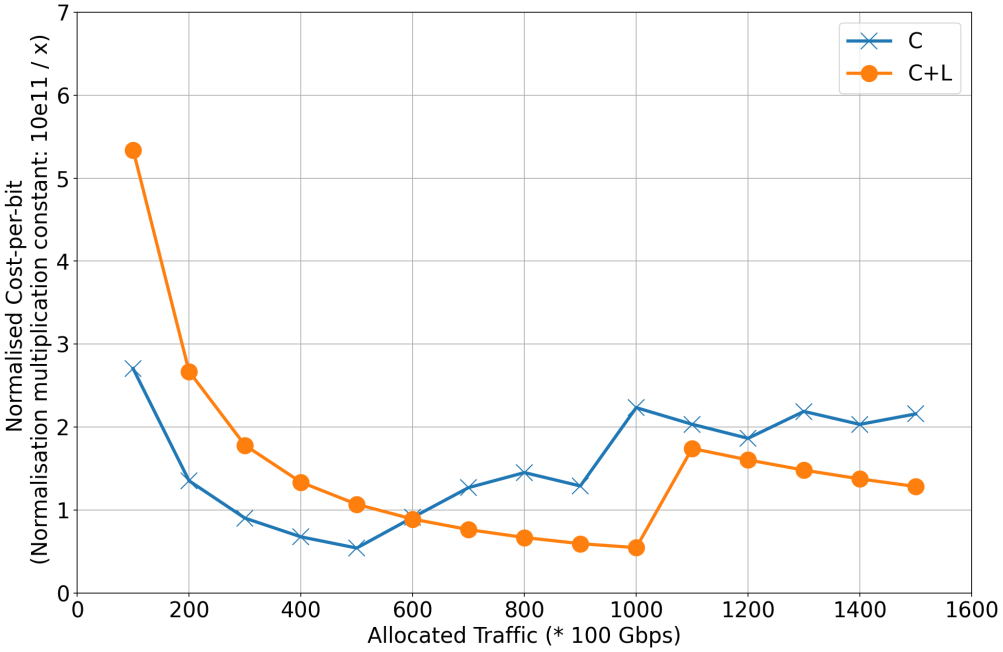

(a)

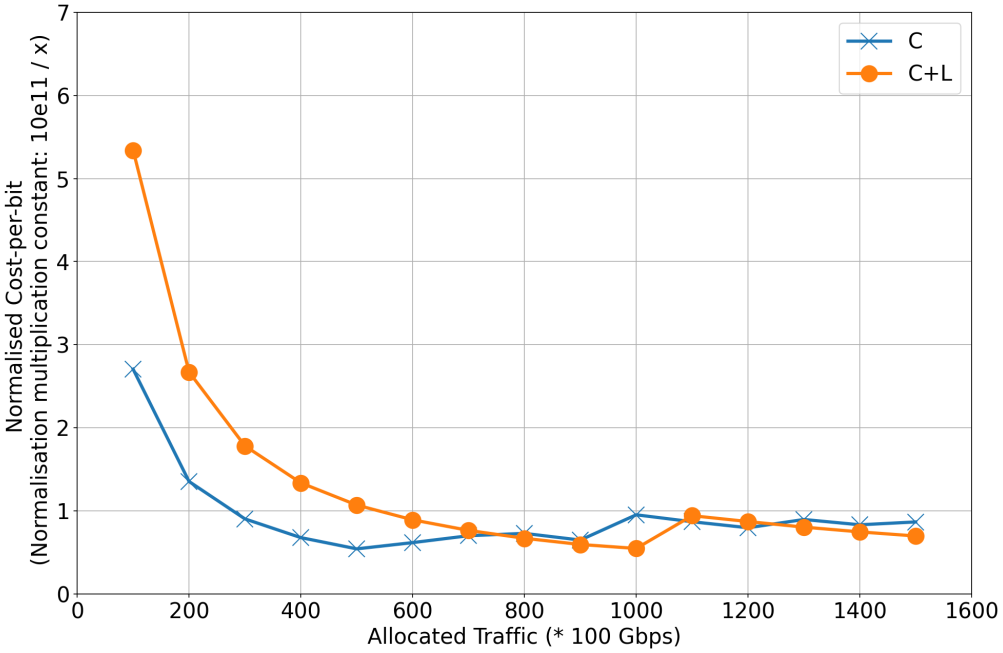

(b)

Figure 4.12: Cost-per-bit Analysis: (a) case 3 with dark fiber leasing, (b) case 3 with optical cable deployment.

are considered the same as discussed in Chapter 3. As the placement of GFF at ROADMs can significantly affect the QoT of lightpaths in longer geography [20], GFFs are placed after every span to mitigate the effect of ISRS in Pan-Europe network. The same cost model (as discussed

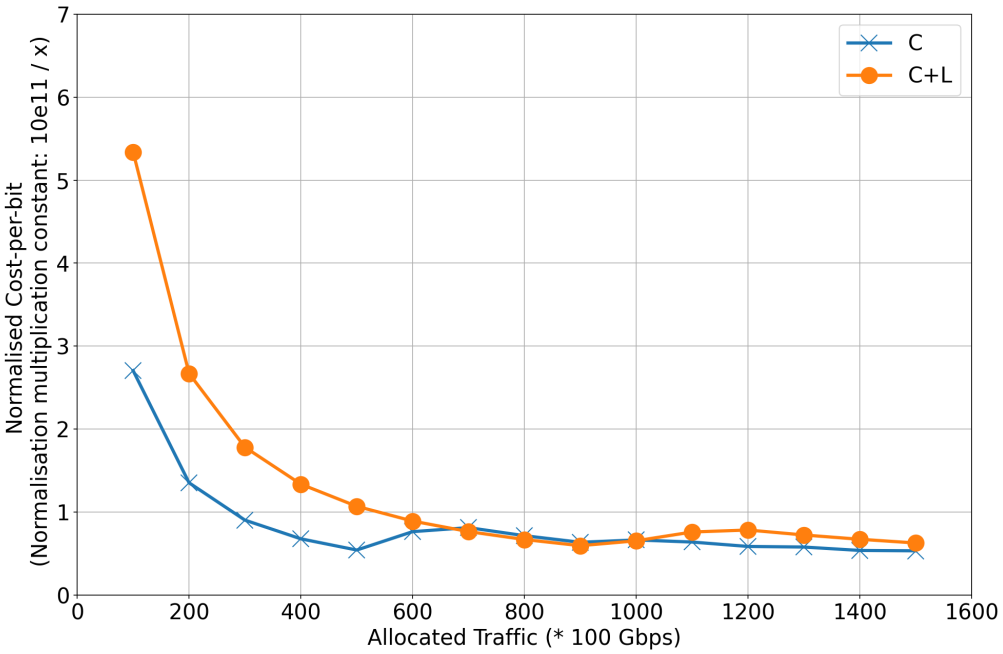

(a)

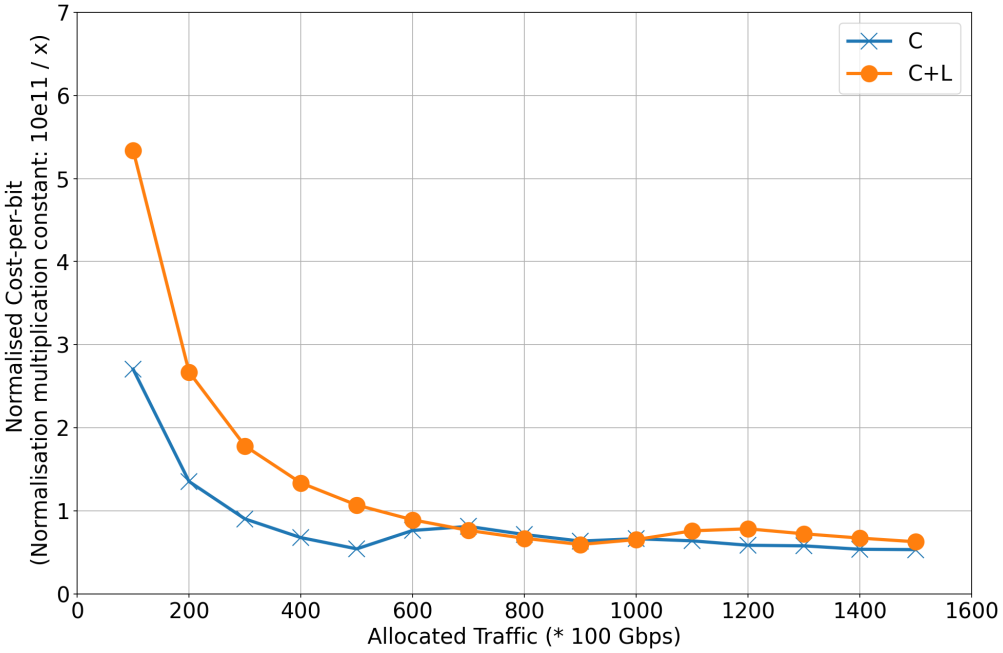

(b)

Figure 4.13: Cost-per-bit Analysis: (a) case 4 with dark fiber leasing, (b) case 4 with optical cable deployment.

in Section 4.2.2) is considered here to determine the network upgrade cost. Traffic matrix for Pan-Europe network is generated using the gravity model [33]. The worst-case scenario (case 6: D_{NL}) is considered here for further analysis, where it is assumed that the operator's owned dark

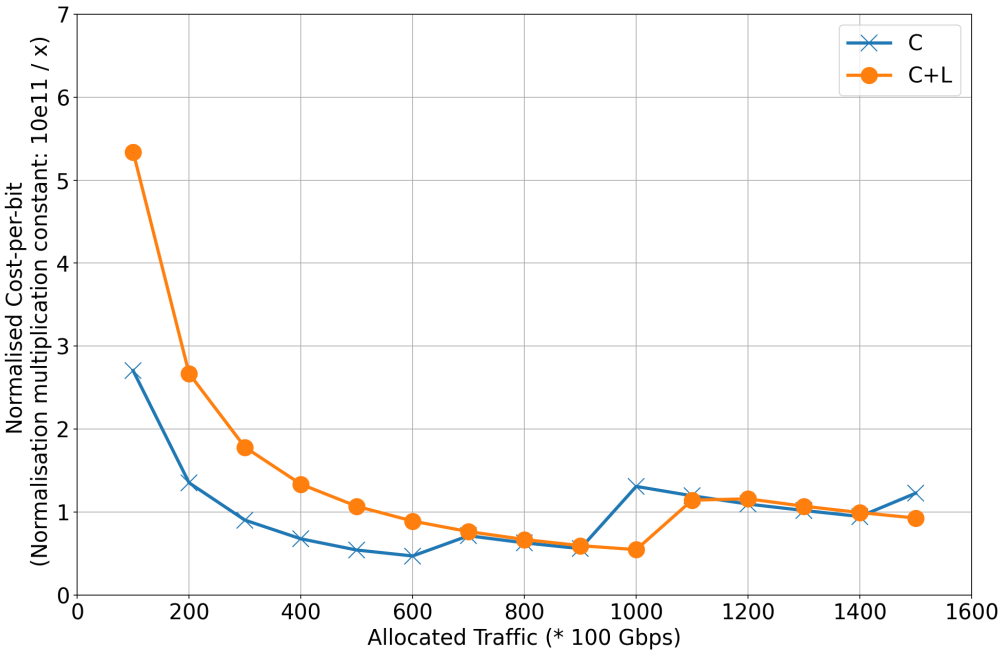

(a)

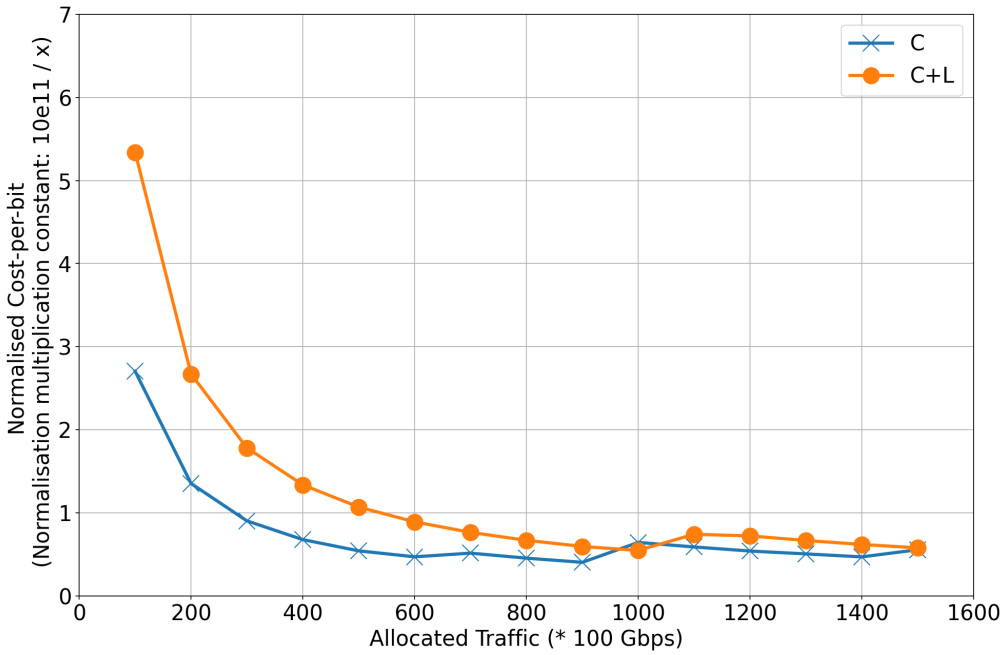

(b)

Figure 4.14: Cost-per-bit Analysis: (a) case 5 with dark fiber leasing, (b) case 5 with optical cable deployment.

fibers are not available in any of links of the Pan Europe network. As the advantage of cable deployment over fiber leasing on CapEx savings is already shown for the smaller network, only cable deployment cases are considered here for further analysis. Table 4.6 shows the variation

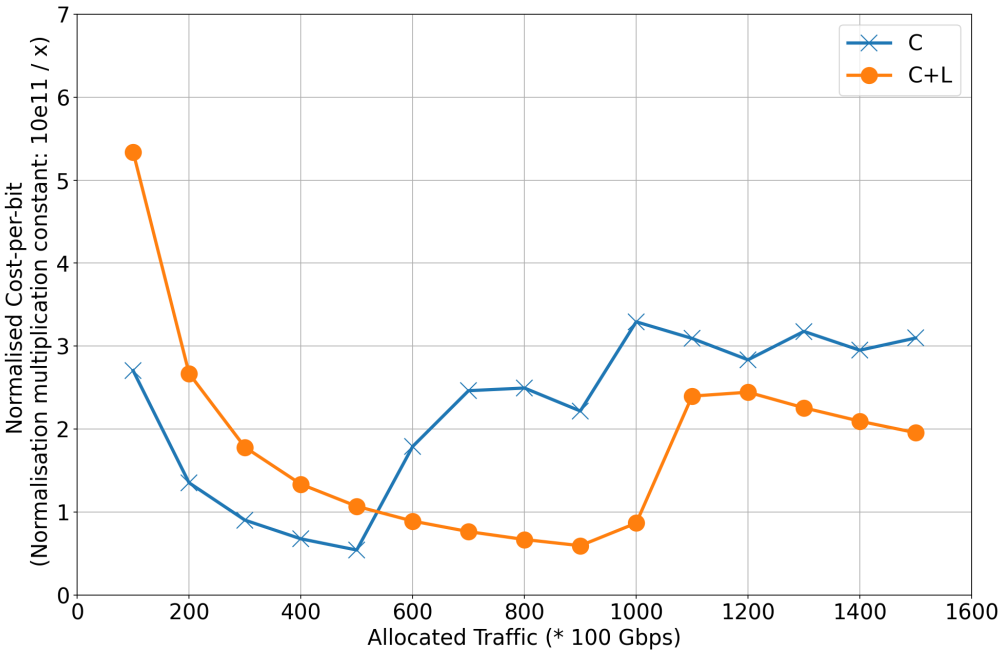

(a)

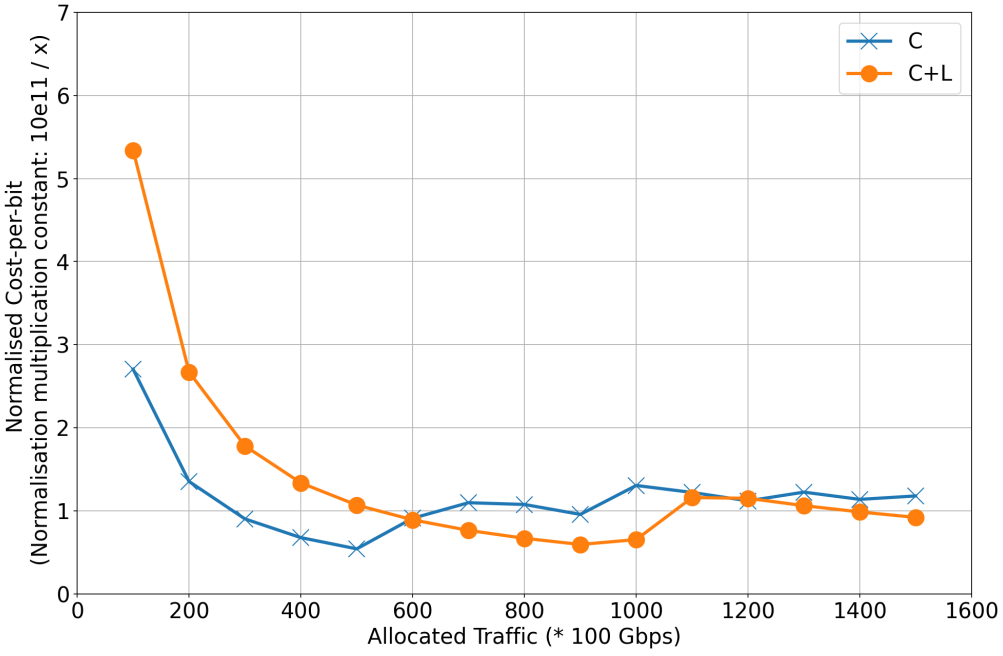

(b)

Figure 4.15: Cost-per-bit Analysis: (a) case 6 with dark fiber leasing, (b) case 6 with optical cable deployment.

of the network upgrade cost for the C and C+L band system with the fixed launch power (same as BT-UK network). As the traffic load grows in the network, the need for extra cable deployments also increases, and that results in the enhancement of upgrade costs for both C

and C+L band systems.

Table 4.6: Cost of Network Upgrade for Pan Europe Network (Launch Power = 0 dBm).

System	Allocated Traffic (Tbps)	Upgrade Cost (x)
C Band	10	1221.15
C Band	50	3825.45
C Band	100	5165.8
C Band	150	6014.5
C+L Band	10	2802.84
C+L Band	50	5016.77
C+L Band	100	5857.64
C+L Band	150	6312.05

The effect of channel launch power for fixed traffic load is shown in Table 4.7. At high launch power (-1.5 dBm), the effect of ISRS dominates in the C+L band system and degrades the average quality of the lightpaths. As a result, the congestion rises in the C+L band network and enhances the network upgrade cost in the long run. However, if the channel launch power is reduced (e.g., from -1.5 dBm to -3 dBm), the average quality of lightpaths improves in the MB network due to the reduction of NLI. As a result, the C+L band system shows an advantage over the C band system (at -3 dBm launch power) in minimizing the network upgrade cost. Nevertheless, too much signal power reduction (e.g., -6 dBm) also reduces the quality of the lightpaths and returns high network upgrade costs.

Table 4.7: Cost of Network Upgrade for Pan Europe Network (Allocated Traffic = 1 Tbps).

System	Launch Power (dBm)	Upgrade Cost (x)
C Band	0	0
C Band	-1.5	0
C Band	-3	2560.75
C Band	-4.5	1932.65
C Band	-6	3108.75
C+L Band	0	0
C+L Band	-1.5	571.16
C+L Band	-3	1377.9
C+L Band	-4.5	3353.23
C+L Band	-6	5252.29

4.5 Conclusion

We investigated the techno-economic comparison between C and C+L band technology while taking a robust cost model. A domain knowledge-assisted cost-effective network upgrade algorithm is proposed in order to enhance the overall network capacity while minimizing CapEx. The comparison between optical cable deployment and fiber leasing is captured in order to upgrade the overall network capacity with minimum cost-per-bit. Reported results show that

the single fiber C+L band system can provide approximately 66.67% gain in terms of traffic admissibility compared to the multifiber C band system while considering fiber leasing in BT-UK network. If the operator's owned dark fibers are not available in any of links, numerical results show that the multifiber C+L band system in BT-UK network can still provide CapEx savings of approximately up to 40.5% compared to the multifiber C band systems while minimizing the cost-per-bit of the network approximately by 21.9% for achieving the targeted network capacity of 150 Tbps. The cost of network upgrade is also analysed for larger networks (like Pan Europe) where the quality of the lightpaths becomes more susceptible to NLI. Reported results show that multifiber C+L band system need 4.95% higher upgrade cost compared to multifiber C band system to achieve 150 Tbps network capacity with high launch power (0 dBm). In addition, the advantage of launch power variation is also explored for minimization of network upgrade cost. Numerical results show that the decrement of launch power from 0 dBm to - 3 dBm can provide approximately 46.2% gain for the upgrade cost minimization in C+L band system compared to C band.

Chapter 5

Fragmentation Management in C+L Band Optical Networks

5.1 Introduction

The advantage of the MB (C+L) network is already illustrated in Chapter 2 to 4. This C+L band system consists of double spectrum resources compared to the C-band system, and efficient management of these important resources is crucial for the network operator in order to avoid blocking in the system. Typically, a major requirement of spectrum management is to reduce the isolated and unutilized spectrum slots that cannot serve a demand request while satisfying the spectrum continuity and contiguity constraints for EONs [34]. These fragmented spectrum chunks need to be re-aligned by the process of defragmentation to create contiguous spectral resources to accommodate future traffic growth.

Considerable literature exists on fragmentation management to enhance the overall network capacity while operating over C band [35]–[37]. In all of these papers, the worst-case NLI assumption (by considering the fully-filled worst case spectrum occupancy in every link) has been considered to avoid the complexity of real-time NLI estimation as per the changes in network dynamics. This assumption makes the computation of the QoT easier and provides a worst-case system capacity for the C band network. On the other hand, currently, network operators are planning to upgrade the deployed infrastructure for the next-generation optical network with less cost per bit. Among various approaches, the MB system (such as C+L) is evolving as a potential solution where the dominance of NLI on the OSNR becomes more prominent due to the presence of ISRS with a high number of channels. Therefore, for such a MB scenario, consideration of the worst-case NLI assumption can reduce the overall achievable capacity of a network very significantly.

Recently, to extract maximum capacity from the deployed infrastructure, operators are focused on designing actual margin [38], and just enough margin-oriented [39] based future networks. The key idea considered in this work is replacing the static-worst-case NLI estimation with the dynamic-real-time NLI estimation by sensing the network's current state of channel occupancy. Accordingly, with the advancement of optical performance monitoring (OPM) equipment [40], researchers also observed that all the links in a network are not fully occupied. Generally, wavelength continuity constraints in WDM networks, as well as spectrum continuity and contiguity constraints in EONs, create unoccupied spectrum regions in every link. These unoccupied spectrum regions are less likely to be filled with increasing traffic due to resource allocation constraints.

Moreover, there has been a growing interest in impairment-aware physical-layer study in the context of EONs, while performing conventional network-layer tasks such as routing, spec-

trum allocation, providing protection, traffic grooming, etc. Following that direction, Ref. [41] presented a dynamic QoT-aware routing and spectrum allocation (RSA) algorithm while considering OSNR for path selection, and spectrum and modulation level assignment. Reported results indicate that the presented scheme performs best in terms of average OSNR for NSFNET and US backbone network. In [42], authors formulated an integer linear program (ILP) to solve the resource-allocation problem for static traffic scenario while considering several common impairments such as amplified spontaneous emission (ASE) noise from in-line amplifiers and NLI from co-propagating lightpaths along the same fiber. Simulation results show that, for Deutsche Telekom (DT) network, the algorithm can provide up to 31% bandwidth savings compared to the baseline methods. Authors in [43] showed the advantage of traffic grooming and multi-path routing to enhance spectral efficiency while considering realistic physical-layer impairments. However, most of these works on defragmentation have considered only the C band while assuming hard values for reach and capacity, due to lack of low-computation-complexity-based QoT estimators.

To the best of our knowledge, no work has accounted for the trade-off between NLI and defragmentation. In case of a MB system operating beyond the C band, the NLI due to ISRS becomes non-negligible [13]. Therefore any spectrum re-tuning will need to account for its detrimental impact on OSNR of other active lightpaths. It is important to account for the impact of defragmentation on existing lightpaths because OSNR is an important figure of merit in guaranteeing a committed QoS by an operator to their customers under their service level agreements (SLA) [44]–[46]. Therefore, while initiating defragmentation to achieve the best ROI, the operator needs to efficiently manage the spectrum while preventing any reduction in the committed QoS due to ISRS for a MB system.

This work proposes, for the first time, a quality-aware proactive defragmentation scheme for the MB EON system while considering C+L bands. It provides insights to develop a QoS maintenance strategy while doing spectrum defragmentation in C+L bands. During the development of the proposed schemes, the work shows the impact of the lightpath selection strategy on the overall network capacity. The proposed scheme prioritizes the minimization of fragmentation index (FI) and QoT maintenance for two different defragmentation algorithms, namely — NLI-aware defragmentation (NAD) and NLI-unaware defragmentation (NUD). Moreover, to leverage the computational advantage of machine learning (ML) techniques, a robust deep neural network (DNN) model is used to predict the OSNR of all the lightpaths, while performing proactive spectrum retuning. Simulation results indicate the advantage of the NAD algorithm with respect to a baseline algorithm (NUD) in terms of blocking probability, traffic admissibility, fragmentation index (FI), contiguous-aligned available slot ratio (CAASR), and cost of defragmentation.

The rest of the work is organized as follows. Section 5.2 discusses related works. Section 5.3 describes the effect of ISRS on defragmentation and the problem statement. Section 5.4 presents the proposed schemes. Section 5.5 introduces the simulation setup followed by traffic matrix generation procedure, and training and testing mechanism of the DNN-based QoT estimator. Section 5.6 evaluates the performance of the proposed scheme. Finally, Section 5.7 concludes the work.

5.2 Related Works

Dynamic establishment and tearing down of lightpaths can create non-aligned, non-continuous, isolated vacant slots in the optical spectrum. Recent evidence suggests that this inevitable situation of fragmentation needs to be handled by efficient approaches, such as non-defragmentation and defragmentation. The non-defragmentation approach tries to manage the spectrum in ad-

vance to avoid fragmentation by incorporating spectrum partitioning and multi-path routing. Several defragmentation approaches have been studied to enhance traffic admissibility, where the fragmented spectrum is managed proactively or reactively. Various attempts have also been made to reroute existing lightpaths to further reduce the blocking probability while following proactive or reactive approaches. Several hitless methods have been investigated to avoid traffic disruptions while following several retuning approaches, such as hop-retuning, push-pull, make-before-break. The following subsections summarize these related works on defragmentation.

5.2.1 Approaches Dealing with Non-defragmentation

The creation of spectrum partition to allocate different lightpaths (in terms of route, requested bandwidth, etc.) can reduce the fragmentation in the network. Taking this direction, Refs. [47], [48] divided the spectrum into multiple dedicated partitions and assigned different lightpath groups into different sections. Grouping of lightpaths can be done based on the requested bandwidth or their routes. The number of partitions can be estimated by formulating a graph-coloring problem. Reported results indicate that the blocking probability can be lowered by reducing the number of partitions in the spectrum; however, statistical multiplexing gain becomes lower. To avoid this drawback, authors in [49], [50] introduced pseudo partitioning techniques by allocating different lightpaths into different portions of the spectrum. Moreover, to suppress the effect of spectrum contiguity in a fragmented scenario, authors in [51] reported a multi-path routing strategy by splitting a demand into multiple smaller sub-demands to avoid blocking.

5.2.2 Approaches Dealing with Defragmentation

A number of cross-sectional studies suggest that, although non-defragmentation approaches can provide lower CAPEX, the admissible traffic is significantly low compared to defragmentation techniques. During defragmentation, existing lightpaths can be sequentially shifted from one part of the spectrum to another to minimize vacant spectrum slots. Following this direction, authors in [52] reported a novel push-pull technique which gradually moves the lightpaths across the available slots in a step-by-step manner without jumping over existing occupied slots during movement. This strategy ensures no additional equipment requirements and zero traffic disruptions. However, sequential movement may lead to the end-of-line situation, where a lightpath can not be shifted without spectral jump in the vacant places of the spectrum due to the presence of other ongoing intermediate lightpaths. This situation can be overcome only by allowing spectral jumps [53] during rearrangement of the spectrum. Following this direction, Ref. [54] compared these two approaches. Reported results indicate the advantages of the hop-retuning methods, including spectrum jumps compared to the push-pull technique to achieve lower bandwidth blocking probability. Several attempts have also been made to learn the effect of defragmentation scheduling time on the admissible traffic load. Defragmentation subroutine can be triggered periodically (called proactive approach) or after the rejection of a request (called reactive approach). In [55], the authors presented both approaches while performing non-disruptive movements. The reported results indicate that reactive approaches can provide a significant advantage while minimizing the defragmentation cost in terms of delay and impact on existing lightpaths.

Overall, all of the above-mentioned defragmentation approaches consider the C band system, where the effect of NLI is smaller than the MB scenario. Therefore, avoidance of NLI during defragmentation does not impact the overall system capacity significantly. However, for the MB system, the effect of NLI becomes severe due to the higher number of channels and ISRS, thereby indicating a need for investigation to monitor the quality of lightpaths during defrag-

mentation. This motivates us to investigate the effect of the physical layer on defragmentation, mainly during MB transmission. Our research considers the disruption-free defragmentation movements while considering ISRS-based NLI in the C+L band scenario.

5.3 Prerequisites for the proposed scheme

This section presents an overview of the effect of ISRS on defragmentation, ML-based QoT estimator, problem statement, and assumptions.

5.3.1 Effect of ISRS on Defragmentation

As described in Section 5.1, ISRS is a significant component for MB transmission, which severely affects the NLI and OSNR of a lightpath. Typically, if two channels are separated by 13 THz, then the maximum power can transfer from a lower wavelength channel to a higher wavelength channel due to ISRS phenomena [56]. As a consequence, the NLI power will also be maximum at the higher wavelength or lower frequency channels as compared to other channels present in the counterparts of the spectrum. As discussed in Chapter 2, the rise in NLI power also decreases the QoT of the lightpaths having higher wavelengths.

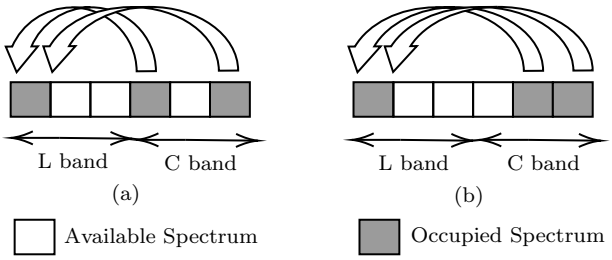

Figure 5.1: Effect of ISRS on defragmentation in C+L band EON: (a) High Fragmentation, Low ISRS; (b) Low Fragmentation, High ISRS.

The primary objective of any defragmentation algorithm is to reduce isolated-available slots in any link to improve a network's overall FI (which can be calculated as the difference between unity and CAASR [57]). Figure 5.1 shows an example to describe the drawback of a conventional defragmentation algorithm, which tries to reduce FI without monitoring QoT of lightpaths. For simplicity, it is assumed that there are six slots across the C+L bands and three lightpaths occupy a total of three slots. The spectrum with isolated vacant slots is considered first, as shown in Fig. 5.1(a), which shows the scenario before defragmentation. Fig. 5.1(b) shows the spectrum scenario after defragmentation, where to minimize the number of isolated-available slots, one of the lightpaths is retuned towards C band. In both scenarios, the possibilities of power transfer due to ISRS are represented by the pair of arrows. Since the presence of more number of contiguous occupied slots in the C band can enhance the ISRS power transfer in the L band, here the quality of the single L band lightpath (in terms of OSNR and associated modulation format) degrades in the post-defragmentation scenario. Typically, L band channels suffer more NLI penalties, ASE noise, and OSNR penalty compared to C band [18]. Therefore, for C+L band transmission, it is not necessary that any choice of spectrum retuning of a lightpath for FI minimization can also maintain the quality of any existing connections. Hence, the quality of lightpaths needs to be checked during defragmentation to handle the trade-off between QoT maintenance and FI minimization.

5.3.2 QoT Estimation using ML

QoT of an optical lightpath is generally quantified in terms of its OSNR. Furthermore, for any wavelength-multiplexed system, the OSNR of any active channel mainly depends on the NLI contribution from other co-propagating channels. Therefore, the calculation of OSNR of active lightpaths according to the changes in network dynamics is an important step for accurately capturing the impact of NLI. In [12], for reduction of computational complexity, the authors give a closed-form approximated formula for NLI estimation while incurring 0.2 dB average error, and it has been adapted in several works [13], [20], [58], [59] to update the OSNR of any active lightpaths. However, as the number of provisioned lightpaths enhances in the network, the complexity of this closed-form-based calculation chances manyfold while considering geographically diverse networks. For example, suppose S is the number of maximum channels in each link, Z is the number of active lightpaths in the network, and n is the number of nodes in the network. If $O(T)$ is the order of complexity for OSNR calculation of a single lightpath, then the overall time complexity for calculating OSNR of all the active lightpaths during defragmentation becomes in the order of $O(Z \times T \times S \times n^2)$.

Recently, in [60]–[66], several attempts have been made to predict the QoT of a lightpath with less computational complexity using Machine Learning (ML) approaches while using synthetic and real data sets. This motivates us to build a DNN-based regression model for predicting the OSNR of active lightpaths. Section 5.5.2 describes the QoT estimator model, which takes features of existing lightpaths as input and estimates the OSNR of a new lightpath. Several hyper-parameters related to DNN (such as the number of hidden layers, hidden nodes, activation functions, etc.) are tuned to train the DNN model, which improves the prediction accuracy.

5.3.3 Problem Statement

Based on discussions in Sections 5.1 and 5.3.1, it can be observed that the effect of defragmentation on the OSNR of existing lightpaths needs to be investigated. Till now, as per our literature survey, no work on fragmentation considers this kind of cross-layer interaction between the physical and network layers during defragmentation. In this work, we propose a QoT-aware proactive defragmentation scheme, which can capture the effect of defragmentation on the established lightpath's QoT and committed SLA.

5.3.4 Assumptions

We assume that all network links have the same number of spectrum slots as resources which includes both C and L bands. We do not consider rerouting of lightpaths during defragmentation, which generally degrades the QoT of the lightpath of interest (LoI) [67]. We also consider traffic grooming during lightpath establishment, where multiple demands are served by the network using higher-order-modulation-based lightpaths [13].

5.4 Proposed Scheme

5.4.1 Overview

Conventional approaches on defragmentation assume that any movement of LoI won't change the QoT of any existing lightpaths, due to the presence of high link margin. As a consequence, these approaches mainly consider the minimization of fragmentation index (FI) during the shifting of lightpaths. However, for low-margin-based [58] multiband systems, this assumption

is inaccurate due to the presence of ISRS. Our proposed scheme is designed for such MB systems where the key objective is to monitor the changes in QoT (in terms of OSNR) of existing lightpaths due to defragmentation. Our study considers two algorithms, namely — NAD, and NUD. To explore the trade-off between the minimization of FI and maintenance of QoT, these two algorithms consider the prioritization of different quantities for lightpath retuning. Algorithm 3 (NAD) prioritizes QoT maintenance of existing lightpaths as compared to FI minimization, whereas Algorithm 4 (NUD) prioritizes in reverse order. Since no existing work considers this kind of quality maintenance issue, the NUD algorithm is considered here as the baseline approach.

During the NAD defragmentation, we explore every possible position where a selected lightpath can be retuned. For each of these positions, the changes in OSNR of all active lightpaths is calculated. Therefore, as more lightpaths are added to the network, the number of OSNR calculations for a given defragmentation movement increases. The DNN-based regression model helps here to ease this computational complexity of OSNR estimation as per the changes in the network's dynamics. This approach during defragmentation helps to elucidate the trade-off between the spectrum defragmentation and OSNR degradation of existing lightpaths.

On the other hand, during the non-defragmentation stage, the quality of all the lightpaths and the corresponding supportable modulation formats are updated as per the addition of network traffic. During any QoT (OSNR) degradation towards lower modulation formats, we ensure the routing of the additional un-accommodated demands over newly established lightpaths.

5.4.2 NLI-aware Defragmentation (NAD) Method

The key objective of the NAD algorithm is to maintain the committed QoS while adhering to the SLA between the customers and operators. To achieve this, we ensure that only selected lightpaths are chosen during the defragmentation process while maintaining the pre-assigned modulation formats for all the lightpaths. We term these lightpaths as "Safe lightpaths" and their retuned operation as "Safe movement". On the contrary, the remaining lightpaths and their corresponding possible movements are termed as "Risky lightpaths" and "Risky movements", respectively. In general, the term "Safe" related to some of the lightpath and their associated movement indicates their higher likelihood of consideration during defragmentation. On the other hand, the rest of the possible lightpaths and movements (termed as "Risky") need to be kept untouched during defragmentation. In a nutshell, NAD method follows the deterministic approach while monitoring the status of each active lightpath during defragmentation. For any possible transition during defragmentation, if the OSNR of any lightpath indicates the degradation to be lower than the threshold for supporting pre-defragmentation modulation formats, the corresponding transition is avoided in the NAD method.

The following subsection describes the strategy of safer lightpath selection while filtering out risky lightpaths and the description of the NAD algorithm. The method of safer lightpath selection from Section 5.4.2.1 is used as lightpath selection policy and fed into the proposed Algorithm 3 of Section 5.4.2.2 as input.

5.4.2.1 Filtering of Risky Lightpaths

Here, we introduce a safer lightpath selection strategy by filtering out all risky lightpaths. As shown in Fig. 5.2, safer lightpath selection and its associated movement depend on three parameters, namely — (i) OSNR of a lightpath before defragmentation, (ii) OSNR degradation of that lightpath for each possible movement, and (iii) number of ongoing demands into that lightpaths.

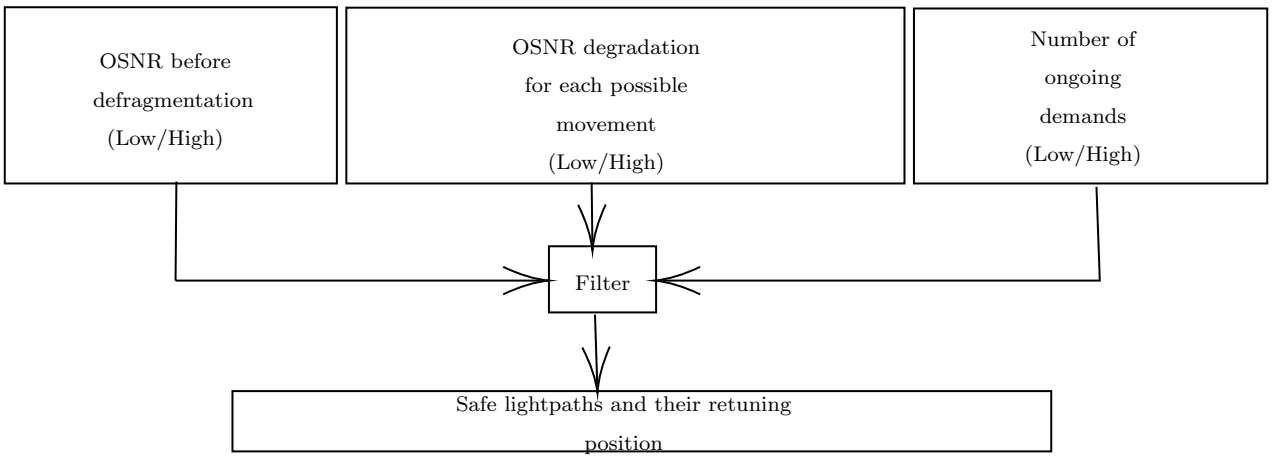

Figure 5.2: Safer lightpath selection strategy for defragmentation.

We formulate a multi-variable binary decision problem using these three parameters to choose safer lightpaths and filter out risky lightpaths. As a start, we pass each of these three parameters through different binary classifiers and classify the state of each parameter into standard binary output classes (such as "Low" and "High") as follows.

5.4.2.1.1 Classification of OSNR before defragmentation (Current OSNR): The quality of a lightpath, its associated modulation format, and capacity depend on its OSNR value. As an example, for symbol rate of 28-32 GBaud and BER of 10^{-3}, the OSNR threshold of PM-BPSK, PM-QPSK, PM-8QAM, PM-16QAM, PM-32QAM, and PM-64QAM modulations are 9, 12, 16, 18.6, 21.6, and 24.6 dB, respectively, whereas the corresponding capacities are 50, 100, 150, 200, 250, and 300 Gbps, respectively [13]. As shown in Table 5.1, we divide the OSNR range of each modulation format into two equal parts. The region near the lower bound is classified as "Low", whereas the remaining portion is termed as "High". For retuning during defragmentation, the probability of selection of lightpaths from the "High" region is greater than that from the "Low" region due to the constraint of quality maintenance.

Table 5.1: Classification of OSNR before defragmentation.

Modulation	Current OSNR (dB)	Decision
PM-BPSK	9-10.5	Low
	10.5-11.9	High
PM-QPSK	12-14	Low
	14-15.9	High
PM-8QAM	16-17.3	Low
	17.3-18.5	High
PM-16QAM	18.6-20.1	Low
	20.1-21.5	High
PM-32QAM	21.6-23.1	Low
	23.1-24.5	High
PM-64QAM	24.6-27.3	Low
	27.3-30	High

5.4.2.1.2 Classification of OSNR degradation for each possible movement: Generally, the modulation format of a lightpath is supported over a range of OSNR. Therefore,

if the updated OSNR of the lightpath due to retuning remains within this range, its modulation format (or committed QoS) remains unaltered. Therefore, the difference between OSNR lower limit of two consecutive modulation formats can be defined as the OSNR window of each modulation format (and symbolized by δ). As shown in Table 5.2, we use δ to classify the degradation of each lightpath. If the degradation of the OSNR of a particular modulation format is greater than 50% of its δ value, we classify it as high degradation, whereas the rest of the cases belong to the low degradation class. Moreover, to obtain the updated OSNR of LoI for each possible movement, the trained DNN model is used, as discussed in Section 5.5.2.

Table 5.2: Classification of OSNR degradation.

Modulation	Degradation OSNR (dB)	Decision
PM-BPSK ($\delta = 3$)	$\leq 50\%\ \delta$	Low
	$> 50\%\ \delta$	High
PM-QPSK ($\delta = 4$)	$\leq 50\%\ \delta$	Low
	$> 50\%\ \delta$	High
PM-8QAM ($\delta = 2.6$)	$\leq 50\%\ \delta$	Low
	$> 50\%\ \delta$	High
PM-16QAM ($\delta = 3$)	$\leq 50\%\ \delta$	Low
	$> 50\%\ \delta$	High
PM-32QAM ($\delta = 3$)	$\leq 50\%\ \delta$	Low
	$> 50\%\ \delta$	High
PM-64QAM ($\delta = 5.4$)	$\leq 50\%\ \delta$	Low
	$> 50\%\ \delta$	High

5.4.2.1.3 Classification of number of ongoing demands into a lightpaths: The capacity of higher-order-modulation-based lightpaths is much more compared to the lower-order ones. For example, three 100 Gbps demands can be groomed within one PM-64QAM lightpath, whereas only one 100 Gbps demand can be served using a single PM-QPSK lightpath. Therefore, as per the operator's capacity enhancement perspective, higher-demand-carrying lightpaths are always preferable compared to single-demand-carrying lightpaths. Hence, retuning of high-demand-carrying lightpaths needs to be avoided during defragmentation to reduce traffic disruption. Table 5.3 shows our method to classify each demand. Typically, more than one demand is placed in the "High" demand group, whereas others are termed as "Low" demand. Therefore, in NAD method, the likelihood of selecting lightpaths having "Low" demands is more; however, the impact of other two decision variables (current OSNR and OSNR degradation) needs to be monitored before finalising the choice of retuning.

Table 5.3: Classification of number of ongoing demands into a lightpath.

Modulation	100 Gbps Demand	Decision
PM-BPSK	0.5	Low
PM-QPSK	1	Low
PM-8QAM	1.5	High
PM-16QAM	2	High
PM-32QAM	2.5	High
PM-64QAM	3	High

5.4.2.1.4 Classification of lightpaths and their possible movement: Now, the lightpaths and their associated movement can be classified as safe or risky as per the strategy mentioned in Table 5.4. As shown in Fig. 5.2, based on the status of the three input parameters, the operator can filter out the risky lightpaths and their associated movements. For example, if the OSNR of a lightpath before defragmentation is already in the lower region, we termed this lightpath as "risky", irrespective of the other two parameters (i.e., OSNR degradation and the number of ongoing demands in the lightpath), since it has a higher chance of blocking after retuning. However, as per the network dynamics, operators of different networks can also decide the allowable degree of lower granular OSNR degradation movements (e.g., OSNR degradation $\sim$ 10% δ or 5% δ with current OSNR at low state), if the modulation-invariant policy of NAD method holds. For the current study, we have not considered such smaller granular transitions when the current state of OSNR belongs to low region. On the other hand, if any lightpath is at a high OSNR region before defragmentation and degradation of the OSNR after retuning in some particular positions is also low, we termed them as safer lightpath and safer movements, respectively. The number of demands in the lightpath does not matter in this latter scenario as the probability of the lightpath's QoT change after retuning becomes very low. It may happen that one safer lightpath may have multiple safer movements. For such cases, the best movements would be the ones which can minimize the existing FI as much as possible.

Table 5.4: Classification of lightpaths.

Current OSNR	OSNR Degradation	Demand	Decision
Low	Low	Low	Risky
Low	Low	High	Risky
Low	High	Low	Risky
Low	High	High	Risky
High	Low	Low	Safe
High	Low	High	Safe
High	High	Low	Safe
High	High	High	Risky

5.4.2.2 NLI-aware Defragmentation (NAD) Algorithm

In this section, we describe our proposed heuristic algorithm to address the trade-off between ISRS and defragmentation for a multiband EON. Table 5.5 presents the notations for the given parameters and decision variables, which are frequently used in our work. Algorithm 3 takes the network topology, traffic matrix, launch power of each channel, defragmentation scheduling threshold, trained DNN model, and lightpath selection policy as inputs. It finds the defragmented spectrum, blocking probability, traffic admissibility (in terms of number of served demands) at various situations (e.g., the instance of first blocking and 1% blocking), network fragmentation index, and cost of defragmentation.

The algorithm starts with the routing, modulation, and spectrum allocation *(RMSA)* operation for each requested demand t from the traffic matrix T (lines 1-2). By using the *RMSA* function, this algorithm attempts first for traffic grooming. If grooming is not possible, it tries to find the available spectrum resource for demand t as per the spectrum allocation policy into the shortest route between source and destination, while maintaining spectrum continuity and contiguity constraints.

After finding the required resources, the possible quality (in terms of OSNR) of the lightpath and its possible modulation format are checked as per the OSNR threshold [13]. If the demand

finds a route with required spectrum and acceptable modulation format, it is placed in the network with the help of a lightpath and counter N_s is incremented. Otherwise, the demand is blocked and we update the B_P. *RMSA* function also calculates the network fragmentation index [57] with the help of all established lightpaths (L_{all}) and their corresponding spectrum occupancy (f_l).

A scheduling threshold (D_{ST}) is chosen for the proactive defragmentation process which helps to manage the spectrum. After placement of (D_{ST}) number of new demands in the network (which resembles the batch size), the *RMSA* operation is paused and fragmentation subroutine is initiated (lines 3-4). During defragmentation, specific lightpaths are chosen for retuning with the help of the function *Select*, which helps to maintain the QoS of all the lightpaths (line 5). Trained deep neural network model (T_{DNNM}), list of all existing lightpaths (L_{all}), and lightpath selection policy (L_{SP}) are fed into the function *Select*, which returns the list of safe lightpaths (L_S) and their specific safe movements (f'_{l_s} from f_{l_s}) as output. This function works on the principle of the filter, which is discussed in Section 5.4.2.1.

If the algorithm finds more than one choice for the safe movement of a safe lightpath, a specific movement is chosen to minimize the FI. Now, these sets of lightpaths are sequentially retuned to their specific safe positions with the hop retuning mechanism [57] to get the defragmented spectrum in terms of updated spectral occupancy (lines 6-8). As a consequence of retuning, the algorithm updates information of all the lightpaths as per their new occupied spectrum in L_{all}, followed by the updated calculation of network fragmentation index and cost of defragmentation in terms of the number of shifted lightpaths (lines 9-11). Each of the defragmentation instances is ended by the OSNR upgrade for the retuned safe lightpaths and their adjacent co-propagating lightpaths with the help of the function $OSNR_{Update}$, which takes the list of all lightpaths and the spectrum occupancy information of LoI as inputs (lines 13-14). At the end of the defragmentation subroutine, RMSA operation is resumed for the next set of new demands in the traffic matrix T (line 15). After processing each of the requested demands for allocation, the algorithm finds the overall traffic admissibility by using the function *Capacity*, which takes N_s and B_P as inputs, and returns N_{SF} and N_{SO} as outputs (line 20).

5.4.3 NLI-unaware Defragmentation (NUD) Method

The work flow of the NUD algorithm is summarized in the following, where the key intention is to overlook the effect on the quality of lightpaths during defragmentation. As a start, the NUD algorithm moves all existing lightpaths of the network into different positions of the spectrum for minimization of the fragmentation index of the network, without monitoring the QoT. However, at the end of all possible movements, the quality of each lightpath is recalculated using the defragmented spectrum.

5.4.3.1 NLI-unaware Defragmentation (NUD) Algorithm

This section describes NUD as Algorithm 4, which takes the network topology, traffic matrix, and channel launch power only as inputs; and provides the defragmented spectrum, network traffic admissibility, and cost of defragmentation index as outputs. All of these output parameters are discussed in detail in Section 5.6. Like Algorithm 3, this algorithm also starts with resource allocation for each requested demand using the function *RMSA* (lines 1-2), followed by the initiation of defragmentation subroutine (lines 3-4). However, Algorithm 4 chooses all the ongoing lightpaths during defragmentation and moves each lightpath to a new position (from f_l to f'_l) by hop retuning without monitoring the associated QoT changes (line 5-6). For each movement, the list of lightpaths, spectral occupancy, fragmentation index, and cost of defragmentation are also updated (lines 7-10) as in Algorithm 3. At the end of the defragmentation subroutine, the $OSNR_{Update}$ function is used to update the QoT of all ongoing lightpaths, while

Table 5.5: List of notations used in the algorithms.

Notation	Description
	Given Parameters:
$G(V, E)$	Network topology; V = set of nodes, E = set of links.
T	Traffic matrix.
P_{Ch}	Launch power of each channel.
D_{ST}	Defragmentation scheduling threshold.
T_{DNNM}	Trained deep neural network model.
L_{SP}	Lightpath selection policy.
	Decision Variables:
D_S	Defragmented spectrum.
B_P	Blocking probability.
N_s	Number of total served demands.
N_{SF}	Number of served demands before first blocking.
N_{SO}	Number of served demands till one percent blocking.
N_L	Number of ongoing lightpaths.
L_{all}	Set of all ongoing lightpaths.
L_S	Set of ongoing safe lightpaths.
f_{l_s}	Operating frequency of the l_s^{th} safe lightpath before hop retuning, where $l_s \in L_S$.
$f_{l_{s,a}}$	Operating frequency of the adjacent lightpath with respect to lightpath of interest l_s.
f'_{l_s}	Operating frequency of the l_s^{th} safe lightpath after hop retuning, where $l_s \in L_S$.
f_l	Operating frequency of the l^{th} lightpath before hop retuning, where $l \in L_{all}$.
f'_l	Operating frequency of the l^{th} lightpath after hop retuning, where $l \in L_{all}$.
$OSNR_{l_s}$	OSNR of the l_s^{th} ongoing safe lightpath.
$OSNR_{l_{s,a}}$	OSNR of adjacent ongoing lightpath with operating frequency $f_{l_{s,a}}$.
$OSNR_l$	OSNR of the l^{th} ongoing lightpath.
FI_N	Fragmentation index of the network.
C_D	Cost of defragmentation.

using the updated spectral occupancy after retuning as input (line 12). This recalculation of OSNR by using updated defragmented spectrum affects the QoT of many lightpaths and hence affects the B_P. Finally, the defragmentation instance is stopped while resuming the RMSA operation for the next set of requested demands (line 14). In the end, the *Capacity* function

Algorithm 3 NLI-aware defragmentation (NAD)

Input: $G(V, E)$, T, P_{Ch}, D_{ST}, T_{DNNM}, L_{SP};
Output: D_S, B_P, N_{SF}, N_{SO}, FI_N, C_D;

for each demand request t in T sequentially **do**
  N_s, L_{all}, f_l, FI_N, $B_P \leftarrow RMSA(G(V, E), t, P_{Ch})$;
  if (N_s **mod** $D_{ST} == 0$) **then**
    Pause RMSA and initiate defragmentation;
    L_S, $f'_{l_s} \leftarrow Select(L_{all}, T_{DNNM}, L_{SP})$;
    for each safe lightpath l_s in L_S sequentially **do**
      $f_{l_s} \leftarrow f'_{l_s}$;
      $D_S \leftarrow$ Spectral occupancy;
      Update L_{all};
      Update FI_N;
      $C_D \leftarrow$ Number of shifted lightpaths;
    end for
    $OSNR_{l_s} \leftarrow OSNR_{Update}$ (L_{all}, f_{l_s});
    $OSNR_{l_{s,a}} \leftarrow OSNR_{Update}$ (L_{all}, $f_{l_{s,a}}$);
    Resume RMSA;
  end if
  else
  Continue;
end for
N_{SF}, $N_{SO} \leftarrow Capacity(N_s, B_P)$;

Algorithm 4 NLI-unaware defragmentation (NUD)

Input: $G(V, E)$, T, P_{Ch};
Output: D_S, B_P, N_{SF}, N_{SO}, FI_N, C_D;

for each demand request t in T sequentially **do**
  N_s, L_{all}, f_l, FI_N, $B_P \leftarrow$ RMSA($G(V, E)$, t, P_{Ch});
  if (N_s **mod** $D_{ST} == 0$) **then**
    Pause RMSA and initiate defragmentation;
    for each lightpath l in L_{all} sequentially **do**
      $f_l \leftarrow f'_l$;
      $D_S \leftarrow$ Spectral occupancy;
      Update L_{all};
      Update FI_N;
      $C_D \leftarrow$ Number of shifted lightpaths;
    end for
    $OSNR_l \leftarrow OSNR_{Update}$ (L_{all}, f_l);
    Update B_P;
    Resume RMSA;
  end if
  else
  Continue;
end for
N_{SF}, $N_{SO} \leftarrow Capacity(N_s, B_P)$;

captures the traffic admissibility as in Algorithm 3.

5.5 Simulation Setup

A custom-built, event-driven, Python simulator is used to emulate the proposed defragmentation scenario while incorporating accurate physical-layer modeling. Two networks, namely — BT-UK network (22 nodes, 35 links, average link length 147 km) [13], and 24-node US network (24 nodes, 43 links, average link length 991 km) [68] are considered. The details of these topologies are illustrated in Appendix B. RMSA are done based on the k-shortest path and First-Fit policy. Modulation formats of each lightpath are selected based on the OSNR threshold [13]. Moreover, D_{ST} value is chosen as 250 for the entire simulation, which can vary as per the operator's choice. We run the simulations for 20 seeds, each with 2000 demands. The average results from these different seeds are reported with approximately less than 5% margin of error at a 95% confidence interval.

5.5.1 Traffic Matrix

Core networks typically exhibit accumulation of static traffic. A total of 2000 100 Gbps static demand requests are considered for the simulation. To resemble the high traffic flow between special nodes in different geographies, a biased traffic matrix is generated as reported in [20]. Source-destination pairs are chosen probabilistically by using dropped wavelength data for the BT-UK network, whereas population metric is used for the 24-node USA network.

5.5.2 Training and testing of DNN-based QoT estimator

A DNN model is trained to predict the updated OSNR of all the lightpaths during defragmentation. At first, to create training and testing data set, our network simulator takes network topology and traffic matrix as inputs and allocates the requested demands with the help of lightpaths while considering the C+L band physical-layer model (as described in Section 5.3). This simulation does not consider any defragmentation instances. Different features of each lightpath such as launch power of each channel (P_{ch}), number of total traversed links or hop count (H_c), link length (L_{link}), number of traversed intermediate ROADMs, the channel of interest (F_{COI}), total number of active C band interfering channels throughout the link ($N_{int,C}$), total number of active L band interfering channels throughout the link ($N_{int,L}$), total number of in-line link amplifiers (N_{amp}) and fill factor of traversed link (FF) [58], and OSNR are stored to generate the training and testing data. The full data set is split into a 70:30 ratio for training and testing. As shown in Fig. 5.3, different features are fed into the DNN-based regression model which provides the lightpath's OSNR as output. Tuning of hyperparameters is an essential step for the DNN-based regressor to minimize the error between predicted and actual simulated values. To choose the number of hidden layers and their associated number of neurons, we started from a baseline [61] which consists of 3 hidden layers with 20 neurons in each. Furthermore, we varied the number of hidden neurons and layers to achieve maximum prediction accuracy and no overfitting. Although we also tested other activation functions such as Sigmoid, Arctan, and Tanh, ReLU provided the minimum error for our data set. The error of the DNN is monitored in terms of maximum absolute error (MAE), mean square error (MSE), root mean square error (RMSE), and R-squared value. As a result, this hyperparameter tuning leads to a DNN model (consisting of 5 hidden layers (32, 32, 32, 32, 32 neurons) and ReLU activation function) with the prediction accuracy of 99.69%.

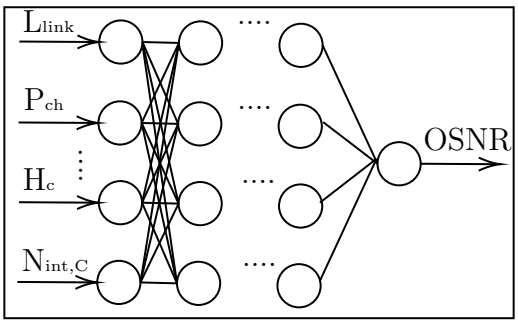

Figure 5.3: DNN-based QoT estimator for OSNR prediction.

5.6 Performance Evaluation

We evaluate the performance of the proposed scheme in terms of blocking probability, traffic admissibility, fragmentation index, contiguous aligned available slot ratio (CAASR), and the cost of defragmentation. Blocking probability is defined as the ratio of the number of blocked requests to the total number of requests in the network. Traffic admissibility is calculated in two ways, namely the number of allocated demands in the network before first blocking and till 1% blocking. The cost of the defragmentation is determined as the total number of retuned lightpaths during defragmentation. The fragmentation index (χ) of the network and CAASR (ϕ) are calculated using Eq. 5.1 and 5.2, respectively [57].

$$\chi = 1 - \phi \tag{5.1}$$

$$\phi = \sum_{d \in D} \sum_{k \in K_D} w_{dk}.\psi_{dk}, \tag{5.2}$$

where D and K_D donate the set of all the source-destination pairs and the set of routes of source-destination $d \in D$, respectively. ψ_{dk} is the ratio of γ_{dk} and Z, where Z represents the number of spectrum slots in each link and γ_{dk} denotes the maximum number of contiguous aligned available slots for route $k \in K_d$ of source-destination pair $d \in D$. Furthermore, w_{dk} represents a weight that is proportional to the traffic load of route $k \in K_D$ of source-destination pair $d \in D$, where $\sum_{d \in D} \sum_{k \in K_D} w_{dk} = 1$.

Initially, we consider uniform channel launch powers of -6 dBm, -4.5 dBm, -3 dBm, -1.5 dBm, and 0 dBm to obtain the information on blocking probability. As shown in Figs. 5.4 and 5.5, for all the launch powers, Algorithm 1 (NAD) performs better in terms of blocking probability compared to Algorithm 2 (NUD) in both topologies. Figures 5.4 and 5.5 also show that - 4 dBm and -3 dBm are the optimum launch powers for NUD and NAD algorithms, respectively. Following this direction, we consider two optimum launch powers (-4 dBm, and -3 dBm) and one sub-optimal launch power (-1.5 dBm) for further study.

Figure 5.6 shows the variation of blocking probability with traffic load in BT-UK network for different launch powers. We observe that the NAD algorithm with optimum launch power (-3 dBm) provides the least blocking compared to the other scenarios. Tables 5.6 and 5.7 capture the traffic admissibility in the BT-UK network. Numerical data shows that Algorithm 1 with optimum launch power can provide the highest capacity in the network at both the instance of first blocking and 1% blocking.

The variation of blocking probability with traffic load for USA network is shown in Fig. 5.7. Reported trends emphasize the ability of the NAD algorithm to reduce blocking probability with optimum launch power. Generally, the presence of the longer links accumulates a larger amount of ASE noise and NLI in the USA network compared to BT-UK network, and thereby reduces

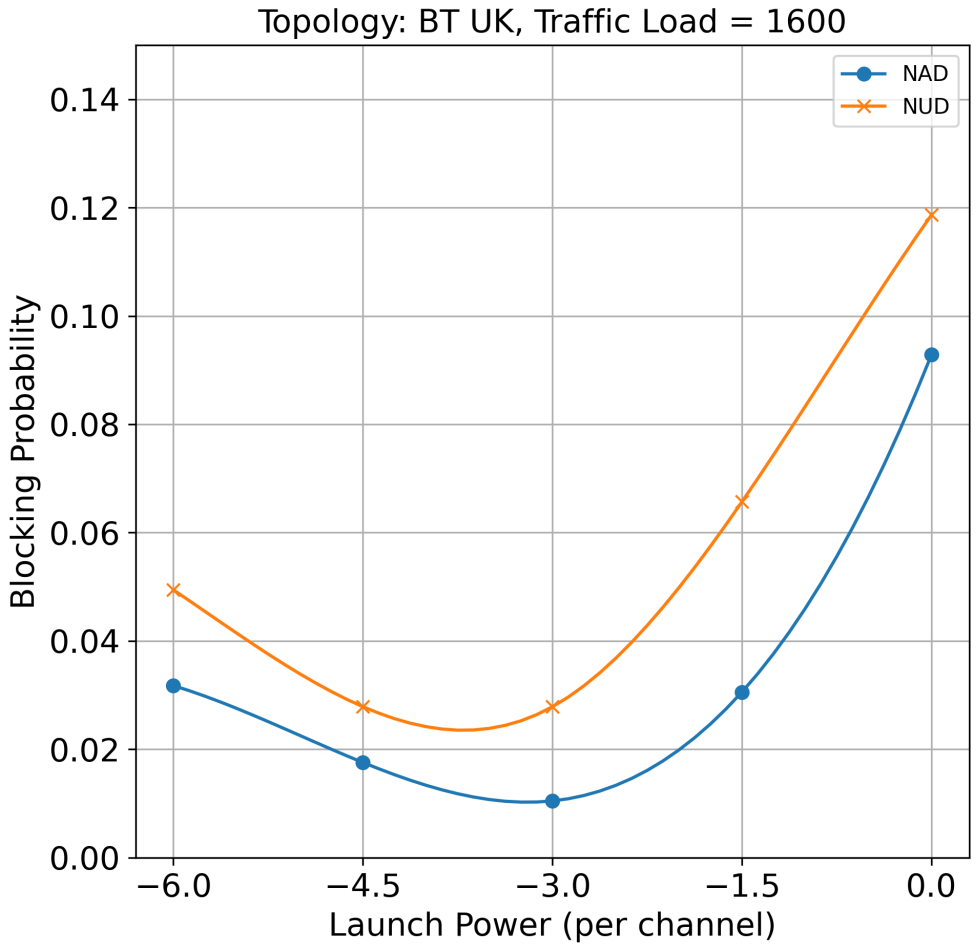

Figure 5.4: Blocking probability vs. launch power in BT-UK network.

Table 5.6: Number of served demands before first blocking for BT-UK network.

Strategy	Launch power (dBm)	Served demands
NUD	-4	1191
NAD	-4	1234
NUD	-3	1069
NAD	-3	1183
NUD	-1.5	882
NAD	-1.5	1003

Table 5.7: Number of served demands at 1% blocking for BT-UK network.

Strategy	Launch power (dBm)	Served demands
NUD	-4	1518
NAD	-4	1615
NUD	-3	1501
NAD	-3	1673
NUD	-1.5	1350
NAD	-1.5	1552

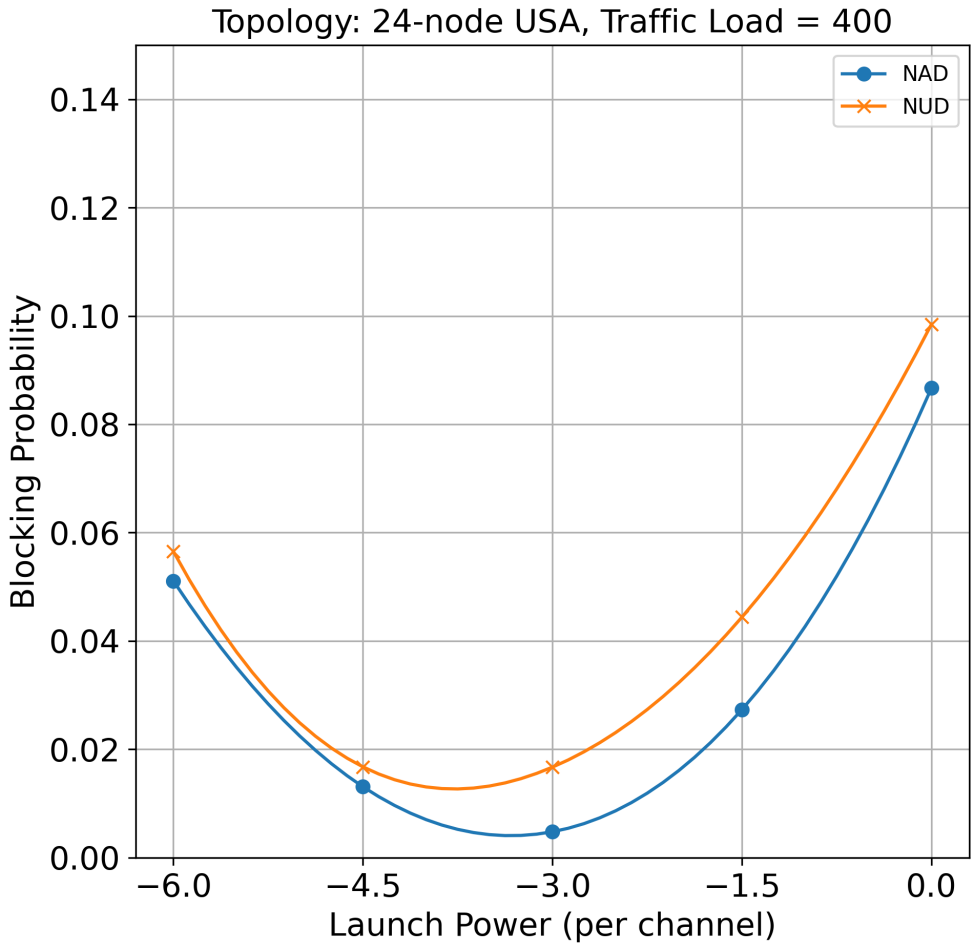

Figure 5.5: Blocking probability vs. launch power in USA network.

Table 5.8: Number of served demands before first blocking for USA network.

Strategy	Launch power (dBm)	Served demands
NUD	-4	250
NAD	-4	350
NUD	-3	250
NAD	-3	350
NUD	-1.5	250
NAD	-1.5	300

Table 5.9: Number of served demands at 1% blocking for USA network.

Strategy	Launch power (dBm)	Served demands
NUD	-4	376
NAD	-4	421
NUD	-3	365
NAD	-3	450
NUD	-1.5	322
NAD	-1.5	383

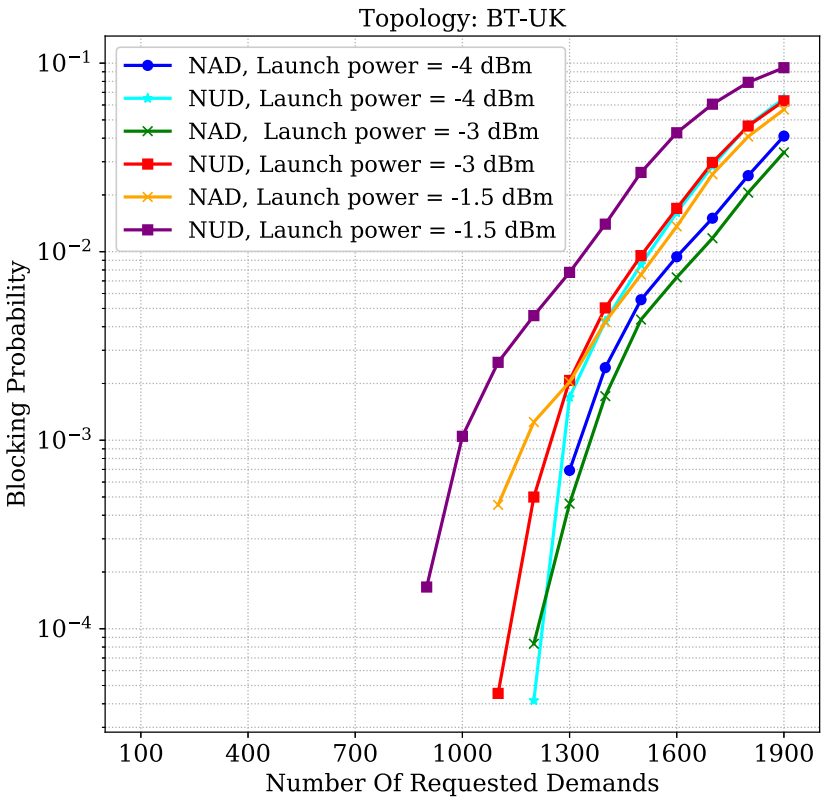

Figure 5.6: Blocking probability vs. traffic load in BT-UK network.

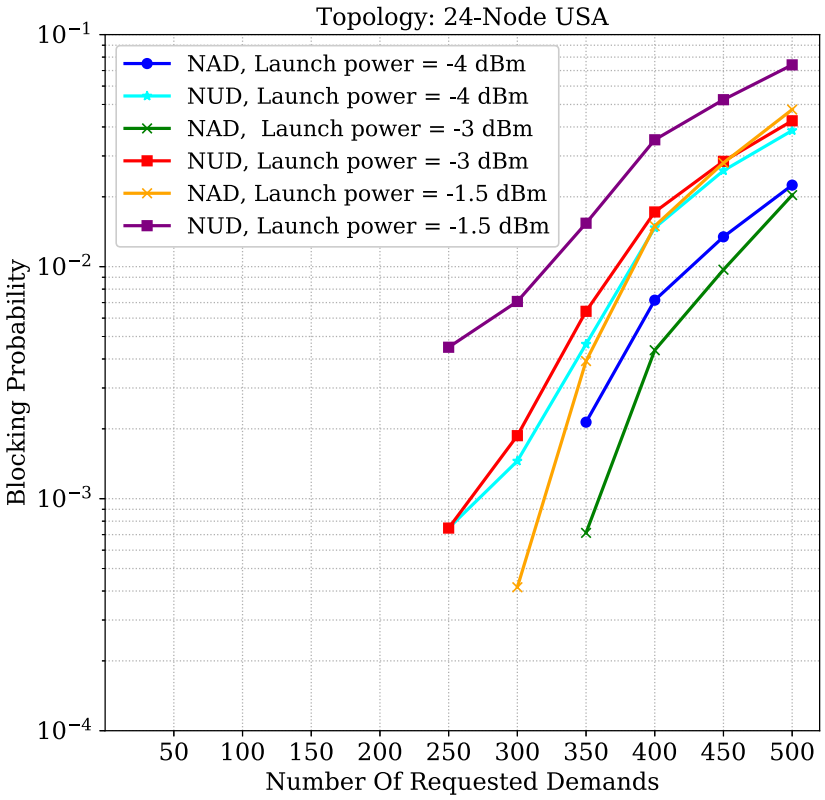

Figure 5.7: Blocking probability vs. traffic load in USA network.

the overall capacity. Tables 5.8 and 5.9 provide information on the number of served demands at the instance of first blocking and 1% blocking, respectively. Numerical data in Tables 5.7

Table 5.10: Normalised cost, FI, and CAASR for BT-UK network.

Strategy	Normalized cost	FI	CAASR
NUD	1	0.69	0.31
NAD	0.16	0.88	0.12

Table 5.11: Normalised cost, FI, and CAASR for USA network.

Strategy	Normalized cost	FI	CAASR
NUD	1	0.01	0.99
NAD	0.0	0.73	0.27

and 5.9 shows that NAD algorithm can provide a maximum of 15% traffic admissibility gain in BT-UK network, whereas in USA network, this gain becomes 23%.

Tables 5.10 and 5.11 show the variation of the normalized cost of defragmentation, FI, and CSSSR values for Algorithms 3 and 4 in BT-UK and USA network, respectively. As NAD algorithm considers the maintenance of the quality of all existing lightpaths by selectively choosing safer lightpaths for retuning, it achieves higher traffic admissibility, lower cost of defragmentation, while incorporating a higher value of fragmentation index (or, lower CAASR). On the other hand, selection of all the lightpaths during defragmentation in NUD algorithm leads to higher CAASR; and, in the long run, it provides higher cost of defragmentation and lower traffic admissibility.

5.7 Conclusion

We investigated spectrum retuning via hitless defragmentation for EON to enhance efficient spectrum accommodation while reducing the unused fragmented spaces in the spectrum. As the presence of ISRS for transmission beyond the conventional C band can severely degrade the quality of the signal during defragmentation, we investigated the importance of QoT monitoring during defragmentation in C+L band EONs. A signal-quality-aware proactive defragmentation scheme for the C + L band system has been proposed. The proposed scheme prioritizes the minimization of the fragmentation index and QoT maintenance for two different defragmentation algorithms, namely, NAD and NUD. We leverage ML techniques for QoT estimation of ongoing lightpaths during spectrum retuning. The OSNR of a lightpath is predicted for each choice of spectrum retuning, which helps to monitor the effect of defragmentation on the quality of ongoing lightpaths (in terms of assigned modulation format). Numerical results show that, compared to a baseline algorithm (NUD), the proposed NAD algorithm provides up to 15% traffic admissibility gain for smaller networks such as BT-UK, while for larger networks such as the 24-node USA network, a capacity benefit of 23% is achieved in terms of the number of served demands at 1% blocking. Mainly, the effect of ISRS on the existing lightpaths during defragmentation is minimized by selectively choosing safer lightpaths for retuning in the C+L band system while considering the NAD algorithm. As a result, the NAD algorithm outperforms in terms of traffic admissibility compared to the NUD algorithm.

Moreover, the performance of the proposed scheme is also evaluated in terms of FI, CAASR, and cost of defragmentation. As selected lightpaths are chosen for retuning in the NAD algorithm, the cost of defragmentation becomes lower compared to the NUD algorithm. On the contrary, the NUD algorithm prioritizes the minimization of FI while selecting all active lightpaths during defragmentation instead of QoT maintenance. As a result, the NUD algorithm outperforms in terms of FI minimization and CAASR maximization compared to the NAD algorithm.

Chapter 6

Efficient Resource Provisioning in C+L Band Optical Networks

6.1 Introduction

Chapter 5 shows the advantage of periodic spectrum management (namely, defragmentation) for improving the capacity of multiband EON. The underlying resource provisioning policy also plays a crucial role in this context, as the major challenge in EON remains in the maintenance of spectrum continuity and contiguity constraints. Several attempts have been made to reduce the rate of blocking in EON while designing different spectrum allocation policies, such as first fit (FF), last fit (LF), random fit (RF), etc [34]. Although these algorithms reduce blocking, they assume fully-filled worst conditions to estimate NLI, and that leads to poor resource utilization. As a result, these algorithms return the overall network capacity under the worst-case assumption.

The effect of this worst-case NLI estimation becomes severe in the context of MB-EON [6], [69] due to the presence of ISRS [12]. To overcome this drawback of worst-case NLI estimation on network capacity, recent work has started to consider the real-time spectrum occupancy during QoT estimation and resource allocation [13], [58], [59]. Moreover, as the effect of NLI also depends on the allocated wavelength of the channel of interest, recent research has also focused on intelligent spectrum allocation policies for lightpaths based on its several characteristics, such as the link distance for reducing the overall blocking probability of the network while enhancing the transmission reach. For example, in [70], the authors assign longer lightpath requests in the smallest indexed spectrum slot, where the dispersion effect is less, whereas the shorter lightpath requests are assigned in the largest indexed spectrum slot, where the dispersion effect is higher. Although digital signal processing (DSP) based dispersion compensation techniques can be used to mitigate the effect of dispersion, authors in [70] have not considered it to avoid the additional cost and proposed resource allocation algorithm for dispersion uncompensated network. The result of this dispersion adaptive spectrum allocation scheme shows an improvement compared to distance adaptive FF schemes in terms of blocking probability reduction and fragmentation minimization. In [50], a spectrum provisioning strategy based on the lightpath's route is studied to separately place joint and disjoint lightpaths at different ends of the spectrum for minimizing the number of non-contiguous and non-aligned available slots.

In addition to NLI variation based on spectrum occupancy, the presence of different band-specific discrete amplifiers in MB-EON changes the QoT of connections in different bands due to the variation of ASE noise. Thus conventional RSA policies [34] that have been utilized for C-band-only systems may not provide the best performance in the MB-EON context due to the presence of heterogeneous, complex, and nonlinear physical-layer impairments (PLI) due

to band-specific characteristics.

All these works indicate some fundamental question:

- Is it possible to build a new resource provisioning framework for allocating requested traffic demands in the network while considering the behavior of ISRS in C+L band EON?

To address this question, this work proposes a novel quality-aware resource provisioning scheme for C+L band EON while considering the impact of ISRS on NLI. Unlike conventional schemes, the proposed scheme takes the effect of PLI before the choice of the spectrum during resource allocation to reduce the likelihood of blocking. An algorithm under this scheme, namely, OSNR adaptive first-last-fit (OA-FLF), is proposed while leveraging the heterogeneity of MB-EON. The proposed algorithm selectively chooses the available channels from different bands to achieve the maximum network capacity in the long run. Furthermore, to leverage the computational advantage of ML techniques (as discussed in Chapter 5), a deep neural network (DNN) model is used to predict the OSNR of all lightpaths during provisioning. The performance of the algorithm is analyzed in terms of traffic admissibility, quality of the established lightpaths, and CAASR monitoring.

In summary, the key contributions of this chapter are as follows.

- Efficiency of the conventional C-band spectrum provisioning algorithms is elaborately analyzed for C+L band EON.
- A deep-learning assisted QoT estimator is modeled with the robust synthetic dataset for predicting the OSNR of lightpaths as per the changes in the network dynamics with an accuracy of 99.65%.
- A quality-aware resource provisioning scheme and an algorithm under this scheme are proposed for C+L band EON to enhance the overall network capacity.
- The performance of the proposed scheme is evaluated in terms of traffic admissibility, quality of the established lightpaths, and CAASR.

The remainder of this chapter is organized as follows. Section 6.2 summarizes the related works on resource provisioning. The deep-learning framework for OSNR estimation of lightpaths is presented in Section 6.3. The efficiencies of the conventional spectrum allocation policies are analyzed in Section 6.4. Section 6.5 presents the proposed scheme, whose performance is evaluated in Section 6.5.5. Finally, Section 6.6 concludes the work.

6.2 Related Works

Generally, the choice of the spectrum allocation strategy affects the overall capacity of a network due to the variation of the continuous and contiguous spectrum slots. This section summarizes related works on spectrum provisioning along with the ML-assisted QoT estimation strategy.

6.2.1 Spectrum Provisioning without Considering PLI

Conventional spectrum allocation approaches focus on lightpath placement from one end of the spectrum. Authors in [37] started the allocation of lightpaths from the low-frequency region of the spectrum and termed it the FF allocation policy, whereas Ref. [47] followed the reverse approach and called the allocation LF. In [71], authors investigated a worst-case scenario by

making a random choice during resource allocation and termed it RF. Furthermore, to minimize the fragmentation in the network, the authors in [48], [70] reported an FLF approach, where the disjoint and non-disjoint lightpaths are allocated separately in the spectrum using FF and LF approaches, respectively. As all of these approaches consider the C band transmission with worst-case interference conditions, the effect of PLI during resource allocation is ignored.

6.2.2 Spectrum Provisioning Considering PLI

There has been a growing interest in monitoring the effect of adjacent channel interference on the signal quality after the resource allocation. Ref. [72] investigated a load-aware NLI estimation model for the C band scenario and reported a step-wise margin reduction strategy according to the load profile while considering the FF spectrum allocation. Authors in [73] started the spectrum allocation using FF and calculated the effect of aggregated interference on signal-to-interference-plus-noise ratio (SINR). These resource provisioning approaches consider the C band-only system, where the impact of NLI is significantly less compared to the MB scenario.

Recently, provisioning strategy in MB scenario has also got attention, as reported in [74]–[77]. For example, the authors in [74] considered fixed values of optical reach to model distance adaptive resource allocation strategy. However, consideration of these fixed values can not provide the highest capacity from the deployed network due to the approximated PLI assumption. In [75], authors considered multicore, multimode, and MB system, simultaneously, and proposed a ML framework for resource allocation. However, in practical scenario, the simultaneous use of all these technologies needs proper modelling of PLIs. On the other hand, band allocation algorithms are investigated during resource allocation in [76], where hard values of optical reach for different bands is considered without monitoring the evolution of PLI with traffic growth. In [77], authors also considered the band allocation step during resource allocation, but randomly considered different band preference for all the connections. Moreover, all of the above MB resource provisioning schemes considered FF spectrum allocation policy. Since, the effect of PLI on each active lightpath changes as per the growth of network traffic, the resource provisioning strategies by considering the characteristics of individual connection needs investigation.

6.2.3 Lightpath's QoT Prediction using ML

Recently, the adaptation of ML techniques for solving several complex problems of optical networks has shown a significant advantage [60]. Several authors predict the QoT using different ML frameworks, such as multi-layer perceptron (MLP)-based regressor, transfer learning, etc. For example, in [61], authors use transfer learning approaches while using synthetic dataset to mitigate the uncertainties of QoT computation in an unused network using an in-service network. The work in [62] used three regression models to predict the probability density function for the QoT of unestablished lightpaths with the aid of the synthetic dataset. On the other hand, the authors in [63] summarize several ML techniques and discuss the sources of inaccuracy in the QoT estimator, followed by the difficulty of ML training by the accurate data set in brownfield and greenfield scenarios. Moreover, a comparative study between the analytical and artificial neural network (ANN) models for QoT estimation is explored in [64]. Authors in [65] started knowledge transferring between different lightpaths having different characteristics such as nodes, modulation formats, device conditions, etc.

Overall, all of the above impairment-aware resource provisioning schemes started with a conventional baseline allocation such as FF, and later on explored several readjustment strategies, such as modulation format level reduction, alternate paths routing, and adjacent contiguous slot selection to incorporate the effect of PLI. This approach to PLI handling at the post resource

allocation stage adds extra complexity to the system and enhances the likelihood of blocking for a multi-channel system, such as MB-EON. This work proposes a resource provisioning scheme where the effect of PLI is considered prior to resource allocation. The underlying technique of the proposed scheme avoids the complexity of readjustment and prioritizes the establishment of higher-order modulation (HoM) based lightpaths by monitoring the effect of PLI during the resource allocation to enhance the overall capacity of the network.

6.3 Deep-learning Framework for OSNR Estimation

Conventionally, the quality of a lightpath in terms of OSNR is determined using two methods, namely, split-step Fourier method (SSFM) and Gaussian noise (GN) model. Although these expressions can calculate the OSNR easily at the beginning-of-life (BoL) of the network, the complexity rises when the network evolves towards the mid-of-life (MoL) or end-of-life (EoL) situations as the number of connections rises in ultra-wideband systems. The network dynamics change during progressive loading of the network due to the appearance of new demands, and their associated lightpath start impacting the OSNR of existing connections. Therefore, as the network gets filled up, the need for the OSNR re-evaluation of all existing lightpaths becomes computationally intensive. As a solution, advantage of ML techniques is leveraged and DNN-based regression model is used to predict the quality of a lightpath in a self-adaptive manner [78].

Figure 6.1 shows the architecture of the DNN-assisted QoT estimator considered, which takes different features of a lightpath and predicts the corresponding OSNR. The selection of these features is very important for accurate prediction. First, several baseline features, such as path length, number of hops, etc., [79] are taken to predict the OSNR. Then, several combinations of other features are tested to improve the prediction accuracy while capturing the effect of complex nonlinear interactions among several active channels in MB-EON. Finally, the most affecting parameters for in-line ASE noise, ROADM ASE noise, NLI are considered; and nine features of each lightpath such as the total path length, number of hops, frequency of the selected channel, number of in-line link amplifiers, intermediate ROADMS, total number of active C and L and interfering channels, channel launch power, and fill factor [14] are selected.

In addition, the modeling of the QoT estimator is developed by following several consecutive steps.

- **Training data-set generation:** First, allocation of 10,000 traffic requests is considered, where the source-destination pairs of each traffic are generated using a biased traffic matrix (as discussed in Section 6.5.5.1). The pattern of the source-destination distribution in this traffic matrix resembles the high traffic flow between special nodes of the network. Before allocating spectrum resources for each of these traffic requests, the OSNR of the corresponding lightpath at each possible position of the spectrum is calculated using the analytical closed-form expressions (as discussed in Chapter 2) and saved as the training data-set. In addition, it needs to be noted that the generated OSNR data-set for training depends on the underlying physical layer model, where several assumptions, such as uniform launch power, EDFA gain flattening, constant fiber attenuation, etc., are taken into consideration. After storing the OSNR of each lightpath for every possible position, the lightpath is finally allocated at the best OSNR-supportive position. At the end of 1% blocking, the simulator stops and provides the data of all the established lightpaths with their possible values of OSNR at the different parts of the spectrum.

- **Feature extraction:** Next, different features of individual lightpaths and their impact on the corresponding OSNR are extracted from this data set. The extracted data is split into an 80:20 ratio to train and test a DNN model.

- **Hyperparameter tuning:** Initially, the training simulation started with a baseline architecture of 3 hidden layers with 20 neurons in each. Finally, hyperparameter tuning returns a DNN model consisting of 5 hidden layers with 64 neurons per layer and the ReLU activation function in each neuron.

Figure 6.2 shows the accuracy of the calculated OSNR using DNN (termed as DNN-predicted OSNR) with the value of analytical computation (termed as Analytical OSNR) using the testing data set. In Figure 6.2, the red dashed line represents the expected accuracy of the QoT estimator, whereas the blue stars show the actual predicted values of the OSNR by the designed QoT estimator. Overall, the proposed DNN model provides an average estimation error [80] less than 0.4% (with a variance of 0.012 dB), and achieves average prediction accuracy of 99.65% .

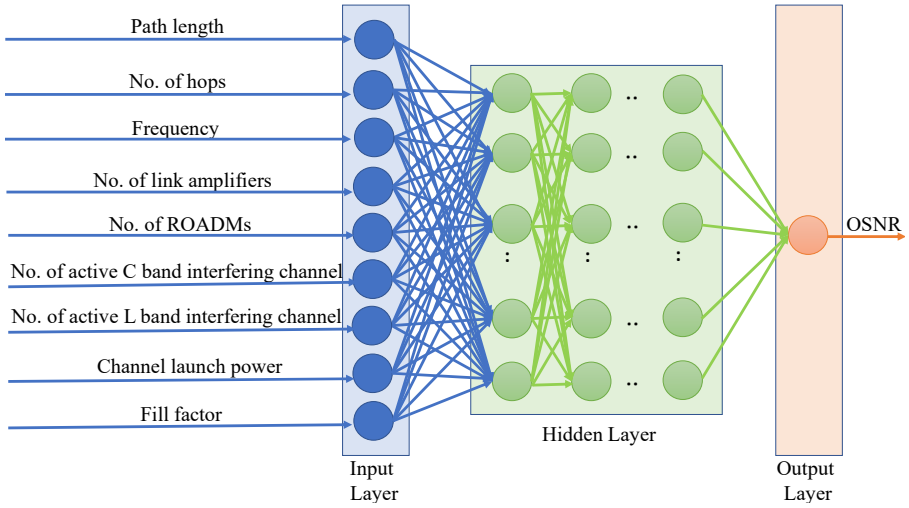

Figure 6.1: DNN-assisted QoT estimator.

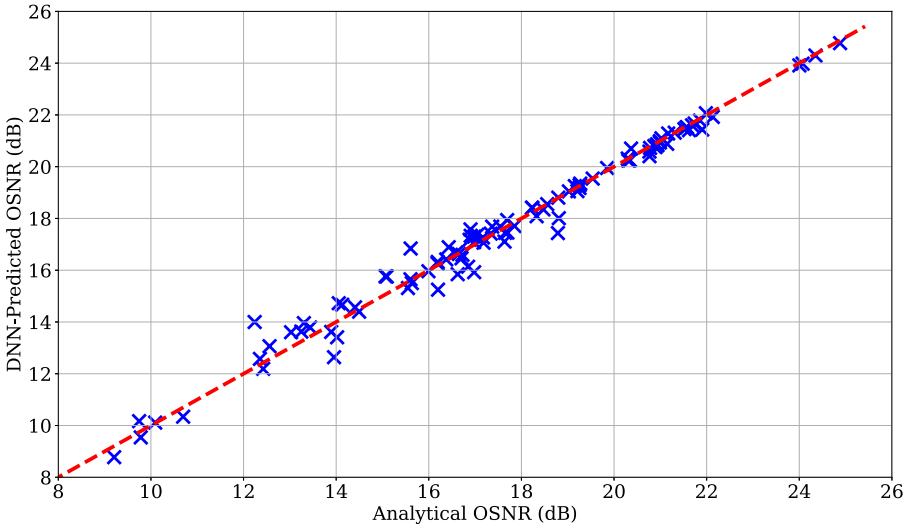

Figure 6.2: Analytical OSNR vs. DNN-predicted OSNR.

6.4 Performance Evaluation of Conventional Spectrum-Allocation Policies

Conventional RSA approaches select the shortest path for each requested demand using k-shortest paths (KSP) algorithm depending on the availability of spectral resources, while maintaining spectrum continuity and contiguity constraints. Recently, several works [13], [20], [58] upgraded the RSA problem into the RMSA problem, where the lightpath's route, spectrum, and modulation format are assigned by considering its OSNR. Algorithm 5 describes the overall flow of the RMSA operation while considering physical-layer impairments (PLI).

The algorithm starts with the search of continuous and contiguous spectrum slots in the shortest path (lines 1-2) for each requested demand, followed by the lightpath's OSNR estimation (lines 3-4). If the OSNR of the lightpath is in acceptable range, the demand is admitted into the network either using traffic grooming, or by the establishment of a new lightpath with suitable modulation format (lines 5-11). If there is no possible route for a demand with requested number of contiguous slots or if the OSNR of the lightpath for a demand in any possible route remains less than the acceptable limit, the demand is blocked (lines 12-22). At the end, the algorithm returns the traffic admissibility (number of served demands at different instances) and spectral occupancy in the overall network (lines 24-25).

6.4.1 Simulation Setup

Two geographically-diverse networks, namely BT-UK network (22 nodes, 35 links, average link length 147 km) [20], and Indian RailTel network (19 nodes, 28 links, average link length 531 km) [59] are considered for analysis. The details of these topologies are illustrated in Appendix A. Four conventional spectrum-allocation policies, namely FF, LF, FLF, and RF, are taken for comparison along with k-shortest path routing for RMSA operation. We have not considered the exact fit (EF) [34] and best fit (BF) [81] spectrum allocation policy in this study because EF policy leads to higher blocking ratio compared to FLF, whereas BF policy achieves similar performance to the FF strategy for single path routing. Two conventional launch powers (-3 dBm and -1.5 dBm) are considered in this study. The FF policy starts with the channels from the L band, whereas C band channels are taken first for the Last-Fit approach. Accumulation of 2000 (100 Gbps) static demand requests are taken while considering the dropped wavelength model and population model for traffic matrix generation in BT-UK and Indian network, respectively [20]. 30 seeds of simulations are performed in this study, and average results with approximately less than 5% margin of error at 95% confidence interval are reported.

6.4.2 Performance Evaluation

This section analyses the performance of conventional spectrum-allocation policies in terms of the following parameters:

- **Blocking Probability:** It is defined as the ratio of the number of blocked demands to the total number of requested demands in the network.
- **Traffic Admissibility:** This parameter measures the overall capacity of the network. It is defined as the number of allocated requested demands in the network till predefined thresholds. We have considered two scenarios. First, we capture the number of allocated demands until any demand block in the network, and it is named the first blocking scenario. Later on, we also recorded the number of allocated demands in the network

Algorithm 5 PLI-Aware RMSA

Input: Physical topology, Launch power, OSNR threshold for allowable modulation formats, Traffic matrix, k-shortest paths for each demand, Spectrum-allocation policy;
Output: Traffic admissibility, Spectrum occupancy;
Initialisation: $k = 1$, Number of Blocked demands = 0

```
for each demand in the traffic matrix do
    Check availability of continuous and contiguous spectrum slots in route k as per the
    spectrum-allocation policy;
    if (spectrum availability == True) then
        Calculate OSNR using Eqn. (2.7);
        if (OSNR ≥ acceptable threshold) then
            Check the possibility of traffic grooming into existing lightpaths;
            if (grooming possibility == True) then
                Groom the demand into higher-capacity lightpath;
            else
                Establish a lightpath to admit the demand in the network, while choosing a suit-
                able modulation formats as per Table 6.1 (from [13]);
            end if
        else
            k += 1;
            if (k > maximum possible link disjoint shortest path) then
                Number of Blocked demands += 1;
            else
                Go to Step 2;
            end if
        end if
    else
        Go to Step 13;
    end if
end for
Calculate spectral occupancy of each link;
Calculate traffic admissibility in the network;
```

till 1% of the requested demands were blocked in the network. The latter condition is referred to as a 1% blocking scenario in the subsequent sections.

- **Resource Utilization:** It is defined as the ratio of the total number of occupied slots to the total number of slots in the network.
- **CAASR:** It is calculated as the difference between unity and network's fragmentation [82]. The details of CAASR calculation are elaborately discussed in section 5.6.
- **Quality of Established Lightpaths:** It is measured in terms of assigned modulation formats (BPSK, QPSK, PM-8QAM, PM-16QAM, PM-32QAM, PM-64QAM), and its associated OSNR threshold is given in Table 6.1.

Figures 6.3 and 6.4 show the variation of the blocking probability with traffic load (number requested demand), while considering a uniform channel launch power of -3 dBm, for BT-UK and Indian networks, respectively. We observe that the Last-Fit policy performs best compared to the other policies in both networks. In the C+L band system, the Last-Fit policy starts with filling of C band channels where link attenuation, amplifier noise figures (NF), and NLI

Table 6.1: Quality of lightpaths for 28 GBaud system [13].

Modulation	Data Rate (Gbps)	OSNR Threshold (dB)
PM-BPSK	50	9
PM-QPSK	100	12
PM-8QAM	150	16
PM-16QAM	200	18.6
PM-32QAM	250	21.6
PM-64QAM	300	24.6

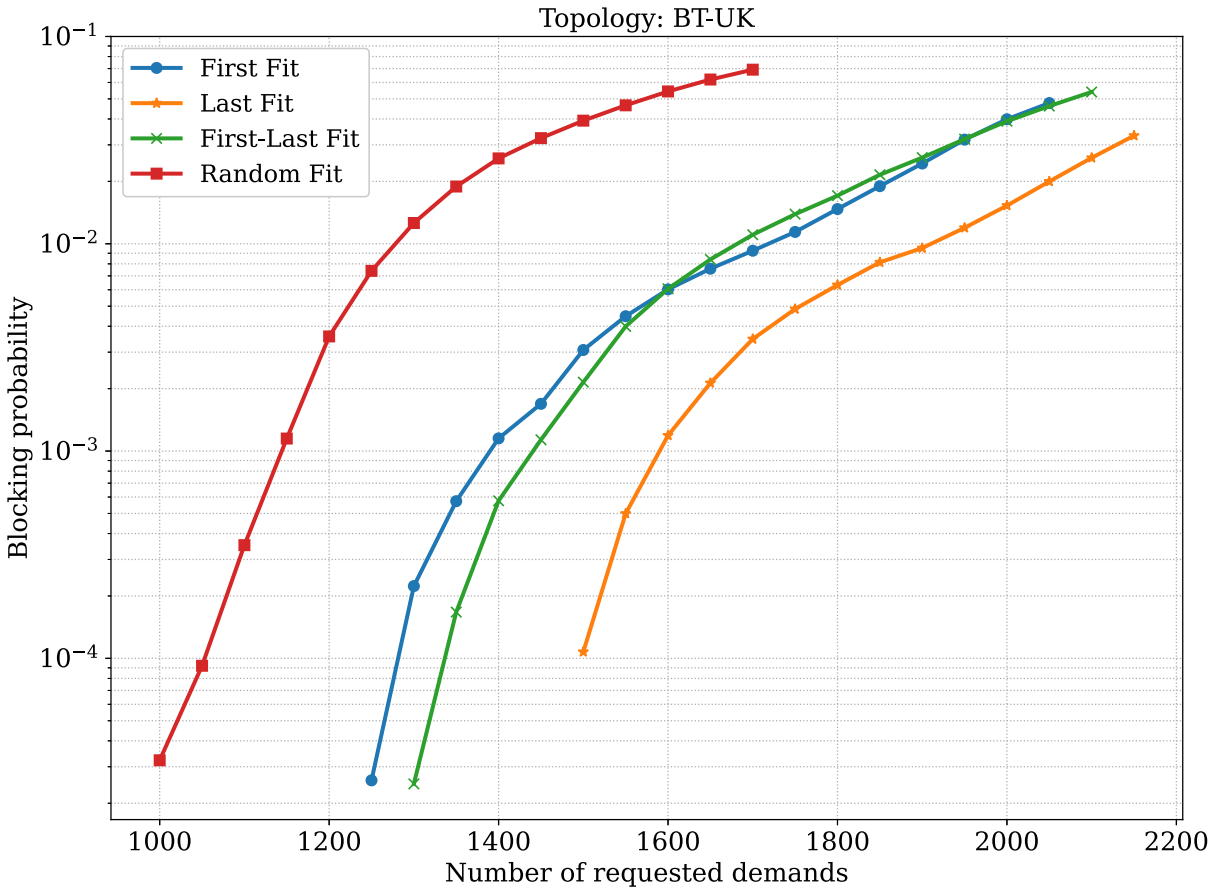

Figure 6.3: Blocking probability vs. traffic load in BT-UK network.

effect are lower compared to the other end of the spectrum. Thus, the Last-Fit policy leads to higher OSNR of lightpaths and hence higher capacity in the network.

Tables 6.2 and 6.3 capture the traffic admissibility (with launch power of -1.5 and -3 dBm) in terms of number of served demands at the instance of 1% blocking and first blocking, respectively, in the BT-UK network, whereas Tables 6.4 and 6.5 show the same information for the Indian network. Numerical data shows that, in terms of number of served demands at 1% blocking with -3 dBm launch power, Last-Fit policy achieves approximately 10%, 12.5%, and 46.6% gain in BT-UK network compared to First Fit, First-Last Fit, and Random Fit, respectively, whereas in Indian network, these gain becomes 25%, 128%, and 99%.

Figures 6.5 and 6.6 show the variation of resource utilization with the spectrum-allocation polices in the BT-UK and Indian network, respectively, whereas Figures 6.7 and 6.8 capture

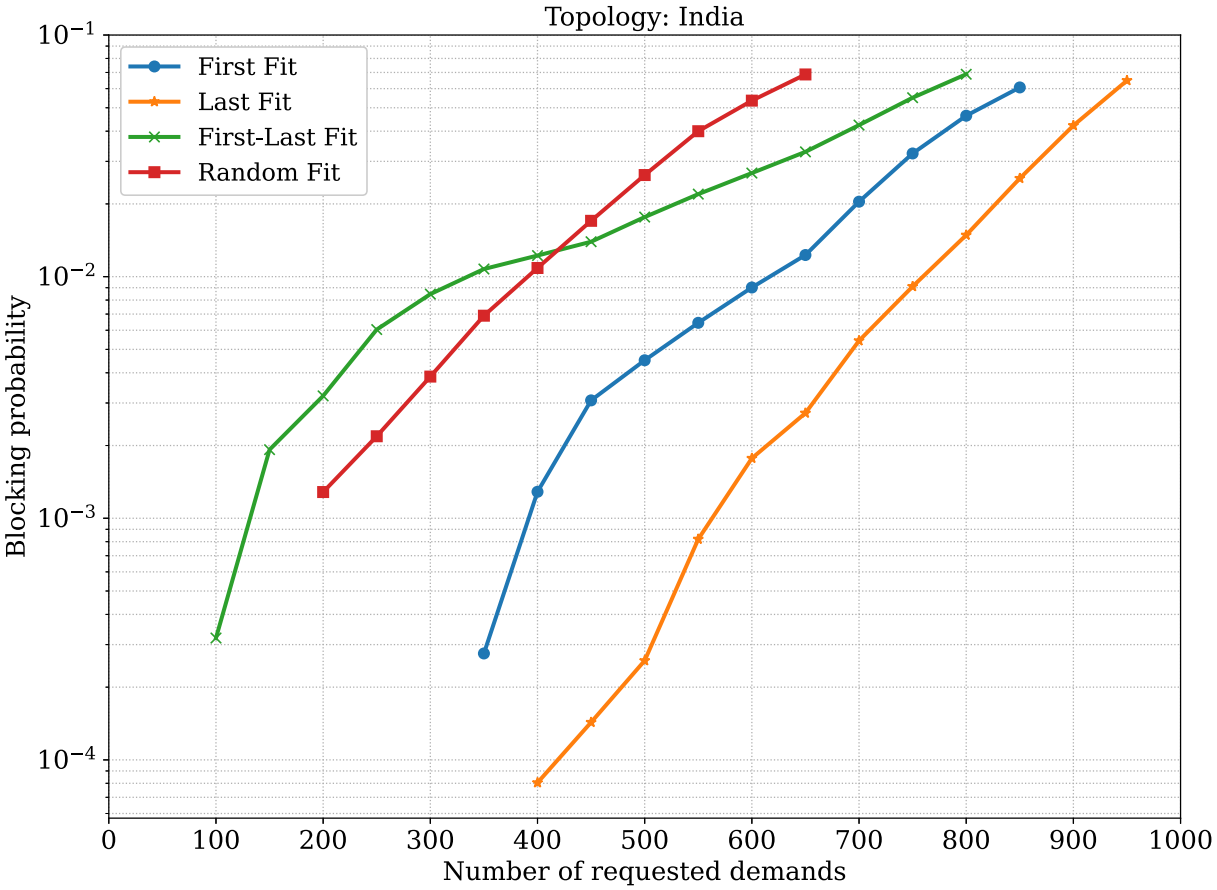

Figure 6.4: Blocking probability vs. traffic load in Indian network.

Table 6.2: Number of served demands at 1% blocking for BT-UK network.

Allocation Policy	**Launch Power (dBm)**	**Served Demands**
First Fit	-3	1722
Last Fit	-3	1894
First-Last Fit	-3	1683
Random Fit	-3	1292
First Fit	-1.5	1562
Last Fit	-1.5	1850
First-Last Fit	-1.5	1503
Random Fit	-1.5	1376

the condition of network fragmentation in terms of CAASR for the two networks. Simulation results show that the allocation of lightpaths using Last-Fit policy leads to higher spectrum utilization and lower fragmentation (higher CAASR). Moreover, the drastic reduction of the availability of contiguous slots is captured for Random Fit in Figs. 6.7 and 6.8, i.e., as expected, random spectrum allocation leads to a fragmented network with least capacity, higher blocking, and lower resource utilization.

The variation of the quality of lightpaths till 1% blocking (with launch power of -3 dBm) for BT-UK and Indian network is captured in Figs. 6.9 and 6.10, respectively. Results show

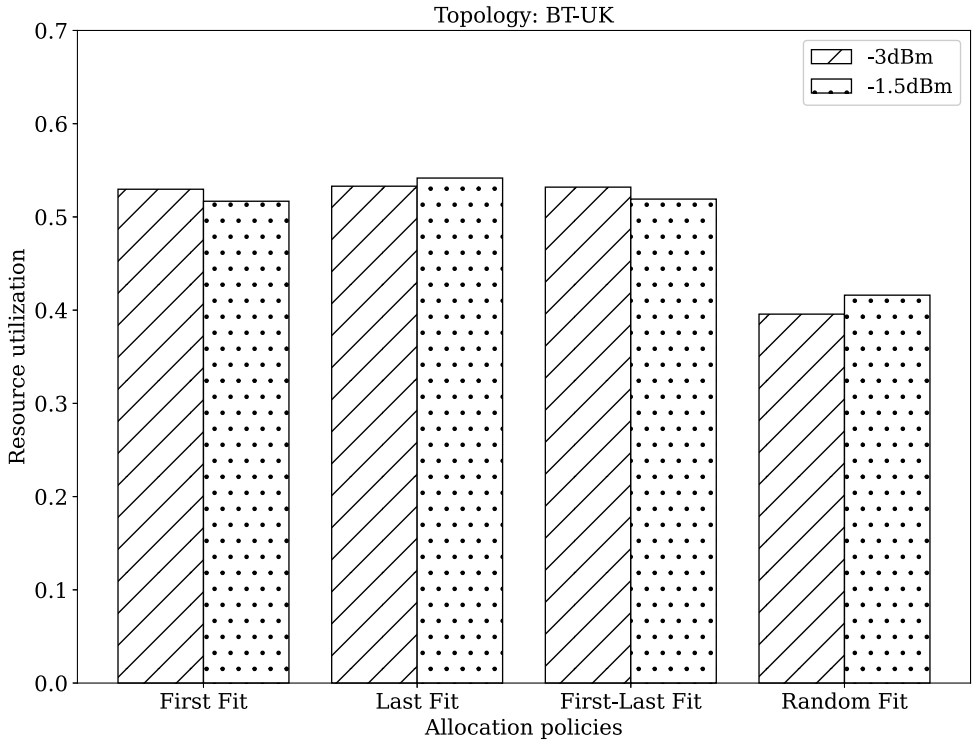

Figure 6.5: Resource utilization in BT-UK network.

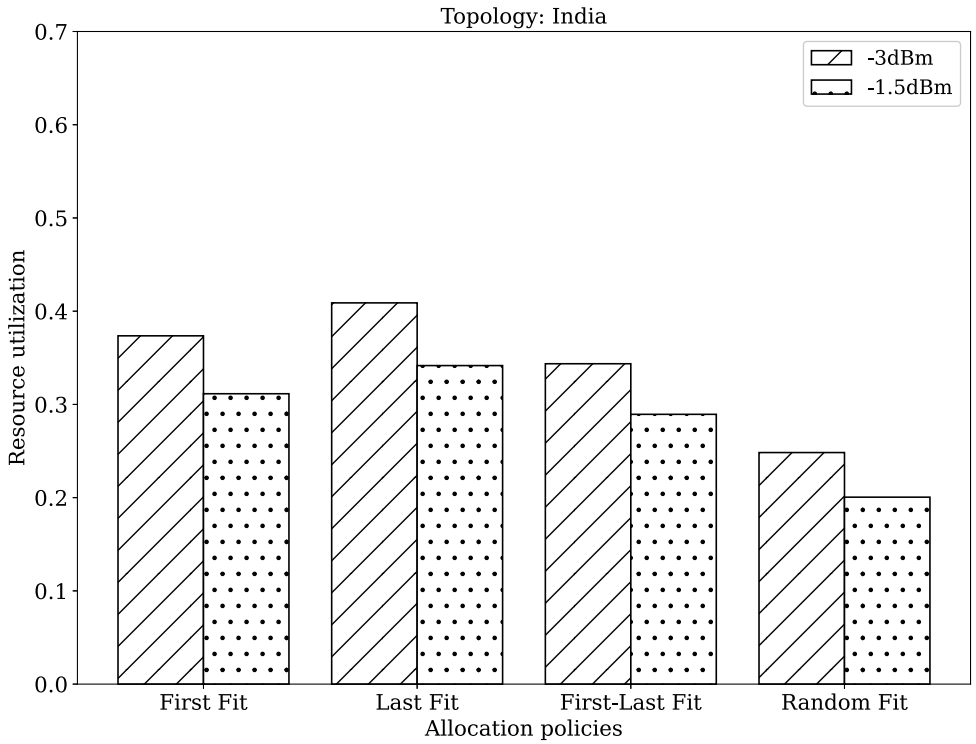

Figure 6.6: Resource utilization in Indian network.

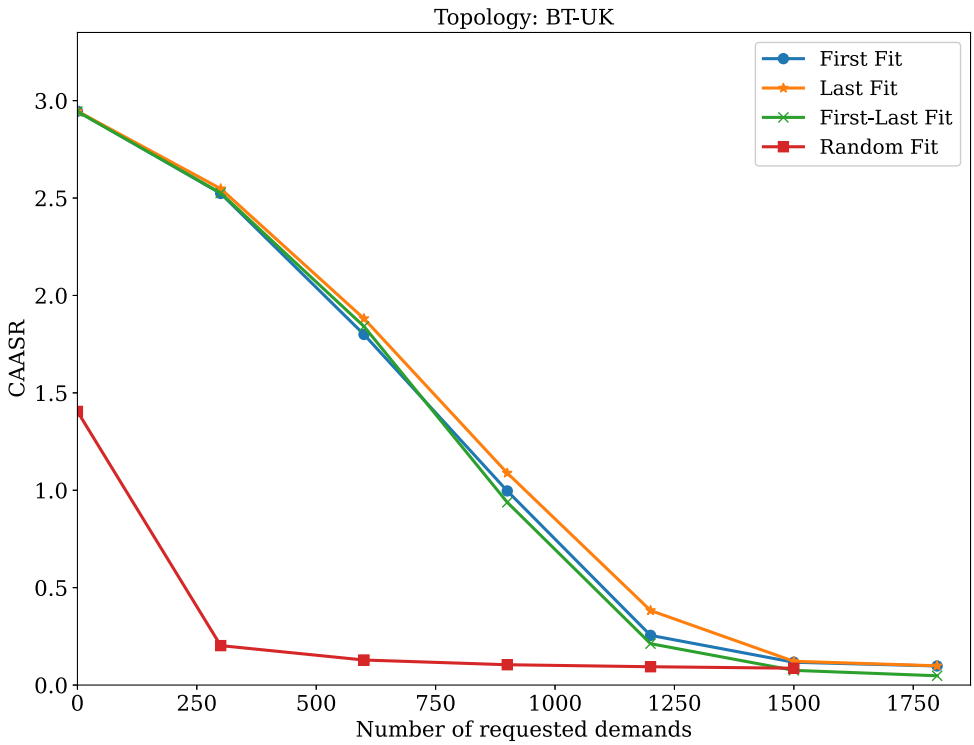

Figure 6.7: CAASR in BT-UK network.

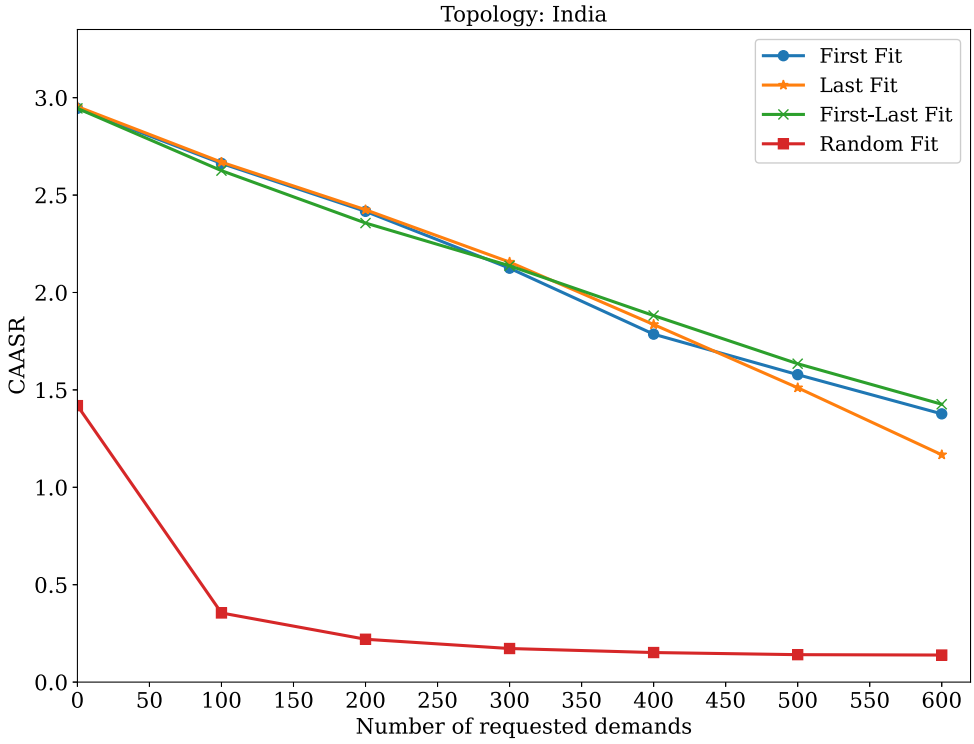

Figure 6.8: CAASR in Indian network.

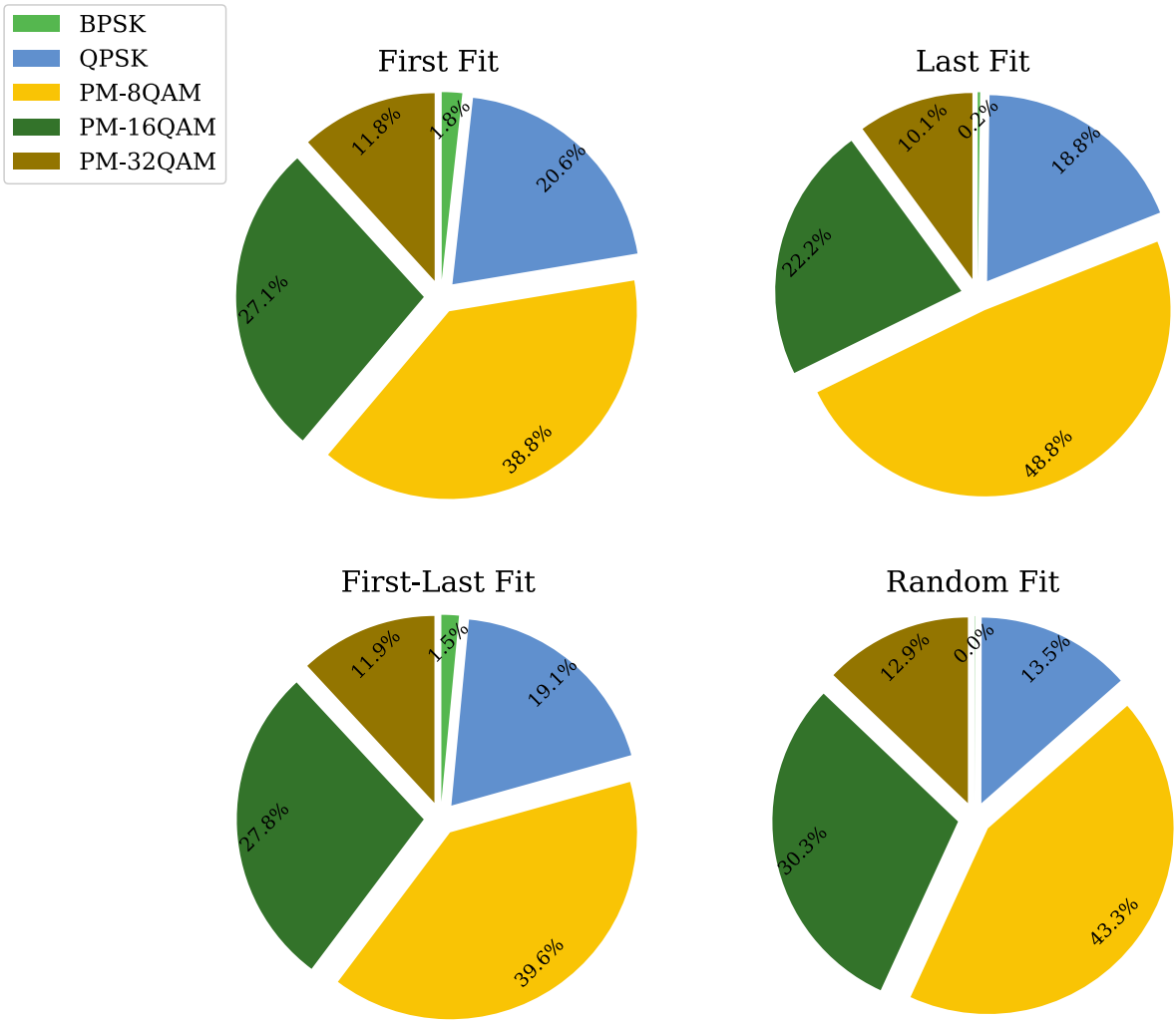

Figure 6.9: Quality of lightpaths in BT-UK network.

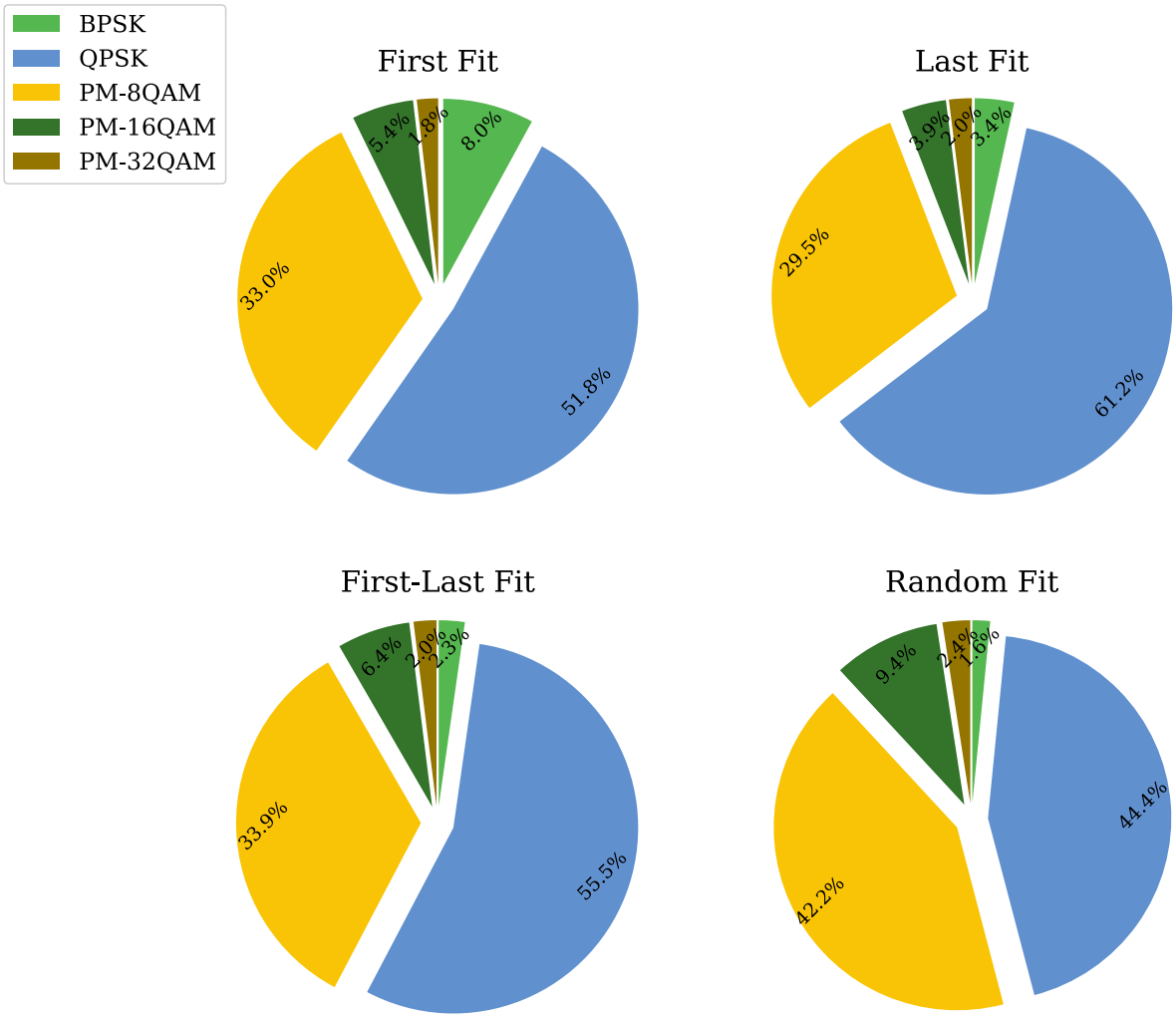

Figure 6.10: Quality of lightpaths in Indian network.

Table 6.3: Number of served demands at first blocking for BT-UK network.

Allocation Policy	Launch Power (dBm)	Served Demands
First Fit	-3	1335
Last Fit	-3	1568
First-Last Fit	-3	1406
Random Fit	-3	1145
First Fit	-1.5	1163
Last Fit	-1.5	1553
First-Last Fit	-1.5	1215
Random Fit	-1.5	1104

Table 6.4: Number of served demands at 1% blocking for Indian network.

Allocation Policy	Launch Power (dBm)	Served Demands
First Fit	-3	608
Last Fit	-3	761
First-Last Fit	-3	334
Random Fit	-3	382
First Fit	-1.5	498
Last Fit	-1.5	609
First-Last Fit	-1.5	238
Random Fit	-1.5	309

Table 6.5: Number of served demands at first blocking for Indian network.

Allocation Policy	Launch Power (dBm)	Served Demands
First Fit	-3	419
Last Fit	-3	593
First-Last Fit	-3	218
Random Fit	-3	274
First Fit	-1.5	382
Last Fit	-1.5	490
First-Last Fit	-1.5	168
Random Fit	-1.5	236

that Last-Fit policy can place maximum number of higher-order modulation (HOM)-based lightpaths, which include PM-8QAM, PM-16QAM, PM-32QAM and PM-64QAM for a smaller geography, such as BT-UK. However, for a larger geography, such as India, dominance of lower-order modulation (LOM) lightpaths is observed, which includes BPSK and QPSK modulations, due to presence of longer links, large ASE noise, and low OSNR of the lightpaths.

6.5 Quality-Aware Resource Provisioning Scheme

6.5.1 Overview

Conventional approaches to resource provisioning either consider the allocation from one end of the spectrum or provision the spectrum based on the lightpath's route or distance. However, for MB-EON, the overall capacity of the network depends on the quality of individual established lightpaths, which can vary based on the choice of spectrum selection. This section describes the proposed scheme, which prioritizes the placement of high-quality lightpaths in the network during resource allocation to achieve high network capacity in the long run.

6.5.2 Model and Assumptions

We assume that all of the links in the network are operating across the C+L band, where an equal number of spectrum slots are considered in each link. As the spectral occupancy in the network changes with the progressive traffic allocation, the QoT of all existing lightpaths is updated by considering the physical layer model as discussed in Chapter 2. Moreover, the possibility of traffic grooming is considered by adjusting the establishment of the small-capacity-based lightpaths using large-capacity-based lightpaths to save spectrum resources for future traffic growth [13].

6.5.3 Concept Illustration of the Proposed Scheme

To illustrate our concept, we consider a sample four-node network with an average link length of 224 km, as shown in Fig. 6.11. Mainly, five sequential requests (r_1, r_2, r_3, r_4, r_5) are considered and their shortest route with corresponding path length are given in the adjacent table. Four conventional approaches, namely FF, LF, route adaptive first-last-fit (RA-FLF), and distance adaptive first-last-fit (DA-FLF), are considered; and their associated spectrum allocation is shown in Fig. 6.12. Generally, FF starts the allocation from the lower channel index region, whereas LF follows the reverse approach. RA-FLF places disjoint lightpaths using the FF approach and non-disjoint lightpaths using the LF approach. DA-FLF policy places longer lightpaths (if the path length is greater than the average link length) in the high channel index region and shorter lightpaths in the low channel index region.

Overall, all of these baseline approaches allocate the spectrum without concern about the effect of channel selection on the quality of lightpaths. Typically, each channel in MB-EON has different characteristics, which may create variation in the QoT of a lightpath. As shown in Fig. 6.12, lower index channels belong to the L band, where the impact of NLI becomes larger due to the presence of the ISRS power transfer (as shown by the arrow). On the other hand, the high NF (6 dB, [83]) of in-line L band-amplifiers raises the ASE noise power compared to the high-frequency channels of the C band. Since QoT of a lightpath depends on the value of NLI and ASE noise, the proper selection of a channel for a specific lightpath can enhance its OSNR and also boost the network capacity. To achieve this, a quality-aware resource provisioning scheme and its associated algorithm, namely OA-FLF, is proposed in next subsection to execute the routing, modulation, band, and spectrum allocation (RMBSA) for each traffic demand. The key objective of the proposed scheme targets the enhancement of the individual lightpath's quality to achieve high network capacity in the long run.

6.5.4 Proposed OA-FLF Algorithm

Figure 6.13 shows the pattern of spectrum filling using the OA-FLF algorithm for the same sample network and traffic requests. The key objective of this algorithm is to allocate the

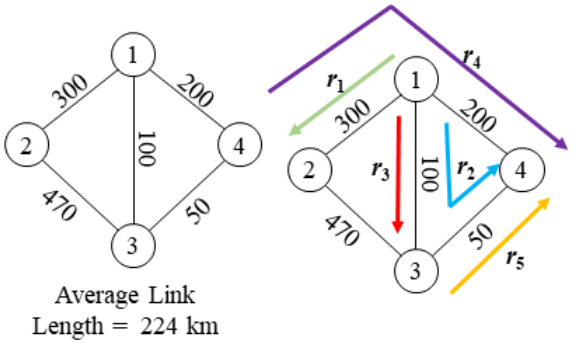

Requests	S-D pairs	Shortest Route	Distance (km)	FF	LF	RA-FLF	DA-FLF
r_1	1 - 2	1 ➔ 2	300	Ch_1	Ch_{10}	Ch_1	Ch_{10}
r_2	1 - 4	1 ➔ 3 ➔ 4	150	Ch_1	Ch_{10}	Ch_1	Ch_1
r_3	1 - 3	1 ➔ 3	100	Ch_2	Ch_9	Ch_{10}	Ch_2
r_4	2 - 4	2 ➔ 1 ➔ 4	500	Ch_2	Ch_9	Ch_{10}	Ch_9
r_5	3 - 4	3 ➔ 4	50	Ch_2	Ch_9	Ch_{10}	Ch_2

Figure 6.11: Physical topology and traffic demands.

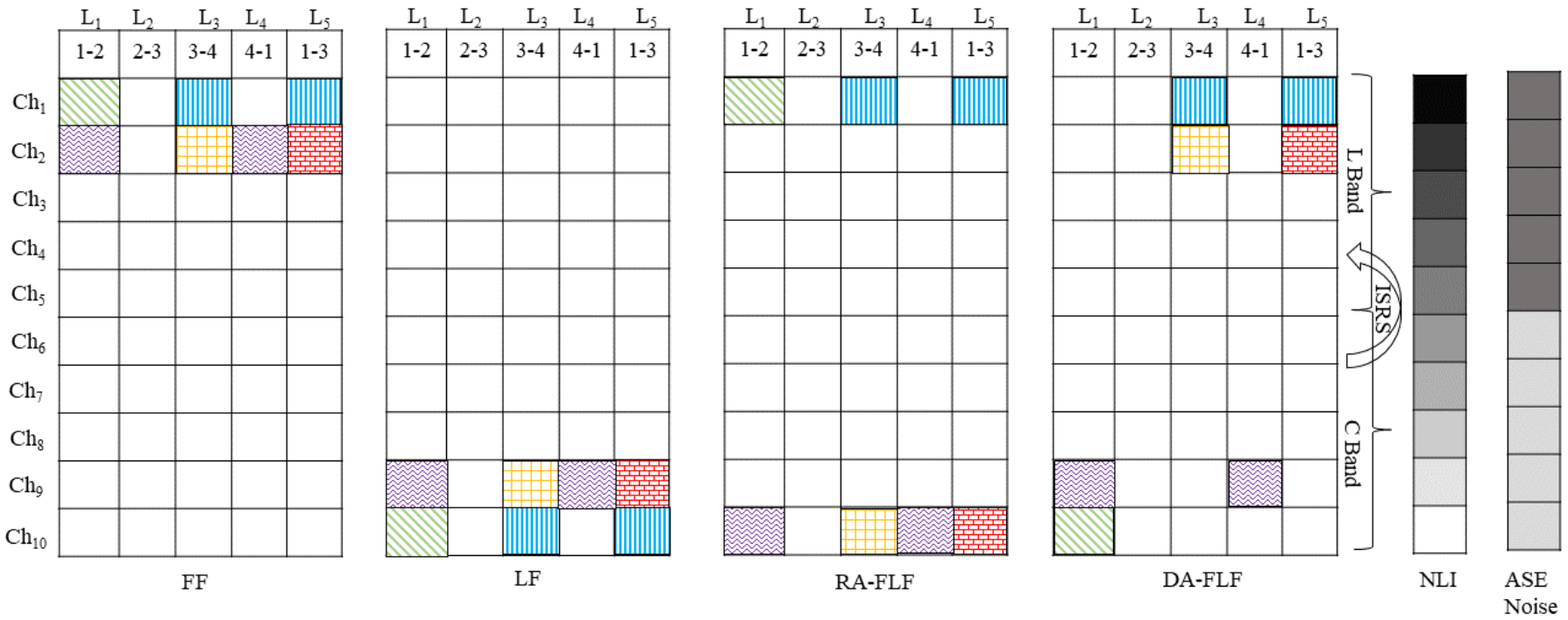

Figure 6.12: Spectrum allocation in FF, LF, RA-FLF, and DA-FLF.

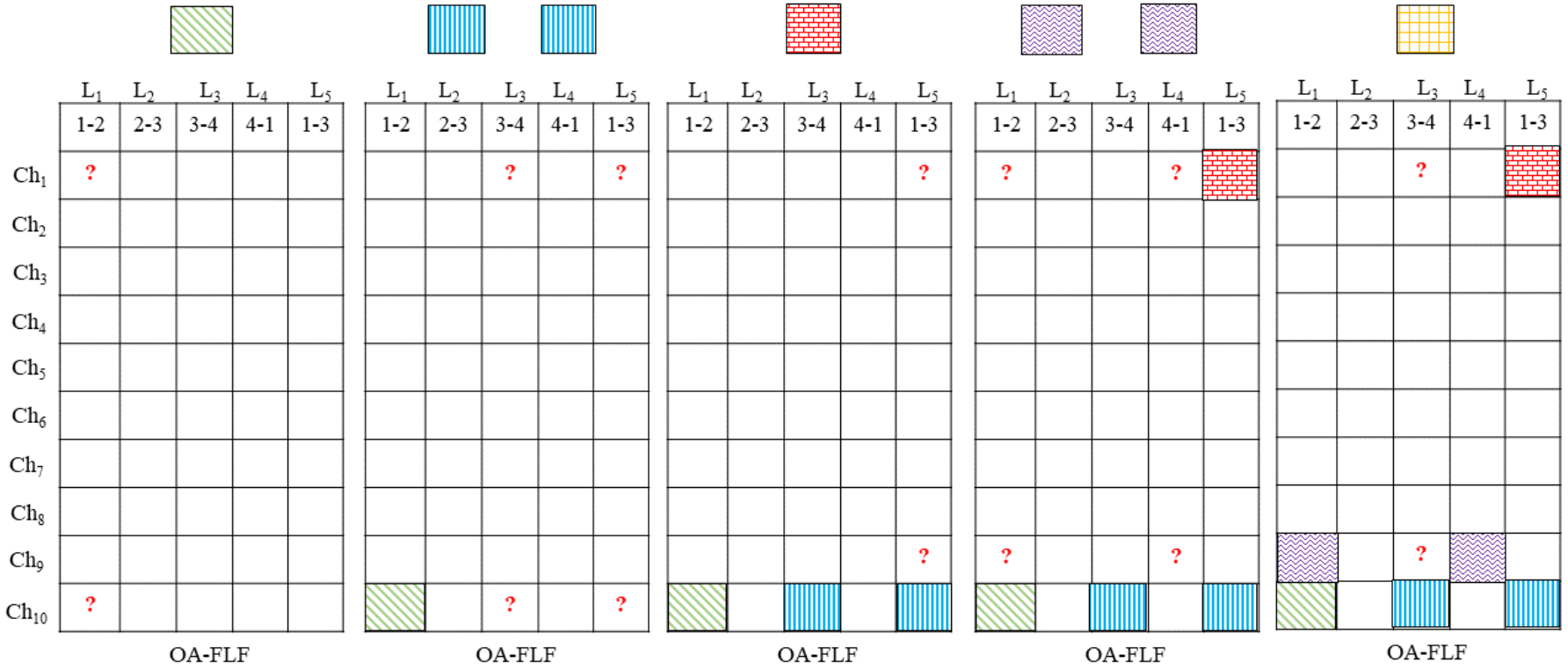

Figure 6.13: Spectrum allocation in OA-FLF.

spectrum for a lightpath at the best OSNR-supportive position while maintaining the filling of the spectrum in a contiguous manner (to reduce fragmentation). One-by-one demands are provisioned in the network using the lightpath while searching for the best OSNR-supportive position at the two ends of the spectrum. The red question mark in Fig. 6.13 at each stage shows the choice of spectrum allocation available for a particular request at each stage to maintain the contiguous filling rule. Among the available free channels at the lowest and highest index positions of the spectrum, the lightpath is allocated using only that channel which can provide the best OSNR. Table 6.6 summarizes the notations of the given parameters, decision variables, and functions, which are elaborately used in the proposed algorithm.

Algorithm 6 starts by taking several inputs, such as network topology, traffic matrix, channel launch power, OSNR threshold, trained DNN model, and the maximum number of the allowable shortest paths. Initially, before starting the allocation, traffic admissibility and the number of blocked demands are set at zero, whereas the binary variable for the possibility of traffic grooming is set as False for any request. Other sets such as spectrum occupancy and list of all lightpaths do not contain any elements before the start of any allocation.

At the beginning of the allocation of each request, the possibility of traffic grooming into existing lightpaths is explored using the function TG (lines 1-9). Generally, when the list of lightpaths is not empty, the TG function takes the current demand request and information of ongoing lightpaths as input (lines 2-3). As an output, it returns the location of possible traffic grooming. Mainly, if there is spare capacity in the existing lightpath L_{TG} to allocate the current request t, the binary variable related to the possibility of traffic grooming (${P_{TG}}^t$) is updated as True (line 4), and requested demand t is allocated using lightpath L_{TG} (line 7).

On the other hand, if grooming is not possible for a particular request, the CRSA function is used to check the availability of the spectrum slot for a new lightpath establishment (line 11). It takes the information of network topology, demand information, and index of the shortest path as input; and returns the availability of continuous and contiguous free spectrum slots in the possible route R_k. If there are available slots (i.e., ACCSS = True), all of the corresponding frequency indexes are extracted using the function GAF (line 14). Hence, the other two functions, namely FFA and LFA, are used to determine the positions of the lowest index and highest index of the free slots in the spectrum (lines 15-16). Consequently, the OSNR of the lightpath at these two positions is predicted using the trained DNN model while taking several input features such as channel power, frequency of operation, spectrum occupancy, etc (lines 17-18). Furthermore, these two OSNRs are compared to provision lightpaths at the highest OSNR-based position (lines 19-24). If both of the available frequencies provide OSNR less than O_{Th}, then an alternate path needs to be explored for lightpath establishment (line 32). After exhausting all the alternate shortest paths (till k_{max}), if the algorithm does not find any sufficient available free spectrum for a demand in any of the routes or the estimated OSNR of the lightpath for a demand becomes less than the acceptable limit in all the considered paths, the demand is blocked (lines 33-41).

6.5.5 Performance Evaluation

This section explains the simulation framework, followed by the computational gain of the DNN-assisted QoT estimator. Then, the advantage of the proposed algorithm compared to the baseline algorithms is discussed.

6.5.5.1 Simulation Framework

This section describes the simulation setup for analyzing the performance of the proposed scheme. An event-driven, custom-built Python simulator is designed to implement all of the

Table 6.6: List of notations for different given parameters, decision variables, sets, and functions used in the algorithm.

Notation	Description
	Given Parameters:
$G(V, E)$	Network topology; V = set of nodes, E = set of links.
T	Traffic matrix.
P_{Ch}	Launch power of each channel.
O_{Th}	OSNR threshold for allowable modulation formats.
T_{DNNM}	Trained deep neural network model.
k_{max}	Maximum number of allowable shortest paths for each demand.
	Decision Variables:
k	Index of the shortest path $\in \mathbb{N}$.
T_A	Traffic admissibility $\in \mathbb{W}$.
N_B	Number of total blocked demands $\in \mathbb{W}$.
${P_{TG}}^t$	Possibility of traffic grooming for demand request $t \in$ {True, False}.
L_{TG}	Location of traffic grooming.
R_k	Route for the k^{th} shortest path.
$ACCSS$	Availability of continuous and contiguous spectrum slots $\in$ {True, False}.
$F_{Available}$	Available frequencies.
f_l	Available lower-index frequency.
f_h	Available higher-index frequency.
$OSNR_{f_l}$	OSNR at lower-index frequency.
$OSNR_{f_h}$	OSNR at higher-index frequency.
$M_{OSNR_{f_l}}$	Modulation format according to OSNR at lower-index frequency
$M_{OSNR_{f_h}}$	Modulation format according to OSNR at higher-index frequency.
	Sets:
S_O	Spectrum occupancy.
L_{All}	Set of all ongoing lightpaths.
	Functions:
TG	Traffic grooming.
CRSA	Check route and spectrum availability.
GAF	Get available frequencies.
FFA	First fit availability.
LFA	Last fit availability.

Algorithm 6 OA-FLF algorithm for MB-EON

Input: $G(V, E)$, T, P_{Ch}, O_{Th}, T_{DNNM}, k_{Max};
Output: T_A, N_B, S_O;
***Initialisation*:** $k = 1$, $T_A = 0$, $N_B = 0$, $S_O = \{\emptyset\}$, $L_{All} = \{\emptyset\}$, ${P_{TG}}^t$ = False;

1: **for each** demand request t in T sequentially **do**
2: **while** $L_{All} \neq \{\emptyset\}$ **do**
3: $L_{TG} \leftarrow$ TG(t, L_{All});
4: Update ${P_{TG}}^t$;
5: **end while**
6: **if** (${P_{TG}}^t$ == True) **then**
7: Allocate demand request t using L_{TG};
8: $T_A = T_A + 1$;
9: Update S_O, L_{All};
10: **else**
11: R_k, ACCSS $\leftarrow$ CRSA($G(V, E)$, t, k);
12: **if** (ACCSS == True) **then**
13: Pause CRSA for next demand request
14: $F_{Available} \leftarrow$ GAF(ACCSS, S_O, R_k);
15: $f_l \leftarrow$ FFA($F_{Available}$);
16: $f_h \leftarrow$ LFA($F_{Available}$);
17: $OSNR_{f_l} \leftarrow T_{DNNM}(t, R_k, P_{Ch}, f_l \in F_{Available}, S_O)$;
18: $OSNR_{f_h} \leftarrow T_{DNNM}(t, R_k, P_{Ch}, f_h \in F_{Available}, S_O)$;
19: **if** $(OSNR_{f_l} \geq O_{Th})$ **and** $(OSNR_{f_h} \geq O_{Th})$ **then**
20: **if** $OSNR_{f_l} \geq OSNR_{f_h}$ **then**
21: Select $M_{OSNR_{f_l}}$, Occupy f_l;
22: $T_A = T_A + 1$;
23: Update S_O, L_{All};
24: Resume CRSA for next demand request
25: **else**
26: Select $M_{OSNR_{f_h}}$, Occupy f_h;
27: $T_A = T_A + 1$;
28: Update S_O, L_{All};
29: Resume CRSA for next demand request
30: **end if**
31: **else**
32: $k = k + 1$;
33: **if** $(k > k_{Max})$ **then**
34: $N_B = N_B + 1$;
35: Resume CRSA for next demand request
36: **else**
37: Try reallocation by following Step 11-29;
38: **end if**
39: **end if**
40: **else**
41: Check the next shortest path and try reallocation by following step 32-37;
42: **end if**
43: **end if**
44: **end for**

baselines and the proposed algorithm; and all of the reported results are generated using Intel(R) Xeon(R) Gold 5220 CPU @ 2.20 GHz and Intel(R) Xeon(R) CPU E5-2670 v2 @ 2.50 GHz with 264 cores and 96 GB of memory. Simulations are focused on two geographically diverse core networks, namely, the BT-UK network (22 nodes, 35 links, average link length 147 km) and the 24-node USA network (24 nodes, 43 links, average link length 991 km). The details of these topologies are illustrated in Appendix B. It is assumed that the same fiber, namely ITU-T G.652.D, is used for both the networks where the fiber attenuation coefficient is considered as 0.2 dB/km for both C and L bands. In addition, dispersion, Raman, and non-linear coefficients are assumed to be same as [12]. Moreover, a total of 10 THz optical bandwidth in each fiber is considered for the C+L band transmission. In addition, to mimic the high traffic flow between special nodes of these networks, a biased traffic matrix is considered for selecting the source-destinations pairs probabilistically. For BT-UK network, this matrix is generated using the dropped wavelength data [20], whereas the gravity model [84] is used for the same purpose in case of 24-node USA network. Moreover, the network is progressively loaded with 100 Gbps static demand requests [14], where for each demand k-shortest path (k=3) routing is taken into consideration. Although only 100 Gbps data rate based requests are considered for the current study, variable data-rate based demands can also be allocated into the network using traffic grooming. Traffic requests with path lengths greater than 7500 km are avoided during the biased traffic generation since the QoT of the lightpath becomes unacceptable due to high ASE noise. The signal bandwidth (B_Z) and B_{ref} are considered same as 37.5 GHz which is nearly equal to the considered baud rate of the system (28-32 Gbaud). Average results of 20 seeds are reported at 95% confidence interval with less than 5% margin of error for two cases with uniform channel launch power (-3 dBm and -1.5 dBm).

6.5.5.2 Computational Gain using QoT Estimator

The key purpose of the DNN-based QoT estimation is the reduction of computational time compared to the complex analytical approach while ensuring a similar capacity at the end of the simulation. Figure 6.14 compares the analytical approach with the ML technique in terms of the computational time (in minutes) and the number of allocated demands till 1% blocking for the OA-FLF resource allocation algorithm. Reported result shows the DNN-based approach can provide 96.6% and 96.5% computational gain (in minutes) in the BT-UK network for uniform channel launch power of -3 dBm and -1.5 dBm, whereas this gain becomes 96.92% and 96.94% for 24-node USA network.

To account for the effect on the end capacity using these two approaches, we define a metric, called normalized accuracy, as the ratio of the number of allocated demands with the computational time. For BT-UK, the value of normalized accuracy becomes 177.9 and 6.09 for -3 dBm launch power using DNN and analytical approach, respectively, whereas these numbers become 71.4 and 2.4 for the USA network. This data indicates that the DNN method of OSNR estimation can provide a significant gain in terms of computation time reduction compared to the analytical approach while ensuring a similar capacity of the network. Therefore, instead of analytical calculation, the results of the proposed algorithm with the DNN-assisted approach are considered in the subsequent sections of this work.

6.5.5.3 Traffic Admissibility Analysis

The performance of the proposed quality-aware resource allocation algorithm on the overall network capacity is evaluated in terms of traffic admissibility till 1% blocking.

Figure 6.15 shows the advantage of the proposed algorithm compared to the baseline algorithms in terms of traffic admissibility for the two considered geographies with two uniform channel launch powers. For smaller geographies, such as the BT-UK network, the availability of

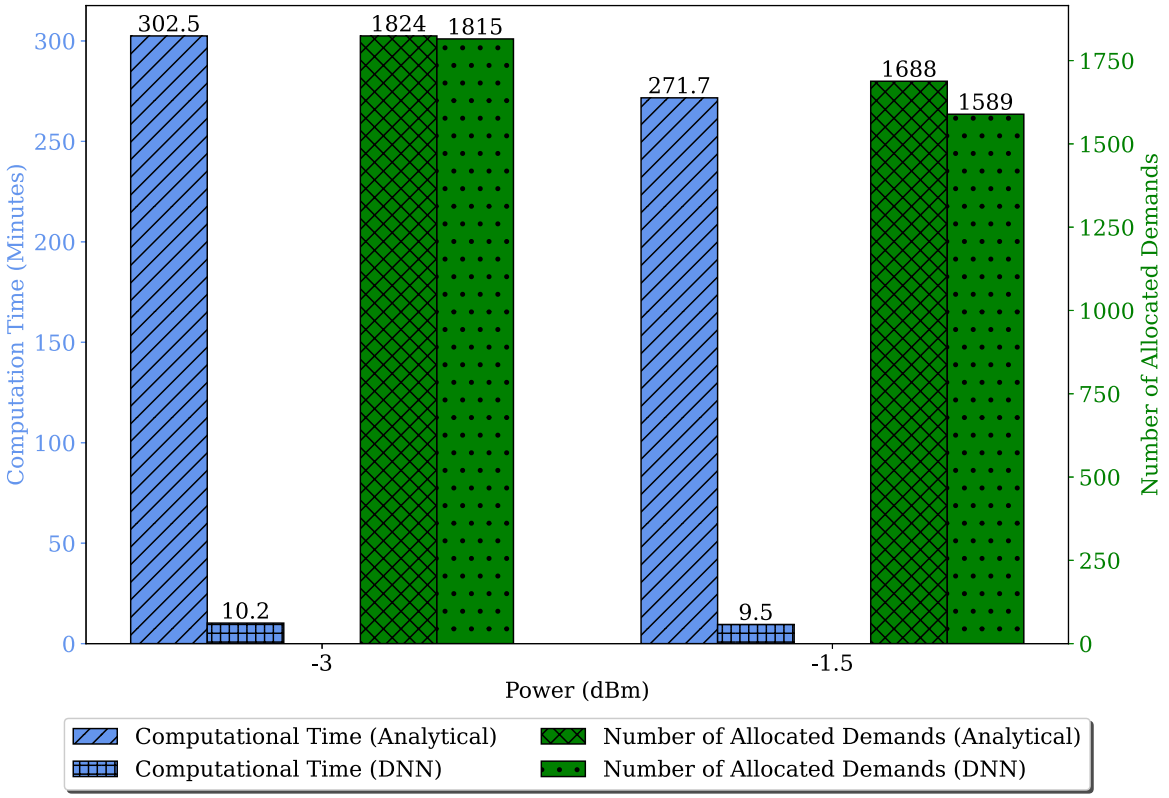

(a) Topology: BT-UK network.

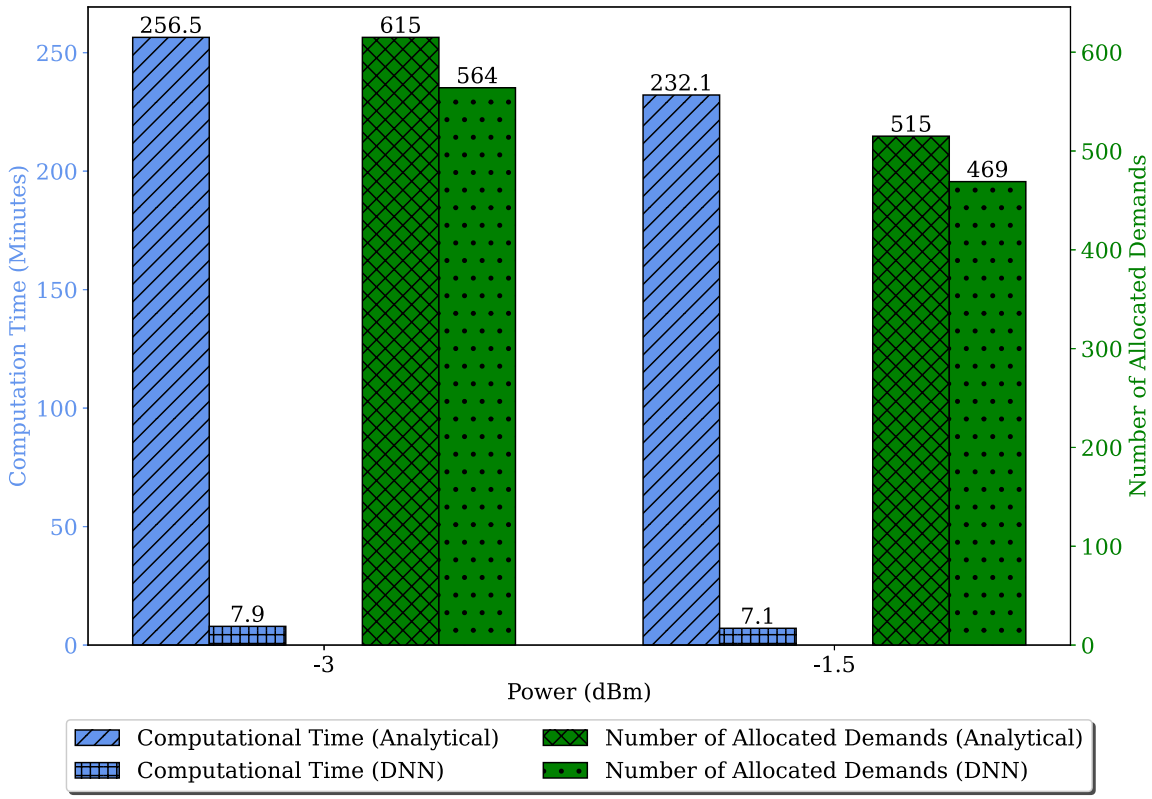

(b) Topology: 24-node USA network.

Figure 6.14: Computational gain using QoT estimator for the proposed algorithm

high-quality lightpaths (such as PM-8QAM, PM-16QAM, PM-32QAM) enhances the chances of traffic grooming by utilizing the surplus capacity of existing lightpaths in the network. As a

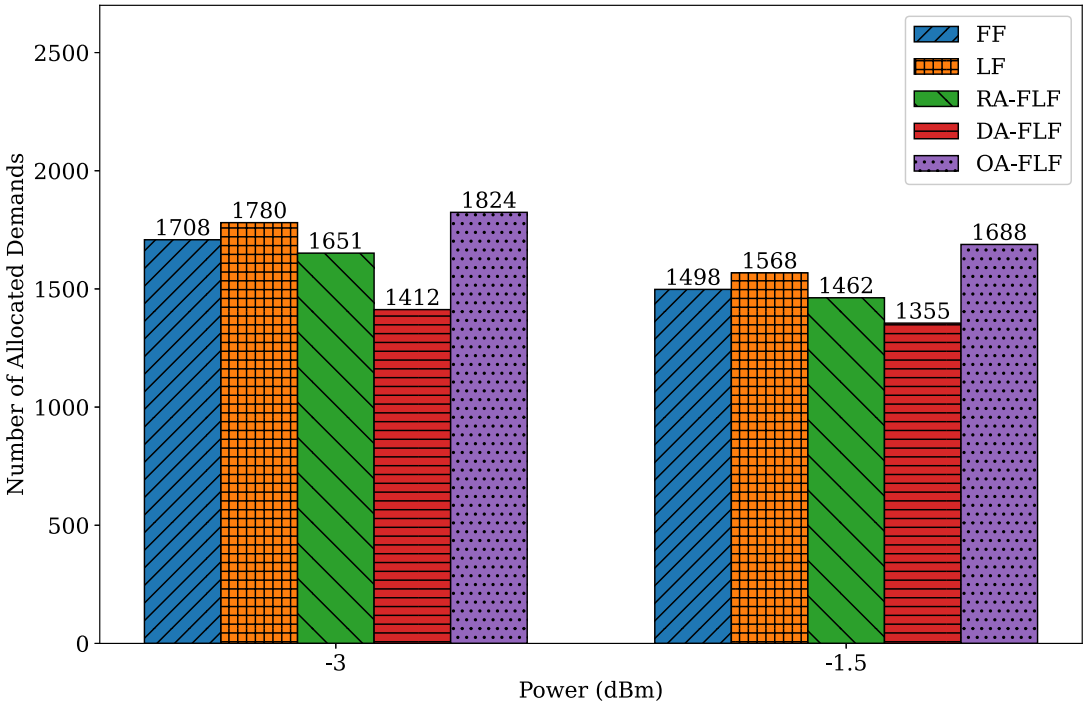

(a) Topology: BT-UK network.

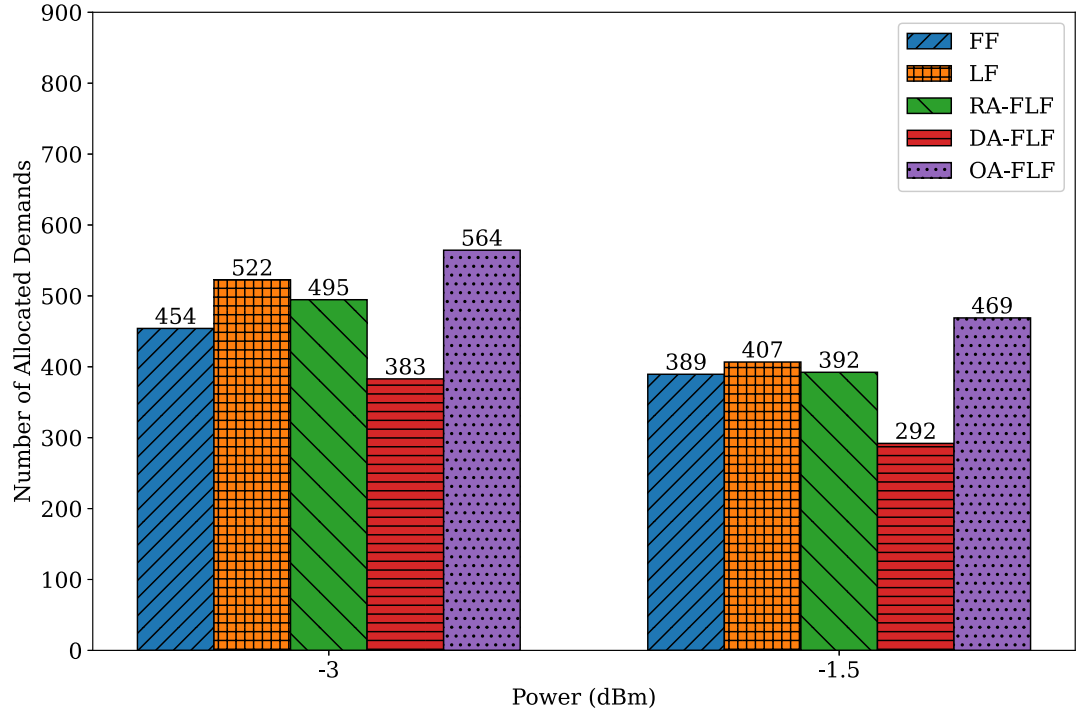

(b) Topology: 24-node USA network.

Figure 6.15: Comparison of traffic admissibility

result, the end capacity of this network becomes much higher compared to larger geographies (such as the 24-node USA network), where the quality of most of the established lightpaths belongs to lower order modulation formats (such as PM-BPSK, PM-QPSK). The numerical results suggest that the OA-FLF algorithm can provide 6.3%, 2.4%, 10.5%, and 29.2% gain, respectively, compared to FF, LF, RA-FLF, and DA-FLF algorithms while using a launch power of -3 dBm in BT-UK network. Although the increment of launch power from -3 dBm to -1.5

dBm reduces the overall capacity of the network for any of the algorithms due to enhancement of the NLI impact on the OSNR of lightpaths, the advantage of OA-FLF compared to other baseline algorithms remains unaltered.

On the other hand, in larger geography, such as the 24-node USA network, the presence of high accumulated ASE noise degrades the OSNR of the lightpaths manyfold. In addition, if the launch power is increased from -3 dBm to -1.5 dBm, the overall capacity of the larger network becomes very low. However, a gain of 20.6%, 15.2%, 19.6%, and 60.6% can be achievable by the OA-FLF algorithm compared to the FF, LF, RA-FLF, and DA-FLF algorithms, respectively. Moreover, as shown in Fig. 6.14, the DNN-based OA-FLF approach, with the help of a 99.65% accurate QoT estimator, predicts a maximum of 5.9 % and 8.9% less capacity compared to the analytical approach in the BT-UK network and 24-node USA network, respectively. Therefore, it can be easily observed that the OA-FLF algorithm with the analytical approach can provide slightly better traffic admissibility than the DNN-based approach with the aid of high computational complexity. Furthermore, as the LF algorithm appears as the best baseline algorithm compared to others in terms of traffic admissibility, the subsequent sections only consider the proposed algorithm OA-FLF and LF for further analysis.

6.5.5.4 Quality of Lightpath Analysis

This subsection analyses the distribution of established lightpath in the network and shows its effect on the traffic admissibility. Generally, the quality of the lightpath severely impacts the overall capacity of the network. The establishment of high-order modulation-based lightpaths enhances the chances of traffic grooming and saves spectrum for future connections. In this work, two lower-order modulations (LoM) (such as PM-BPSK and PM-QPSK) and four HoM (e.g., PM-8QAM, PM-16QAM, PM-32QAM, and PM-64QAM) are considered as likely choices for the quality of the lightpaths. The supported data rate and required OSNR threshold for each of these modulation formats is considered as shown in [14]. Table 6.7 captures the distribution of LoM and HoM-based lightpaths till 1% blocking while using the proposed and the best baseline algorithm with launch power of -3 dBm, which provides the highest capacity. Numerical data suggests that the OSNR adaptive policy can significantly reduce the LoM distribution compared to the best baseline algorithm (i.e., LF) and provides a notable capacity gain by increasing the distribution of HoM-based lightpaths.

Table 6.7: Comparison of quality of lightpaths till 1% blocking (P_{Ch} = -3 dBm).

Topology	Algorithm	LoM	HoM
BT-UK	OA-FLF	17%	83%
BT-UK	LF	20%	80%
24-node USA	OA-FLF	76%	24%
24-node USA	LF	83%	17%

6.5.5.5 Fragmentation Analysis

This section analyses the impact of the proposed quality-aware resource allocation algorithm on the overall fragmentation of the network. Table 6.8 shows the CAASR value at the end of 1% blocking for the proposed and the best baseline resource allocation algorithm with two launch powers. As LF policy starts the allocation of the spectrum from one end of the spectrum, it is expected that the overall network fragmentation should be lower. However, it is not guaranteed

that allocation with minimum fragmentation can provide the highest network capacity. The reported results in Table 6.8 indicate that the OA-FLF algorithm can provide a capacity gain of up to 7.7% compared to the LF approach while achieving approximately similar values of CAASR in the smaller geography (i.e., the BT-UK network) due to the ability of high-quality lightpath provisioning and possibilities of traffic grooming. In addition, a capacity gain of up to 15.2% is also achieved in the larger geography (i.e., the 24-node USA network) using the OA-FLF algorithm compared to the LF strategy. Furthermore, the OA-FLF algorithm also minimizes fragmentation (and maximizes the CAASR metric) significantly in the 24-node USA network. As the majority of lightpaths are generally provisioned over LoM formats in longer geography, the priority for lightpath's quality selection before spectrum allocation under the OA-FLF algorithm outperforms in terms of fragmentation minimization compared to the LF approach. Numerical data suggests that the OA-FLF algorithm returns 14.9% and 4% gain in CAASR improvement compared to the LF algorithm under -3 dBm and -1.5 dBm channel power, respectively.

Table 6.8: Comparison of $CAASR$ till 1% blocking.

Topology	P_{Ch} (dBm)	Algorithm	N_A	CAASR
BT-UK	-3	LF	1780	0.110
BT-UK	-3	OA-FLF	1824	0.108
BT-UK	-1.5	LF	1568	0.113
BT-UK	-1.5	OA-FLF	1688	0.109
24-node USA	-3	LF	522	1.688
24-node USA	-3	OA-FLF	564	1.940
24-node USA	-1.5	LF	407	1.884
24-node USA	-1.5	OA-FLF	469	1.958

6.6 Conclusion

We investigated the importance of the quality-aware resource allocation strategy in the context of MB-EON. To ease the computational complexity of quality calculation of a lightpath, a DNN-assisted QoT estimator is considered instead for analytical OSNR calculation while ensuring acceptable accuracy in the OSNR estimation. The numerical results show that the DNN-based QoT estimator can provide a maximum computational gain of 96.94% while ensuring an average prediction accuracy of 99.65%. Furthermore, a resource provisioning algorithm, namely OA-FLF, is proposed, where the placement of HoM-based lightpaths is prioritized during resource allocation. Reported results show that, compared to the baseline algorithms, the proposed OA-FLF algorithm can provide a maximum gain of nearly 30% in terms of traffic admissibility for smaller networks such as BT-UK, whereas, for larger geography such as a 24-node USA network, this traffic admissibility gain becomes over 60% till 1% blocking.

Chapter 7

Effect of Resource Re-provisioning on Network Upgrade

7.1 Introduction

Chapter 5 and 6 show the effect of the efficient spectrum management policies on the C+L band optical network. As the existing C-band-based network can't adopt these emerging technologies instantaneously, strategic planning needs to be done to upgrade the existing network infrastructure. A network can be upgraded either gradually or all once, depending on the network operator's objective. Upgrading all links of the network topology at the same time without checking the specific link conditions, generally results in an investment of enormous CapEx. Whereas gradual upgrades while following a pay-as-you-grow approach can avoid the requirement of unessential upgrades and hence minimize extra CapEx requirements. In this regard, authors in [84] showed that a network operator needs to wisely select a set/sequence of link(s) to upgrade from C to C+L, which can delay future network upgrades, thereby achieving cost benefits.

A network upgrade can be further delayed by employing a mechanism called re-provisioning. We define re-provisioning as the movement of existing lightpaths from the C band to the L band. By moving more lightpaths to the L band over the C+L band upgraded links, the availability of the valuable C-band spectrum increases. This approach may be cost-effective because early upgrades can be expensive. Hence, re-provisioning is an important mechanism to delay network upgrades and efficiently use network resources. A distance-based re-provisioning strategy for C+L upgrade was proposed in [85]. Despite its effectiveness, re-provisioning lightpaths from one band to another may degrade the signal quality, i.e., OSNR of lightpaths, leading to increased service disruptions, which operators would like to avoid as much as possible. To reduce disruption in the network, we propose new and improved re-provisioning strategies when upgrading a network to C+L bands. Also, although OSNR can be calculated analytically, we incorporate a synthetic, data-driven, ML model to estimate OSNR of lightpaths, which decreases computation times of lightpath-feasibility checks.

The two proposed OSNR-aware re-provisioning strategies, called budget-based (BB) and margin-aware (MA), aim at reducing lightpath disruption in the network, thereby improving spectrum utilization. In BB, a network operator is allowed to re-provision a fixed number of lightpaths from C band to L band after each batch upgrade, while in MA, existing C-band lightpaths are re-provisioned to L band based on their OSNR margin set by the network operator. We evaluate the performance of the proposed strategies with a baseline distance-based strategy in the BT-UK network. Results show that the BB and MA strategies significantly reduce disruption and blocking in the network, compared to the distance-based strategy in [85].

The remaining portion of this study is organized as follows: In Section 7.2, related works are reviewed. Section 7.3 describes the physical-layer model and the regression models used for Quality-of-Transmission (QoT) estimation. Section 7.4 describes the proposed re-provisioning strategies for C+L networks and also presents the algorithms. Section 7.5 introduces the simulation settings and traffic matrices, and shows the numerical results. Section 7.6 concludes the study.

7.2 Related Works

How to deal with capacity crunch using MB transmission in optical networks is a topic of significant interest. Prior works, [69], [77], [86], [87], have considered different scenarios in MB to enhance transmission capacity. Ref. [69] developed a planning tool that exploits physical-layer-aware routing, modulation, and spectrum assignment (RMSA) algorithm to activate optical bands based on incoming traffic. Ref. [86] proposed a provisioning scheme considering C+L and C+L+S bands with the flexibility to assign preference to a specific transmission band. Their findings indicate that, despite the signal-strength degradation caused by neighboring bands in the C band, significant reduction in blocking probability can be achieved with MB transmission. Ref. [77] considered a lightpath-provisioning scheme for different MB scenarios (C only, C+L, C+L+S, C+L+S+E, and C+L+S+E+O), showing a significant increase in transmission capacity. However, technical maturity and commercial availability of the necessary optical devices for different bands must be considered. Among the different bands, L-band technology has significantly matured, and previous studies [8], [88] provide a strong motivation for expanding to C+L. Also, network upgrades from C to C+L bands have been implemented in industry [89].

Considering these prior works, modeling the physical layer is an essential part to plan a practical MB expansion. Some major factors that need to be considered during MB operation are stimulated Raman scattering (SRS), nonlinear interference (NLI), noise figure, and type of optical amplifier required to operate in each band. Ref. [90] considered the above factors and showed that network traffic in MB might increase with an optimized power assignment. Ref. [5] discusses the potential challenges in MB by considering the effects of ASE noise (due to optical amplifiers) and non-linear effects such as SRS and NLI. Other works, such as [12], [19], [21], [91] have also modeled and evaluated the impact of ISRS in MB networks. Refs. [13], [58] investigate MB scenarios limited to C+L systems by accounting for ASE due to in-line amplifiers and SRS.

The above factors add to signal impairments, thereby affecting the OSNR of lightpaths. Previous work [85] considered a worst-case scenario to calculate the OSNR of lightpaths for incoming requests. In fact, determining OSNR using analytical calculations can be cumbersome, especially when a large number of lightpaths are provisioned in a network. Hence to predict lightpaths' QoT, in this study, we use ML-based QoT estimation for unestablished lightpaths based on the current network state. Multiple studies have demonstrated how to use ML-based QoT estimators to verify the feasibility of lightpaths for deployment. We review below some studies related to ML-based QoT estimation.

Ref. [92] proposed regression approaches which consider the effect of variations and uncertainties on fiber attenuation, non-linear coefficients, or amplifier noise figure per span, to estimate QoT. Ref. [93] showed the benefits of using neural networks and support vector machines (SVM) for modulation-format classification and OSNR estimation. In [94], effectiveness of various ML models such as k-nearest neighbors, logistic regression, and SVM for QoT estimation were described. Ref. [95] investigated the performance of a data-driven QoT model on dynamic and unicast metro optical networks capable of supporting both unicast and multicast

connections. The model predicts nearly-accurate QoT of lightpaths that need to be established. Other works, such as [60], [62], [65], [79], show the application of ML to predict OSNR of lightpaths where real and synthetic data were used. Our work uses the predicted OSNR for lightpath provisioning and re-estimates OSNR using the ML model during migration to MB.

Operators choose to migrate to MB networks to sustain traffic growth. However, upgrading the entire network at once can incur large CapEx and operational expenditures (OpEx). Prior works, [22], [23], [83], [84], [96], [97], have proposed cost models and upgrade strategies for MB expansion. Ref. [96] focused on a pay-as-you-grow order of band deployment in MB networks. Ref. [23] developed a cost model to assess migration scenarios from C band to C+L and C+L+S bands. Ref. [22] emphasized the importance of link selection by proposing a framework in which fiber-capacity upgrade is geographically dependent. Ref. [84] modeled a multi-period batch upgrade from C to C+L networks by considering traffic demands and annual traffic growth, and discussed the significance of selecting appropriate links for C+L upgrade.

Our work focuses on C+L networks where all links initially operate in C band. Building on previous research, we use a link-selection technique from [84] that groups links into batches based on their spectrum utilization. This enables network upgrades from C to C+L with minimal cost. To further reduce upgrade cost, Ref. [84] extended their work to [85] and introduced a mechanism of distance-based re-provisioning, which delays upgrades by moving lightpaths, from C band to L band, based on their path length. For instance, upgrading the network in year 3, year 5, and year 10 may reduce the overall network upgrade cost. To show the effectiveness of our newly-proposed re-provisioning strategies, we use link-selection technique from [84] and upgrade times from [85]. Accordingly, Ref. [85] is significantly extended in this work by demonstrating that selectively moving lightpaths based on their QoT can reduce the number of disrupted connections in the network and hence limit the adverse impact of re-provisioning.

7.3 ML-Based Regression Models for QoT Estimation

The QoT of an optical lightpath is usually expressed using OSNR, as discussed in Chapter 2. Our study relies on ML models to estimate the OSNR of lightpaths. We have used the same physical layer model as discussed in Chapter 2 for generating data for training purposes. Note that, since the network is upgraded in batches, we need two estimators - a C-band estimator and a C+L-band estimator - which are described in Section 7.3.1.

7.3.1 C and C+L-Band QoT Estimators

In previous work [85], OSNR calculation of a lightpath assumed that all channels in a route are occupied (fully-filled spectrum). Here, we observe that, it is important to calculate OSNR with growing traffic so that a network operator, given the state of the network, can assess the current QoT of a lightpath. Hence, in this work, we estimate the OSNR achieved for the actual current load in the network. Since repeating QoT estimations for a large number of lightpaths every time a network state changes could lead to unsustainable computational burden, we adopt a supervised ML model for QoT estimation, leveraging a well-known Random-Forest algorithm. The proposed model is fed with features that represent the state of the network: route, COI, number of intermediate links or hop counts, distance between source and destination, and number of active interfering channels in C or L band. To depict the route in which a lightpath operates, we encode all links of a route. ML algorithms require numerical inputs for data processing. Hence, we choose to encode a route in binary, i.e., if the lightpath traverses a link, we assign a binary value '1' to the link variable, else '0'. Next, we discuss the necessity of using two estimators for OSNR estimation.

Since network upgrade occurs in batches [85], with each batch containing a set of links, the network will exist in a mixed state, where certain links will operate only in C band, while others are capable of operating in both C and L bands. Consequently, it becomes imperative to employ two distinct estimators to ensure necessary OSNR estimation, accounting for the impact of both C and L bands. We accomplish this by using the physical-layer model of Chapter 2 to generate synthetic data for C and C+L band transmission while considering the simulation parameters discussed in Section 7.5.1.

We now discuss an example on how different links are encoded during multi-period batch upgrade for model training. In Fig. 7.1(a), blue links operate in C band and red links operate in C+L band. For each link, total number of channels and number of active channels are known. Consider lightpath λ_1, which is provisioned over links AF, FE, and ED (named e_6, e_5, and e_4, respectively). These links are assigned value '1', while other links in the network are assigned with '0'. If the link variables (e) are arranged in a matrix as [e_1, e_2, e_3, e_4, e_5, e_6, e_7, e_8], then the lightpath is encoded as [0, 0, 0, 1, 1, 1, 0, 0]. Since there are eight links in the network topology (Fig. 7.1(a)), a route can be expressed using eight binary variables. This encoding technique allows the model to effectively capture the presence or absence of a connection. The input to the estimator is an array composed of link variables and other parameters required to predict OSNR. If a route operates only in C band (e.g., λ_1 in Fig. 7.1(a)), a C-band estimator is used. Similarly, if all links of the route are upgraded to C+L (e.g., λ_2 in Fig. 7.1(a)), then a C+L-band estimator would be used.

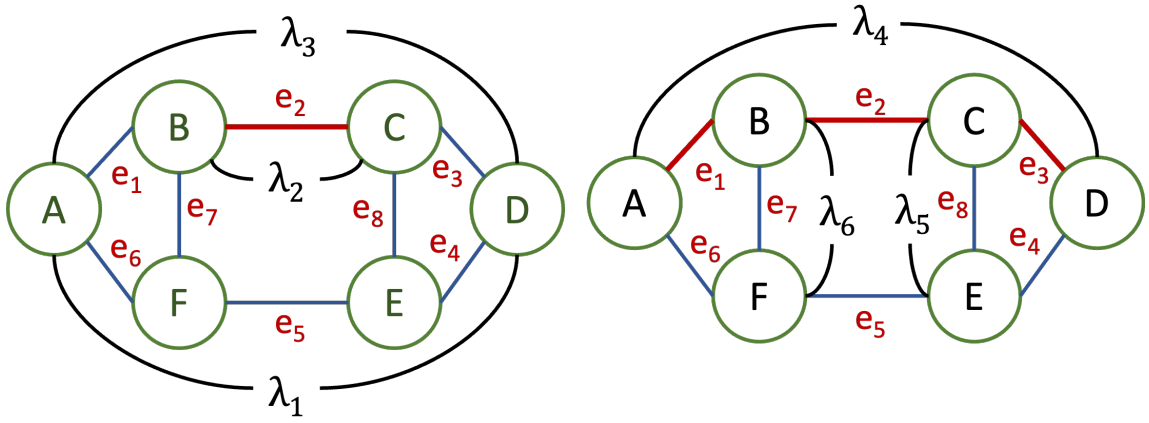

(a) A sample network containing a single link in C+L band.

(b) A sample network operating with multiple upgraded links.

Figure 7.1: Two scenarios of network operation

Now, let us consider a scenario in which a lightpath traverses a route containing an upgraded link. For example, consider a lightpath λ_3 going through links e_1, e_2, and e_3. As shown in Fig. 7.1(a), only link e_2 is upgraded to C+L. In such case, we calculate the OSNR of the entire route on a per-link basis, i.e., links in C and C+L are fed into respective estimators. Therefore, OSNR of lightpath λ_3 can be calculated as shown below.

$$OSNR_{\lambda_3}^{-1} = OSNR_{e_1}^{-1} + OSNR_{e_2}^{-1} + OSNR_{e_3}^{-1} \tag{7.1}$$

By using historical data of relevant network features (for training and validation) and tuning the model for optimal performance, OSNR can be estimated. The predicted OSNR can be used to estimate the impact of new lightpaths in the network. These values are also used to determine lightpath capacity (as shown in Table 7.1). To improve model prediction, we conduct an exhaustive search to optimize the ML parameters that minimize the loss function

of the algorithm. We evaluate the performance of the model according to the following metrics: R-squared (R^2), mean squared error (MSE), and mean absolute error (MAE). Both models have an R^2 score higher than 96%, where R^2 represents the proportion of variance in OSNR explained by the network features used to train the QoT estimator. The C-band estimator exhibits an MSE of 0.1725 and an MAE of 0.2808, while the C+L-band estimator yields an MSE of 0.5698 and an MAE of 0.5126.

7.4 OSNR-Aware Re-provisioning

7.4.1 Problem Description

In this section, we describe the problem of re-provisioning in MB optical networks, and then we propose two OSNR-aware re-provisioning strategies. These strategies move the lightpaths (from C to L band) based on the signal quality with the aim of reducing the overall disruption in the network. To implement the strategies, we adopt a multi-period upgrade strategy and upgrade times from [84] and [85], respectively.

Expansion to MB, which involves network upgrades, comes at a cost. Upgrading the entire network at once to address concerns of growing network traffic will lead to a high upgrade cost. Instead, by carefully selecting a set of links in a network, traffic growth could be sustained. In this regard, Ref. [84] proposed a multi-period, batch-upgrade strategy (where each batch contains a subset of links for upgrade), which reduces network upgrade cost over time. By sorting links in decreasing order of their spectrum utilization and grouping a set of links, network upgrades from C to C+L can be significantly delayed, thereby further reducing the upgrade cost. It was also established, for the parameter settings considered in [84], that upgrading the network in three batches would be most beneficial in terms of cost. To determine the timing of upgrade of each batch, extensive statistical analysis was conducted, guided by a target blocking probability set by the network operator.

While multi-period network upgrades lead to lower network upgrade cost, they cause the network to exist in a mix of C and C+L links. In doing so, lightpaths may exist on routes which contain upgraded links (e.g., λ_3 in Fig. 7.1(a)). After each batch upgrade, the network operator will likely continue to serve most of the requests in C band, as only a subset of links can accommodate requests in L band. Hence, to maximize availability of C-band spectrum and delay future network upgrade, we choose to move some of the existing lightpaths in C band to L band, if possible.

In this regard, Ref. [85] proposed a re-provisioning strategy that relied on distance to delay network upgrades, thereby lowering network upgrade costs further. Although re-provisioning helps in lowering upgrade costs, it adds to an important practical problem of disruption. This so-called disruption (denoted as $N_{Disruption}$) is an effect occurring due to three factors, namely: Re-provisioning (denoted as $N_{Re-provisioned}$), Provisioning Overflow requests (denoted as $N_{Overflow}$), and Re-adjustment (denoted as $N_{Re-adjusted}$), where N is the number of lightpaths. Hence, disruption in a network can be computed as:

$$N_{Disruption} = N_{Re-provisioned} + N_{Overflow} + N_{Re-adjusted} \tag{7.2}$$

In this study, re-provisioning, re-adjustment, and provisioning of Overflow requests are initiated after each batch upgrade in the network. To demonstrate how/when re-provisioning (the first factor in disruption) is triggered, we consider the following scenario: if a lightpath λ_3 originates from node A and terminates at node D (in Fig. 7.1(a)), λ_3 cannot be re-provisioned to L band, as not all links in the route have been upgraded. On the contrary, a lightpath λ_2 starting at node B and terminating at node C could be moved to L band. However, moving a lightpath from one band to another comes at the cost of sacrificing its signal quality (OSNR).

Table 7.1: OSNR Classification for Modulation Assignment [58].

Modulation	Data Rate (Gbps)	OSNR Window (dB)
PM-BPSK	50	9 − 11.9
PM-QPSK	100	12 − 15.9
PM-8QAM	150	16 − 18.5
PM-16QAM	200	18.6 − 21.5
PM-32QAM	250	21.6 − 24.5
PM-64QAM	300	24.6 − 30

OSNR of a lightpath decides the modulation format it supports. Usually, modulation format of a lightpath supports a range of OSNRs, as shown in Table 7.1. Growing network traffic and change in spectrum occupation (e.g., due to link upgrade to L band) can cause OSNR of lightpaths to degrade during their lifetime. A degraded lightpath needs to either be re-adjusted (i.e., modulation format should be down-shifted) or an additional overflow request must be provisioned on a new lightpath. Section 7.4.2 provides an example for overflow and re-adjustment, the second and third factors in disruption, respectively. As network traffic increases, it could impact existing lightpaths due to NLI effects, which leads to OSNR degradation. Hence, it is necessary to monitor lightpaths based on OSNR degradation.

7.4.2 Strategies for Re-provisioning

We propose two OSNR-aware re-provisioning strategies, namely, Margin-Aware and Budget-Based. MA re-provisioning allows a network operator to move a lightpath to L band based on its proximity to the lower-bound OSNR value for the corresponding modulation format. Consider a lightpath λ_4, as shown in Fig. 7.1(b), that was provisioned in C band with an OSNR of 23.5 dB. Assume that the first batch of links was upgraded, and it contained all links on which λ_4 is provisioned. We now re-estimate the OSNR of λ_4 and find it to be 22 dB, which is close to the threshold (21.6 dB) as seen in Table 7.1. This lightpath is a good candidate to be re-provisioned, as lightpaths whose OSNR is close to the threshold are more likely to be affected due to NLI (with increasing traffic) and will anyway drop to a lower modulation format (and hence be disrupted) regardless of them being re-provisioned.

Alternatively, if a network operator has a budget based on the number of lightpaths that could be moved, BB re-provisioning may be employed. In this approach, like MA, we calculate the OSNR margin of lightpaths and select lightpaths whose margin is closest to the threshold. We continue to select and re-provision such lightpaths until a budget is reached.

After each batch upgrade, OSNR re-estimation is required for all existing lightpaths whose links have been upgraded. Existing degraded lightpaths may encounter the following scenarios: (a) Overflow requests can be provisioned on new lightpaths; and (b) C-band lightpaths can be re-adjusted.

Now, let us consider an example for overflow requests. Loss in signal quality can cause lightpaths to possibly drop modulation formats, which may lead to reduced capacity. This reduced capacity causes some requests to overflow and such requests need to be provisioned on new lightpaths. Consider the following example: suppose a lightpath λ_5, as shown in Fig. 7.1(b), has a OSNR of 25 dB when provisioned in C band and based on Table 7.1, has a corresponding data rate of 300 Gbps. Since we assume all lightpaths to have a uniform data rate of 100 Gbps, λ_5 can serve at most three requests. Assume that subsequent lightpaths are provisioned thereafter, and we re-estimate the OSNR of λ_5 to be 23 dB. This indicates that λ_5 can now serve at most two requests. Hence, one of the three requests needs to be served by provisioning a new lightpath.

Now, let us consider an example for re-adjustment of lightpaths in C band. If a lightpath degrades such that it drops below its current modulation format but can still serve the existing requests, then such lightpaths are re-adjusted. Consider the following example: suppose a lightpath λ_6, as shown in Fig. 7.1(b), has a OSNR of 27 dB when provisioned in C band and from Table 7.1, has a capacity of 300 Gbps. Assume λ_6 serves two requests (of 100 Gbps each). If the OSNR degrades to 23 dB, it indicates that the modulation format has changed (from Table 7.1). λ_6 can continue to serve the existing requests with the new modulation format because of the data rate it supports. Hence, this lightpath would only be re-adjusted.

7.4.3 Algorithms for Re-provisioning

We now describe the algorithms for our proposed re-provisioning strategies in MB networks. Given parameters:
- $G(V, E)$: Network topology; V set of nodes, E set of links.
- T: Traffic matrix.
- E': Set of links sorted in descending order of spectrum utilization, where $E' \subset E$.
- E_{C}: Set of links in C band, where $E_{\mathrm{C}} \subset E$.
- $E_{\mathrm{C+L}}$: Set of links in C+L bands, where $E_{\mathrm{C+L}} \subset E$.
- R_p: Set of connection requests in a lightpath p.
- q_p: OSNR of lightpath p.
- m_p: Modulation format of a lightpath p.
- P_{C}: Set of lightpaths in C band.
- P'_{C}: Set of lightpaths in C band sorted based on OSNR proximity.
- P_{L}: Set of lightpaths in L band.
- q'_p: Lower-bound OSNR threshold of lightpath p.
- N: Number of upgrade batches.
- k_N: Upgrade time of a batch N.
- $b(N)$: Set of un-upgraded links in batch number N.
- B: Set of links upgraded in each batch b; where $b \in B$.
- X_N: Number of lightpaths that can be moved (*budget* set by network operator) in each batch number N.
- Q: OSNR margin set by network operator.

Our algorithms take as input the network topology and number of upgrade batches. We adopt a link-selection technique from [84] and fix the set of links that are upgraded per batch. These links are stored in E'.

Here, we describe Algorithm 7. In this strategy, we assume that the network operator decides to re-provision a certain number (X_N) of existing lightpaths in C band. We obtain E' which is the set of links sorted in descending order of spectrum utilization, and we upgrade the links in E' in N batches. When N is greater than 0 and at a fixed upgrade time k_N, a set of un-upgraded links, $b(N)$, from E' is upgraded and is added to $E_{\mathrm{C+L}}$ (line 3). For each lightpath p in P_{C}, the algorithm extracts the corresponding features to recompute OSNR (q_p), corresponding modulation format (m_p) (lines 5-6), and proximity to the lower OSNR window of the current modulation format (line 7). Lightpaths in P_{C} are then sorted in ascending order of their OSNR proximity and are stored in P'_{C} (line 8). For lightpaths in P'_{C}, re-provision (if possible) the ones whose links are upgraded to L band (lines 10-17); and if a request in the re-provisioned lightpath overflows in L band, it is served by a new lightpath (lines 18-20). We count the number of lightpaths that were re-provisioned (line 22) and check if it exceeds the budget, X_N (line 25). We continue to re-provision lightpaths as long as the number is less than the budget decided by the network operator. After the re-provisioning phase, OSNR of the

remaining lightpaths in C band, whose links are upgraded to L band, are re-calculated (lines 29-31), and the modulation format is updated accordingly. If a request in a path overflows the lightpath capacity due to the updated OSNR, it is served by a newly-provisioned lightpath (lines 32-34). If the OSNR of the lightpath changes such that its modulation format remains unaltered, the request remains in the same lightpath with the updated OSNR. After the first batch upgrade, new requests are allocated in L band first. We store the set of upgraded links from each batch in B (line 38). The algorithm checks for any remaining batches to upgrade (line 39); if so, it continues to upgrade until all links in the network are upgraded (line 1).

Now, we describe Algorithm 8. This algorithm works in a similar way to Algorithm 1, except that the network operator provides a OSNR margin (Q) instead of a budget (X_N). Then, we check if each lightpath p in P_C is eligible to be re-provisioned (lines 4-5) and if its OSNR (q_p) lies within the OSNR margin (lines 9-10). All such lightpaths would be re-provisioned to L band (lines 11-14). Overflow requests of re-provisioned lightpath p will be served by a new lightpath in L band (lines 15-17). After the re-provisioning phase, OSNR of all remaining lightpaths in C band will be updated and the overflow requests will be served by newly-provisioned lightpaths in C band (lines 23-28). The upgraded links from each batch are stored in B (line 32). The algorithm checks for remaining batches (line 33), and continues to upgrade until the entire network is upgraded (line 1).

Time complexities of both Algorithms 7 and 8 are: $O(N.|P_C|.T.log(n))$, where N is the number of batches, T is the number of decision trees in the Random-Forest model, and n is the number of samples in the dataset.

7.5 Results and Discussion

7.5.1 Simulation Setup

An event-driven, custom-built simulator is used to emulate an upgrade environment from C to C+L bands while incorporating physical-layer modeling. For our simulation, the BT-UK network is considered, which consists of 22 nodes and 35 links, as shown in Appendix B. A uniform channel launch power of 0 dBm is considered for every lightpath. To build the QoT Estimator, synthetic data was generated using the same physical-layer model as discussed in Chapter 2, while considering the system parameters from Table 7.2. Using these parameters, we generate 1000 datapoints for C and C+L bands separately. These datapoints were subsequently partitioned, with 70% allocated for training and 30% for testing. Routing and spectrum selection are carried out using k-shortest path and first-fit methods, respectively. Modulation format of each lightpath is selected according to the OSNR window shown in Table 7.1. We run the simulation for 20 seeds, each with 3000 demands.

Table 7.2: System Parameters.

Parameters	Values
Channel bandwidth (THz) for C band [98]	5
Channel bandwidth (THz) for C+L band [12]	10
Symbol rate (GBaud) [13]	28−32
Channel spacing (GHz) [13]	37.5
Span length (km) for both C and L band [14]	60
Loss co-efficient (dB/km) [13]	0.2
Noise figure (dB) for C-band EDFA [14]	5.5
Noise figure (dB) for L-band EDFA [14]	6
Non-linearity co-efficient (1/Watt/km) [13]	1.2

Algorithm 7 Budget-Based re-provisioning

```
1: while N > 0 do
2:    k_N ← Fixed upgrade time;
3:    E_C+L ← E_C+L ∪ b(N); % Upgrade set of un-upgraded links, b(N), from E' to E_C+L at
      k_N;
4:    for each lightpath p in P_C do
5:       Update q_p ← QoT Estimator;
6:       Update m_p;
7:       OSNR proximity ← q_p − q'_p;
8:       Add p to P'_C in sorted order of OSNR proximity;
9:    end for
10:   counter ← 0;
11:   for each lightpath p in P'_C do
12:      if (All links of p are upgraded to L band) then
13:         if (Bandwidth available in L band) then
14:            Update q_p ← QoT Estimator;
15:            Update m_p;
16:            Allocate requests R_p in L, p ∈ P_L;
17:            Remove p from C band, update P_C;
18:            if Capacity of R_p overflows p then
19:               Provision overflow requests;
20:               Update P_L with new lightpaths;
21:            end if
22:            counter ← counter + 1;
23:         end if
24:      end if
25:      if (counter > X_N) then
26:         break;
27:      end if
28:   end for
29:   for each lightpath p in P_C do
30:      if (All links of p are upgraded to L band) then
31:         Update q_p and m_p;
32:         if Capacity of R_p overflows p then
33:            Provision overflow requests;
34:            Update P_C with new lightpaths;
35:         end if
36:      end if
37:   end for
38:   B ← B ∪ b(N);
39:   N ← N − 1;
40: end while
```

Algorithm 8 Margin-Aware re-provisioning

while $N > 0$ **do**
  $k_N \leftarrow$ Fixed upgrade time;
  $E_{\mathrm{C+L}} \leftarrow E_{\mathrm{C+L}} \cup b(N)$; % Upgrade set of un-upgraded links, $b(N)$, from E' to $E_{\mathrm{C+L}}$ at k_N;
  for each lightpath p **in** P_{C} **do**
    if (All links of p are upgraded to L band) **then**
      if (Bandwidth available in L band) **then**
        Update $q_p \leftarrow$ QoT Estimator;
        Update m_p;
        OSNR proximity $\leftarrow q_p - q'_p$;
        if OSNR proximity $\leq Q$ **then**
          Update $q_p \leftarrow$ QoT Estimator;
          Update m_p;
          Allocate requests R_p in L, $p \in P_{\mathrm{L}}$;
          Remove p from C band, update P_{C};
          if Capacity of R_p overflows p **then**
            Provision overflow requests;
            Update P_{L} with new lightpaths;
          end if
        end if
      end if
    end if
  end for
  for each lightpath p **in** P_{C} **do**
    if (All links of p are upgraded to L band) **then**
      Update q_p and m_p;
      if Capacity of R_p overflows p **then**
        Provision overflow requests;
        Update P_{C} with new lightpaths;
      end if
    end if
  end for
  $B \leftarrow B \cup b(N)$;
  $N \leftarrow N - 1$;
end while

The network topology, along with a traffic matrix, are provided as inputs. Incoming connection requests are allocated with available modulation format based on the physical-layer modeling of spectrum bands. Initially, the network operates exclusively in C band, where all connection requests are provisioned. We adopt a multi-period upgrade strategy from [84] to support transmission in C+L. After each batch upgrade, new requests are allocated (if possible) in L band first.

Traffic in backbone networks is typically quasi-static. To resemble traffic flow, a biased traffic matrix of the BT-UK network is used (an incrementally-growing traffic with a growth factor of 30% per year [85]). Source-Destination pairs are selected according to a gravity model consisting of the traffic generation probability of each node [84]. Data rate of all requests is assumed to be uniform, and 3000 connection requests of 100 Gbps are considered for simulation [84].

7.5.2 Baseline Strategies

To evaluate the effectiveness of our proposed OSNR-aware re-provisioning strategies, we compare them with a set of distance-based re-provisioning strategies introduced in [85]. In these distance-based strategies, re-provisioning of existing C-band lightpaths to L band is guided by the evaluation of their path lengths. By calculating the median path length of all allocated ligthpaths, various versions of the distance-based strategy presented in [85] are listed below:

- R: In this strategy, all existing lightpaths whose links are upgraded to L band are re-provisioned.
- R^{long}: In this strategy, we identify and re-provision all lightpaths whose path length is longer than the median path length of existing lightpaths.
- R^{short}: In this strategy, we identify and re-provision all lightpaths whose path length is shorter than the median path length of existing lightpaths.

7.5.3 Total Disruption in the Network

In this subsection, we assess the impact of the proposed OSNR-aware re-provisioning strategies compared to the distance-based re-provisioning strategies by evaluating the disruption metric in the network. It is calculated using Eq. 7.2 (a detailed description of the factors involved in disruption is provided in Sections 7.4.1 and 7.4.2).

To represent the variations of the Budget-Based and Margin-Aware re-provisioning strategies, we use notations BB_x and MA_y, respectively. Here, x indicates the budget or the percentage of the existing C-band lightpaths (whose OSNR is closest to the lower limit of their OSNR window as per Table 1) that can be moved to the L band; and y indicates the OSNR margin set by the network operator such that the lightpaths within y dB of their OSNR threshold (as per Table 1) can be moved to L band.

With BB re-provisioning, we show in Fig. 7.2 that $BB_{5\%}$ yields the least disruption in the network by re-provisioning 5% of the lightpaths that are close to the OSNR threshold. In comparison to R^{short}, R^{long}, and R, $BB_{5\%}$ results in about 22%, 19%, and 29% lower disruption, respectively. As the budget (i.e., the number of lightpaths that can be moved) increases (e.g., from $BB_{5\%}$ to $BB_{15\%}$), more lightpaths are re-provisioned, causing higher disruption in the network; however, the disruption still remains lower compared to the distance-based re-provisioning strategies. Unlike the distance-based strategies, BB takes into account the QoT of lightpaths and restricts the number of lightpaths that may be re-provisioned after every batch upgrade. Hence, BB is an effective strategy to minimize disruption in the network.

With MA re-provisioning, we observe that disruption in the network is least when lightpaths whose OSNR is within 0.1 dB of the OSNR threshold ($MA_{0.1}$) are re-provisioned. As shown in Fig. 7.2, compared to R^{short}, R^{long}, and R, $MA_{0.1}$ results in about 27%, 24%, and 34% lower disruption, respectively. As OSNR margin increases (e.g., from $MA_{0.1}$ to $MA_{0.5}$), more lightpaths become candidates for re-provisioning, which leads to higher disruption in the network, but it still remains lower than the disruption caused by distance-based re-provisioning. Unlike distance-based strategies, MA preemptively moves lightpaths that are likely to drop to lower modulation formats and thus avoids those lightpaths from contributing to disruption. Hence, MA is an effective strategy to minimize disruption in the network.

Among the distance-based re-provisioning strategies, R causes the highest disruption as it re-provisions all candidate lightpaths. R^{long}, which re-provisions only the longer lightpaths to the L band, results in the least disruption. However, to re-provision longer lightpaths, additional links must be upgraded to ensure sufficient bandwidth availability, resulting in higher upgrade cost. On the other hand, R^{short} re-provisions lightpaths with shorter path lengths, causing higher disruption than R^{long} but lower disruption than R. By re-provisioning only shorter lightpaths, network operations can continue in the C band, which delays future batch upgrades and reduces overall upgrade cost. Thus, R^{short} is the most cost-effective option [85]. In this context, it is most relevant to compare our proposed OSNR-aware re-provisioning strategies to R^{short} to evaluate their effectiveness in mitigating disruptions.

Besides disruption, we also evaluate the number of requests that were blocked in the network. As shown in Fig. 7.3, $BB_{5\%}$ blocks about 11% fewer requests compared to R^{short}, and $MA_{0.1}$ blocks 17% fewer requests compared to R^{short}. Note that increasing the budget in BB or the OSNR margin in MA results in higher disruption, which leads to more blocked requests. Also, we observe that $MA_{0.1}$ blocks fewer requests compared to $BB_{5\%}$, making it a better strategy.

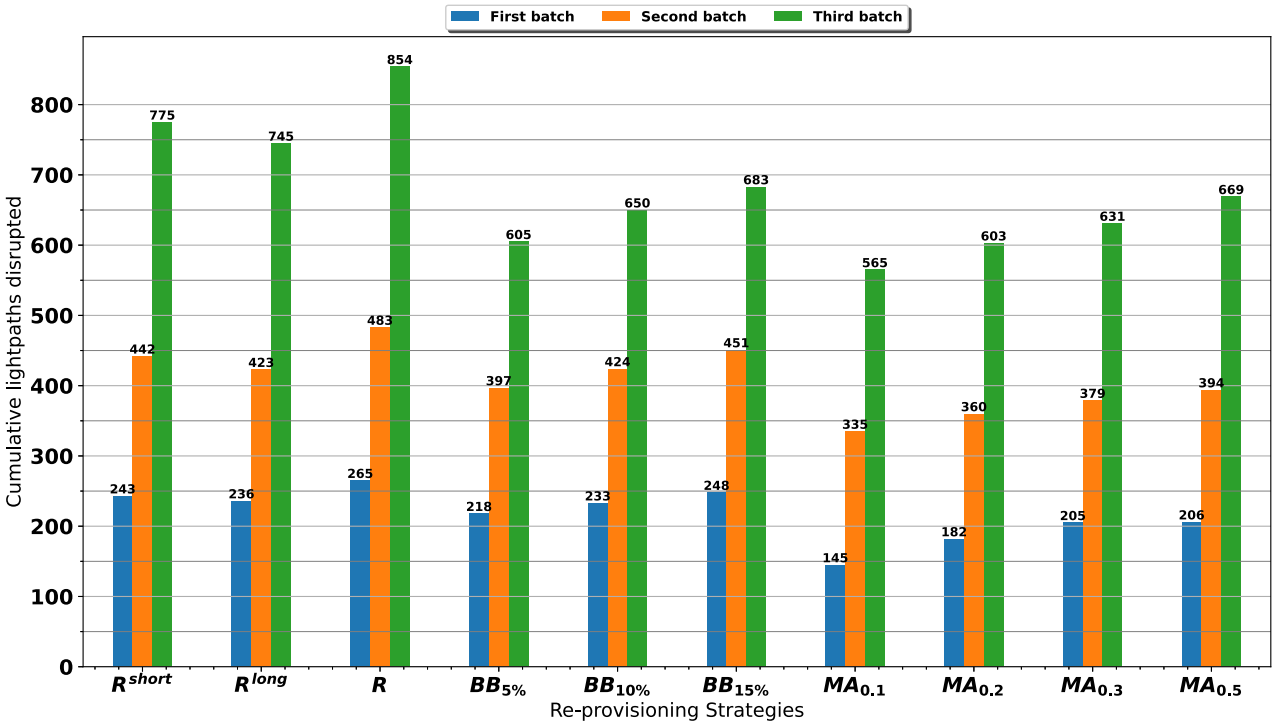

Figure 7.2: Total lightpath disruption in the network due to different re-provisioning strategies.

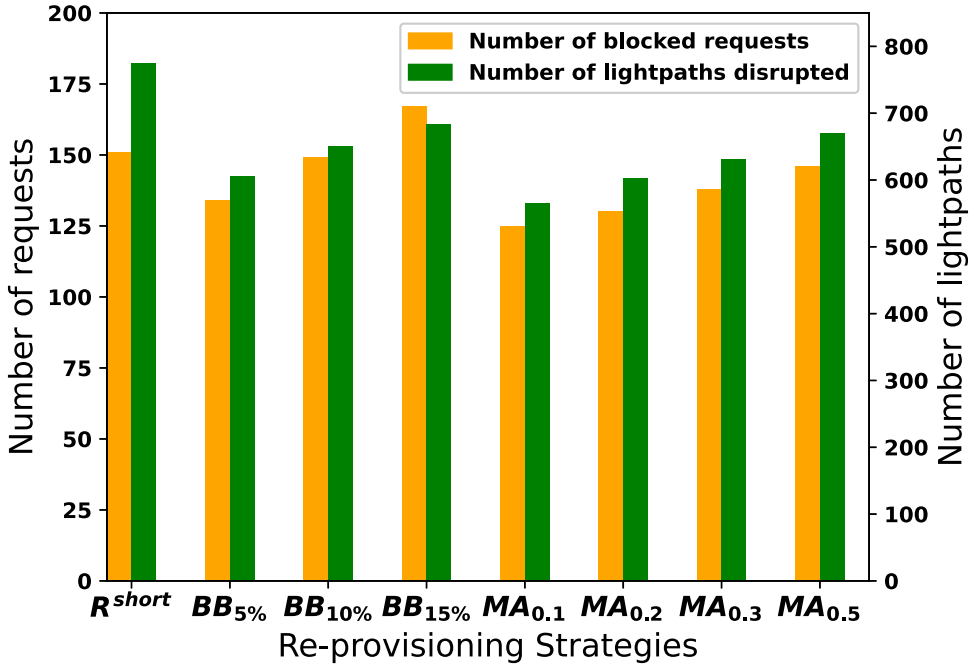

Figure 7.3: Total lightpath disruption and number of blocked requests in the network due to different re-provisioning strategies.

Table 7.3: Cumulative lightpaths re-provisioned with R^{short}, BB, and MA.

Upgrade Batches	R^{short}	$BB_{5\%}$	$BB_{10\%}$	$BB_{15\%}$	$MA_{0.1}$	$MA_{0.2}$	$MA_{0.3}$	$MA_{0.5}$
First	56	26	52	78	3	8	9	15
Second	124	52	102	151	8	16	20	42
Third	324	84	164	237	35	69	92	144

7.5.4 Evaluation of Different Factors of Disruption

This section evaluates the potential impact of the proposed OSNR-aware re-provisioning strategies on the different factors involved in disruption.

7.5.4.1 Impact of Re-provisioning on Disruption

Table 7.3 highlights the effectiveness of BB and MA strategies in terms of cumulative lightpaths re-provisioned in the network. With BB strategy, we observe that $BB_{5\%}$, compared to R^{short}, significantly reduces the number of re-provisioned lightpaths by approximately 54% after the first batch upgrade, by 58% after the second batch upgrade, and by 74% after upgrading all links in the network. In addition, we see that, as the budget increases (e.g., from $BB_{5\%}$ to $BB_{15\%}$), more lightpaths are re-provisioned to L band in the network. Although re-provisioning more lightpaths is desirable to delay future upgrades and lower the upgrade cost, a network operator must consider the consequences of disturbing a large number of existing lightpaths as they can increase disruption. Hence, given a certain network upgrade cost, a network operator must aim to minimize the total disruption in the network.

With MA strategy, we show that, compared to R^{short}, $MA_{0.1}$ yields significant reduction of almost 95% and 94% in the number of re-provisioned lightpaths after the first and second batch, respectively. Furthermore, upgrading all links in the network resulted in 89% decrease in the number of re-provisioned lightpaths. Increasing the OSNR margin (e.g., from $MA_{0.1}$ to $MA_{0.5}$) results in higher number of re-provisioned lightpaths in every batch. Therefore, a network operator must carefully select the OSNR margin to minimize disruptions when moving

Table 7.4: Cumulative lightpaths re-adjusted with R^{short}, BB, and MA.

Upgrade Batches	R^{short}	$BB_{5\%}$	$BB_{10\%}$	$BB_{15\%}$	$MA_{0.1}$	$MA_{0.2}$	$MA_{0.3}$	$MA_{0.5}$
First	112	112	107	100	71	96	114	112
Second	170	181	172	160	156	165	180	183
Third	257	301	287	261	297	294	296	299

Table 7.5: Cumulative overflow requests provisioned with R^{short}, BB, and MA.

Upgrade Batches	R^{short}	$BB_{5\%}$	$BB_{10\%}$	$BB_{15\%}$	$MA_{0.1}$	$MA_{0.2}$	$MA_{0.3}$	$MA_{0.5}$
First	75	80	74	70	71	78	82	79
Second	148	164	150	140	171	179	179	169
Third	194	220	199	185	233	240	243	226

a certain volume of lightpaths.

As more lightpaths are added to accommodate traffic growth, degradation of OSNR in these lightpaths due to NLI may become increasingly significant. This trend is demonstrated for MA re-provisioning in Table 7.3. For instance, in $MA_{0.1}$, only three lightpaths could be re-provisioned after the first batch upgrade. However, with subsequent batch upgrades, more lightpaths are affected and need to be re-provisioned (8 in the second and 35 in the third batch). This could also be attributed to the fact that only a few links are upgraded after the first batch, resulting in fewer eligible lightpaths for re-provisioning. Note that this trend, which is consistent with MA with increasing OSNR margin (e.g., from 0.1 dB to 0.5 dB), contributes to the increasing disruption in the network (as shown in Fig. 7.2).

7.5.4.2 Impact of Re-adjustment and Overflow requests on Disruption

With increasing network traffic, lightpaths may experience degradation in OSNR, which may necessitate their re-adjustment or the provisioning of overflow requests on new C-band lightpaths. Tables 7.4 and 7.5 show the number of lightpaths re-adjusted and overflow requests that were provisioned on new lightpaths after every batch upgrade, respectively. As more lightpaths are re-provisioned (in R^{short} and BB_x), we see that the number of lightpaths that are re-adjusted or new lightpaths that were provisioned to support overflow requests are lower. However, employing MA re-provisioning with low OSNR margins may still result in significant re-adjustment and overflow, particularly during the first and second batches due to the large number of lightpaths remaining in the C band. Increasing the OSNR margin, e.g., to 1 dB, 1.5 dB, or higher, follows a pattern which is similar to BB. Although re-provisioning is a major factor that contributes to disruption, re-adjustment and provisioning of overflow requests are by-products of OSNR degradation and cannot be ignored.

7.6 Conclusion

We investigated different re-provisioning strategies to be employed during the upgrade of a C-band-only optical backbone network to a C+L network. We adopted a multi-batch upgrade strategy and leveraged Machine Learning techniques for QoT estimation of lightpaths. We proposed two OSNR-aware re-provisioning strategies, namely, Budget-Based and Margin-Aware, to minimize disruption in the network. In Budget-Based re-provisioning, a network operator sets a budget on the number of lightpaths to be re-provisioned while in Margin-Aware re-provisioning, OSNR margin is used as a parameter to re-provision lightpaths. We compared the proposed strategies with a baseline distance-based strategy to evaluate disruptions inflicted in the network. Numerical results show that disruptions are reduced by almost 22% with Budget-Based

re-provisioning and by almost 27% with Margin-Aware. Furthermore, the proposed strategies are capable of accommodating more requests in the network. Results show decrement of about 11% and 17% in the number of blocked requests with Budget-Based and Margin-Aware re-provisioning, respectively. Hence, we showed how a network operator can reduce disruptions in the network while keeping the upgrade cost to a minimum.

Chapter 8

Effective Network Upgrade towards C+L Band Optical Networks

8.1 Introduction

Chapter 3 and 4 illustrates that the network operator needs to upgrade several links in the network to enable the MB transmission; however, this action is associated with significant CapEx. Prior works have proposed several link-upgrade strategies for MB expansion while considering the impact of upgrade costs. For example, authors in [22] showed the significance of proper link selection by introducing a framework that accounts for the geographical dependence of fiber-capacity upgrades. Authors in [97] proposed a planning strategy for determining the set of fibers for an upgrade, which could lower upgrade costs. Similarly, authors in [84] proposed a multi-period batch-upgrade model from C to C+L using resource utilization as a metric to select a group of links for the upgrade. Although these studies offer various upgrade strategies, they consider only current resource utilization in the network to assess the need for upgrades and do not consider a monitoring-based prediction mechanism for timely and effective link selection for upgrades.

Emphasizing the significance of timely upgrades, we note that while early upgrades can mitigate the occurrence of blocked connections, i.e., reduce blocking probability (BP) in the network, delaying upgrades can yield cost benefits stemming from equipment depreciation. Therefore, it is important for network operators to carefully choose times for upgrades to reduce blocking and reduce upgrade costs in the network. Since dynamics of blocking and cost are time-dependent, an ML-based model capable of continuously monitoring changes in the network state would be ideal for predicting suitable links for an upgrade at appropriate times. The long short-term memory (LSTM) variant of recurrent neural network (RNN), thanks to its capability of storing/retrieving information over both short and long-time periods and of capturing non-linear patterns, makes it a strong candidate for tracking changes over time [99]. In this work, we propose a novel link-upgrade strategy, named C to C+L upgrade (CLU), and develop an LSTM-based model that leverages information such as resource utilization, fragmentation, etc., over time to efficiently predict the links that will more likely need an upgrade. Our objective is to reduce BP in the network while increasing cost savings by adhering to a given upgrade budget.

8.2 System Model

We consider an elastic backbone optical network topology, $G(V, E)$, comprising $|V|$ nodes and $|E|$ links, where V represents the set of nodes and E represents the set of links. In our study,

we consider C and L bands, with each band comprising 133 channels (considering 37.5 GHz frequency spacing [59]), and the network initially operates only in C band. Incoming traffic is quasi-static where requests enter and remain in the network (which is a common scenario for telecom network operators catering to clients requesting high-bandwidth pipes). Source-destination pairs are generated using a gravity model where traffic generation probability of each node is based on its population density. The set of requests is denoted by R; each request $i \in R$ is represented by a tuple (S_i, D_i, F_i) where S, D, and F are source, destination, and required frequency slots (FSs), respectively. We define an upgrade budget $\hat{J}$, which is decremented after each link upgrade in the network.

In this work, given an EON operating in the C band, a set of requests, and an upgrade budget, we employ one ML model to effectively select which links to upgrade at what time, such that BP and upgrade costs are reduced.

8.2.1 Upgrade Cost Model

Authors in [100] show that the cost of upgrading a link is influenced by two key factors: the number of EDFAs and the type of switches employed on links. When upgrading from C to C+L bands, the cost significantly rises due to the necessity of installing separate EDFAs to support L-band transmission [97], [101]. On the other hand, to support both C and L-band transmission, wavelength-selective, band-switchable, multi-band optical cross-connect switches (MB-OXCs) must be installed at all nodes.

We denote d_e and d^* as the length of link e and the maximum amplifier span for C and L bands, respectively. Taking into account one pre-amplifier and one post-amplifier on each link, the total number of L-band EDFAs required for upgrade on link e is given by $(\lceil d_e/d^* \rceil + 2)$ [101]. We denote J_{EDFA} as the cost of each EDFA on link e and J_{WSS} as the cost of a WSS at each end of link e. Considering an equipment depreciation factor of $\delta \in [0, 1]$ for EDFA over a span of y years [84] (impact of cost depreciation for WSS is considered negligible due to its lower cost), the cost of upgrade for link e is given by:

$$J_e = \left(\left\lceil \frac{d_e}{d^*} \right\rceil + 2 \right) \cdot J_{EDFA} \cdot (1 - \delta)^y + 2 \cdot J_{WSS} \tag{8.1}$$

Eq. (8.1) implies that the upgrade cost exponentially decreases with respect to the upgrade time so that delaying an upgrade can lead to significant cost savings. However, it can increase BP; hence, determining the appropriate upgrade time is crucial.

8.2.2 Cumulative Blocking Probability per Link

Total BP in a network depends on the spectrum utilization (SU) and fragmentation ratio (FR) of the links. SU is defined as the ratio of FSs occupied on a link to the total bandwidth of the link [102]. Considering $R_e(t)$ as the set of requests provisioned over link e at time t and B_e as the total capacity of link e, SU (denoted by μ_e) is given as:

$$\mu_e(t) = \frac{\sum_{i \in R_e(t)} F_i}{B_e}, \tag{8.2}$$

where F_i denotes the total number of occupied FSs by the i^{th} request $\in R_e(t)$ over link e. On the other hand, FR of a link depends on sets of available continuous FSs, known as slot blocks (SBs). Considering $G_e(t)$ as the set of available SBs on link e at time t and H_j as the size of the j-th available SB on link e, FR (denoted by η_e) is expressed as [103]:

$$\eta_e(t) = 1 - \frac{\max_{j \in G_e(t)} H_j}{\sum_{j \in G_e(t)} H_j} \tag{8.3}$$

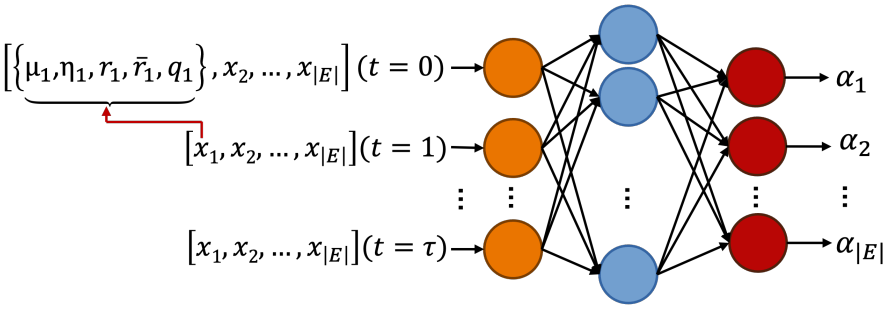

Figure 8.1: Proposed RNN-based model incorporating link features.

To alleviate total BP in the network, links over which more requests are likely to be blocked need to be upgraded sooner. In this regard, we define cumulative blocking probability per link (CBPL) as the ratio of the number of blocked requests to the total number of requests over a link. Since requests are provisioned using a routing and spectrum allocation (RSA) strategy, which influences the SU and FR of a link, exact mathematical representation of CBPL is challenging. Hence, we develop a LSTM (variant of RNN)-based model to predict CBPL of the links as a function of SU and FR; details of the model are described in Section 8.3.1.

8.3 CLU: C to C+L Upgrade Strategy

During MB upgrades, it is crucial to reduce both blocking and upgrade cost in the network. We propose a novel upgrade strategy, namely CLU, to reduce BP and avoid untimely upgrades leading to high cost. To achieve this goal, we design an algorithm to identify the most suitable link(s), based on CBPL threshold (i.e., the maximum allowable CBPL as set by the operator) and budget constraint, for upgrade at appropriate times. The upgrade budget ($\hat{J}$) is derived by calculating the cost of upgrading *all* links in the network at the beginning, which results in the maximum cost as it does not consider any link selection criteria and equipment cost depreciation.

8.3.1 RNN-Based CBPL Estimation Model

To efficiently predict CBPL of the links, we develop an RNN-based model employing a LSTM architecture. In Fig. 8.1, we show the structure of the proposed model, which comprises an input layer, a hidden layer, and an output layer. Each link $e \in E$ has a set of five features, indicated by $x_e(t) = \{\mu_e(t), \eta_e(t), r_e(t), \bar{r}_e(t), q_e(t)\}$, where $\mu_e(t)$, $\eta_e(t)$, $r_e(t)$, $\bar{r}_e(t)$, and $q_e(t)$ represent SU, FR, total number of served requests, total number of blocked requests, and number of remaining FSs on link e, respectively. The input layer is composed of the features of all links for τ time steps, e.g., in Fig. 8.1, we show the features of link 1 (x_1) at time $t = 0$. On the other hand, the output layer consists of $|E|$ nodes, each corresponding to CBPL (denoted by α_e) of a link $e \in E$; the model observes previous time steps to predict CBPL at $t + 1$.

8.3.2 Algorithm

Algorithm 9 summarizes the steps of CLU which takes network topology, set of requests (R), CBPL threshold ($\tilde{\alpha}$), and upgrade budget ($\hat{J}$) as inputs. Total BP (A_{Total}) is initially set to 0. Then, it employs the k-Shortest Path algorithm to identify candidate paths for the incoming requests and allocates FSs to each request using the first-fit (FF) mechanism. Requests unable to secure FSs are classified as blocked. Following this, A_{Total} is updated based on the number of blocked requests and the number of served requests in the network. In the next step, CLU estimates the CBPL of all un-upgraded links for the next time instance (t+1) using the proposed

Algorithm 9 CLU Algorithm

Input: $G(V, E)$, R, $\tilde{\alpha}$, $\hat{J}$;
Output: Total upgrade cost, upgraded links, A_{Total};

Initialize: $\mathrm{A}_{Total} = 0$;
for each time t **do**
  for all incoming requests **do**
    Perform corresponding RSA;
  end for
  Update A_{Total} accordingly;
  for each $e \in E$ **do**
    Estimate $\alpha_e(t+1)$ using the RNN-based model;
    Calculate J_e using Eq. (8.1);
  end for
  $E' \leftarrow$ Sorted links in descending order of $\alpha_e(t+1)$;
  for each $e \in E'$ **do**
    if $\alpha_e(t+1) \geq \tilde{\alpha}$ && $J_e \leq \hat{J}$ **then**
      Upgrade e and remove it from E;
      $\hat{J} -= J_e$;
    end if
  end for
end for

RNN-based model and sorts them in descending order of CBPL. In addition, upgrade cost of each link at time t is calculated using Eq. (8.1). Finally, it chooses the links that satisfy both $\tilde{\alpha}$ and $\hat{J}$ for upgrade, removes them from the set of candidate links, and updates $\hat{J}$.

8.4 Numerical Evaluation

8.4.1 Modeling and Simulation Setup

An event-driven, custom-built Python simulator is used to emulate a C to C+L upgrade environment. Simulations are performed on the Indian RailTel network (see Appendix B) consisting of 19 nodes and 28 bi-directional links. We repeat and average the simulations for 15 different seeds, each with about 1800 quasi-static demands. We assume equipment cost to upgrade one link from C to C+L as $J_{EDFA} = 1$ unit, with yearly depreciation of $\delta = 5\%$, and $J_{WSS} = 0.5$ unit. Using Eq. (8.1), we derive $\hat{J} = 512$ units. To train/test the CBPL model, dataset is obtained by simulating over numerous seeds and extracting necessary link features. The data is split in chunks of τ time steps (for our simulation, τ is set to 10).

8.4.2 Preliminary Evaluation of Baseline Approaches

To demonstrate the efficiency of CLU, we consider two intuitive baseline approaches: basic spectrum utilization (BSU) and cost-aware spectrum utilization (CSU). In BSU, links that exceed a predefined SU threshold ($\tilde{\mu}$) are candidates for upgrade. Since it does not consider budget constraint, we introduce, as an extension of BSU, a cost-aware approach, CSU, which not only checks $\tilde{\mu}$, but also checks if the candidate links can accommodate one or more requests (over a single hop) so as to delay upgrades and reduce cost. We model CSU to postpone upgrades for up to n iterations (e.g., if $n = 3$, we check upto three times if a link can accommodate one more request and hence delay the upgrade).

Since performance of CSU varies over n, we evaluate its performance w.r.t. n. As shown in Fig. 8.3, we compare BP of CSU for different values of n with BSU. Since BSU relies only on $\tilde{\mu}$

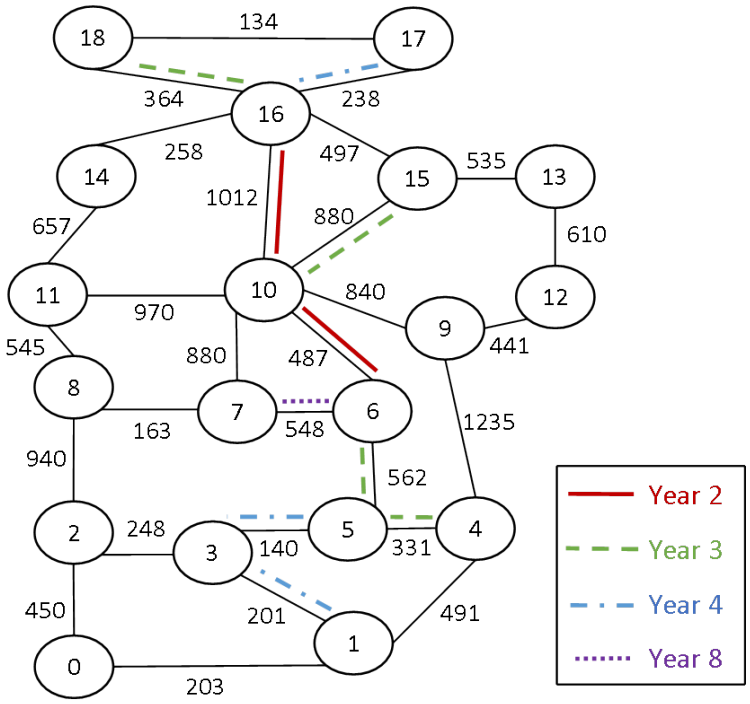

Figure 8.2: Indian RailTel network with link lengths in km. Gradual link upgrades by CLU (for $\tilde{\alpha} = 0.05$) are shown by solid and dashed lines.

to initiate an upgrade and does not wait to accommodate additional requests, BSU exhibits the lowest BP compared to CSU. Results also show that, with every increment of n, BP continues to rise in CSU as postponing the upgrade leads to higher BP. However, it also leads to lower cost as shown in Fig. 8.4 which compares the total upgrade cost of CSU for different values of n with BSU. Here, the cost of BSU is almost comparable to CSU when $n = 1$ and $n = 3$ for $\tilde{\mu} = 0.4$. However, when $n = 8$, the upgrade cost is lower for all values of $\tilde{\mu}$. Since CSU aims to delay upgrade, higher values of n will lead to lower cost. Considering both blocking and cost evaluation, CSU ($n = 3$) is selected for comparison with CLU as it gives reasonable trade-off between BP and upgrade cost compared to BSU and other variations of CSU.

8.4.3 CLU vs. Baseline Approaches

In Fig. 8.5, we evaluate the performance of CLU and analyze the trade-off between BP (blue solid line) and upgrade cost (red dashed line). In addition to comparing with CSU ($n = 3$) (as discussed in Section 8.4.2), we also consider two extreme cases: early upgrade (EU) and no upgrade (NU). EU initiates network operation by upgrading all links without considering any selection criteria which leads to highest cost (512 units) with lowest blocking. In NU, the entire network operates only in C band without any upgrade, which leads to highest BP (about 16%) and lowest upgrade cost.

In Fig. 8.5, our strategy CLU outperforms CSU ($n = 3$) for different values of $\tilde{\mu}$. With $\tilde{\alpha} = 0.05$, CLU leads to lower BP of about 4% compared to about 7% and 9% BP by CSU for $\tilde{\mu} = 0.5$ and 0.6, respectively. CLU also significantly curtails upgrade cost by about 32% and 15% compared to CSU for $\tilde{\mu} = 0.5$ and 0.6, respectively. As CBPL threshold is increased, i.e., $\tilde{\alpha} = 0.1$, CLU delays the upgrade lowering the cost slightly but it leads to higher BP of about 6% (which is still lower than BP of CSU). In terms of cost savings, CLU reduces upgrade cost by about 41% and 26% compared to CSU for $\tilde{\mu} = 0.5$ and 0.6, respectively. It is evident that increasing SU threshold reduces upgrade cost at the expense of increased BP. Hence, a network operator could benefit from using CLU, which reduces both BP and upgrade cost compared to CSU.

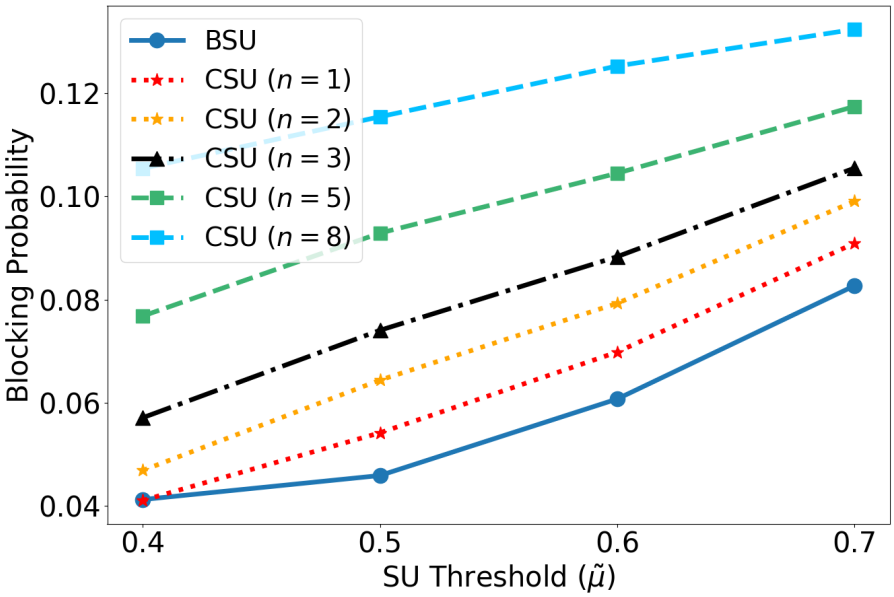

Figure 8.3: Blocking probability comparison of CSU and BSU.

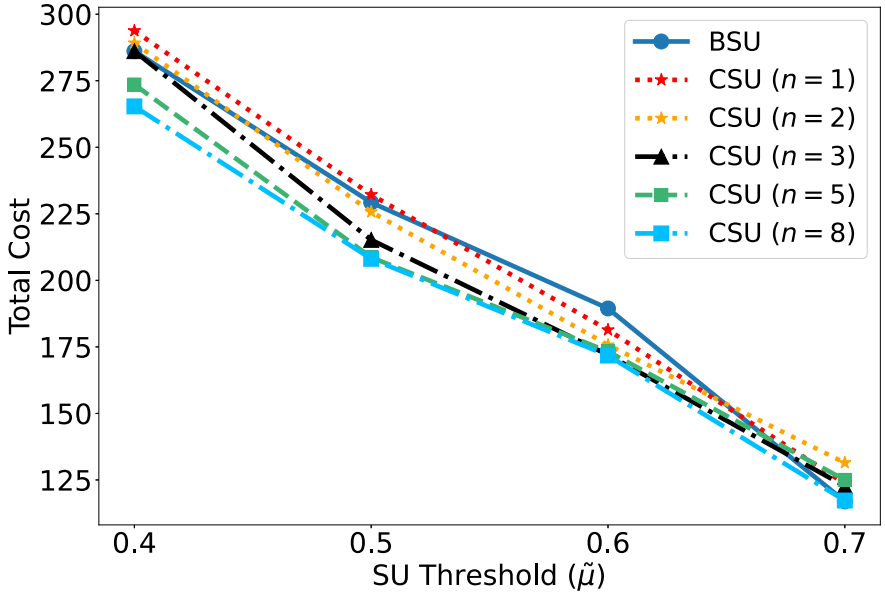

Figure 8.4: Upgrade cost comparison of CSU and BSU.

To analyze the impact of upgrades at appropriate times, Table 8.1 compares the number of links upgraded in a year by each strategy. We see that BSU and CLU start upgrading at year 1 and 2, respectively, while CSU starts at year 3. For CSU, since upgrades are delayed by $n = 3$ times, most link upgrades occur much later, e.g., at year 6 and beyond. As shown in Table 8.1, with increasing $\tilde{\mu}$, fewer links are upgraded by the baseline strategies (since not all links in the network reach the SU threshold). For example, for $\tilde{\mu} = 0.5$, 18 and 16 links are upgraded by BSU and CSU, respectively, whereas 13 links are upgraded for $\tilde{\mu} = 0.6$. On the other hand, we show that CLU significantly outperforms both BSU and CSU as it upgrades only 10 links in appropriate years for $\tilde{\alpha} = 0.05$ and 0.1. In Fig. 8.2, we show which 10 links in the topology are upgraded by CLU for $\tilde{\alpha} = 0.05$ in years 2, 3, 4, and 8.

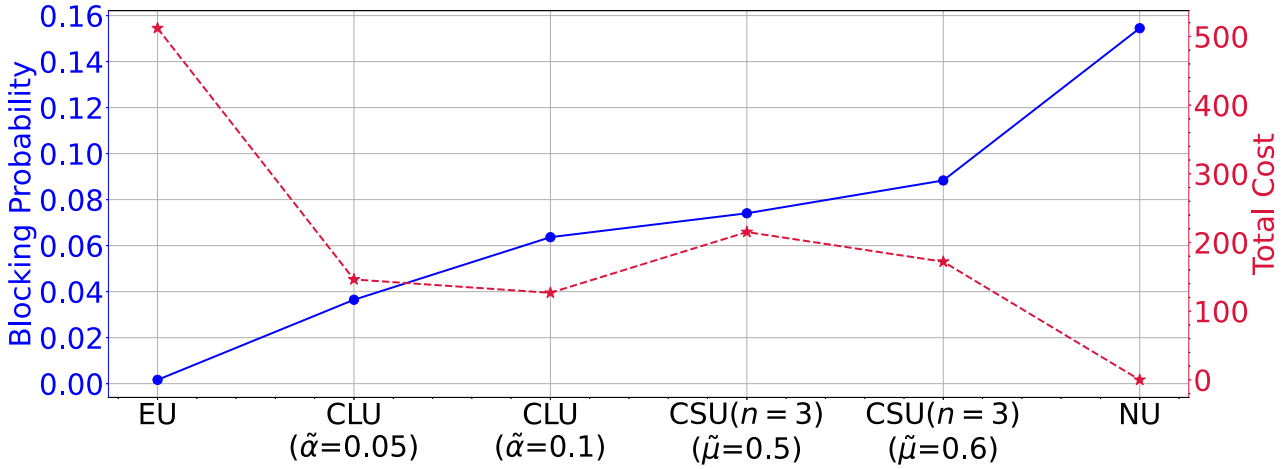

Figure 8.5: Comparison of CLU with baseline strategies.

Table 8.1: Number of Links Upgraded per Year

Method \ Year		1	2	3	4	5	6	7	8	9	10	Total
BSU	$\tilde{\mu} = 0.5$	2	1	1	2	3	2	2	3	2	0	18
	$\tilde{\mu} = 0.6$	1	1	1	1	2	1	2	2	2	0	13
CSU ($n = 3$)	$\tilde{\mu} = 0.5$	0	0	1	1	1	2	3	4	4	0	16
	$\tilde{\mu} = 0.6$	0	0	0	1	1	1	2	3	5	0	13
CLU	$\tilde{\alpha} = 0.05$	0	2	4	3	0	0	0	1	0	0	10
	$\tilde{\alpha} = 0.1$	0	0	2	4	2	1	1	0	0	0	10

8.5 Conclusion

We proposed a novel upgrade strategy, named CLU, utilizing an RNN-based model that effectively identifies links for upgrade in the network. Numerical results show that our proposed strategy outperforms the baseline strategies in terms of both BP and upgrade cost. These findings highlight the potential for significant cost savings and reduced BP when a network operator employs a trained ML model for upgrade decisions.

Chapter 9

Effect of Adaptive Margin Allocation on Network Upgrade

9.1 Introduction

Chapter 7 and 8 indicates that the availability of adequate spectrum resources by upgrading the current C-band-based network infrastructure is crucial for the network operator to support enormous future traffic growth [11]. Recently, numerous studies [1], [15], [20], [26] compare the possible solutions for network upgrades, and it is reported that usage of parallel C-band fiber solution will be beneficial for those network operators who have their own available dark-fibers. However, before the enlightenment of additional dark fibers in the duct, the maximum achievable capacity of the active fibers needs to be explored to postpone the requirement of upgrade and minimization of the additional CapEx and cost-per-bit in the long run.

This chapter focuses on extracting the true capacity of the deployed infrastructure and investigates the effect of adaptive margin allocation on network upgrades. Our proposed approach considers periodic feedback from the network to gain domain knowledge and prioritizes adequate margin allocation before network upgrade initiation. Figure 9.1 depicts the considered simplified architecture of the core optical network while reflecting the important components of the data plane and network management plane. The deployed optical devices (optical fibers, amplifiers (EDFA), optical performance monitoring (OPM) equipment) are shown in the data plane, whereas network controllers are considered in the management plane. The lightpaths in the underlying physical layer between different sources and destinations are routed over multiple links while considering several linear and non-linear impairments, as discussed in Chapter 2. The QoT is evaluated in terms of the received OSNR [20] at the coherent receivers while considering the cumulative noises from in-line devices.

9.2 Domain Knowledge-Assisted Adaptive Margin Allocation Framework

The true capacity of the network not only depends on these accumulative noises but also depends on the considered link margin [104], [105], which operators incorporate to safeguard against service interruption caused by link degradation. Traditionally, at the beginning of life (BoL) of the network, operators do not rely on the performance of the deployed equipment and network performance, thereby allocating a high link margin [104] in the network. However, as the network is operated towards the end of life (EoL), the operator can get more insights from OPM data and would expect greater certainty about its actual state of performance and

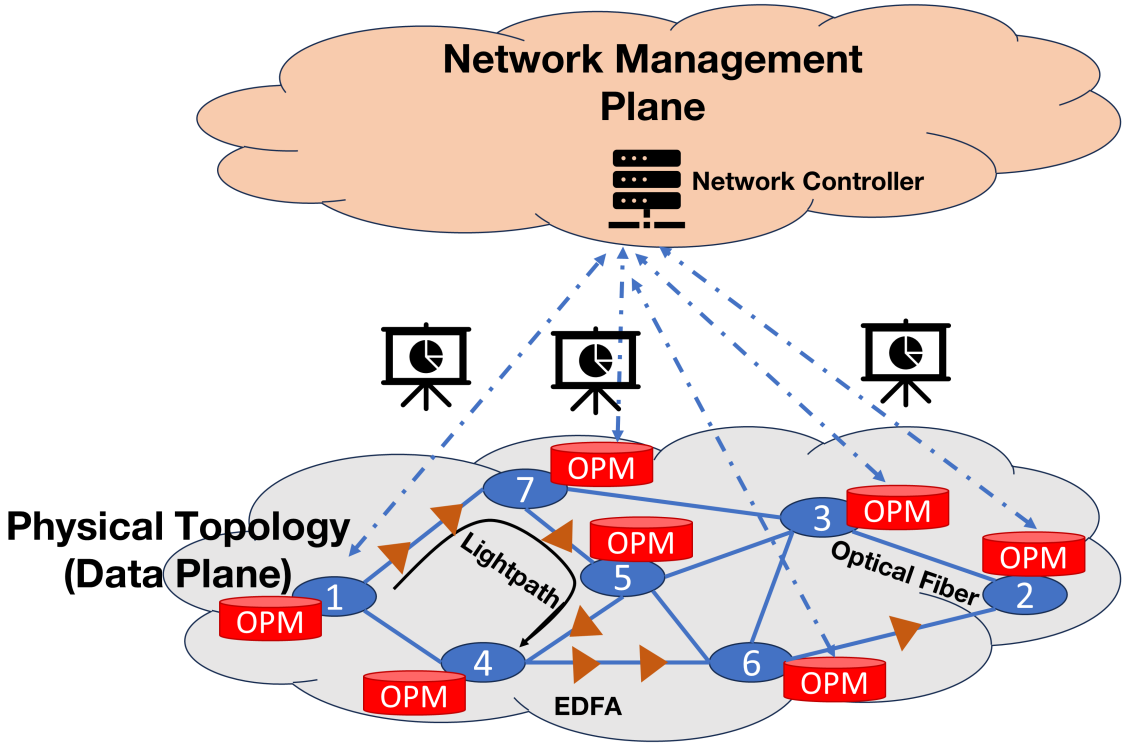

Figure 9.1: Physical and Network Layer Model.

variability. This knowledge can be beneficial for the operator to reduce margins later in the network's life, and that could be useful to support the required additional spectrum resources for future connections.

This section proposes an adaptive margin allocation framework by considering feedback from the deployed network, and its steps are briefly summarised as follows. First, the performance of the network for different time horizons needs to be predicted in advance by analytical modeling while considering the worst case (highest margin) and ideal scenarios (no margin). This analytical data can be compared with the available real-field data at the network controller level. This real-field data is generally collected from the OPMs and forwarded to the network controller. After statistical analysis at the network controller, the average deviation on the QoT is predicted, and that can be adapted as a margin for the subsequent connection. To emulate and collect data from a real network scenario (termed as 'Field'), we have done simulations by varying the NF of the in-line amplifiers and attenuation of optical fibers. The maximum period of periodic data collection from OPMs is considered as an operator's choice. We have considered field data of four consecutive half-years (termed as HY_1, HY_2, HY_3 and HY_4) and assumed a maximum period of periodic data collection as two years. In the statistical toolbox of the network controller, these field data are compared with the predicted data, and different values of adaptive margin are suggested for the respective time horizons.

9.3 Network Upgrade Strategy

Figure 9.2 captures the flow of network update strategy in the presence of domain knowledge-assisted adaptive margin scenario. At first, the RMSA has been solved for every incoming request by considering the worst-case hard margin. Later on, the availability of monitoring data from OPM has been used to choose the adaptive margin for the subsequent connections in the network. The network is upgraded by adding additional optical fibers in the specific links and additional optical amplifiers to minimize the blocking ratio (BR).

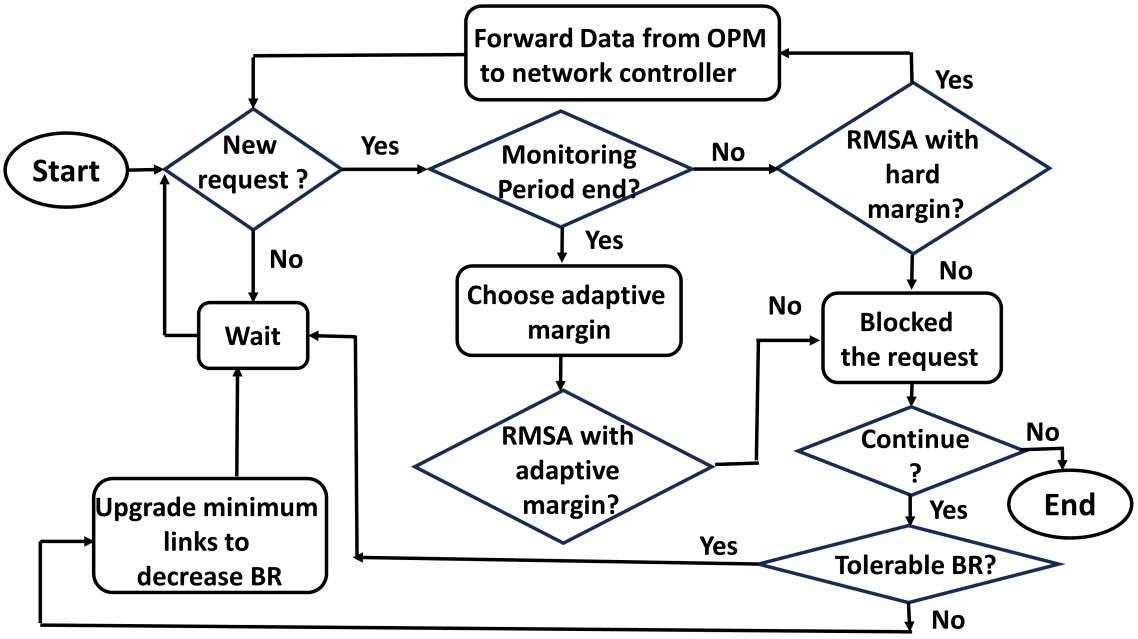

Figure 9.2: Flowchart of network upgrade strategy.

9.4 Simulation Framework and Assumptions

In this work, a custom-built event-driven in-house Python simulator is developed for adaptive margin allocation. Network simulations are focused on the BT-UK network (22 nodes, 35 links, average link length 147 km) with a uniform launch power of 0 dBm/channel. We consider the symbol rate of 28 GBaud with a channel spacing of 37.5 GHz while incorporating six modulation formats (PM-BPSK, PM-QPSK, PM-8QAM, PM-16QAM, PM-32QAM, and PM-64QAM) with corresponding supportable data rates (50, 100, 150, 200, 250 and 300 Gb/s) and required OSNR thresholds (9, 12, 16, 18.6, 21.6 and 24.6 dB)[14].

The subsequent section presents the average outcomes derived from multiple seeds, ensuring a margin of error of less than 5% within a 95% confidence interval. During simulation, the traffic growth rate of 35% with the baseline traffic of 20 Tbps is assumed while considering a biased traffic metrics generator [20]. Each link within the network is presumed to utilize the C-band of ITU-T G.652.D fibers, along with the standard system parameters tuple (attenuation coefficient = 0.2 dB/ km, dispersion = 17 ps/nm/km, dispersion slope = 0.067 ps/nm^2/km, non-linear coefficient = 1.2 /W/km, Raman gain slope = 0.028 /W/km/THz). Furthermore, the k–shortest path (k = 3) routing algorithm is considered for the selection of shortest routes between source-destination pair and the last-fit allocation policy (i.e., choice of shortest wavelength first) is considered for the spectrum selection of individual lightpaths. Moreover, it is assumed that the BT-UK network has its own dark fibers throughout the network, which have been used for network upgrades; therefore, only the amplifier upgrade cost is taken into consideration for techno-economic comparison. Furthermore, the cost of individual C-band EDFAs ($\sim$ 4000$) is taken as x unit for reference [20].

9.5 Results and Discussion

The performance of the proposed adaptive margin allocation algorithm is evaluated in terms of the percentage of margin reduction (PMR), the cumulative number of additional required fibers and amplifiers for network upgrade, QoT in terms of lower order modulation (LoM), and

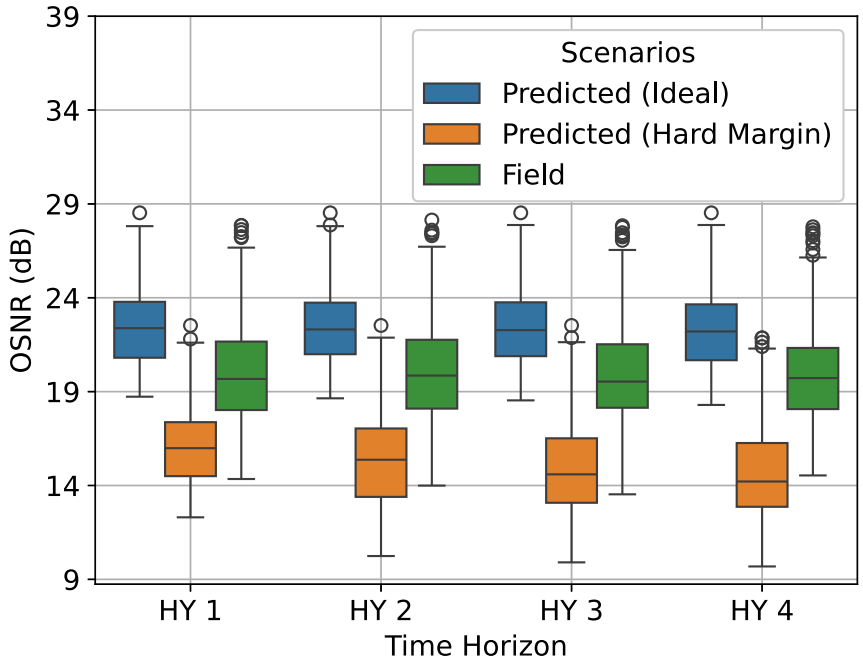

Figure 9.3: OSNR Distribution with Time Horizon.

higher order modulation (HoM) based lightpaths, normalized upgrade cost-per-bit (NUCpB), and operational expenditure (OpEx).

Figure 9.3 captures the OSNR distribution of active lightpaths in the network under different time horizons. Predicted OSNR of lightpaths at BoL is captured using blue and orange bars for ideal (no margin) and hard margins (6 dB), respectively. Whereas the emulated results of the real field scenario are shown by green bars, which is analogous to the collected data from field OPM.

The amount of PMR by considering different stages of monitoring data is captured in 9.4. Reported results show that, on average, a maximum of 50% PMR can be achieved using the monitoring data compared to hard margin scenarios.

The instances of additional fiber additions under various margin scenarios are depicted in Fig. 9.5 for achieving a targeted capacity of 150 Tbps (which resembles seven years of network traffic). Numerical results show that the addition of a hard margin of 6 dB prepones the need for network upgrade and reduces the achievable capacity of the non-upgraded network by 50.4 Tbps compared to the ideal scenario (no margin). In the case of adaptive margin, lightpath allocation started with a high margin of 6 dB due to the absence of domain knowledge at the BoL of the network. However, as the margin gets updated with domain knowledge using the monitoring data from different quarters, a significant advantage is observed in terms of traffic admissibility. Results indicate that adaptive margin allocation can show a maximum of 57.3% less upgrade compared to the hard margin of 6 dB.

Table 9.1 summarizes the benefits of the proposed margin allocation framework compared to the baseline solutions. Reported results show that the allocation of a hard margin of 6 dB degrades the quality of transmission and enhances the LoM, such as PM-BPSK and PM-QPSK, by 22.4% compared to the ideal scenario (i.e., no margin). As the total length of additional fibers (TLAF), the percentage of upgraded links (#Links), and the total number of additional amplifiers (TNAA) increase in the case of hard margin, it reflects the requirement of the highest OpEx and NUCpB. The proposed domain-knowledge-assisted adaptive margin allocation algorithms show the maximum reduction of upgrade cost and NUCpB by 58% compared to the

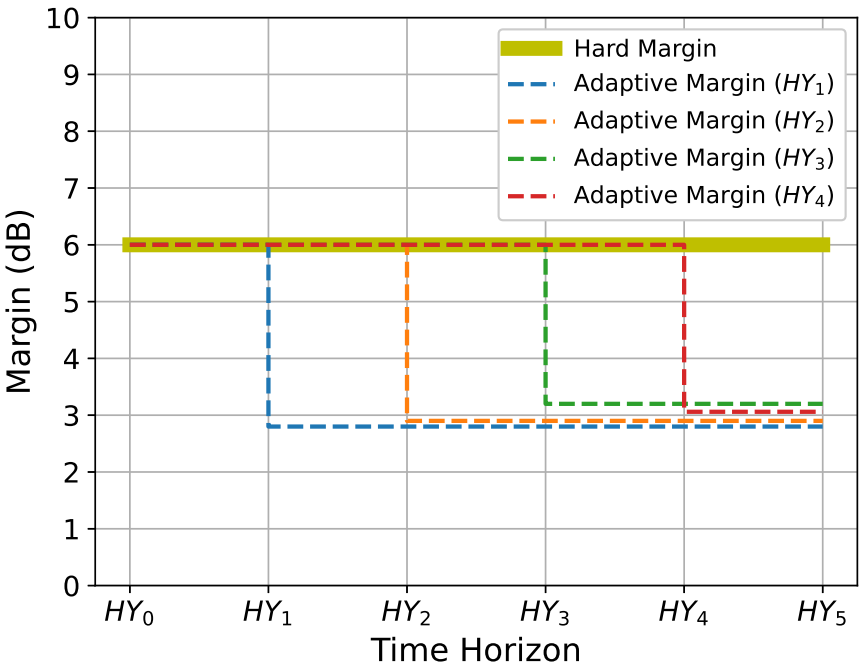

Figure 9.4: Margin Reduction from BoL to EoL.

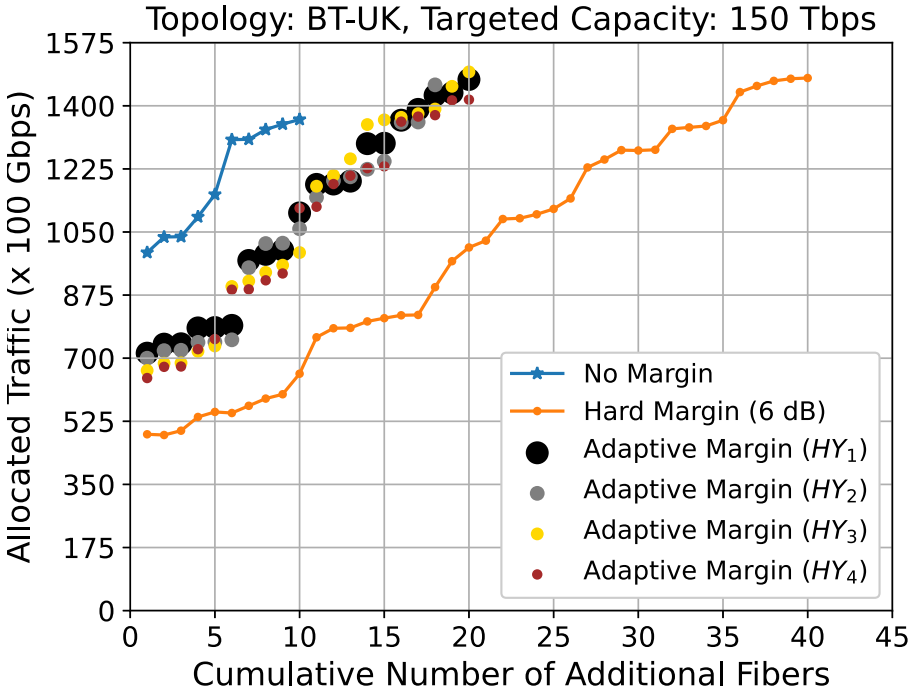

Figure 9.5: Additional fiber requirement with traffic loading.

Table 9.1: Effectiveness of proposed adaptive margin allocation strategies for targeted capacity of 150 Tbps.

Margin	LoM	HoM	TLAF (km)	TNAA	#Links	NUCpB (x/Tbps)
No Margin	7.3%	92.7%	1,238	26	28.6%	0.17
Hard Margin (6 dB)	84.7%	15.3%	4,923	103	68.6 %	0.69
Adaptive Margin (HY_1)	55.3%	44.7%	2,261	49	42.8 %	0.33
Adaptive Margin (HY_2)	59.0%	41.0%	2,028	45	42.8 %	0.30
Adaptive Margin (HY_3)	62.4%	37.6%	2,224	49	42.8 %	0.33
Adaptive Margin (HY_4)	58.2%	41.8%	1,978	44	40.0 %	0.29

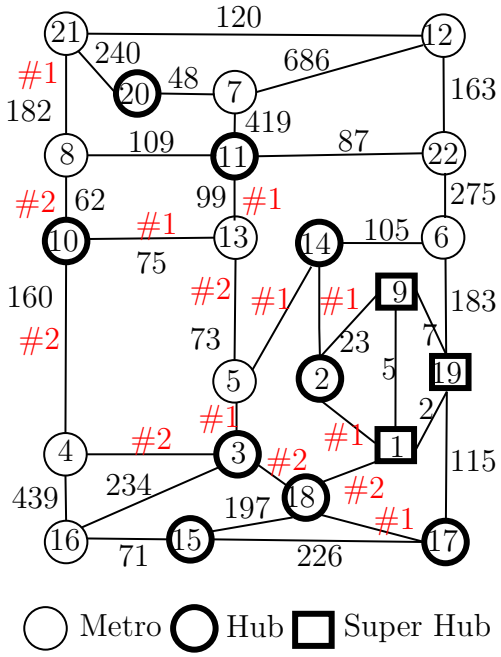

Figure 9.6: Upgraded BT-UK network with adaptive margin (HY_4) (numbers in # red represents additional upgraded fibers in specific locations).

worst hard margin scenario. The effect of monitoring period variation during adaptive margin allocation is also captured in the last four rows of Table 9.1. Numerical results indicate that the collected monitoring data from HY_4 outperforms in terms of NUCpB and OpEx minimization, whereas it falls behind in terms of QoT compared to the remaining adaptive strategies.

Figure 9.6 shows the location of the additional fibers in the network for the targeted capacity of 150 Tbps under the best adaptive margin (HY_4) scenario.

9.6 Conclusion

This work shows the benefits of adaptive margin allocation compared to hard margin by leveraging input from network health monitoring equipment. Enhancement of the collected monitoring data can provide certainty and variability around the actual state of network performance, and that can be helpful in adjusting the margin from BoL to EoL. However, trade-offs exist between the duration of the monitoring period and the net profit from the adaptive margin allocation.

Chapter 10

Network Survivability for C+L Band Optical networks

10.1 Introduction

Upgrading the core optical network beyond the existing C-band-based infrastructure becomes necessary for the network operator to support the exponential growth of global IP traffic. As discussed in Chapters 3 and 4, operations over the C+L band can be a short-term, cost-effective solution for minimizing network upgrade cost and the cost-per-bit in the long run. However, to assess the overall potential of the multiband solution, network reliability due to component failures needs to be studied.

This chapter considered the inline amplifier failure scenario and showed the benefits of C+L band systems compared to conventional C-band systems. Our approach measures the overall protection space of the network and the quality of the allocated lightpaths in two geographically diverse networks. As a final step, we show the effect of the required OSNR cushion variation for absorbing adjacent channel impairments (called Fill Margin (FM) [13], [106]) on the achievable protection space and reliability of the network. We have considered the same physical layer model for C+L band transmission as discussed in Chapter 2. The remaining parts of this work are arranged as follows. Section 10.2 captures the details of the proposed protection strategy. The effect of FM on network protection is illustrated in Section 10.3. The simulation setup and simulated results are reported in Sections 10.4 and 10.5, respectively. Finally, Section 10.6 concludes the work.

10.2 Protection Strategy

This section discusses the proposed methodology that has been considered for ensuring 1+1 protection in the network. In this work, we consider only single-band (either C or L band) inline amplifier failure scenarios for the C+L band system, and hence, the provisioning of the backup lightpaths is prioritized over the same route as primary lightpaths using the alternate band. If the spectrum is unavailable in the primary route then alternate routes are explored (like conventional C-band system) for backup path provisioning in the C+L band system. Figure 10.1 shows the flow of the protection strategy where the possibility of provisioning one dedicated backup lightpath and one primary lightpath is explored for every requested connection in the network. If a backup lightpath is not feasible in the network for certain connections, only primary lightpaths are allocated for them. When the network reaches its targeted capacity, the process of resource allocation ends.

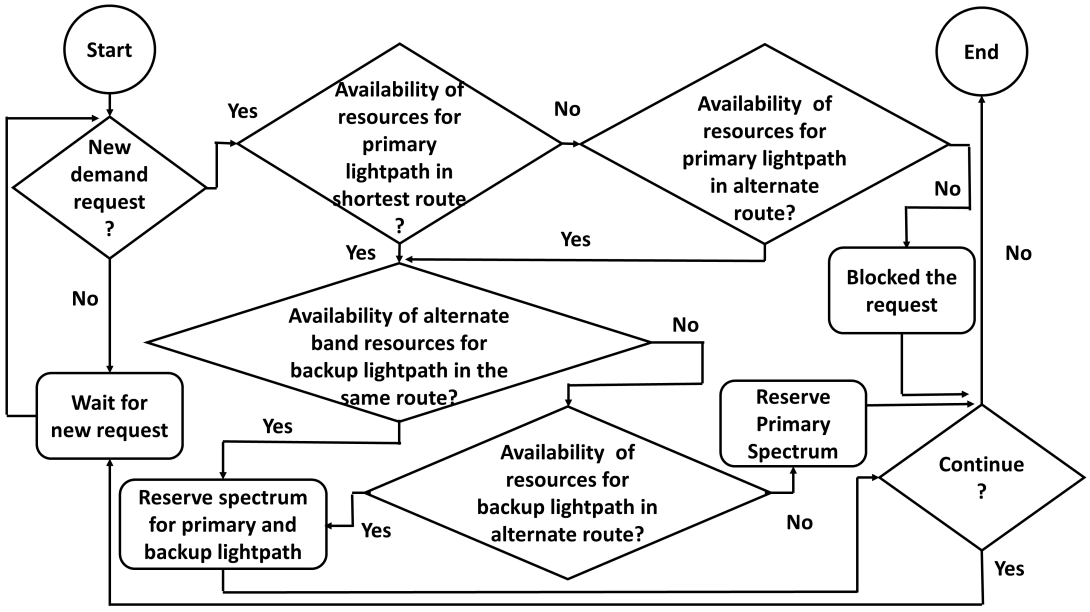

Figure 10.1: Flowchart of 1+1 protection strategy.

10.3 Effect of Fill Margin on Network Protection

FM is a well-studied metric for link designing in optical networks, and it is defined as the required OSNR cushion that is needed to absorb the effect of channel loading on the existing connections in the network. Mainly, FM is employed to protect against the NLI from the nearby channels and allows the network operators to maintain the quality of the lightpath. However, the FM can severely impact the network survivability in the multiband scenario. The additional spectrum resources of the multiband system can be used to provide protection in the network. Figure 10.2 shows such a scenario, where the C-band system is used for provisioning primary connections (denoted by: C1(P), C2(P)) and their dedicated backup connections (denoted by: C1(B), C2(B)) are provisioned over L-bands on the same route. If any new connections (say, C3(P) and C3 (B)) appear, then depending on the choice of FM, the situation may arise to allocate a backup lightpath in an alternate route. Considering an FM of 0 dB, upon the addition of a new request, an operator may allow the OSNR of existing lightpaths to degrade up to the threshold; however, for FM 2 dB, the new threshold for tolerable degradation will be 2 dB higher than the original threshold. Therefore, as any new connection arrives under high FM, the likelihood of the OSNR dropping beyond the new threshold will be higher. This may prevent the allocation of backup lightpath over the same route, and consequently, spectral space over an alternative route shall be utilized, leading to higher spectrum occupancy.

10.4 Simulation Setup

In this work, two diverse network topologies, namely, BT-UK network (22 nodes, 35 links, average link length 147 km) and USA24 network (24 nodes, 43 links, average link length 991 km) [16] have been considered for simulation. The details of these topologies are discussed in Appendix B. As discussed in Chapter 2, GFF placement is considered at each EDFA module for the longer USA24 network, whereas GFF is considered at each ROADM block for the smaller BT-UK network. Lightpaths are allocated into the network with individual launch power of 0 dBm while considering three available modulation formats (PM-QPSK, PM-8QAM, and PM-16QAM) at 64 GBuad, with channel spacing of 75 GHz [26]. A traffic growth rate of 35%

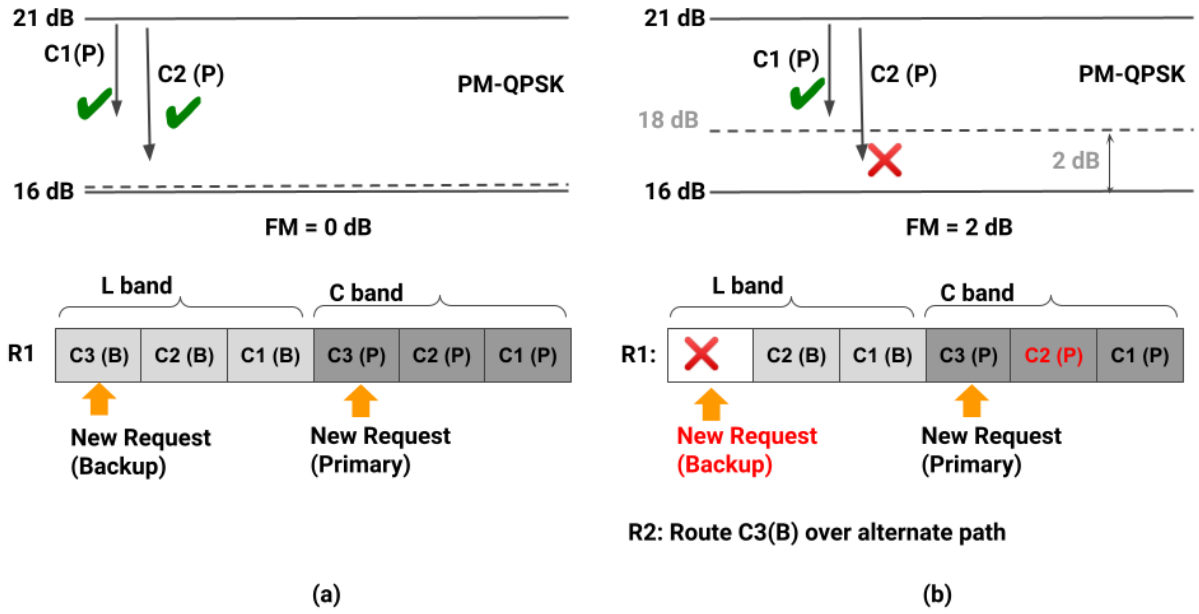

Figure 10.2: Concept of Fill Margin. (a): Tolerable degradation up to 16 dB threshold for the existing connections C1(P) and C2(P), FM = 0 dB, (b): Due to FM of 2 dB, the addition of C3(B) degrades the C2(P) beyond 18 dB, thereby triggering the backup lightpath route R2.

with baseline traffic of 20 Tbps is considered in the network while using a biased traffic matrix generator [20]. Average results of multiple seeds with less than 5% margin of error at a 95% confidence interval are reported in the following section.

10.5 Results and Discussion

We evaluate the performance of the proposed protection strategy in terms of the overall protection space of the network, and the quality of the allocated lightpaths under different FM conditions. Protection space is an indicator of how many requests in the network have a backup lightpath over which it can be routed in an event of single C-band or L-band equipment failure. The quality of lightpaths and associated capacity is decided while comparing the OSNR of a lightpath against OSNR thresholds of PM-QPSK, PM-8QAM, and PM-16QAM.

The effect of FM variation on the protection space in the BT-UK network is captured in Fig. 10.3. For a targeted capacity of 80 Tbps with 0 dB FM, the C+L band system allocates 55.6% more demands than the C-band system in the network with 1+1 protection. As the FM of the network enhances, the flexibility of backup lightpath establishment in the same route as of primary is reduced in the C+L band system. Hence, backup lightpaths for the C+L band system start routing over longer link disjoint paths leading to the reduction of the quality of backup lightpaths and overall protection of the network. Figure 10.3 shows that increment of FM from 0 to 2 dB, reduces the protection space by 9.6% for C+L band system as multiple backup paths are allocated over lower order modulation formats (as shown in Fig. 10.4). Moreover, if the targeted capacity of the network is increased along with FM enhancement, the probability of spectrum availability in alternate band/route is reduced and as a result, the protection space reduction (PSR) for the C+L band system can also further enhanced as indicated in Table 10.1.

As the C+L band protection strategy first explores the availability of spectral resources in an alternate band for protection in the same route of the primary lightpath, the average

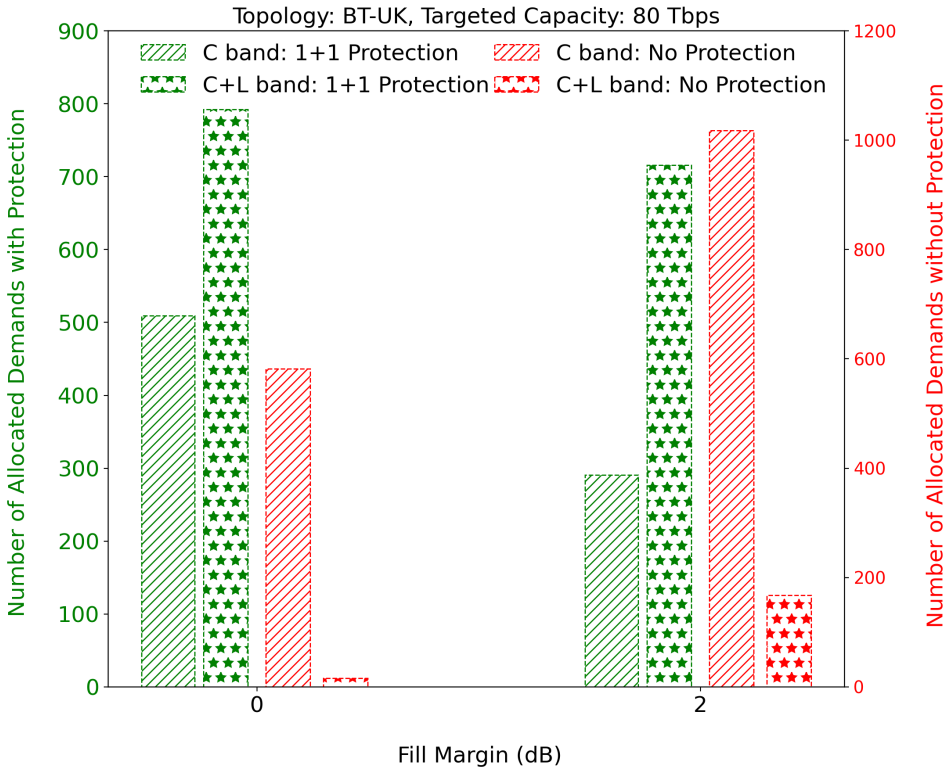

Figure 10.3: Effect of FM on protection space of BT-UK network.

Table 10.1: Effect FM enhancement (0 to 2 dB) on the protection space of C+L band system in BT-UK network.

Targeted Capacity (Tbps)	**PSR** (%)
80	9.6
100	12.3
125	15.5
150	18.8

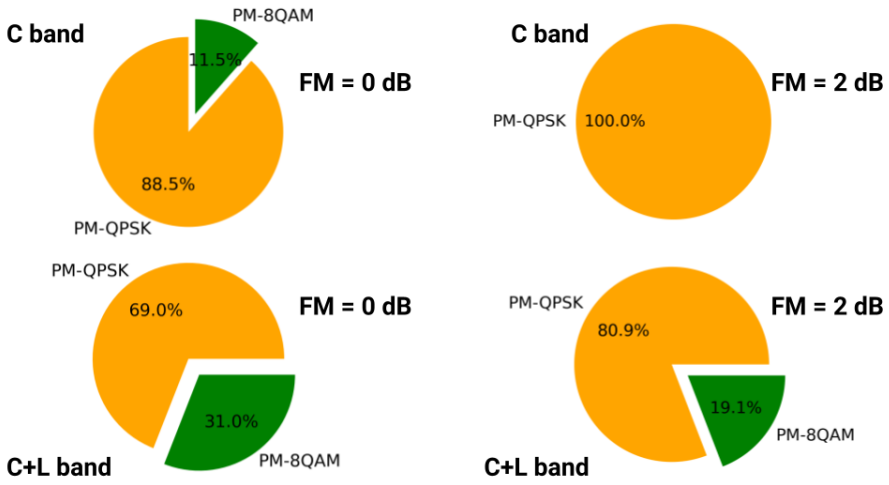

Figure 10.4: Quality of backup lightpath for BT-UK network (Targeted Capacity: 80 Tbps).

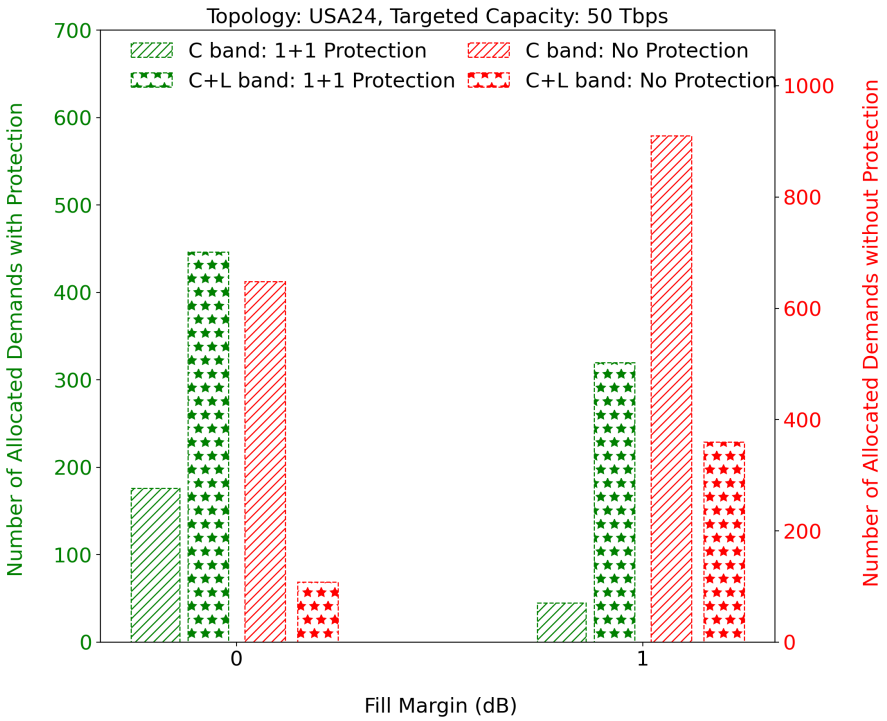

Figure 10.5: Effect of FM on protection space of USA24 network.

quality of the backup lightpath is higher compared to the C-band system (protection over a separate link disjoint path). Figure 10.4 shows that 31% of backup lightpaths can be placed with PM-8QAM for the C+L band with 0 dB FM, whereas it becomes only 11.5% for the C-band system. As all the backup lightpaths are placed using link disjoint alternate routes in the C-band system, the longer link length of the backup lightpath majorly supports low-quality modulations such as PM-QPSK.

Nevertheless, the impact of FM enhancement provides lower protection in C-band since the average quality of the backup lightpath is further reduced from the lowest available modulation format PM-QPSK. Figure 10.3 shows that the protection space of the C-band system reduces by 42.8% due to the 2 dB FM increment in the BT-UK network. The numerical result indicates that the availability of high-quality based backup lightpaths in the C+L band system provides a gain of ∼146% protection space compared to the C-band even in the presence of 2 dB FM.

In the case of longer geography such as the USA24 network, the presence of long link length degrades the average quality of lightpath. In addition, the increment of FM further reduces the achievable protection space in the network. Figure 10.5 shows the impact of FM variation on the survivability of the USA24 network. Results indicate that a variation of only 1 dB FM can reduce the protection gain by 74.4% and 28.2% in C and C+L band systems, respectively. Nevertheless, the C+L band system still outperforms compared to the C-band system even in the high FM scenario due to its inherent protection space.

10.6 Conclusion

This study shows that the C+L band system can ensure more reliability compared to the C-band system for ensuring connection survivability in smaller (BT-UK) and as well as larger networks (USA24). Increasing the FM allows the operators to maintain the signal quality, however, the trade-off would be in terms of achievable protection space. Hence an individual allocation of FM for every lightpath may be required to find the right balance between signal

quality and protection space in C+L band networks.

Chapter 11

Conclusions and Future Work

The research in this thesis is entirely focused on the multiband (C+L) optical networks while considering the inter-dependency between the network layer and the underlying physical layer. Numerous significant aspects, such as techno-economic comparisons, cost-per-bit minimization, efficient spectrum resource management, periodic network upgrades, reliability issues, etc., have been explored in various parts of this thesis. The research output on these perspectives will be truly essential for network operators and vendors for practically enabling C+L band transmission in the core optical network.

11.1 Summary of Contributions

The main contributions of this dissertation can be summarized as follows:

- The research in this thesis first considered the C+L band physical layer model and summarized the presence of significant challenges from several non-linear PLIs, such as ISRS, and band-dependent transmission impairments, such as attenuation, dispersion, etc. In order to enhance the QoT and the overall capacity of the network while mitigating the effect of PLIs, the use of GFFs in different parts of the network has been explored.

- The next part of this thesis is focused on the techno-economic comparisons between the C+L band optical network with the multifiber C band scenario, which have appeared as the alternative immediate solutions to solve the fiber capacity problem. In this context, we have taken the CapEx of different in-line components and considered geographically diverse networks. A domain-knowledge-assisted, cost-effective network upgrade algorithm is proposed to enhance the overall capacity of the network while minimizing CapEx. The performance of the proposed algorithm is assessed in terms of network upgrade cost, overall CapEx, and cost-per-bit while considering EON with incremental traffic. In addition, the comparison between optical cable deployment and fiber leasing is also captured to upgrade the capacity of the optical core network with minimum cost-per-bit.

- After showcasing the benefits of C+L band transmission on cost-per-bit minimization, the next part of this thesis is focused on the designing of efficient spectrum management policies for the C+L band network to enhance the overall network capacity. Hitless spectrum defragmentation is mainly considered for the efficient utilization of spectral resources. The proposed work provides in sights for network operators to develop the QoS maintenance strategy while doing spectrum defragmentation in the C + L bands. The proposed scheme prioritizes the minimization of the fragmentation index while maintaining the QoT for

two different defragmentation algorithms, namely, nonlinear-impairment (NLI)-aware defragmentation (NAD) and NLI-unaware defragmentation (NUD). We also leveraged ML techniques for QoT estimation of ongoing lightpaths during spectrum reprovisioning. The OSNR of a lightpath is predicted for each choice of spectrum reprovisioning, which helps to monitor the effect of defragmentation on the quality of active lightpaths (in terms of assigned modulation format).

- As the C+L band network is highly vulnerable to NLI, appropriate channel allocation during lightpath provisioning also becomes crucial for boosting the achievable capacity of the overall network. As a consequence, the next part of this thesis is focused on the development of efficient spectrum allocation strategies for C+L band networks. First, the performance of the existing spectrum allocation policies is investigated for C+L band systems while considering geographically diverse networks and different channel launch powers. Hence, a novel quality-aware resource provisioning scheme is proposed to enhance the overall network capacity. Unlike conventional schemes, the proposed scheme takes the effect of PLI before the choice of the spectrum during resource allocation to reduce the likelihood of blocking. An algorithm under this scheme, named OA-FLF, is proposed while leveraging the heterogeneity of the C+L band EON.

- As the existing C-band-based network can't adopt these above-mentioned emerging technologies instantaneously, strategic planning needs to be done to upgrade the existing network infrastructure. Hence, the later part of this thesis focuses on efficient network upgrade strategies. First, the advantage of resource re-provisioning via selective movement of lightpaths from C-band to L-band is explored before upgrading the C-band network to C+L-bands. Later on, a novel strategy, named CLU, is proposed to upgrade links from C to C+L bands gradually. Moreover, as the parallel multifiber C-band-based solution is beneficial for the network operators in the presence of their own dark-fibers availability, the later section of this thesis also explored the strategic network upgrade methodologies in this context. Later on, the advantage of adaptive margin allocation on network upgrades while effectively utilizing the monitoring data from optical performance monitoring equipment is shown for multifiber-based upgrade scenarios.

- Although operations over the C+L band can be an immediate and cost-effective solution for minimizing network upgrade costs, the impact on overall network reliability due to component failures needs to be considered for comprehensively assessing the true potential of the C+L band solution. Hence, the last part of this thesis is focused on the network survivability for C+L band networks while considering geographically diverse networks. In this context, we consider only single-band (either C or L band) inline amplifier failure scenarios. Our approach measures the overall protection space of the network and the quality of the allocated lightpaths in geographically diverse networks. As a final step, we show the effect of the required FM on the achievable protection space and reliability of the network.

11.2 Future Work

There are many relevant research directions in which the reported work of this dissertation can be extended. Some of the selected future research verticals in this context are described as follows:

- **Development of S+C+L band optical network:** The next step for MB optical transmission beyond the C+L band wavelength window relies on the expansion of the overall

transmission bandwidth to 20 THz wide while enabling the use of the short wavelength band (S-band) which covers the wavelength range of 1460 to 1530 nm. Research in recent years [107]–[110] have already started to look into this aspect; however, commercial deployment of S+C+L band requires more time since there exist several open questions and challenges in terms of S-band amplifier choice and QoT estimation [7]. In this dissertation, we have designed the network upgrade methodologies for hybrid C/C+L band scenarios. However, it will be interesting to investigate the optimum strategy for network upgrades toward the S+C+L band scenario for geographically diverse networks, and we will explore this in future research.

- **Multiband Network Survivability in the Presence of Fiber Cuts:** This dissertation has explored the survivability aspects in the C+L band systems while considering only single-band (either C or L band) inline amplifier failure scenarios. It will be interesting to re-investigate this problem in the presence of the fiber cuts scenario as well. As the frequency of network disruptions due to optical fiber cuts is common in longer geographies like India, the applicability of multiband networks can also be explored for resiliency maintenance in this context. An interesting open question is whether the deployment of the multiband optical network at specific parts of the network could be helpful for the minimization of network disruption and maintenance of service level agreements (SLA). We have kept this objective for our future research work.

- **Application of AI for Soft-Failure Detection and Management in Multiband Optical Network:** Detection of soft-failures in the in-line equipment (such as EDFA [111]–[113], wavelength selective switch (WSS) [111], [112], [114]) plays a crucial role in order to avoid hard-failures and service disruptions. Literature suggests that machine learning methods can be helpful in this context for predicting the soft failures in the network while monitoring BER [111]–[113] and optical spectral shape [114], [115]. As the number of inline components becomes almost double in the case of the multiband scenario, the likelihood of component failure and their associated consequences needs a separate investigation. One of our future objectives is to develop AI-assisted methodologies for proactively identifying the presence of any soft failures in band-specific inline network equipment (such as amplifiers and WSSes) and demonstrate its utilization for the designing of intelligent network control strategies in order to minimize the network downtime in the commercial C+L band optical network.

- **Techno-Economic Comparison in the Presence of Space Division Multiplexing:** In this dissertation, we have shown the techno-economic comparison between the C+L band system and parallel C-band solutions. However, it will be interesting to revisit this problem in the presence of space division multiplexing. Mainly, as the usage of multicore fiber emerges as a long-term solution [116]–[118] for the network operator, a separate study needs to be done in this context. One of our future research objectives is to explore the requirement of MCF upgrades with the growth of network traffic, followed by capturing the impact of multicore upgrades on the cost-per-bit. However, the key challenge in this context of the hybrid SMF/MCF scenario will come from the estimation of QoT while considering the impact of all linear and non-linear impairments.

Chapter 12

Publications

The following section captures the selected list of the author's journal and conference publications, whose research output has been discussed in detail in different sections of this thesis.

12.1 Peer-Reviewed Journal Papers

1. R. Kalkunte, **R. K. Jana**, S. Ferdousi, A. Srivastava, A. Mitra, M. Tornatore, A. Lord, and B. Mukherjee, "GSNR-aware resource re-provisioning for C to C+L-bands upgrade in optical backbone networks," in ***Photonic Network Communications***, vol. 47, pp. 139-153, July 2024, doi: 10.1007/s11107-024-01023-6, [**Impact Factor: 1.8**].

2. **R. K. Jana**, A. Srivastava, A. Lord, and A. Mitra, "Optical Cable Deployment vs. Fiber Leasing: An Operator's Perspective on CapEx Savings for Capacity Upgrade in Elastic Optical Core Network," in ***Journal of Optical Communications and Networking***, vol. 15, no. 8, pp. C179-C191, August 2023, doi: 10.1364/JOCN.483200, [**Impact Factor: 4.0**].

3. **R. K. Jana**, B. C. Chatterjee, A. P. Singh, A. Srivastava, B. Mukherjee, A. Lord, and A. Mitra, "Quality-Aware Resource Provisioning for Multiband Elastic Optical Networks: A Deep Learning-Assisted Approach," in ***Journal of Optical Communications and Networking***, vol. 14, no. 11, pp. 882-893, Nov 2022, doi: 10.1364/JOCN.465782, [**Impact Factor: 4.0**].

4. **R. K. Jana**, B. C. Chatterjee, A. P. Singh, A. Srivastava, B. Mukherjee, A. Lord, and A. Mitra, "Machine learning-assisted nonlinear-impairment-aware proactive defragmentation for C+L band elastic optical networks," in ***Journal of Optical Communications and Networking***, vol. 14, no. 3, pp. 56-68, March 2022, doi: 10.1364/JOCN.440214 [**Impact Factor: 4.0**].

12.2 Peer-Reviewed International Conference Papers

1. **R. K. Jana**, A. Lord, A. Srivastava and A. Mitra., "An Operator's Perspective on the Introduction of Domain Knowledge-Assisted Adaptive Margin Ahead of Network Upgrade," ***2024 European Conference on Optical Communications (ECOC)***, Frankfurt, Germany, 2024, pp. 1-4, (Accepted).

2. R. Kalkunte, F. S. Abkenar, **R. K. Jana**, D. Aureli, S. Ferdousi, A. Srivastava, A. Mitra, M. Tornatore and B. Mukherjee, "An Effective Strategy for Link Upgrade from C to C+L

Band in Elastic Optical Backbone Networks," ***2023 IEEE International Conference on Advanced Networks and Telecommunications Systems (ANTS)***, Jaipur, India, 2023, pp. 437-440, doi: 10.1109/ANTS59832.2023.104696492023.

3. **R. K. Jana**, A. Srivastava, A. Lord and A. Mitra, "Effect of Gain Flattening Filter Placement for Nonlinear Impairment Mitigation in Multiband Optical Transport Network," ***2023 IEEE International Conference on Advanced Networks and Telecommunications Systems (ANTS)***, Jaipur, India, 2023, pp. 102-107, doi: 10.1109/AN TS59832.2023.10469529.

4. **R. K. Jana**, A. Srivastava, A. Lord and A. Mitra, "Effect of fill margin on network survivability for C+L band optical networks," ***49th European Conference on Optical Communications (ECOC)***, Glasgow, UK, 2023, pp. 1453-1456, doi: 10.1049/icp.2023. 2589.

5. **R. K. Jana**, M. A. Iqbal, N. Parkin, A. Srivastava, A. Mishra, J. Balakrishnan, P. Coppin, A. Lord and A. Mitra, "Multifiber vs. Ultra-Wideband Upgrade: A Techno-Economic Comparison for Elastic Optical Backbone Network," ***2022 European Conference on Optical Communications (ECOC)***, Basel, Switzerland, 2022, pp. 1-4, doi: 10.1364/ECEOC.2022.We1A.5.

6. **R. K. Jana**, B. C. Chatterjee, A. P. Singh, A. Srivastava, B. Mukherjee, A. Lord, and A. Mitra, "Performance Evaluation of Conventional Spectrum-Allocation Policies for C+L Band Elastic Optical Networks," ***2021 IEEE International Conference on Advanced Networks and Telecommunications Systems (ANTS)***, Hyderabad, India, 2021, pp. 348-353, doi: 10.1109/ANTS52808.2021.9937024.

7. **R. K. Jana**, A. Mitra, A. Pradhan, K. Grattan, A. Srivastava, B. Mukherjee and A. Lord, "When Is Operation Over C + L Bands More Economical than Multifiber for Capacity Upgrade of an Optical Backbone Network?," ***2020 European Conference on Optical Communications (ECOC)***, Brussels, Belgium, 2020, pp. 1-4, doi: 10.1109/ECOC48923.2020.9333276.

Appendices

Appendix A

Inter-channel Stimulated Raman Scattering (ISRS)

Nonlinear power transfer among the adjacent active channels in the network due to the ISRS effect becomes significant in the scenario of multiband transmission. In general, the power spectral density (PSD) of the nonlinear interference (NLI) power due to optical Kerr non-linearity for a single span can be written as follows [19]:

$$G(f) = \frac{16}{27}\gamma^2 \int df_1 \int df_2 G_{Tx}(f_1) G_{Tx}(f_2) G_{Tx}(f_1+f_2-f) \cdot \left| \int_0^L d\zeta \sqrt{\frac{\rho(\zeta,f_1)\rho(\zeta,f_2)\rho(\zeta,f_1+f_2-f)}{\rho(\zeta,f)}} e^{j\phi(f_1,f_2,f,\zeta)} \right|^2 \tag{A.1}$$

where $G_{Tx}(.)$ denotes the PSD of different input signals, γ indicates the non-linearity coefficient, ϕ is related to group velocity dispersion (GVD) parameter, and $\rho(z,f)$ denotes normalized signal power profile. Moreover, in the presence of ISRS, the signal power profile evolution of every active WDM channel (say M) can be found by solving the following coupled differential equation [119]:

$$\frac{\partial P_i}{\partial z} = -\sum_{k=i+1}^{M} \frac{f_k}{f_i} g_r(\Delta f) P_k P_i + \sum_{k=1}^{i-1} g_r(\Delta f) P_k P_i - \alpha(f_i) P_i \tag{A.2}$$

where $\alpha(.)$ denotes the attenuation coefficient, P_k and P_i indicates the launch power of k^{th} and i^{th} channels, $g_r(.)$ captures the effect of normalized Raman gain spectrum corresponds to the frequency separation of Δf. If the triangular assumption [120] is considered for the Raman gain spectrum, Eq. A.2 can be solved analytically, and the normalized signal power profile or ISRS gain for frequency f can be written as follows :

$$\rho(z,f) = \frac{P_{tot} e^{-\alpha z - P_{tot} C_r L_{eff} f}}{\int G_{Tx}(\nu) e^{-P_{tot} C_r L_{eff} \nu} d\nu} \tag{A.3}$$

where C_r denotes Raman gain slope, P_{tot} is the total optical launch power. Furthermore, if the Eq. A.3 is combined with Eq. A.1, the gaussian noise (GN) model with ISRS consideration can be written as follows, which have been widely used in the literature as a baseline for QoT estimation in ultra-wideband transmission [12] system:

$$G(f) = \frac{16}{27}\gamma^2 \int df_1 \int df_2 G_{Tx}(f_1) G_{Tx}(f_2) G_{Tx}(f_1+f_2-f) \cdot \left| \int_0^L d\zeta \frac{P_{tot} e^{-\alpha\zeta - P_{tot} C_r L_{eff}(f_1+f_2-f)}}{\int G_{Tx}(\nu) e^{-P_{tot} C_r L_{eff} \nu} d\nu} e^{j\phi(f_1,f_2,f,\zeta)} \right|^2 \tag{A.4}$$

Appendix B

Network Topologies

Geographically diverse networks are considered in different chapters of this thesis, and their details are summarized below:

- **Smaller Network:**
  - BT-UK Network (22 nodes, 35 links, average link length of 147 km)
- **Larger Network:**
  - Pan-Europe Network (16 nodes, 23 links, average link length of 486 km)
  - Indian RailTel Network (19 nodes, 28 links, average link length 531 km)
  - USA-24 Network (24 nodes, 43 links, average link length 991 km)

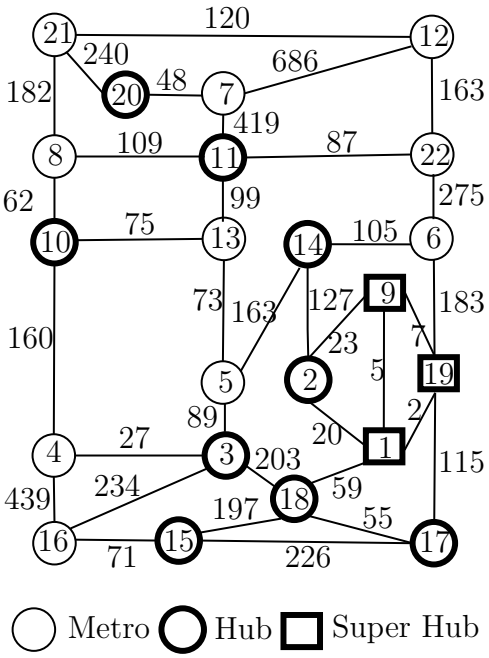

Figure B.1: BT-UK network with link lengths in km.

Table B.1 captures different metrics of individual nodes in the BT-UK network.

Table B.1: Node Metric in BT-UK Network.

Node Index	Population	Dropped Wavelength
1	2700	508
2	13900	192
3	20200	266
4	12100	121
5	30200	97
6	49200	186
7	43400	69
8	12400	124
9	12900	468
10	9000	189
11	10400	223
12	17300	117
13	50800	189
14	27800	238
15	4500	153
16	27400	57
17	59600	224
18	47200	294
19	15400	442
20	2700	137
21	45100	100
22	7800	9

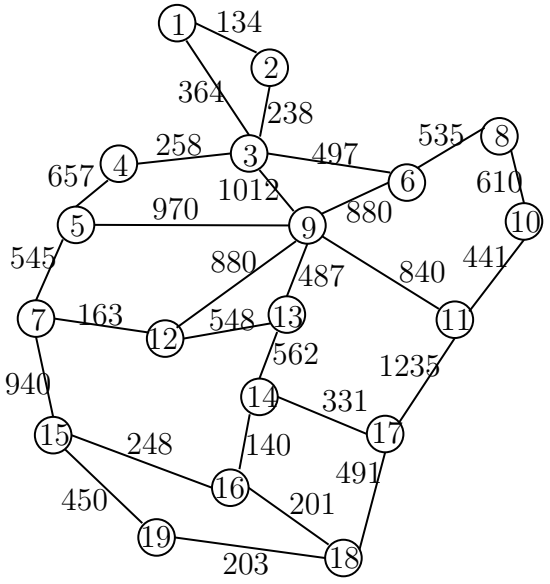

Figure B.2: Indian RailTel network with link lengths in km.

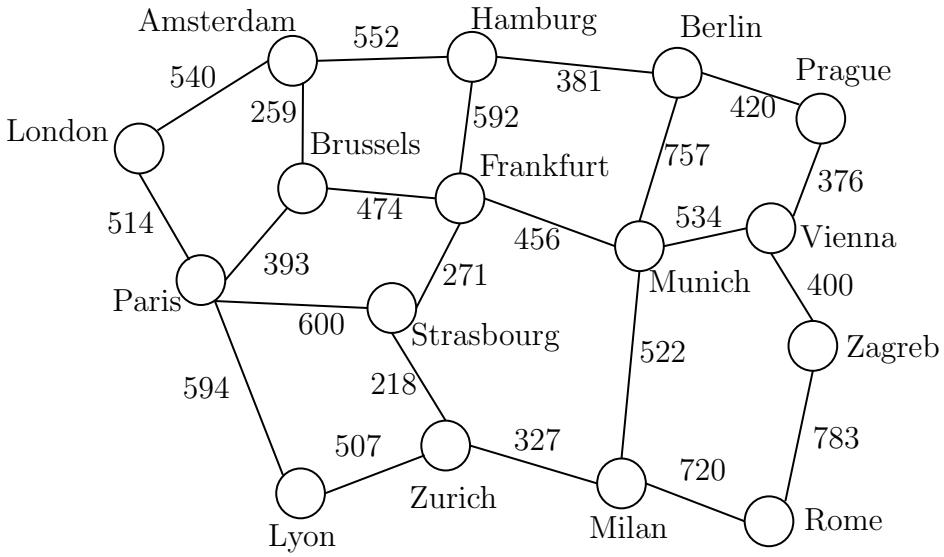

Figure B.3: 16-node Pan EU network with link length in km.

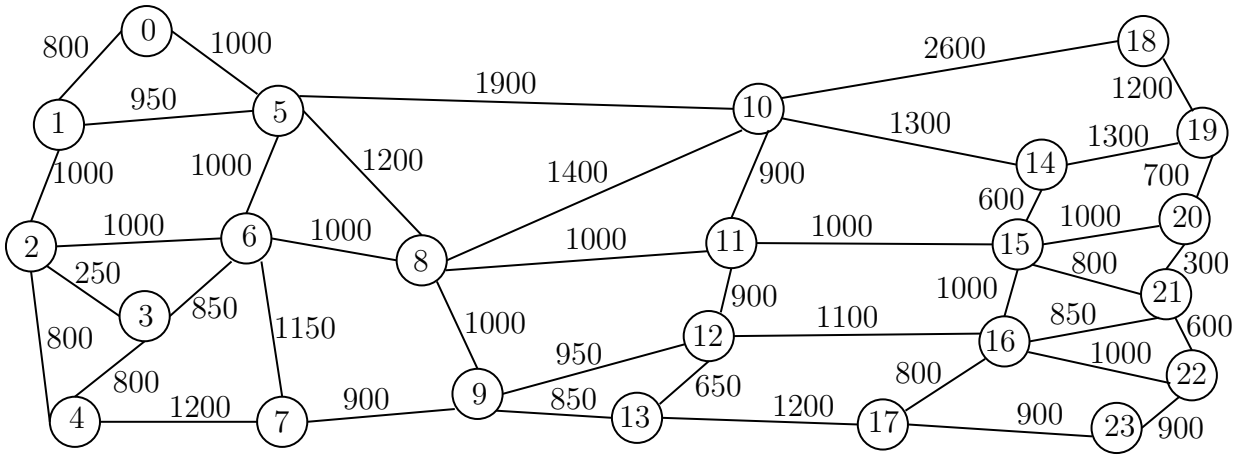

Figure B.4: 24-node USA network with link lengths in km.

Bibliography

[1] A. Lord, S. J. Savory, M. Tornatore, and A. Mitra, "Flexible Technologies to Increase Optical Network Capacity," *Proceedings of the IEEE*, vol. 110, no. 11, pp. 1714–1724, 2022.

[2] M. Jinno, "Elastic Optical Networking: Roles and Benefits in Beyond 100-Gb/s Era," *Journal of Lightwave Technology*, vol. 35, no. 5, pp. 1116–1124, Mar. 2017, ISSN: 1558-2213. DOI: 10.1109/JLT.2016.2642480.

[3] O. Gerstel, M. Jinno, A. Lord, and S. B. Yoo, "Elastic Optical Networking: A New Dawn for the Optical Layer?" *IEEE Communications Magazine*, vol. 50, no. 2, s12–s20, Feb. 2012, ISSN: 1558-1896. DOI: 10.1109/MCOM.2012.6146481.

[4] P. J. Winzer, D. T. Neilson, and A. R. Chraplyvy, "Fiber-optic transmission and networking: the previous 20 and the next 20 years," *Opt. Express*, vol. 26, no. 18, pp. 24 190–24 239, Sep. 2018. DOI: 10.1364/OE.26.024190. [Online]. Available: https://opg.optica.org/oe/abstract.cfm?URI=oe-26-18-24190.

[5] A. Ferrari, A. Napoli, J. K. Fischer, *et al.*, "Assessment on the Achievable Throughput of Multi-Band ITU-T G.652.D Fiber Transmission Systems," *Journal of Lightwave Technology*, vol. 38, no. 16, pp. 4279–4291, Aug. 2020, ISSN: 1558-2213. DOI: 10.1109/JLT.2020.2989620.

[6] A. Napoli, N. Costa, J. K. Fischer, *et al.*, "Towards multiband optical systems," *Advanced Photonics 2018 (BGPP, IPR, NP, NOMA, Sensors, Networks, SPPCom, SOF)*, 2018.

[7] L. Rapp and M. Eiselt, "Optical Amplifiers for Multi–Band Optical Transmission Systems," *Journal of Lightwave Technology*, vol. 40, no. 6, pp. 1579–1589, Mar. 2022, ISSN: 1558-2213. DOI: 10.1109/JLT.2021.3120944.

[8] M. Cantono, R. Schmogrow, M. Newland, V. Vusirikala, and T. Hofmeister, "Opportunities and Challenges of C+L Transmission Systems," *Journal of Lightwave Technology*, vol. 38, no. 5, pp. 1050–1060, Mar. 2020, ISSN: 1558-2213. DOI: 10.1109/JLT.2019.2959272.

[9] Cisco, "Cisco Annual Internet Report (2018–2023) White Paper," Accessed: March 26, 2021. [Online]. Available: https://www.cisco.com/c/en/us/solutions/collateral/executive-perspectives/annual-internet-report/white-paper-c11-741490.html.

[10] A. Yassine and M. S. Hossain, "COVID-19 Networking Demand: An Auction-based Mechanism for Automated Selection of Edge Computing Services," *IEEE Transactions on Network Science and Engineering*, vol. 9, no. 1, pp. 308–318, 2022. DOI: 10.1109/TNSE.2020.3026637.

[11] A. Lord, C. White, and A. Iqbal, "Future Optical Networks in a 10 Year Time Frame," in *Optical Fiber Communication Conference (OFC) 2021*, Optica Publishing Group, 2021, M2A.3. DOI: 10.1364/OFC.2021.M2A.3. [Online]. Available: https://opg.optica.org/abstract.cfm?URI=OFC-2021-M2A.3.

[12] D. Semrau, R. I. Killey, and P. Bayvel, "A Closed-Form Approximation of the Gaussian Noise Model in the Presence of Inter-Channel Stimulated Raman Scattering," *Journal of Lightwave Technology*, vol. 37, no. 9, pp. 1924–1936, 2019. DOI: 10.1109/JLT.2019.2895237.

[13] A. Mitra, D. Semrau, N. Gahlawat, A. Srivastava, P. Bayvel, and A. Lord, "Effect of Channel Launch Power on Fill Margin in C+L Band Elastic Optical Networks," *Journal of Lightwave Technology*, vol. 38, no. 5, pp. 1032–1040, Mar. 2020, ISSN: 1558-2213. DOI: 10.1109/JLT.2019.2952876.

[14] R. K. Jana, B. C. Chatterjee, A. P. Singh, *et al.*, "Machine learning-assisted nonlinear-impairment-aware proactive defragmentation for C+L band elastic optical networks," *Journal of Optical Communications and Networking*, vol. 14, no. 3, pp. 56–68, 2022. DOI: 10.1364/JOCN.440214.

[15] R. K. Jana, A. Srivastava, A. Lord, and A. Mitra, "Optical cable deployment versus fiber leasing: An operator's perspective on CapEx savings for capacity upgrade in an elastic optical core network," *Journal of Optical Communications and Networking*, vol. 15, no. 8, pp. C179–C191, 2023. DOI: 10.1364/JOCN.483200.

[16] R. K. Jana, B. C. Chatterjee, A. P. Singh, *et al.*, "Quality-aware resource provisioning for multiband elastic optical networks: A deep-learning-assisted approach," *Journal of Optical Communications and Networking*, vol. 14, no. 11, pp. 882–893, 2022. DOI: 10.1364/JOCN.465782.

[17] H. Yang, R. Wang, P. Wright, *et al.*, "Impact of WSS passband narrowing effect on the capacity of the flexible-spectrum networks," in *2017 Optical Fiber Communications Conference and Exhibition (OFC)*, Mar. 2017, pp. 1–3.

[18] R. K. Jana, B. C. Chatterjee, A. P. Singh, *et al.*, "Performance Evaluation of Conventional Spectrum-Allocation Policies for C+L Band Elastic Optical Networks," in *2021 IEEE International Conference on Advanced Networks and Telecommunications Systems (ANTS)*, 2021, pp. 348–353. DOI: 10.1109/ANTS52808.2021.9937024.

[19] D. Semrau, R. I. Killey, and P. Bayvel, "The Gaussian Noise Model in the Presence of Inter-Channel Stimulated Raman Scattering," *Journal of Lightwave Technology*, vol. 36, no. 14, pp. 3046–3055, 2018. DOI: 10.1109/JLT.2018.2830973.

[20] R. K. Jana, A. Mitra, A. Pradhan, *et al.*, "When Is Operation Over C + L Bands More Economical than Multifiber for Capacity Upgrade of an Optical Backbone Network?" In *2020 European Conference on Optical Communications (ECOC)*, 2020, pp. 1–4. DOI: 10.1109/ECOC48923.2020.9333276.

[21] D. Semrau, E. Sillekens, R. I. Killey, and P. Bayvel, "The ISRS GN Model, an Efficient Tool in Modeling Ultra-Wideband Transmission in Point-to-Point and Network Scenarios," in *2018 European Conference on Optical Communication (ECOC)*, 2018, pp. 1–3. DOI: 10.1109/ECOC.2018.8535146.

[22] D. Moniz, V. Lopez, and J. Pedro, "Design Strategies Exploiting C+L-band in Networks with Geographically-dependent Fiber Upgrade Expenditures," in *Optical Fiber Communication Conference (OFC) 2020*, Optica Publishing Group, 2020, M2G.3. DOI: 10.1364/OFC.2020.M2G.3. [Online]. Available: http://opg.optica.org/abstract.cfm?URI=OFC-2020-M2G.3.

[23] B. Shariati, P. S. Khodashenas, J. M. Rivas-Moscoso, *et al.*, "Investigation of Mid-term Network Migration Scenarios Comparing Multi-Band and Multi-Fiber Deployments," in *Optical Fiber Communication Conference*, Optica Publishing Group, 2016, Th1E.1. DOI: 10.1364/OFC.2016.Th1E.1. [Online]. Available: http://opg.optica.org/abstract.cfm?URI=OFC-2016-Th1E.1.

[24] R. J. Pandya, V. Chandra, and D. Chadha, "Simultaneous Optimization of Power Economy and Impairment Awareness by Traffic Grooming, Mixed Regeneration, and All Optical Wavelength Conversion With an Experimental Demonstration," *J. Lightwave Technol.*, vol. 32, no. 24, pp. 4166–4177, Dec. 2014. [Online]. Available: http://opg.optica.org/jlt/abstract.cfm?URI=jlt-32-24-4166.

[25] Sterlite, "Sterlite Technologies Limited," Accessed: Jan 29, 2020. [Online]. Available: https://stl.tech/.

[26] R. K. Jana, M. A. Iqbal, N. Parkin, *et al.*, "Multifiber vs. Ultra-Wideband Upgrade: A Techno-Economic Comparison for Elastic Optical Backbone Network," in *European Conference on Optical Communication (ECOC) 2022*, Optica Publishing Group, 2022, We1A.5. DOI: 10.1364/ECEOC.2022.We1A.5. [Online]. Available: https://opg.optica.org/abstract.cfm?URI=ECEOC-2022-We1A.5.

[27] G. of India, "Census of INDIA," Accessed: January 20, 2020. [Online]. Available: https://censusindia.gov.in/census.website/data/census-tables.

[28] Thorlabs, "Erbium-Doped Fiber Amplifiers (EDFA)," Accessed: Jan 29, 2020. [Online]. Available: https://www.thorlabs.com/newgrouppage9.cfm?objectgroup_id=10680.

[29] OEQuest, "C/L Band Combiners-Splitters," Accessed: Jan 29, 2020). [Online]. Available: https://www.oequest.com/cat/1148.

[30] S. Verbrugge, D. Colle, M. Pickavet, and P. Demeester, "Cost Versus Flexibility of Different Capacity Leasing Approaches on the Optical Network Layer," in *Optical Network Design and Modeling*, I. Tomkos, F. Neri, J. Solé Pareta, X. Masip Bruin, and S. Sánchez Lopez, Eds., Berlin, Heidelberg: Springer Berlin Heidelberg, 2007, pp. 418–427, ISBN: 978-3-540-72731-6.

[31] OpenZR+, "Open ZR+ MSA Technical Specification," Accessed: July 20, 2022. [Online]. Available: www.openzrplus.org/documents.

[32] R. Sadeghi, B. Correia, E. Virgillito, *et al.*, "Network Comparison of C+L-band Transparent versus C-band Translucent Upgrade," in *2021 International Conference on Optical Network Design and Modeling (ONDM)*, Jun. 2021, pp. 1–6. DOI: 10.23919/ONDM51796.2021.9492468.

[33] M. Klinkowski and K. Walkowiak, "On the Advantages of Elastic Optical Networks for Provisioning of Cloud Computing Traffic," *IEEE Network*, vol. 27, no. 6, pp. 44–51, 2013. DOI: 10.1109/MNET.2013.6678926.

[34] B. C. Chatterjee, N. Sarma, and E. Oki, "Routing and Spectrum Allocation in Elastic Optical Networks: A Tutorial," *IEEE Communications Surveys Tutorials*, vol. 17, no. 3, pp. 1776–1800, Third Quarter 2015, ISSN: 1553-877X. DOI: 10.1109/COMST.2015.2431731.

[35] P. Wright, M. C. Parker, and A. Lord, "Simulation Results of Shannon Entropy Based Flexgrid Routing and Spectrum Assignment on a Real Network Topology," in *39th European Conference and Exhibition on Optical Communication (ECOC 2013)*, Sep. 2013. DOI: 10.1049/cp.2013.1428.

[36] P. Wright, M. C. Parker, and A. Lord, "Minimum- and Maximum-Entropy Routing and Spectrum Assignment for Flexgrid Elastic Optical Networking [Invited]," *IEEE/OSA Journal of Optical Communications and Networking*, vol. 7, no. 1, A66–A72, Jan. 2015, ISSN: 1943-0639. DOI: 10.1364/JOCN.7.000A66.

[37] R. Wang and B. Mukherjee, "Spectrum Management in Heterogeneous Bandwidth Optical Networks," en, *Optical Switching and Networking*, vol. 11, pp. 83–91, Jan. 2014, ISSN: 1573-4277. DOI: 10.1016/j.osn.2013.09.003.

[38] P. Soumplis, K. Christodoulopoulos, M. Quagliotti, A. Pagano, and E. Varvarigos, "Network Planning With Actual Margins," *Journal of Lightwave Technology*, vol. 35, no. 23, pp. 5105–5120, Dec. 2017, ISSN: 1558-2213. DOI: 10.1109/JLT.2017.2743461.

[39] C. Chen, F. Zhou, Y. Liu, and S. Xiao, "Throughput Maximization Leveraging Just-Enough SNR Margin and Channel Spacing Optimization," *arXiv:2106.07536 [cs, eess]*, Jul. 2021. arXiv: 2106.07536 [cs, eess].

[40] I. Sartzetakis, K. Christodoulopoulos, C. P. Tsekrekos, D. Syvridis, and E. Varvarigos, "Estimating QoT of Unestablished Lightpaths," in *Optical Fiber Communication Conference*, Anaheim, California: OSA, 2016, Tu3F.2, ISBN: 978-1-943580-07-1. DOI: 10.1364/OFC.2016.Tu3F.2.

[41] H. Beyranvand and J. A. Salehi, "A Quality-of-Transmission Aware Dynamic Routing and Spectrum Assignment Scheme for Future Elastic Optical Networks," *Journal of Lightwave Technology*, vol. 31, no. 18, pp. 3043–3054, Sep. 2013, ISSN: 1558-2213. DOI: 10.1109/JLT.2013.2278572.

[42] J. Zhao, H. Wymeersch, and E. Agrell, "Nonlinear Impairment-Aware Static Resource Allocation in Elastic Optical Networks," *Journal of Lightwave Technology*, vol. 33, no. 22, pp. 4554–4564, Nov. 2015, ISSN: 1558-2213. DOI: 10.1109/JLT.2015.2474130.

[43] M. N. Dharmaweera, J. Zhao, L. Yan, M. Karlsson, and E. Agrell, "Traffic-Grooming- and Multipath-Routing-Enabled Impairment-Aware Elastic Optical Networks," *IEEE/OSA Journal of Optical Communications and Networking*, vol. 8, no. 2, pp. 58–70, Feb. 2016, ISSN: 1943-0639. DOI: 10.1364/JOCN.8.000058.

[44] M. Du-Pond, O. Audouin, B. Berde, *et al.*, "Service Level Agreement in Optical Networks," en, in *Network Control and Engineering for QoS, Security and Mobility II*, D. Gaïti, G. Pujolle, A. Al-Naamany, H. Bourdoucen, and L. Khriji, Eds., vol. 133, Boston, MA: Springer US, 2003, pp. 225–237, ISBN: 978-1-4757-5950-1 978-0-387-35703-4. DOI: 10.1007/978-0-387-35703-4_17.

[45] W. Fawaz, B. Daheb, O. Audouin, M. Du-Pond, and G. Pujolle, "Service Level Agreement and Provisioning in Optical Networks," en, *IEEE Communications Magazine*, vol. 42, no. 1, pp. 36–43, Jan. 2004, ISSN: 0163-6804. DOI: 10.1109/MCOM.2004.1262160.

[46] A. Agrawal, U. Vyas, V. Bhatia, and S. Prakash, "SLA-Aware Differentiated QoS in Elastic Optical Networks," en, *Optical Fiber Technology*, vol. 36, pp. 41–50, Jul. 2017, ISSN: 10685200. DOI: 10.1016/j.yofte.2017.01.012.

[47] W. Fadini and E. Oki, "A Subcarrier-Slot Partition Scheme for Wavelength Assignment in Elastic Optical Networks," in *2014 IEEE 15th International Conference on High Performance Switching and Routing (HPSR)*, Jul. 2014, pp. 7–12. DOI: 10.1109/HPSR.2014.6900874.

[48] W. Fadini, B. C. Chatterjee, and E. Oki, "A Subcarrier-Slot Partition Scheme with First-Last Fit Spectrum Allocation for Elastic Optical Networks," en, *Computer Networks*, vol. 91, pp. 700–711, Nov. 2015, ISSN: 1389-1286. DOI: 10.1016/j.comnet.2015.08.048.

[49] R. Wang and B. Mukherjee, "Spectrum Management in Heterogeneous Bandwidth Networks," in *2012 IEEE Global Communications Conference (GLOBECOM)*, Dec. 2012, pp. 2907–2911. DOI: 10.1109/GLOCOM.2012.6503558.

[50] B. C. Chatterjee, W. Fadini, and E. Oki, "A Spectrum Allocation Scheme Based on First–Last-Exact Fit Policy for Elastic Optical Networks," en, *Journal of Network and Computer Applications*, vol. 68, pp. 164–172, Jun. 2016, ISSN: 1084-8045. DOI: 10.1016/j.jnca.2016.02.020.

[51] A. Pagès, J. Perelló, S. Spadaro, and J. Comellas, "Optimal Route, Spectrum and Modulation Level Assignment in Split-Spectrum-Enabled Dynamic Elastic Optical Networks," *IEEE/OSA Journal of Optical Communications and Networking*, vol. 6, no. 2, pp. 114–126, Feb. 2014, ISSN: 1943-0639. DOI: 10.1364/JOCN.6.000114.

[52] F. Cugini, F. Paolucci, G. Meloni, *et al.*, "Push-Pull Defragmentation Without Traffic Disruption in Flexible Grid Optical Networks," *Journal of Lightwave Technology*, vol. 31, no. 1, pp. 125–133, Jan. 2013, ISSN: 1558-2213. DOI: 10.1109/JLT.2012.2225600.

[53] R. Proietti, C. Qin, B. Guan, *et al.*, "Rapid and Complete Hitless Defragmentation Method Using a Coherent RX LO with Fast Wavelength Tracking in Elastic Optical Networks," EN, *Optics Express*, vol. 20, no. 24, pp. 26 958–26 968, Nov. 2012, ISSN: 1094-4087. DOI: 10.1364/OE.20.026958.

[54] M. Zhang, Y. Yin, R. Proietti, Z. Zhu, and S. J. B. Yoo, "Spectrum Defragmentation Algorithms for Elastic Optical Networks using Hitless Spectrum Retuning Techniques," en, in *Optical Fiber Communication Conference/National Fiber Optic Engineers Conference 2013*, Anaheim, California: OSA, 2013, OW3A.4, ISBN: 978-1-55752-962-6. DOI: 10.1364/OFC.2013.OW3A.4.

[55] R. Wang and B. Mukherjee, "Provisioning in Elastic Optical Networks with Non-Disruptive Defragmentation," *Journal of Lightwave Technology*, vol. 31, no. 15, pp. 2491–2500, Aug. 2013, ISSN: 1558-2213. DOI: 10.1109/JLT.2013.2268535.

[56] J. Bromage, "Raman Amplification for Fiber Communications Systems," *Journal of Lightwave Technology*, vol. 22, no. 1, pp. 79–93, Jan. 2004, ISSN: 1558-2213. DOI: 10.1109/JLT.2003.822828.

[57] B. C. Chatterjee, S. Ba, and E. Oki, "Fragmentation Problems and Management Approaches in Elastic Optical Networks: A Survey," en, *IEEE Communications Surveys & Tutorials*, vol. 20, no. 1, pp. 183–210, 21, ISSN: 1553-877X. DOI: 10.1109/COMST.2017.2769102.

[58] A. Mitra, D. Semrau, N. Gahlawat, A. Srivastava, P. Bayvel, and A. Lord, "Effect of reduced link margins on C + L band elastic optical networks," *IEEE/OSA Journal of Optical Communications and Networking*, vol. 11, no. 10, pp. C86–C93, Oct. 2019, ISSN: 1943-0639. DOI: 10.1364/JOCN.11.000C86.

[59] A. Mitra, D. Semrau, N. Gahlawat, *et al.*, "Capacity Benefits of Operation Over C+ L Band Elastic Optical Network in the Indian Network Scenario," in *2019 IEEE International Conference on Advanced Networks and Telecommunications Systems (ANTS)*, Dec. 2019. DOI: 10.1109/ANTS47819.2019.9117992.

[60] F. Musumeci, C. Rottondi, A. Nag, *et al.*, "An Overview on Application of Machine Learning Techniques in Optical Networks," *IEEE Communications Surveys Tutorials*, vol. 21, no. 2, pp. 1383–1408, Second Quarter 2019, ISSN: 1553-877X. DOI: 10.1109/COMST.2018.2880039.

[61] I. Khan, M. Bilal, M. Umar Masood, A. D'Amico, and V. Curri, "Lightpath QoT Computation in Optical Networks Assisted by Transfer Learning," *Journal of Optical Communications and Networking*, vol. 13, no. 4, B72–B82, Apr. 2021, ISSN: 1943-0620, 1943-0639. DOI: 10.1364/JOCN.409538.

[62] M. Ibrahimi, H. Abdollahi, C. Rottondi, *et al.*, "Machine Learning Regression for QoT Estimation of Unestablished Lightpaths," *Journal of Optical Communications and Networking*, vol. 13, no. 4, B92–B101, Apr. 2021, ISSN: 1943-0620, 1943-0639. DOI: 10.1364/JOCN.410694.

[63] Y. Pointurier, "Machine Learning Techniques for Quality of Transmission Estimation in Optical Networks," *Journal of Optical Communications and Networking*, vol. 13, no. 4, B60–B71, Apr. 2021, ISSN: 1943-0620, 1943-0639. DOI: 10.1364/JOCN.417434.

[64] J. Lu, G. Zhou, Q. Fan, *et al.*, "Performance Comparisons between Machine Learning and Analytical Models for Quality of Transmission Estimation in Wavelength-Division-Multiplexed Systems [Invited]," *Journal of Optical Communications and Networking*, vol. 13, no. 4, B35–B44, Apr. 2021, ISSN: 1943-0620, 1943-0639. DOI: 10.1364/JOCN.410876.

[65] C.-Y. Liu, X. Chen, R. Proietti, and S. J. B. Yoo, "Performance studies of evolutionary transfer learning for end-to-end QoT estimation in multi-domain optical networks [Invited]," en, *Journal of Optical Communications and Networking*, vol. 13, no. 4, B1–B11, Apr. 2021, ISSN: 1943-0620, 1943-0639. DOI: 10.1364/JOCN.409817.

[66] A. Mahajan, K. Christodoulopoulos, R. Martinez, R. Munoz, and S. Spadaro, "Quality of Transmission Estimator Retraining for Dynamic Optimization in Optical Networks," *Journal of Optical Communications and Networking*, vol. 13, no. 4, B45–B59, Apr. 2021, ISSN: 1943-0620, 1943-0639. DOI: 10.1364/JOCN.411524.

[67] J. Comellas, L. Vicario, and G. Junyent, "Proactive Defragmentation in Elastic Optical Networks under Dynamic Load Conditions," *Photonic Network Communications*, vol. 36, no. 1, pp. 26–34, 2018.

[68] S. Dahlfort, M. Xia, R. Proietti, and S. J. B. Yoo, "Split Spectrum Approach to Elastic Optical Networking," en, in *European Conference and Exhibition on Optical Communication*, Amsterdam: OSA, 2012, Tu.3.D.4, ISBN: 978-1-55752-950-3. DOI: 10.1364/ECEOC.2012.Tu.3.D.4.

[69] D. Uzunidis, E. Kosmatos, C. Matrakidis, A. Stavdas, and A. Lord, "Strategies for Upgrading an Operator's Backbone Network Beyond the C-Band: Towards Multi-Band Optical Networks," *IEEE Photonics Journal*, vol. 13, no. 2, pp. 1–18, Apr. 2021, ISSN: 1943-0655. DOI: 10.1109/JPHOT.2021.3054849.

[70] B. C. Chatterjee and E. Oki, "Dispersion-Adaptive First–Last Fit Spectrum Allocation Scheme for Elastic Optical Networks," *IEEE Communications Letters*, vol. 20, no. 4, pp. 696–699, Apr. 2016, ISSN: 1089-7798. DOI: 10.1109/LCOMM.2016.2526998.

[71] A. Rosa, C. Cavdar, S. Carvalho, J. Costa, and L. Wosinska, "Spectrum Allocation Policy Modeling for Elastic Optical Networks," in *High Capacity Optical Networks and Emerging/Enabling Technologies*, Dec. 2012, pp. 242–246. DOI: 10.1109/HONET.2012.6421472.

[72] R. Wang, S. Bidkar, R. Nejabati, and D. Simeonidou, "Load and Nonlinearity Aware Resource Allocation in Elastic Optical Networks," in *Optical Fiber Communication Conference*, Los Angeles, California: OSA, 2017, W1H.5, ISBN: 978-1-943580-23-1. DOI: 10.1364/OFC.2017.W1H.5.

[73] S. Behera, A. Deb, G. Das, and B. Mukherjee, "Impairment Aware Routing, Bit Loading, and Spectrum Allocation in Elastic Optical Networks," *Journal of Lightwave Technology*, vol. 37, no. 13, pp. 3009–3020, Jul. 2019, ISSN: 1558-2213. DOI: 10.1109/JLT.2019.2909125.

[74] M. Nakagawa, H. Kawahara, K. Masumoto, T. Matsuda, and K. Matsumura, "Performance Evaluation of Multi-Band Optical Networks Employing Distance-Adaptive Resource Allocation," in *2020 Opto-Electronics and Communications Conference (OECC)*, Oct. 2020, pp. 1–3. DOI: 10.1109/OECC48412.2020.9273660.

[75] R. Jashvantbhai Pandya, "Machine Learning-Oriented Resource Allocation in C + L + S Bands Extended SDM–EONs," *IET Communications*, vol. 14, no. 12, pp. 1957–1967, 2020, ISSN: 1751-8636. DOI: 10.1049/iet-com.2019.1191.

[76] F. Calderón, A. Lozada, P. Morales, *et al.*, "Heuristic Approaches for Dynamic Provisioning in Multi-Band Elastic Optical Networks," *IEEE Communications Letters*, vol. 26, no. 2, pp. 379–383, Feb. 2022, ISSN: 1558-2558. DOI: 10.1109/LCOMM.2021.3132054.

[77] N. Sambo, A. Ferrari, A. Napoli, *et al.*, "Provisioning in Multi-Band Optical Networks," *Journal of Lightwave Technology*, vol. 38, no. 9, pp. 2598–2605, May 2020, ISSN: 1558-2213. DOI: 10.1109/JLT.2020.2983227.

[78] L. Zhang, X. Li, Y. Tang, J. Xin, and S. Huang, "A Survey on QoT Prediction using Machine Learning in Optical Networks," *Optical Fiber Technology*, vol. 68, p. 102 804, 2022, ISSN: 1068-5200. DOI: https://doi.org/10.1016/j.yofte.2021.102804. [Online]. Available: https://www.sciencedirect.com/science/article/pii/S1068520021003540.

[79] L. Barletta, A. Giusti, C. Rottondi, and M. Tornatore, "QoT Estimation for Unestablished Lighpaths using Machine Learning," in *2017 Optical Fiber Communications Conference and Exhibition (OFC)*, 2017, pp. 1–3.

[80] R. Proietti, X. Chen, K. Zhang, *et al.*, "Experimental Demonstration of Machine-Learning-Aided QoT Estimation in Multi-Domain Elastic Optical Networks with Alien Wavelengths," *Journal of Optical Communications and Networking*, vol. 11, no. 1, A1–A10, Jan. 2019, ISSN: 1943-0639.

[81] R. Ahumada Cortes, A. Leiva Lopez, F. Alonso Villalobos, S. Fingerhuth Massmann, and G. Farias Castro, "Spectrum Allocation Algorithms for Elastic DWDM Networks on Dynamic Operation," *IEEE Latin America Transactions*, vol. 12, no. 6, pp. 1012–1018, 2014. DOI: 10.1109/TLA.2014.6893994.

[82] B. C. Chatterjee, A. Wadud, and E. Oki, "Proactive Fragmentation Management Scheme Based on Crosstalk-Avoided Batch Processing for Spectrally-Spatially Elastic Optical Networks," en, *IEEE Journal on Selected Areas in Communications*, 2021, ISSN: 0733-8716, 1558-0008. DOI: 10.1109/JSAC.2021.3064594.

[83] A. Ferrari, A. Napoli, J. K. Fischer, *et al.*, "Upgrade Capacity Scenarios Enabled by Multi-band Optical Systems," in *2019 21st International Conference on Transparent Optical Networks (ICTON)*, 2019, pp. 1–4. DOI: 10.1109/ICTON.2019.8840550.

[84] T. Ahmed, A. Mitra, S. Rahman, M. Tornatore, A. Lord, and B. Mukherjee, "C+L-band Upgrade Strategies to Sustain Traffic Growth in Optical Backbone Networks," *Journal of Optical Communications and Networking*, vol. 13, no. 7, pp. 193–203, Jul. 2021, ISSN: 1943-0639. DOI: 10.1364/JOCN.427097.

[85] T. Ahmed, S. Rahman, A. Pradhan, *et al.*, "C to C+ L Bands Upgrade with Resource Re-provisioning in Optical Backbone Networks," in *Optical Fiber Communication Conference*, Optica Publishing Group, 2021, W1F–7.

[86] N. Sambo, A. Ferrari, A. Napoli, *et al.*, "Provisioning in Multi-band Optical Networks: A C+L+S-band Use Case," in *45th European Conference on Optical Communication (ECOC 2019)*, IET, 2019, pp. 1–4.

[87] B. Correia, R. Sadeghi, E. Virgillito, *et al.*, "Networking Performance of Power Optimized C+L+S Multiband Transmission," in *Proc. IEEE Global Communications Conference (GLOBECOM)*, Dec. 2020.

[88] E. Virgillito, R. Sadeghi, A. Ferrari, A. Napoli, B. Correia, and V. Curri, "Network Performance Assessment with Uniform and Non-Uniform Nodes Distribution in C+L Upgrades vs. Fiber Doubling SDM Solutions," in *Proc. International Conference on Optical Network Design and Modeling (ONDM)*, May 2020.

[89] Infinera, "Windstream Deploys Infinera C+L Solution, Sets Foundation to Double Fiber Capacity," Accessed: May 2021. [Online]. Available: https://www.infinera.com/press-release/windstream-deploys-infinera-c-l-solution-sets-foundation-double-fiber-capacity.

[90] B. Correia, R. Sadeghi, E. Virgillito, *et al.*, "Power Control Strategies and Network Performance Assessment for C+L+S Multiband Optical Transport," *Journal of Optical Communications and Networking*, vol. 13, no. 7, pp. 147–157, 2021.

[91] M. Cantono, J. L. Auge, and V. Curri, "Modelling the Impact of SRS on NLI Generation in Commercial Equipment: An Experimental Investigation," in *Proc. Optical Fiber Communications Conference*, Mar. 2018.

[92] I. Sartzetakis, K. K. Christodoulopoulos, and E. M. Varvarigos, "Accurate Quality of Transmission Estimation with Machine Learning," *Journal of Optical Communications and Networking*, vol. 11, no. 3, pp. 140–150, 2019.

[93] J. Thrane, J. Wass, M. Piels, J. C. Diniz, R. Jones, and D. Zibar, "Machine Learning Techniques for Optical Performance Monitoring from Directly Detected PDM-QAM Signals," *Journal of Lightwave Technology*, vol. 35, no. 4, pp. 868–875, 2016.

[94] R. M. Morais and J. Pedro, "Machine Learning Models for Estimating Quality of Transmission in DWDM Networks," *Journal of Optical Communications and Networking*, vol. 10, no. 10, pp. D84–D99, 2018.

[95] T. Panayiotou, S. P. Chatzis, and G. Ellinas, "Performance Analysis of a Data-Driven Quality-of-Transmission Decision Approach on a Dynamic Multicast-Capable Metro Optical Network," *Journal of Optical Communications and Networking*, vol. 9, no. 1, pp. 98–108, 2017.

[96] A. Souza *et al.*, "Optimal Pay-As-You-Grow Deployment on S+C+L Multi-band Systems," in *Proc. Optical Fiber Communications Conference*, Mar. 2022.

[97] S. Hosseini *et al.*, "Migration Strategy from C-Band Elastic Optical Network to C+L Multiband Optical Network," in *Proc. International Telecommunication Networks and Applications Conference*, Wellington, New Zealand, Nov. 2022.

[98] J. L. Ravipudi and M. Brandt-Pearce, "Impairment-and Fragmentation-Aware Dynamic Routing, Modulation and Spectrum Allocation in C+L Band Elastic Optical Networks using Q-Learning," *Optical Switching and Networking*, vol. 47, p. 100 717, 2023.

[99] S. Hochreiter and J. Schmidhuber, "Long Short-Term Memory," *Neural Computation*, vol. 9, no. 8, pp. 1735–1780, Nov. 1997.

[100] M. Nakagawa, T. Seki, and T. Miyamura, "Techno-Economic Potential of Wavelength-Selective Band-Switchable OXC in S+C+L Band Optical Networks," in *Proc. Optical Fiber Communications Conference*, San Diego, CA, USA, Mar. 2022.

[101] Y. Gu, Y. Li, N. Guo, X. You, and G. Shen, "L-Band Amplifier Placement in C+L-Band Elastic Optical Networks," in *Proc. Asia Communications and Photonics Conference*, Shanghai, China, Oct. 2021.

[102] W. Shi, Z. Zhu, M. Zhang, and N. Ansari, "On the Effect of Bandwidth Fragmentation on Blocking Probability in Elastic Optical Networks," *IEEE Transactions on Communications*, vol. 61, no. 7, pp. 2970–2978, Jul. 2013.

[103] D. Amar, E. Rouzic, N. Brochier, J. Auge, C. Lepers, and N. Perrot, "Spectrum Fragmentation Issue in Flexible Optical Networks: Analysis and Good Practices," *Photonic Network Communications*, vol. 29, no. 3, pp. 230–243, Mar. 2015.

[104] Y. Pointurier, "Design of Low-Margin Optical Networks," *Journal of Optical Communications and Networking*, vol. 9, no. 1, A9–A17, 2017. DOI: 10.1364/JOCN.9.0000A9.

[105] J. Pesic and A. Morea, "Operating a Network Close to the "Zero Margin" Regime Thanks to Elastic Devices," in *2015 17th International Conference on Transparent Optical Networks (ICTON)*, 2015, pp. 1–1. DOI: 10.1109/ICTON.2015.7193719.

[106] M. S. Zefreh and S. Asselin, "Capacity Enhancement in Optical Networks using Margin Extraction," in *2018 Optical Fiber Communications Conference and Exposition (OFC)*, 2018, pp. 1–3.

[107] F. Hamaoka, M. Nakamura, S. Okamoto, *et al.*, "Ultra-Wideband WDM Transmission in S-, C-, and L-Bands Using Signal Power Optimization Scheme," *Journal of Lightwave Technology*, vol. 37, no. 8, pp. 1764–1771, 2019. DOI: 10.1109/JLT.2019.2894827.

[108] D. Semrau, E. Sillekens, R. I. Killey, and P. Bayvel, "The Benefits of Using the S-Band in Optical Fiber Communications and How to Get There," in *2020 IEEE Photonics Conference (IPC)*, 2020, pp. 1–2. DOI: 10.1109/IPC47351.2020.9252426.

[109] B. J. Puttnam, R. S. Luís, G. Rademacher, M. Mendez-Astudilio, Y. Awaji, and H. Furukawa, "S, C and Extended L-Band Transmission with Doped Fiber and Distributed Raman Amplification," in *2021 Optical Fiber Communications Conference and Exhibition (OFC)*, 2021, pp. 1–3.

[110] T. Hoshida, V. Curri, L. Galdino, *et al.*, "Ultrawideband Systems and Networks: Beyond C + L-Band," *Proceedings of the IEEE*, vol. 110, no. 11, pp. 1725–1741, 2022. DOI: 10.1109/JPROC.2022.3202103.

[111] S. Shahkarami, F. Musumeci, F. Cugini, and M. Tornatore, "Machine-Learning-Based Soft-Failure Detection and Identification in Optical Networks," in *2018 Optical Fiber Communications Conference and Exposition (OFC)*, IEEE, 2018, pp. 1–3.

[112] F. Musumeci, C. Rottondi, G. Corani, S. Shahkarami, F. Cugini, and M. Tornatore, "A Tutorial on Machine Learning for Failure Management in Optical Networks," *Journal of Lightwave Technology*, vol. 37, no. 16, pp. 4125–4139, 2019.

[113] S. Behera, T. Panayiotou, and G. Ellinas, "Machine Learning Framework for Timely Soft-Failure Detection and Localization in Elastic Optical Networks," *Journal of Optical Communications and Networking*, vol. 15, no. 10, E74–E85, 2023.

[114] L. Shu, Z. Yu, Z. Wan, J. Zhang, S. Hu, and K. Xu, "Dual-Stage Soft Failure Detection and Identification for Low-Margin Elastic Optical Network by Exploiting Digital Spectrum Information," *Journal of Lightwave Technology*, vol. 38, no. 9, pp. 2669–2679, 2019.

[115] L. Velasco, B. Shariati, A. P. Vela, J. Comellas, and M. Ruiz, "Learning from the Optical Spectrum: Soft-Failure Identification and Localization," in *2018 Optical Fiber Communications Conference and Exposition (OFC)*, IEEE, 2018, pp. 1–3.

[116] G. M. Saridis, D. Alexandropoulos, G. Zervas, and D. Simeonidou, "Survey and Evaluation of Space Division Multiplexing: From Technologies to Optical Networks," *IEEE Communications Surveys & Tutorials*, vol. 17, no. 4, pp. 2136–2156, 2015.

[117] Í. Brasileiro, L. Costa, and A. Drummond, "A Survey on Challenges of Spatial Division Multiplexing Enabled Elastic Optical Networks," *Optical Switching and Networking*, vol. 38, p. 100 584, 2020, ISSN: 1573-4277. DOI: https://doi.org/10.1016/j.osn.2020.100584. [Online]. Available: https://www.sciencedirect.com/science/article/pii/S1573427720300461.

[118] B. J. Puttnam, G. Rademacher, and R. S. Luís, "Space-Division Multiplexing for Optical Fiber Communications," *Optica*, vol. 8, no. 9, pp. 1186–1203, Sep. 2021. DOI: 10.1364/OPTICA.427631. [Online]. Available: https://opg.optica.org/optica/abstract.cfm?URI=optica-8-9-1186.

[119] S. Tariq and J. C. Palais, "A Computer Model of Non-Dispersion-Limited Stimulated Raman Scattering in Optical Fiber Multiple-Channel Communications," *Journal of Lightwave Technology*, vol. 11, no. 12, pp. 1914–1924, 1993.

[120] M. Zirngibl, "Analytical Model of Raman Gain Effects in Massive Wavelength Division Multiplexed Transmission Systems," *Electronics letters*, vol. 34, no. 8, pp. 789–790, 1998.